Carbon-efficient Wastewater Treatment Through Resource Recovery, Process Intensification, and Partial Denitrification Anammox

Jiefu Wang

Dissertation submitted to the faculty of the Virginia Polytechnic Institute and State University in partial fulfillment of the requirements for the degree of

Doctor of Philosophy
in
Civil Engineering

Zhi-Wu (Drew) Wang, Chair
Amy Pruden-Bagchi
John Novak
Christopher Wilson

April 30th, 2024
Blacksburg, VA

Keywords: Carbon efficient; biological nutrient removal; anammox; process intensification; anaerobic digestion; thermal hydrolysis pretreatment

Copyright © 2024, Jiefu Wang

Carbon-efficient Wastewater Treatment Through Resource Recovery, Process Intensification, and Partial Denitrification Anammox

Jiefu Wang

Abstract (academic)

Facing the pressure of population growth and global warming, this dissertation provided an array of innovative carbon-efficient wastewater treatment technologies for resource recovery, process intensification, and anammox featured next generation biological nutrient removal (BNR) technologies. These technologies aim to supplant traditional carbon-intensive treatment processes with more sustainable alternatives. To this end, the dissertation first comprehensively reviewed what resources can be recovered from wastewater, and how these valuable resources can contribute to the carbon neutrality in water resource reclamation facilities (WRRFs) and help achieve sustainable society development. Then, the effect of mixed liquor recycle (MLR) configurations on the process intensification through continuous-flow aerobic granulation was explored in plug flow reactors. The results demonstrated that MLR configuration could hinder the sludge granulation, but the hindrance could be alleviated to some extent by its location change. In order to eliminate the energy consuming MLR, endogenous denitrification was taken advantage through a synergistic integration with partial nitrification, partial denitrification anammox (PdNA), and enhanced biological phosphorus removal (EBPR). This idea was tested in a pilot setup treating real primary effluent under highly variable influent conditions and low temperatures. The results showcased substantial carbon savings while meeting the stringent effluent requirements. To take a deeper dive into the PdNA performance and the underlying mechanisms, two parallel pilot-scale moving bed biofilm reactor (MBBR) treatment trains fed with methanol and glycerol, respectively, were operated in a local WRRF. Their efficacies in achieving stringent nutrient removal targets and carbon savings were compared. The impacts of operational conditions on the mechanisms and performance were elucidated. In the culmination of this dissertation, a sidestream process intensification and resource recovery technique, namely thermal hydrolysis pretreatment (THP) enhanced anaerobic digestion (AD), was experimented to compare the efficiencies between thermophilic and mesophilic AD when integrated with THP. To sum up, this dissertation not only advanced our understanding of carbon-efficient wastewater treatment processes but also laid the groundwork for their practical implementation, contributing to the global effort towards sustainability.

Carbon-efficient Wastewater Treatment Through Resource Recovery, Process Intensification, and Partial Denitrification Anammox

Jiefu Wang

Abstract (general audience)

Wastewater treatment consumes 3-4% of the energy produced in the U.S. and contributes to approximately 1.6% global greenhouse gas emissions. This dissertation aims to advance a series of carbon-efficient technologies specifically tailored for sustainable wastewater treatment. To this end, a variety of valuable resources that can be recovered or reused in wastewater treatment plants was firstly reviewed. Then, an advanced technology that can turn dispersed bacteria into bacteria aggregates was tested with real wastewater in a local wastewater treatment plant. Although these bacteria aggregates allow more wastewater to be treated with less small footprint, which was great, it was realized from this study that the formation of these bacteria aggregates was hindered by the nitrate water recycle which has been commonly practiced for using influent carbon for nitrogen removal. This nitrate water recycle consumed excessive energy for its high flow rate. To save this energy, a novel bioprocessing design was developed to eliminate the need for this nitrate water recycle by using carbon stored in bacterial cells. This new design also incorporated phosphorus recovery capacity and a low carbon nitrogen removal technique into one consolidated system to create an all-in-one solution to meet the stringent wastewater treatment requirement. This low carbon nitrogen removal technique harnessed a special group of bacteria that can use ammonia to reduce nitrite to nitrogen gas. Hence, only minor carbon source needs to be provided to reduce nitrate to nitrite for these bacteria to utilize. Two types of carbon sources, namely methanol and glycerol, were compared in a pilot-scale study to understand their efficiencies in generating nitrite. Results indicated that although both types of carbon sources can work, methanol is better suited for low strength wastewater treatment. These results provided an engineering basis for the full-scale application of the technology in the same wastewater treatment plant where the pilot study was performed. Besides liquid treatment, a carbon efficient solid treatment technology was also studied. The bottleneck constraining the rate of sewage sludge conversion to flammable menthane gas was identified, which provided engineering guidance for the design of the solid treatment process that can destroy more sewage sludge within smaller reactor spaces. In essence, this dissertation offers promising solutions for modern wastewater treatment plants to achieve low carbon wastewater treatment without compromising the treatment performance.

Acknowledgments

During my Ph.D. study, I'm blessed to have the opportunity to work on multiple research projects in five U.S. water resource recovery facilities spread in three states and meet all the excellent and warmhearted people, who supported, guided, and helped me throughout my Ph.D. education journey even during the Covid-19 pandemic. I also have the fortune to receive a very good research scientist job offer from a famous consulting firm I worked with during my Ph.D. study prior to my graduation. I could not have gone this far without you all. Words cannot express how grateful I am.

First, I would like to express my sincere and hearty gratitude to my advisor, Dr. Zhi-Wu Wang, who has supported, guided, and helped my study and research all the way. He was the one who opened the door for me to the world of science and engineering, helped me weather the storm, and gave me confidence even in the darkest moments of my study and research journey. I would not have achieved all of these without him. A great appreciation also goes to Dr. Amy Pruden, Dr. John Novak, and Dr. Chirstopher Wilson for their willingness to serve on my committee and offered me kind help and guidance. Thank you for making this challenging journey easier and rewarding for me!

I would also like to give my special thanks to Dr. Yewei Sun and Dr. Wendell Kunjar from Hazen and Sawyer. I met Yewei in 2019 when he was a Ph.D. student in Dr. Wang's team. For me, Yewei was not only just a lab mate or a colleague, but also a confidant and a mentor. We witnessed each other's growth and transformation. Dr. Wendell Kunjar, as the Director of Wastewater Innovation and an expert process specialist from Hazen and Sawyer, supported, mentored, and supervised me on many projects I did and guided me on paper writing.

I would also like to thank all the people in Occoquan Lab. It was my first time coming to the U.S about five years ago when I joined the Occoquan Lab. Mrs. Marilyn Stull helped me prepare all the paperwork and place orders for chemicals and equipment. Mrs. Dongmei Alvi, Mrs. Joan Wirt, and Mr. Curt Kskridge helped me use new equipment and solve problems during my first semester in the Occoquan Lab. Although I left Occoquan Lab at the beginning of the pandemic, I will never forget our time together and the warmness of the Occoquan Lab family.

I'm also aware that that I would not have been able to do any research without the funding support from our sponsors, including Noman Cole pollution control plant (NCPCP), Upper Occoquan Service Authority (UOSA), Alexandria Renew Enterprise, Arlington water pollution control plant, Everett Wastewater Treatment Plant, National Science Foundation (NSF), Edna Bailey Sussman Foundation, Water Research Foundation (WRF), Hazen and Sawyer, and my alma mater Virginia Tech. I also would like to thank all the people offering support for my fieldwork research including staffs in the utilities, companies, and organizations mentioned above.

Next, I would like to thank my lab mates who helped, accompanied, and supported me during my Ph.D. study. Dr. Dian Zhang, Dr. Zhaohui An, and Dr. Hao Luo, three previous members from Dr. Wang's team, are also great friends of mine. Also, my thanks go to all current teammates, Ms. Xueyao Zhang and Mr. Yitao Li, for their generous help in the lab and in my daily life. I always remember the great time we had together.

Last but not least, my family started to support my oversea study eight years ago. Their unconditional love is like superman's cape that protects me through the hard times. I love you! I appreciate everyone mentioned above and others in my life for supporting my accomplishments today.

Thank you, Virginia Tech! **GO Hokies!**

Publication List

Journal Papers

1. **Wang J.**, An Z., Zhang X., Angelotti B., Brooks M., & Wang Z.W. (2023). Effects of Nitrate Recycle on the Sludge Densification in Plug-Flow Bioreactors Fed with Real Domestic Wastewater. Processes, 11(7), 1876, DOI: https://doi.org/10.3390/pr11071876.
2. **Wang J.**, Sun Y., Xia K., Deines A., Cooper R., Pallansch K., & Wang Z.W. (2022). Pivotal Role of Municipal Wastewater Resource Recovery Facilities in Urban Agriculture: A Review, Water Environment Research, 94(6), e10743, DOI: https://doi.org/10.1002/wer.10743 . (Issue cover of the June 2022 of Water Environment Research).
3. **Wang J.**, Sun Y., Zhang D., Broderick T., Strawn M., Santha H., & Wang Z.W. (2022). Unblocking the rate-limiting step of the municipal sludge anaerobic digestion, Water Environmental Research, e10793, DOI: https://doi.org/10.1002/wer.10793 .
4. **Wang J.**, Sun Y., Khunjar W., Pace G., McGrath M., Ali M., & Wang Z.W. (2024). Kinetic mechanism of methanol-fed partial denitrification anammox in tertiary moving bed biofilm reactors fed with real secondary effluent (Ready for submission).
5. **Wang J.**, Sun Y., Khunjar W., Pace G., McGrath M., Ali M., & Wang Z.W. (2024). Mechanistic understanding of the performance difference between methanol- and glycerol-fed partial denitrification anammox in tertiary moving bed biofilm reactors treating real secondary effluent (Ready for submission).
6. **Wang J.**, Sun Y., Zhang X., Khunjar W., Winkler M., Goel R., Wang Z.W. (2024). Carbon efficient nutrients removal from real municipal wastewater under conditions of highly variable influent quality and low temperature (Ready for submission).
7. **Wang J.**, Liu M., Zheng Y., Kumar S., Umeda, I., Wang Z.W. (2024). Activated sludge is highly efficient in treating hydrothermal liquefaction wastewater (Ready for submission).
8. An Z., **Wang J.**, Zhang X., Bott C. B., Angelotti B., Brooks M., & Wang Z.W. (2023). Coupling physical selection with biological selection for the startup of a pilot-scale, continuous flow, aerobic granular sludge reactor without treatment interruption. Water Research X, 100186, DOI: https://doi.org/10.1016/j.wroa.2023.100186 .

Conference Papers

1. **Wang J.**, Sun Y., Khunjar W., Winkler M. K., Li B., Goel R., Wang Z.W. (2023), Combination of EBPR, endogenous denitrification, partial nitrification/denitrification and anammox to

achieve cost-effective nutrient removal, WEFTEC, Water Environment Federation, DOI: https://www.accesswater.org/?id=-10097669 .

2. **Wang J.**, Sun Y., Khunjar W., Pace G., Pathak A., McGrath M., Ali M., Sun Y., Wang Z.W. (2022), Polishing tertiary effluent nitrogen via the synergy between methanol-driven partial denitrification and anaerobic ammonia oxidation in moving bed biofilm reactors, WEFTEC, Water Environment Federation, DOI: https://www.accesswater.org/?id=-10083928.
3. **Wang J.**, Sun Y., Khunjar W., Pace G., Pathak A., McGrath M., Ali M., Sun Y., Wang Z.W. (2022), Partial denitrification with glycerol as external carbon in moving bed biofilm reactors applied for anaerobic ammonia oxidation of low nitrogen concentration secondary effluent, WEFTEC, Water Environment Federation, DOI: https://www.accesswater.org/?id=-10083918.

Conference Oral Presentations

1. **Wang J.**, Sun Y., Khunjar W., Pace G., McGrath M., Ali M., & Wang Z.W. (2024). Mechanistic understanding of the kinetic difference between the methanol and glycerol-driven partial denitrification anammox in low nitrogen polishing moving bed biofilm reactors, Innovations in Treatment Technology Conference 2024, May 21-24, Virginia Beach, VA (to be presented).
2. **Wang J.**, Liu M., Zheng Y., Kumar S., Umeda I., & Wang Z.W. (2024). Biological treatment of hydrothermal liquefaction wastewater from sewage sludge with municipal wastewater activated sludge, Innovations in Treatment Technology Conference 2024, May 21-24, Virginia Beach, VA (to be presented).
3. **Wang J.**, Sun Y., Khunjar W., Winkler M. K., Li B., Goel R., Wang Z.W. (2023), Combination of EBPR, endogenous denitrification, partial nitrification/denitrification and anammox to achieve cost-effective nutrient removal, WEFTEC 2023, Sep.30 - Oct. 4, Chicago, IL.
4. **Wang J.**, Sun Y., Khunjar W., Winkler M., Goel R., Wang Z.W. (2023), Integration of endogenous denitrification, EBPR, partial nitrification/denitrification and anammox (PANDA) for cost-effective nutrient removal. WaterJAM 2023, September 11-14, Virginia Beach, VA
5. **Wang J.**, Sun Y., Khunjar W., Winkler M., Goel R., Wang Z.W. (2023), Integration of EBPR, endogenous denitrification, partial nitrification/denitrification and anammox for cost-effective nutrient removal, AEESP Research and Education Conference 2023, June 20-23, Boston, MA
6. **Wang J.**, Sun Y., Khunjar W., Winkler M. K., Li B., Goel R., Wang Z.W. (2023), Combination of EBPR, endogenous denitrification, partial nitrification/denitrification and anammox to achieve cost-effective nutrient removal, WEF/IWA Innovations in Process Engineering 2023,

June.6-9, Portland, OR.

7. **Wang J.**, An Z., Zhang X., Angelotti B., Brooks M., & Wang Z.W. (2023), Effects of NRCY and its Location Change on the Startup of Physical and Biological Selection Pressure-Driven Aerobic Granulation for Biological Nitrogen Removal in Plug-Flow Bioreactors Fed with Real Domestic Wastewater, WEF/IWA Innovations in Process Engineering 2023, June.6-9, Portland, OR.
8. **Wang J.**, Sun Y., Khunjar W., Pace G., Pathak A., McGrath M., Ali M., Sun Y., Wang Z.W. (2022), Low nitrogen concentration polishing via the synergy between methanol-driven partial denitrification and anammox in moving bed biofilm reactors, Tri-State ASABE Meeting-3MT Competition (2022), Raleigh, NC, November 3-4.
9. **Wang J.**, Sun Y., Khunjar W., Pace G., Pathak A., McGrath M., Ali M., Sun Y., Wang Z.W. (2022), Polishing tertiary effluent nitrogen via the synergy between methanol-driven partial denitrification and anaerobic ammonia oxidation in moving bed biofilm reactors, WEFTEC 2022, New Orleans, LA, October 9-13.
10. **Wang J.**, Sun Y., Khunjar W., Pace G., Pathak A., McGrath M., Ali M., Sun Y., Wang Z.W. (2022), Partial denitrification with glycerol as external carbon in moving bed biofilm reactors applied for anaerobic ammonia oxidation of low nitrogen concentration secondary effluent, WEFTEC 2022, New Orleans, LA, October 9-13.
11. **Wang J.**, Sun Y., Khunjar W., Pace G., Pathak A., McGrath M., Ali M., Sun Y., Wang Z.W. (2022), Comparison between methanol- and glycerol-driven partial denitrification-anammox for low concentration nitrogen polishing in MBBRs, WaterJam 2022, Virginia Beach, VA, September 12-15.
12. **Wang J.**, Sun Y., Khunjar W., Pace G., Pathak A., McGrath M., Ali M., Sun Y., Wang Z.W. (2022), Glycerol-driven partial denitrification-anammox for low concentration nitrogen polishing in tertiary MBBRs under real-time feedforward control, WEF Innovations in Process Engineering 2022, Miami, FL, June 20-23.
13. **Wang J.**, Sun Y., Khunjar W., Pace G., Pathak A., McGrath M., Ali M., Sun Y., Wang Z.W. (2022), Polishing tertiary effluent nitrogen via the synergy between methanol-driven partial denitrification and anaerobic ammonia oxidation in moving bed biofilm reactors, WEF Innovations in Process Engineering 2022, Miami, FL, June 20-23.
14. **Wang J.**, Sun Y., Khunjar W., Pace G., Pathak A., McGrath M., Ali M., Wang Z.W. (2021), Low concentration nitrogen polishing via the synergy between partial denitrification and anaerobic

ammonia oxidation in moving bed biofilm reactors under real-time feed forward control at Noman M. Cole Jr., Pollution Control Plant, IWA Biofilm Reactors Conference 2021, Virtual, Dec. 6 - 8.

15. **Wang J.,** Broderick T., Strawn M., Wang Z.W. (2020) High-solid anaerobic digestion of biosolids pretreated with thermal hydrolysis, ASABE 2020, Chicago, IL, July 12-15 (Accepted but not presented due to COVID-19).

Conference Posters

1. **Wang J.**, An Z., Angelotti B., Brooks M., Wang Z.W., (2023) Effects of NRCY on the startup of physical and biological selection pressure-driven aerobic granulation for biological nitrogen removal in plug-flow bioreactors fed with real domestic wastewater, WaterJAM 2023, Virginia Beach, VA, September 11-14.
2. **Wang J.**, Sun Y., Khunjar W., Winkler M. K., Li B., Goel R., Wang Z.W. (2022), An integration of EBPR, endogenous denitrification, and partial nitrification/denitrification/anammox (PANDA) for cost-effective nutrient removal, WaterJam 2022, Virginia Beach, VA, September 12-15.
3. **Wang J.**, Sun Y., Khunjar W., Pace G., Pathak A., McGrath M., Ali M., Wang Z.W. (2022), Shortcut nitrogen removal from low-strength tertiary wastewater via partial denitrification and anammox in moving bed biofilm reactors, IWA AD17 2022, Ann Arbor, MI, June 17-22.
4. **Wang J.**, Sun Y., Khunjar W., Pace G., Pathak A., McGrath M., Ali M., Wang Z.W. (2022), Low concentration nitrogen polishing via methanol- and glycerol-driven partial denitrification and anaerobic ammonia oxidation in moving bed biofilm reactors under real-time feed forward control in real tertiary wastewater, AEESP 2022, St. Louis, MO, June 28-30.
5. **Wang J.**, Sun Y., Khunjar W., Pace G., Pathak A., McGrath M., Ali M., Wang Z.W. (2021), Low concentration nitrogen polishing via the synergy between partial denitrification and anaerobic ammonia oxidation in moving bed biofilm reactors under real-time feed forward control at Noman M. Cole Jr., Pollution Control Plant, WaterJAM 2021, Virginia Beach, VA, September 13-16.
6. **Wang J.**, Sun Y., Khunjar W., Pace G., Pathak A., McGrath M., Ali M., Wang Z.W. (2021), Nitrogen removal from secondary clarifier effluent of a domestic wastewater treatment plant via partial denitrification - anaerobic ammonia oxidation in moving bed biofilm reactor under real-time feed forward control, CSAWWA's annual virtual poster competition 2021, June 26.

Technical reports:

1. **Wang J.**, Sun Y., Khunjar W., Winkler M. K., Li B., Goel R., Wang Z.W. (2022), An integration of EBPR, endogenous denitrification, and partial nitrification/denitrification/anammox (PANDA) for cost-effective nutrient removal. Submitted to The Water Research Foundation, December 20.
2. Pace G., Sun Y., **Wang J.**, Khunjar W., Carroll J., and Wang Z.W. (2022), NCPCP primary and secondary infrastructure reinvestment and optimization – MBBR PANDA/PdNA benchtop-scale pilot. Submitted to Noman Cole Jr. Pollution Control Plant, Fairfax County, January 19.

Table of contents

List of Figures

List of Tables

Chapter 1 Introduction

1.1 Background

Municipal wastewater treatment using conventional activated sludge processes faces challenges of intensive energy and carbon consumption, which contributes to greenhouse gas (GHG) emissions and create obstacles in the pursuit of carbon neutrality. Previous studies indicated that wastewater treatment accounts for 3-4% of the energy consumed in the U.S. (Gao et al., 2014; Molinos-Senante and Maziotis, 2022) and contributes to approximately 1.6% global GHG emissions (Lu et al., 2018). Addressing the urgent issue of global warming requires the development of innovative, carbon-efficient wastewater treatment methodologies such as resource recovery technologies, process intensification strategies, and anammox featured next generation biological nutrient removal (BNR) technologies.

There are many valuable resources contained in the municipal wastewater such as water, carbon, energy, nutrients, etc., which can be recovered and reused to help achieve carbon neutrality in water resource reclamation facilities (WRRFs) and sustainable development of modern society. These resources won't become available until innovative technologies are developed to harness them. The advanced bioprocessing technologies such as aerobic granulation and thermal hydrolysis pretreatment (THP) hold promise to allow WRRFs to do with much more with less capital, footprint, energy, and concrete consumption (Kent et al., 2018). A leverage of endogenous denitrification may also help eliminate the energy-consuming mixed liquor recycle (MLR) from the conventional BNR using modified Ludzack–Ettinger (MLE) configurations. Moreover, enriching anammox bacteria in mainstream wastewater treatment through partial denitrification anammox (PdNA) also stands out as a promising strategy to minimize the BNR carbon and energy consumption.

These being said, in the mainstream wastewater treatment, the impact of MLR on aerobic granulation in real municipal wastewater has not been investigated. There is also a lack of understanding on the feasibility of MLR elimination through endogenous denitrification, especially in a pilot setup integrating partial nitrification, PdNA, and enhanced biological phosphorus removal (EBPR) into a consolidated bioprocess to meet the stringent effluent requirements. In addition, there has been a controversy over the

mechanism between methanol and glycerol in driving the performance of PdNA (Campolong, 2019; Ladipo-Obasa et al., 2022; Macmanus et al., 2022), especially in the low strength wastewater polishing process such as tertiary moving bed biofilm reactors (MBBRs).

In the sidestream wastewater treatment, although THP has been implemented to expedite the solid hydrolysis rate for intensifying anaerobic digestion (AD) reactors through the solids retention time (SRT) reduction (Appels et al., 2008), factors constraining the overall rate of sludge AD is still unclear. Therefore, key operational parameters such as solids loading, AD temperature, and AD SRTs should be investigated to understand their synergistic effects on the rates of solids destruction and methane production for unlocking the real rate-limiting step of sludge AD.

Therefore, this dissertation seeks to address these knowledge gaps and advance our understanding of carbon-efficient wastewater treatment processes, which will also lay the groundwork for their practical implementation and contribute to the global effort towards sustainability.

1.2 Outline

This dissertation has 7 chapters in total. These chapters provided an array of innovative carbon-efficient wastewater treatment methodologies to alleviate the imminent pressure of population growth and global warming. Specifically, **Chapter 2** presented a state-of-the-art review of a wide spectrum of valuable resources that can be recovered or reused in WRRFs. The importance of developing applicable technologies to take advantage of these resources for achieving carbon neutral wastewater treatment and sustainable society development was also comprehensively discussed. Subsequently, process intensification through continuous-flow aerobic granulation as an economical option to expand the treatment capacity of WRRFs with a small footprint was explored in plug flow reactors with MLR configurations for BNR in **Chapter 3**. The results demonstrated that MLR configuration could hinder the sludge granulation, but the hindrance could be alleviated to some extent by its location change. Given the energy consumption of the MLR, the possibility to eliminate it through endogenous denitrification was explored in **Chapter 4**. Pilot study results showed that a synergistic integration of partial nitrification, PdNA, EBPR, and endogenous denitrification in one system was able to eliminate MLR and reduce the

footprint, carbon, and energy consumption in the mainstream treatment. This pilot reactor, treating real municipal wastewater under highly fluctuating influent quality and temperature conditions, showcased the robustness of this integrated system in meeting the stringent effluent quality requirements and achieving substantial energy and carbon savings through automatic control strategies. To gain a deeper understanding of PdNA mechanisms with different carbon sources and operating parameters, **Chapters 5 and 6** looked into two parallel pilot-scale MBBR treatment trains fed with methanol and glycerol, respectively, and operated in a local WRRF. Their efficacies in achieving stringent nutrient removal targets and carbon savings were compared. The mechanistic difference of the two types of carbon source in driving PdNA were also elucidated. This first-hand information collected onsite with real wastewater provided an engineering basis for the full-scale application of the PdNA technology in the same WRRF. Alongside these mainstream treatment innovations, **Chapters 7** also gave insights into a sidestream treatment innovation that allowed process intensification and resource recovery, namely THP-enhanced AD. This study compared the efficiencies of thermophilic and mesophilic AD systems when integrated with THP. Results showed that thermophilic AD was superior to mesophilic AD in terms of solids reduction, albeit with a trade-off in methane production efficiency when integrated with THP. To sum up, this dissertation not only advanced our understanding of carbon-efficient wastewater treatment processes but also laid groundwork for their practical implementation, contributing to the global pursuit of sustainability.

1.3 Attribution

All the coauthors are credited with his or her contribution to this work, both in their sharing of ideas and technical expertise.

Zhi-Wu (Drew) Wang, Ph.D., Assistant Professor
Department of Biological System Engineering, Virginia Polytechnic Institute and State University, Blacksburg, VA 24061

Coauthor of Chapters 2, 3, 4, 5, 6, 7

Yewei Sun, Ph.D., Principal scientist
Hazen and Sawyer, Fairfax, VA 20030

Coauthor of Chapters 4, 5, 6

Wendell Khunjar, Ph.D., Associate Vice President
Hazen and Sawyer, Fairfax, VA 20030

Coauthor of Chapters 4, 5, 6

Gregory Pace, Associate
Hazen and Sawyer, Fairfax, VA 20030

Coauthor of Chapters 5, 6

Michael McGrath, Director
Noman M. Cole Jr., Pollution Control Plant, Lorton, VA 22079

Coauthor of Chapters 5, 6

Sajana Chitrakar, Project manager
Noman M. Cole Jr., Pollution Control Plant, Lorton, VA 22079

Coauthor of Chapters 5, 6

Mari. K. Winkler, PhD, Professor
Department of Civil and Environmental Engineering, University of Washington, Seattle, WA 98195

Coauthor of Chapter 4

Bo Li, PhD, Postdoctoral researcher
Department of Civil and Environmental Engineering, University of Washington, Seattle, WA 98195

Coauthor of Chapter 4

Ramesh Goel, PhD, Professor
Department of Civil and Environmental Engineering, University of Utah, Salt Lake City, UT, 84112

Coauthor of Chapter 4

Yuepeng Sun, PhD, Postdoctoral researcher
Department of Civil and Environmental Engineering, George Washington University, Washington DC, 20052

Coauthor of Chapters 2, 7

Kang Xia, PhD, Professor
School of Plant and Environmental Sciences, Virginia Polytechnic Institute and State University, Blacksburg, VA 24061

Coauthor of Chapter 2

Allison Deines, Senior Policy Analyst
Alexandria Renew Enterprises, Alexandria, VA 22314

Coauthor of Chapters 2, 7

Ross Cooper, Water Policy Analyst.
Alexandria Renew Enterprises, Alexandria, VA 22314

Coauthor of Chapters 2, 7

Karen Pallansch. CEO
Alexandria Renew Enterprises, Alexandria, VA 22314

Coauthor of Chapters 2, 7

Dian Zhang, Engineer
Stantec, Washington DC, 20005

Coauthor of Chapter 7

Tom Broderick, Chief Engineer
Arlington County Water Pollution Control Bureau, Arlington, VA 22201

Coauthor of Chapters 2, 7

Mary Strawn, Chief Engineer
Arlington County Water Pollution Control Bureau, Arlington, VA 22201

Coauthor of Chapter 7

Hari Santha, Process/Operations Lead
Alexandria Renew Enterprises, Alexandria, VA 22314

Coauthor of Chapters 2, 7

Zhaohui An, PhD
Department of Biological System Engineering, Virginia Polytechnic Institute and State University, Blacksburg, VA 24061

Coauthor of Chapter 3

Xueyao Zhang, PhD student
Department of Biological System Engineering, Virginia Polytechnic Institute and State University, Blacksburg, VA 24061

Coauthor of Chapters 3, 4

Bob Angelotti, Executive Director
Upper Occoquan Service Authority, 14631 Compton Rd, Centreville, VA 20121

Coauthor of Chapter 3

Matt Brooks, Process Control Engineer
Upper Occoquan Service Authority, 14631 Compton Rd, Centreville, VA 20121

Coauthor of Chapter 3

1.4 References

Appels, L., Baeyens, J., Degrève, J., & Dewil, R. (2008). Principles and potential of the anaerobic digestion of waste activated sludge. Progress in Energy and Combustion Science, 34, 755–781.

Campolong, C.J. (2019) Bioaugmentation and retention of anammox granules to a mainstream deammonification bio-oxidation pilot with a post polishing anoxic partial denitrification/anammox moving bed biofilm reactor, (Master thesis) Virginia Tech.

Gao, H., Scherson, Y.D. and Wells, G.F. 2014. Towards energy neutral wastewater treatment: methodology and state of the art. Environmental science: Processes & impacts 16(6), 1223-1246.

Kent, T.R., Bott, C.B. and Wang, Z.-W. 2018. State of the art of aerobic granulation in continuous flow bioreactors. Biotechnology advances 36(4), 1139-1166.

Ladipo-Obasa, M., Forney, N., Riffat, R., Bott, C., DeBarbadillo, C. and De Clippeleir, H. 2022. Partial denitrification–anammox (PdNA) application in mainstream IFAS configuration using raw fermentate as carbon source. Water Environment Research 94(4), e10711.

Lu, L., Guest, J.S., Peters, C.A., Zhu, X., Rau, G.H. and Ren, Z.J. 2018. Wastewater treatment for carbon capture and utilization. Nature Sustainability 1(12), 750-758.

Macmanus, J., Long, C., Klaus, S., Parsons, M., Chandran, K., De Clippeleir, H. and Bott, C. 2022. Nitrogen removal capacity and carbon demand requirements of partial denitrification/anammox MBBR and IFAS processes. Water Environment Research 94(8), e10766.

Molinos-Senante, M. and Maziotis, A. 2022. Evaluation of energy efficiency of wastewater treatment plants: The influence of the technology and aging factors. Applied Energy 310, 118535.

Chapter 2 Pivotal role of municipal wastewater resource recovery facilities in urban agriculture: A review

(This chapter has been published as "Wang J., Sun Y., Xia K., Deines A., Cooper R., Pallansch K., Wang Z.W. (2022), Pivotal Role of Municipal Wastewater Resource Recovery Facilities in Urban Agriculture: A Review, Water Environment Research, 94(6), e10743, DOI: https://doi.org/10.1002/wer.10743".)

2.1 Abstract

Urban agriculture provides a promising, comprehensive solution to water, energy, and food scarcity challenges resulting from the population growth, urbanization, and the accelerating effects of anthropogenic climate change. Their close access to consumers, profitable business models, and important roles in educational, social, and physical entertainment benefit both developing and developed nations. In this sense, Urban water resource reclamation facilities (WRRFs) can play a pivotal role in the sustainable implementation of urban agriculture. Reclaimed water as a recovered resource has less supply variability, and in certain cases can be of higher quality than other water sources used in agriculture. Another recovered resource, namely biosolids, as byproduct from wastewater treatment can be put to beneficial use as fertilizers, soil amendments, and construction material additives. The renewable electricity, heat, CO2, and bioplastics produced from WRRFs can also serve as essential resources in support of urban agriculture operation with enhanced sustainability. In short, this review exhibits a holistic picture of the state-of-the-art of urban agriculture in which WRRFs can potentially play a pivotal role.

2.2 Keywords

Urban agriculture; wastewater; resource recovery; food; energy; sustainability

2.3 Introduction

With the rapid population growth and urbanization, it would be difficult for rural agriculture industry to meet the food supply need of urban societies by 2050 due to the limited arable land, water scarcity, as well as energy-intensive farming and transportation (Heinemann et al., 2011; Tilman et al., 2001). Urban agriculture (UA) offers close access to consumers, profitable business models, and educational, social, and physical benefits to urban communities, making UA a comprehensive solution to water, energy, and food problems facing modern urban societies (Astee and Kishnani, 2010; Hou et al., 2009; Lohrberg et al., 2016; Lovell, 2010). In order to make the UA concept viable, Water Resource Reclamation Facilities (WRRFs) serving urban municipal wastewater treatment needs could play a pivot role in that they simultaneously recover water, nutrients, and energy, the three essential resources required for UA (Tian et al., 2018). To shed light on this importance, this study reviewed publications collected in Web of Science and Google Scholar between 1983~2021 with regards to the essential roles that WRRFs could play in the context of UA. It is anticipated that the knowledge presented in this study can enlighten researchers and practitioners in the fields of UA and WRRFs to work together for enabling a circular economy along the effort to mitigate the accelerating effects of anthropogenic climate changes.

2.4 Urban agriculture and its benefits

2.4.1 Definition of urban agriculture

As illustrated in Figure 2.1, Mougeot (1996) defined UA as an economic activity correlated to the production of food or non-food products in urban or peri-urban areas. The definition of UA were expanded in the following years, e.g., the processing and distribution of food, livestock breeding, aquaculture and horticulture were added in 1999 (Bailkey and Nasr 1999); urban waste and resources reuse, human and public services, and intensive production methods were added in 2000 Mougeot (2000); wide-ranging activities, economic and business vitality, and individual and community well-being were added in 2002 (Butler and Maronek 2002). The definition of UA currently encompassed the technological innovations

of novel food-production and material reuse methods that maximize output in urban areas (Abelleira-Pereira et al. 2015, Hodgson et al. 2011).

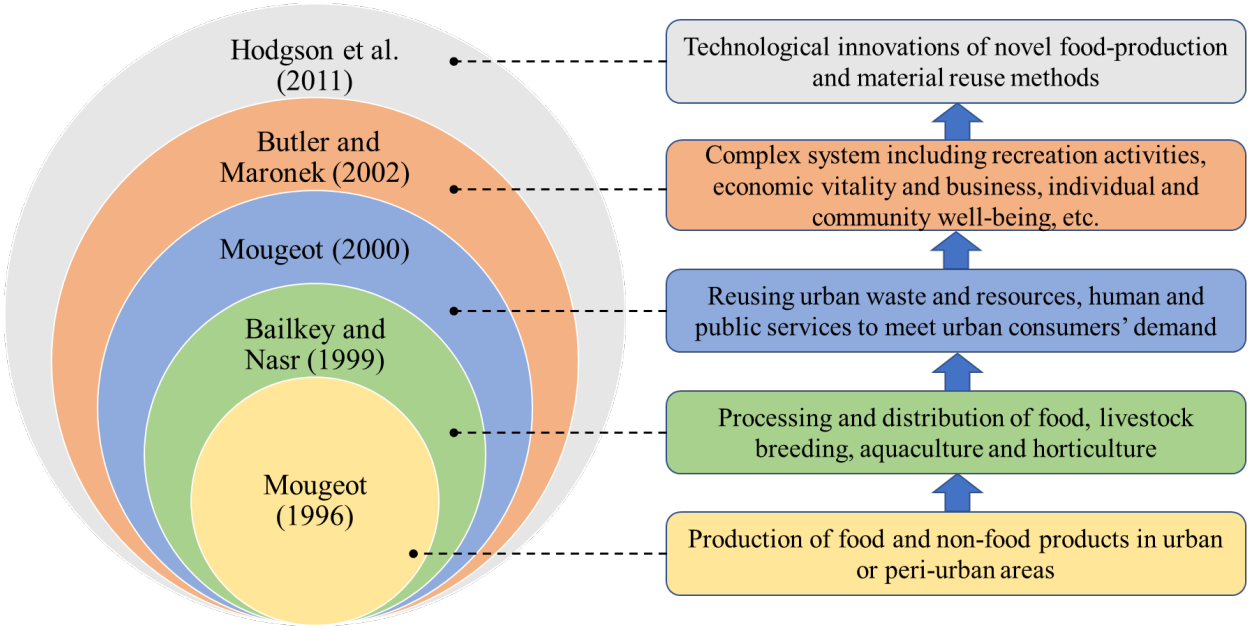

Figure 2.1 Development of UA definition

2.4.2 Benefits of UA

More than three-quarters (76%) of world's population reside in urban areas by 2015 (Congress 2020). Urbanization and population growth have brought new issues related to land shortages, environmental pollution, and urban food security. Thus, more arable land for food supplies is demanded. For example, 40% of the arable land in the UK would have to be dedicated to meeting the food demand of London which houses 12% of the UK population (Miccoli et al. 2016). Moreover, with the growth of urban resident income, the food demand could add further pressure to the global food supply systems. It is projected that the world's agricultural production will increase by between 70 and 100 percent of the current amount by 2050 Heinemann et al. (2011). Global arable land availability is scarce and is only projected to increase by 12% compared to today (Heinemann et al. 2011, Tilman et al. 2001).

Although there is a possibility to meet the food supply demand by increasing the unit productivity of arable land through using fertilizers and pesticides, cultivating newly selected crops, and employing

energy-intensive or water demanding practices (Tilman et al. 2001), rural centric farming approaches alone are environmentally unsustainable due to fossil fuel consumption, greenhouse gas emissions, exploitation of soil and water resources, and aquatic contamination from agricultural runoff (Vandermeer et al. 2009). In addition, the present retail sale and food distribution systems heavily rely on road and air transportation which have high embedded environmental costs due to elevated fuel consumption and air pollution associated with these transport mediums (Paxton 1994).

To ensure urban food security, one option is to split large-scale, centralized rural farming to a multiplicity of small-scale farming systems that interconnects producers, processors, distributors, and consumers in close distance (Brown et al. 2003). UA can offer such an option to address these urbanization challenges through i) transportation distance reduction, ii) profitable business model creation, iii) individual and social wellbeing improvement, iv) climate and ecological effects mitigation, and v) urban waste and spaces utilization.

2.4.2.1 Reduce transportation distance

Food products typically travel between 1,500 and 2,500 miles from rural farms to urban points of sale, which is 25% farther than food products traveled back in 1980 (Halweil 2002). Fruits and vegetables often spend 7 to 14 days in transit before arriving in the supermarket (Brown et al. 2003), which led to 3 to 37% higher grocery price in urban supermarkets (Hunger 1990). UA can reduce transportation distance and energy footprint, as well as shorten supply chains. It also has the potential to minimize product packaging, storage and distribution time/cost, reduce price differentials between producers and consumers, and improve food accessibility to local markets (Aubry et al. 2008). Localizing food production in urban areas can also solve food waste problems due to food spoilage over long distance transporting (Stuart 2009).

2.4.2.2 Profitable business model creation

Investment in UA tends to have a good return rate per dollar input, e.g., every $1 invested in a community garden plot yields approximately $6 worth of vegetables (Bellows et al. 2003). Urban farmers can earn up to $90,000 and $136,000 per acre in Ohio and Philadelphia, respectively, by selecting the proper crops

and growing techniques (Mogk et al. 2010). Other successful examples of UA include Detroit, where the UA grossed $200 million in sales with approximately 5,000 jobs created (Mogk et al. 2010). UA with proper implementation can support economic vitality by providing neighborhood residents with job opportunities and clean public spaces rooted in community involvement (Lovell 2010).

2.4.2.3 Improve individual and social wellbeing

The visibility of trees, grass, and flower gardens as a result of UA can provide easy access to nature and improve general life satisfaction of people in urban areas, reduce irritability and mental fatigue, restore calmness and the ability to concentrate (Kaplan and Kaplan 1990). In addition, UA can create green spaces for social gathering, build a sense of community, and reduce stress, anger and even blood pressure (Ulrich 1992). Blair and Nichaman (2002) found that gardening three to four times a week approximately equals moderate walking or bicycling in terms of health benefits. Honeyman (1992) found that urban built environment with vegetation produced more mental rehabilitation than those without vegetation, and that vegetated urban scenes had more positive psychological impacts than nature only scenes by comparing human response to remote nature scenes and urban built environment scenes. UA have additional functions such as youth education, tourism, and community development through school programs, work programs, and other agriculture-related activities, which can improve the life qualities of current residents and make the city more attractive to new residents (Mogk et al. 2010).

2.4.2.4 Mitigate climate and ecological effects

As a result of urbanization, the area of impervious surfaces such as roads, driveways, sidewalks, parking lots, and rooftops through which water cannot infiltrate have expanded rapidly (Lu and Weng 2006). In the US, the total impervious surface area of the 48 states and Washington DC was estimated to be 112,610 ± 12,725 km^2 (Elvidge et al. 2004). This transformation of urban green land to impervious surface area reduced the amount of carbon fixed through photosynthesis by 1.6% of the pre-urban values and caused urban heat islands effect (Lamptey et al. 2005). Practicing UA can effectively alleviate this phenomenon in various ways. For example, by providing vegetation and facilitating carbon sequestration, UA can potentially increase evapotranspiration and produce cooling, moderate urban climate, and reduce urban

heat island effect (Zasada 2011). In addition, concomitant water usage such as irrigation could reduce air temperature, increase relative humidity, and promote the extent of living comfort by increasing evaporation (Lamptey et al. 2005). Moreover, urban green spaces can play a role in species preservation for birds and butterflies by providing food, resting spaces, and protection along migratory flight paths, and increase a city's biodiversity with plant variety and beneficial soil microorganisms, insects and animals (Brown and Jameton 2000). Plants in UA can not only absorb soil contaminants through their root systems to reduce soil erosion and ground water contamination, but also reduce air pollution by absorbing pollutants through their foliage (Brown and Jameton 2000).

2.4.2.5 Utilize urban waste and spaces

WRRFs can recycle and reuse urban waste to support UA. One of the most efficient ways is through recycling purified wastewater for irrigation. Cheema et al. (1996) reported that California saves 759,000 m^3/day fresh water by recycling and reusing treated effluent from its 200 WRRFs. UA can decrease the burden of WRRFs using combined system by catching and reusing stormwater run-off. Biosolids from WRRFs and composting urban organics such as food waste, leaves, and lawn clippings, also can be applied as fertilizers in UA (Brown et al. 2003).

UA also can function as a substitute for abandoned or vacant lots and yield multiple profits in a short time. The US Accounting Office identified 130,000 to 425,000 contaminated vacant industrial sites or brownfields that could be safely converted to agricultural purposes if properly redeveloped (Bailkey and Nasr 1999). UA regenerate and revitalize a city by transforming these vacant lots from eyesores into bountiful and beautiful gardens which can feed peoples' souls and bodies (Brown et al. 2003). This has been well illustrated by a food project in urban and suburban Boston that staff and volunteers annually raise more than 120,000 pounds of fresh vegetables and 12,000 pounds of other food on vacant lots located less than two miles from downtown Boston (Washington 2000). Thirteen times more food yield per acre than rural farms were produced from urban gardens by utilizing raised beds, soil amendments, and season extenders such as row covers and hoop houses (Washington 2000).

2.4.3 UA in developed countries

Although the status of UA in developing countries has been reviewed in several previous studies (De Bon et al. 2010, Hamilton et al. 2014, Orsini et al. 2013), to our best knowledge, its applicability in developed countries has not been reviewed except for some individual project reports in Singapore, North America, and Europe (Astee and Kishnani 2010, Hou et al. 2009, Lohrberg et al. 2016a, Lovell 2010). To fill this knowledge gap, this section focuses on the various UA types adopted in developed countries. Different taxonomies have been derived to classify the existing forms of UA in developed countries. Features such as temporary or permanent, horizontal, or vertical, monocultures or polycultures, the farm area and annually product selling area, locations and the nature of lands, operating characteristics, capital inputs, and how they interact with urban systems can be used to categorize UA. This review used a taxonomy mainly based on forms, scales, locations, and functions of the UA primarily used in developed countries (Table 2.1).

2.4.3.1 Commercial urban farm

Commercial urban farms sell their products directly through farmers' markets (Table 2.1). In the US, it was reported that the largest direct sales of commercial urban farm products occur in California, New York, Pennsylvania, Michigan, and Ohio (Timmons and Wang 2010). Smaller markets with several vendors are also around in many US urban cities. Some urban farmers even go from door to door with their produce (Brown et al. 2003). These urban farms provide convenience for inner-city residents to access food, while also increasing their own income.

There are 11,760 ha of commercial urban farmland in Greater London (Defra 2011). In terms of production, commercial urban farms account for the overwhelming majority of food grown in London. Garnett and Gillie (1999) reported that the Lower Lea Valley straddling the northeastern boundary of Greater London is the heart of commercial horticulture in London, which has hosted market gardens since the eighteenth century. With the glasshouses and other technologies, Lower Lea Valley is well known for the production of not only ornamental flowers but also vegetables such as cucumbers, tomatoes and peppers, etc.

2.4.3.2 Community garden

Community gardens are places where plants or food are grown in communal settings (Agustina and Beilin 2012). In most cases, community gardens (Table 2.1) are large land divided into smaller plots for each household's use and can be owned by a municipality, an institution, a community group, a land trust, or private ownership (Brown et al. 2003). The Urban Gardening Program, established by US Congress in 1977, provided annual grants of US $150,000 – 250,000 through the Cooperative Extension Service for such gardens (Brown and Jameton 2000, Hynes and Howe 2002). The USDA started a new initiative, called 'The People's Garden', to promote community gardening in 2009 (Mok et al. 2014). Currently, the American Community Gardening Association estimates that there are over 18000 community gardens in the US and Canada, including neighborhood, public housing and school gardens (Kortright and Wakefield 2011). Non-profit organizations and government agencies, such as the 'Homeless Garden Project' in Santa Cruz, California, 'Just Food' in New York City, and 'Food-Share' in Toronto, Canada, work with community gardens to encourage food production and to distribute food to those in need (Johnston and Baker 2005, Saldivar-Tanaka and Krasny 2004).

2.4.3.3 Backyard garden

Urban backyard gardens are plots around homes, including balconies, decks, and courtyards (Table 2.1). Produce can be grown or raised even in the simplest of containers (Brown et al. 2003). Backyard food gardeners are motivated by different factors such as cooking with fresh ingredients, teaching children about nature, environmental sustainability, connecting to cultural or past identity, aesthetics, personal hobby, and neighborhood exchange (Kortright and Wakefield 2011). In much of North America, the harvest from the backyard garden has eased the food budgets of low-income families and their network of family and friends.

2.4.3.4 Allotment garden

An allotment garden is an area subdivided into small plots, which are rented under a tenancy agreement (Table 2.1). They usually stem from municipal initiatives on public land and their regulation is highly formalized, sometimes following specific regional or national laws. They can also be managed by an organized group, or even established as an allotment garden association. Allotment gardens emerged in the eighteenth century to cope with urban poverty, and the First World War prompted their expansion (Lohrberg et al. 2016b). Nowadays, their functions have shifted from self-provision to food supplement, education, social and physical entertainment.

2.4.3.5 Green roof

Green roofs, i.e., roofs with a vegetated surface and substrate, provide ecosystem services in urban areas, including improved storm-water management, better regulation of building temperatures, and increased food production (Table 2.1). Rooftop food production is a more recent addition to the mix of urban food production systems in North America. There are both commercial-scale and community-focused projects in existence, as well as household-scale rooftop gardens (Engelhard 2010). In May 2009, Toronto passed a bylaw requiring green roofs to be installed on new commercial, institutional, and residential developments, and while not specifically addressing the issue of rooftop agriculture, it listed "opportunities for local food production" as one of the many environmental benefits (Kaill-Vinish 2009). There are various plans for large-scale rooftop food production, such as the Brooklyn Grange project in New York which entails a 100,000-ft^2 hydroponic greenhouse and grows over 80,000 lbs. of organically-cultivated produce per year, making it the largest rooftop farm in the world (Plakias 2016). In extensive green roofs, plant species are typically restricted to those that are drought-tolerant and shallow-rooted, minimizing both irrigation and depth of planting media to limit weight (Mok et al. 2014).

2.4.3.6 Vertical farming

Vertical farming (Table 2.1) sometimes called sky farming is based on the concept that the most efficient growing conditions can be built around the crop rather than trying to adapt to the natural environment (Mok et al. 2014). In vertical farming, growing plants are vertically stacked in layers that may reach several stories tall, in controlled indoor environments, with precise light, nutrients, and temperatures. Some common choices of structures to house vertical farming systems include abandoned warehouses in cities, new buildings built on environmentally damaged lands, and even in used shipping containers from ocean transport (Birkby 2016). Vertical farms come in different shapes and sizes, but all vertical farms use one of three soil-free systems for providing nutrients to plants, namely hydroponic, aeroponic, or aquaponic systems (Birkby 2016). Hydroponic system involves growing plants in nutrient solutions that are free of soil. In aeroponic systems, plants grow in an air/mist environment with no soil and using up to 90% less water (Birkby 2016). An aquaponic system takes the hydroponic system one step further by combining plants and fish in the same ecosystem.

2.4.3.7 Rooftop greenhouse

Rooftop greenhouses (Table 2.1) as a new form of UA consists of a greenhouse built on the roof of a building that typically generates produce via soilless culture systems (Cerón-Palma et al. 2012). These structures are considered a component of the “building-based UA” movement, which also covers vertical farming or sky farming (Despommier 2011). Gotham Greens and Lufa Farms are local producers based in New York and Montreal that have built Rooftop greenhouses ranging in size from 830 to 2900 m2 (Sanyé-Mengual et al. 2015). Cerón-Palma et al. (2012) performed a preliminary assessment of Rooftop greenhouses. Energy modelling results illustrated the environmental benefits of energy flow exchange between rooftop greenhouses and office buildings. The results showed that the introduction of residual heat from the greenhouse into the building on an ideal winter day could substitute 87 kWh of the heating demand.

2.4.3.8 Educational and therapeutic garden

Educational gardens are gardens located in educational institutions that provide garden-based learning to their community (schools, kindergartens, etc.) or gardens developed by environmental or social centers that offer educational services to visitors. School gardens are the most common form spreading environmentally and climate-friendly gardening ideas and practices (Lohrberg et al. 2016b). Therapeutic gardens are typically located inside the city, at physical and mental health care institutions, applying basic healing effects through gardening and agriculture (Table 2.1). With a variety of plants and flowers carefully chosen, these gardens can stimulate the sight, smell, and touch, awakening the senses, memories and emotions. They can be used for the treatment of mental disorders, autism, alzheimer's disease or cerebral paralysis, addiction to drugs and alcohol, etc.

Table 2.1 Comparison of different UA types

Categories	Features	Benefits	Examples	References
Commercial urban farm	Directly from farm to markets	Economic benefits for farmers; food provision and other additional values	Smaller markets; Door-to-door peddling with trucks	(Brown et al. 2003); (Timmons and Wang 2010)
Community garden	Communal plots for each household or community use	Food budget saving; promotion of healthy diet; Social and communal benefits	The People's Garden' (USDA); Homeless Garden Project' (Santa Cruz,CA); 'Just Food' (New York City) Community-supported agriculture	(Agustina and Beilin 2012); (Mok et al. 2014); (Johnston and Baker 2005, Saldivar-Tanaka and Krasny 2004)
Backyard garden	Plots around homes, the smallest scale	Food and nutrient supplement, aesthetic, life quality improvement	Balconies, decks, and courtyards	(Brown et al. 2003); (Kortright and Wakefield 2011)
Allotment garden	An area subdivided into small plots, which are rented under a tenancy	Reducing poverty, improving self-provision	Statutory, temporary, and private allotments	(Lohrberg et al. 2016b)
Green roof	Roofs with a vegetated	Increasing food	Intensive and extensive	(Engelhard 2010); (Mok

	surface and substrate	production; storm-water management and building temperature regulation	green roofs	et al. 2014)
Vertical farming	Growing plants are vertically stacked in layers	Hight output, water and space saving	Hydroponic, aeroponic, or aquaponic; building-based vertical farms and shipping-container vertical farms	(Mok et al. 2014); (Birkby 2016)
Rooftop greenhouse	A greenhouse built on the building roof	Increased crop yields; Space and energy saving	Gotham Greens, The Vinegar Factory, and Lufa Farms in New York	(Sanyé-Mengual et al. 2015); Cerón-Palma et al. (2012); (Despommier 2011)
Educational and therapeutic garden	Gardens with educational and healing effects	Raising public awareness; Treatment to mental and physical disorder	School gardens; physical and mental health care institution gardens	(Lohrberg et al. 2016b)

2.5 Pivotal roles of WRRFs in UA

WRRFs in the US alone process an estimated 32 billion gallons of wastewater per day (Pabi et al. 2013). WRRFs discussed herein are centralized in urban areas receiving municipal wastewater with typical inflow compositions reported for developed countries (Davis 2010). Given their centralized nature in the city, drought proof water supply, and the significant infrastructure already in place, WRRFs can play a pivotal role in promoting the concept of UA. Water, nutrient, and energy are three essential resources required for supporting agricultural activities (Tian et al. 2018). WRRFs can recover these three essential resources from domestic wastewater in support of UA (Coats and Wilson 2017, Guest et al. 2009, Takashi et al. 2007). Indeed, resource recovery from wastewater has been aggressively advocated (Cluster 2015) and is the reason why traditional wastewater treatment plants have been rebranded as WRRFs to recognize and reinforce the significant resource recovery potential that exists in wastewater streams (Coats and Wilson 2017). Nowadays, industry professionals have broadly agreed that WRRFs should evolve into resource recovery factories that valorize valuable commodities out of wastewater (Coats and Wilson 2017). To this end, an array of technologies has been developed as illustrated in Figure 2.2 to produce UA relevant commodities such as irrigation water, fertilizers, heat, electricity, carbon source, as well as construction and packaging materials.

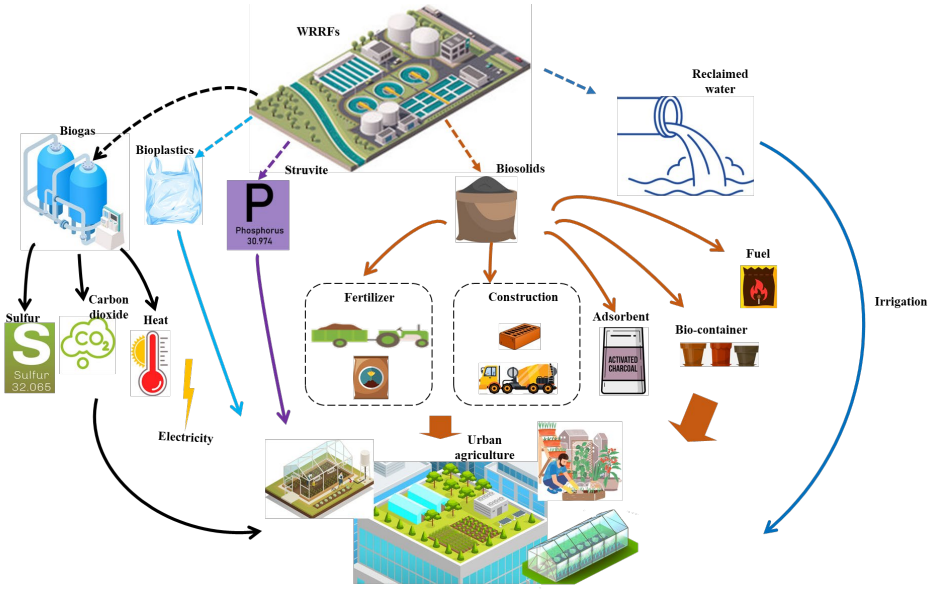

Figure 2.2 Schematic illustration of the pivotal roles of WRRFs in support of UA

2.5.1 Reclaimed water for UA

2.5.1.1 UA irrigation with reclaimed water

Reclaimed water is becoming increasingly attractive as an alternative source to surface and ground water for UA irrigation, because of its high quality, stable supply, and potential energy savings.

High quality irrigation water. The reclaimed water from advanced WWRFs is often with higher quality than the surface water to which it is discharged (Bureau of Reclamation 2010, EPA 2012, Ruetten et al. 2004). For example, Upper Occoquan Service Authority located in Centreville, Virginia, has been practicing indirect potable reuse by generating reclaimed water with quality higher than that in the Occoquan reservoir where it discharges (EPA 2012). The primary chemical constituents to consider for UA irrigation include salinity, sodium, trace elements, chlorine residual, and nutrients, and excess contents of those can cause negative effects on crop growth and human health (EPA 2012). A range of treatment options are available in WRRFs to deliver almost any level of water quality depending upon the expected use of the reclaimed water (EPA 2012).

Stable supply. The generation of wastewater is actually not significantly lower during droughts (EPA 2012). This means that reclaimed water is virtually a drought proof supply. Properly planned, this drought proof supply can be used to increase the reliability of the overall supply (Ruetten et al. 2004). In addition, municipal wastewater generation is relatively constant throughout the year and typically increase with population growth in urban area (EPA 2012). Moreover, reuse of municipal water produced and reclaimed all in the same place within a limited geographical range actually requires less resources for pumping and transport to UA sites.

Energy saving. Water reuse for UA can reduce energy consumption by eliminating additional potable water treatment and associated water conveyance because reclaimed water typically offsets potable water use and is used locally. For example, about 20% of California's electricity is consumed by water-related energy use, including potable water conveyance, storage, treatment, and distribution and wastewater collection, treatment, and discharge (Klein et al. 2005). The

amount of energy required for treatment and transport of potable water is generally much greater than the energy required to treat wastewater for reclamation in southern California. The estimated net energy savings from switching potable water treatment and transport to wastewater reclamation and reuse could range from 0.7 to 1 TWh/yr. At a power cost of $0.075/kWh, the savings would be on the order of $50 to $87 million per year (Schroeder et al. 2012).

2.5.1.2 Applications of reclaimed water for UA irrigation

Water treatment technologies (combined with disinfection) offer a ladder of increasing water quality, and choosing the right level of treatment should be dictated by the end application of the reclaimed water for achieving economic efficiency and environmental sustainability (Council 2012).

Unrestricted irrigation for food crops. Unrestricted use of reclaimed water is the irrigation (surface or spray irrigation) for food crops that are intended for human consumption, including crops eaten raw without processing (Schroeder et al. 2012). An example of large-scale reclaimed water irrigation for raw-eaten food crops is in Monterey County, California. More than 5,000 ha of lettuce, broccoli, cauliflower, fennel, celery, strawberries, and artichokes have been irrigated with recycled water for more than a decade (EPA 2012). World Health Organization (WHO) guidelines and regulations (Organization 2006) have specified treatment processes, water quality standards, and monitoring regimes that minimize risks for use of reclaimed water for irrigation of crops that are ingested by humans. In the US, 27 states or territories have developed rules, regulations, or guidelines regarding this type of reclaimed water use by 2012 (EPA 2012).

Restricted irrigation for food crops. Restricted use of reclaimed water is to irrigate crops that are either processed before human consumption (those prior to sale to the public or others, have undergone chemical or physical processing sufficient to destroy pathogens) or not consumed by humans such as seed crops, industrial crops, fodder crops, orchard crops, and alfalfa plants (EPA 2012). It reduces opportunities of human exposure to the water, resulting in less stringent treatment and water quality requirements than other forms of reuse (EPA 2012). By 2012, 43 states or territories have developed rules, regulations, or guidelines regarding this type of reclaimed water

use, and there are several states that even do not require disinfection if certain parameters are met (EPA 2012).

Other UA relevant reclaimed water application. Reclaimed water can also be used with biosolids for the production of bricks, concrete, and the construction of gardens and other facilities related to UA. In addition, it can be used to control dust generated by these construction sites. Likewise, the reclaimed water requires a minimum of secondary treatment and disinfection prior to use. The details of relative criteria in different states of US or other countries were summarized elsewhere (EPA 2012).

2.5.2 Biosolids for UA

An estimated eight million dry tons of nutrient-rich sludge is produced annually from WRRFs in the US (Coats and Wilson 2017). The produced sewage sludge can be stabilized and processed into biosolids which are nutrient and energy rich materials and can be utilized in many ways in support of UA (Møller et al. 2009). In 1993, the US Environmental Protection Agency (USEPA) promulgated CFR Title 40 Part 503, establishing federal standards for the use or disposal of biosolids. These regulations defined pathogen reduction requirements for municipal sewage sludge resulting in Class A and B biosolids standards. Class B biosolids are treated by processes to significantly reduce, but not totally eliminate, pathogen concentrations and therefore require special handling; whereas Class A biosolids are treated by additional processes to further reduce pathogens to very low concentrations that do not require special handling or other restrictions (1994, USEPA 1990). In addition, Part 503 rule, also uses the term Exceptional Quality (EC) to characterize biosolids that meet low-pollutant and Class A pathogen reduction (virtual absence of pathogens) limits and that have a reduced level of degradable compounds that attract vectors (1994, USEPA 1990). EQ biosolids are considered a product that is virtually unregulated for use, whether used in bulk, or sold or given away in bags or other containers. The Class A requirements shall be met when bulk sewage sludge is applied to a lawn or a home garden or sold or given away in a bag or other container for application to the land. While Class B requirements shall be met when bulk sewage sludge is applied to agricultural land, forest, a public contact site, or a reclamation site (USEPA 1990). Different types of biosolids can be used as fertilizers and soil amenders.

2.5.2.1 Direct farmland application as fertilizers

Biosolids generally contain 1–5% phosphorous and 1–10% nitrogen as well as significant levels of trace metals required by crops for healthy growth (Crocker et al. 2018). Direct land application of biosolids can represent an interesting strategy for improving crop yield by increasing nitrogen and phosphorus contents, soil organic matter contents and fertility (Alvarenga et al. 2015). This blend of nutrients, from an economic standpoint, makes biosolids a very attractive organic alternative to the conventional chemical fertilizers (Darvodelsky and Bridle 2012).

Globally, land application of biosolids is considered to be the most sustainable use of this material (Darvodelsky and Bridle 2012). Additionally, biosolids use in UA can offset the use of chemical fertilizers which can have nonrenewable origins and require large amounts of energy to produce. Based on carbon footprint values of N and P, for every dry tone of biosolids used in agriculture, approximately 192.5 kg of CO_2 emissions are abated from avoided fertilizer production (Goh et al. 2018). Consequently, direct farmland application of biosolids could play an important role in UA especially in commercial farm or community garden for its ability to improve soil properties, nutrient condition, and crop growth.

2.5.2.2 Soil amendment

Because of foot and wheel traffic destroying vegetative cover and compacting the surface soil (Craul 1985, Gregory et al. 2006), a crust on or within several centimeters of the ground surface is typically formed on urban soil, which deteriorates the soil properties. Biosolids have been used to improve soil physical properties, such as reducing bulk density (Punshon et al. 2002), increasing total porosity (Chang et al. 1983) and water-holding capacity (Punshon et al. 2002), improving pore size distribution (Pagliai and Antisari 1993), and chemical properties such as cation exchange capacity and organic matter contents, (Ozores-Hampton et al. 2011, Stoffella et al. 2001), and biological properties such as microbial communities, soil fauna and aboveground plant biomass yield (Sydnor and Redente 2002). Various types of biosolids, i.e., amended biosolids, limed

biosolids, composted biosolids, heat-dried biosolids, hydrochars from hydrothermal carbonization of biosolids, can be applied towards bringing these positive properties to the receiving soil.

Amended biosolids. A blending biosolids with other recycled or reused materials can improve the biosolids properties for UA use. For example, blending biosolids with organic (e.g., sawdust, biochar, lignite) or inorganic (e.g., sand or quarry rock "fines") materials has been practiced for reducing the moisture content for urban soil use (Ervin E. 2013, Yu H. 2013). These organic materials can also reduce nutrients (i.e., nitrogen) leaching from soils amended with biosolids, sorb contaminants, and mitigate negative impacts on the environment (Paramashivam et al. 2017). For example, biochar produced from the pyrolysis of organic waste such forestry, garden, and agricultural wastes can sorb xenobiotic organic contaminants (Spokas et al. 2009, Wang et al. 2010) and metals (Uchimiya et al. 2010). Sawdust can remove pathogens by the toxicity of tannin compounds (Banegas et al. 2007). Lignite amended soil had higher C content (35%), N content (33%), and a C/N ratio than control soil (Budaeva et al. 2006). Hence, lignite mixed with biosolids could reduce heavy metal uptake by plants (Simmler et al. 2013) and inorganic N leaching from soil (Paramashivam et al. 2016). District of Columbia Water Authority (DC Water) has replaced Class B lime-stabilization processing system with a thermal hydrolysis pretreatment enhanced anaerobic digestion process to produce Class A/EQ biosolids (Johnston et al. 2019). The resulting biosolids were successfully blended with woody (e.g., shredded mulch, sawdust) and mineral (e.g., sand) substrates to create byproducts with ideal moisture contents, allowing their handling and application in urban environments.

Limed biosolids. Limed biosolids are biosolids blended with liming agents such as calcium oxide or calcium hydroxide to destroy residual pathogens and minimize odor, as well as limit the attraction of disease vectors such as insects and other living organisms that can transport biosolids-borne pathogens away from site. Therefore, limed biosolids can become Class A biosolids useful in UA as fertilizers or topsoil. To obtain limed biosolids, the pH of the biosolids should be raised with these alkaline materials to a specified level for a specified time according to USEPA promulgated CFR Title 40 Part 503 (USEPA 1990). By increasing pH accordingly, the metal hydroxide precipitation has been formed, and metal leachability has been reduced. This results in

products which have higher alkalinity and low heavy metal bioavailability, which are well suited for use in heavily cropped fields or acidic soils requiring alkaline amendments (Goh et al. 2018).

In Western Australia, the Water Corporation produces lime-amended biosolids from their Subiaco WRRF (Stamatelatou and Tsagarakis 2015). Although this material is suitable to market as-is, blending it with red clay has yielded a product known as Lime-amended BioClay (LaBC®). In addition to functioning as an organic fertilizer for acid sandy soils, LaBC® also overcomes water repellence, a significant issue of arid soil types like those found in Australia (Shanmugam et al. 2014). On the market since 2011, LaBC® is sold to farmers as a three-in-one product to offset the use of agricultural lime and chemical fertilizers as well as to decrease the natural water repellence of sandy soils and increase their water-holding capacity (Stamatelatou and Tsagarakis 2015).

Composted biosolids. Composted biosolids are biosolids blended with organic green waste and composted to achieve volatile solids reduction, odor mitigation and residual pathogen inactivation. Composted biosolids are suitable for horticultural and domestic use and used as top dressing for fields (Goh et al. 2018). Vietor et al. (2010) found that composted biosolids can enhance turfgrass establishment and soil properties. In Australia, Sydney Water has 20% of all biosolids produced ends up in compost with approximately two-thirds of all compost products in Sydney containing a blend of biosolids (Darvodelsky and Bridle, 2012).

Heat-dried biosolids. Heat-dried biosolids are biosolids that have undergone some form of drying which effectively kills all pathogens, concentrates the nutrients in the biosolids, and significantly reduces the volume of material to be transported to farmland. Potential odor and pathogen issues are mitigated during heat-drying, and the resulting products are essentially dried biosolids in a concentrated and commonly pelletized form. These thermally treated biosolids normally meets the requirement of Class A biosolids defined by USEPA. To implement this thermal treatment, the four time-temperature regimes have been proposed by USEPA (1994, USEPA 1990). Treatment temperature and time vary with the solid contents. For example, biosolids with 7% solids or greater in the form of small particles can be heated through the contact with either warmed gases or an immiscible liquid with temperature of 50°C or higher for 15 seconds or longer (1994, USEPA 1990).

These heat-dried biosolid products can be applied in any agricultural, horticultural or domestic application requiring fertilizer use (Goh et al. 2018). A well-established and often cited example is the heat-dried product known as Milorganite® produced in Milwaukee, Wisconsin, US. Touted as the gold-standard of biosolid fertilizers, Milorganite® was first marketed back in 1926 and as of 2016 had been sold for 90 years. In 2006, the sale of 41,500 dry tones of Milorganite® throughout the US and Canada resulted in a USD $5.85 million net revenue for the Milwaukee Metropolitan Sewerage District (LeBlanc et al. 2009).

Hydrochars from hydrothermal carbonization of biosolids. Hydrothermal carbonization (HTC) could be a preferable option for biomass with high moisture. It is typically carried out at a temperature of 180-220 °C, with pressure in the range of 2.5-5 MPa, and for a residence time of 15-120 min in an inert or oxygen-free environment (Kambo and Dutta 2014). HTC required less input energy than conventional drying methods for sewage sludge or biosolids since the hydrothermal treatment process does not involve evaporation of water (Escala et al. 2013). The other advantages of HTC include complete sterilization and destruction of organic pollutants such as pharmaceutically active compounds in sewage sludge or biosolids (Funke and Ziegler 2010, Libra et al. 2011).

The renewable products could be produced during HTC. For example, the peat or lignite-like product derived from HTC of sewage sludge or biosolids is called hydrochar or sewchar (Melo et al. 2019). Hydrochars from sewage sludge or biosolids could be used as soil conditioner or ameliorant (Libra et al. 2011), reducing the demand of synthetic inputs (Tasca et al. 2017). Hydrochar application has been shown to reduce the tensile strength, increase the hydraulic conductivity, enhance the soil water-holding capacity, immobilize and later release the soil nitrogen (Zhang et al. 2014), reducing the leaching potential of this element to groundwater and improve its availability once the crop is present on the field (Bargmann et al. 2014). Nevertheless, the potential of marketing sewchar for UA should be explored.

2.5.2.3 Biosolid-based construction materials

Biosolids reuse for producing bricks and cement like materials can be applied in the construction of UA facilities.

Bricks. Brick manufacturers generally incorporate waste into bricks to achieve quarry activities reduction and costs saving (Association 2009). The incorporation of biosolids into the bricks, possibly blended with other materials (e.g., fly ash, agricultural wastes, forest wastes, etc.) was proposed (Alleman and Berman 1984). The world's first full-scale sewage brick plant started back in 1991 in Tokyo with a capacity of 5,500 bricks a day out of 15,000 kg of incinerated sludge ash. Bricks made with sludge are a resilient material and have not been demonstrated to leach heavy metals (Spinosa 2004). Bricks containing sludge have been shown to perform better under structural tests than traditional bricks. These tests include compression strength, water absorption rates, abrasion strength, and bending strength (Spinosa 2004). Sewage bricks have been applied in public walkways and gardens (Spinosa 2004).

Cement. Biosolids produced in WRRFs contain CaO, SiO_2, Al_2O_3, and Fe_2O_3 which are four major oxides of Portland cement clinker. The Portland cement clinker is a dark grey nodular material made by heating ground limestone and clay at a temperature of about 1400 °C - 1500 °C, and it can be used as the binder in many cement products (Valderrama et al. 2013). Biosolids can be used in the cement kilns to produce cement clinker through co-firing (Stasta et al. 2006). To achieve this technology, dry matter content in the sludge can reach approximately 92% in industrial practice by decreasing the water content in a sludge drier (Stasta et al. 2006). Manufacturers accept incinerated ash, dried sludge, or dewatered sludge cake as raw materials of cement production. The amount of biosolids that can be added as raw material substitute with controlled ratio ranging from 5 to 15 wt% depending on the organic contents to avoid undesirable changes in the mechanical and rheological properties of pastes and mortars (Collivignarelli et al. 2019, Johnson et al. 2014).

2.5.2.4 Biosolid fuels for heating in greenhouses

Greenhouses normally utilize direct combustion of natural gas, liquefied petroleum gas, or fuel oil to provide heat for boilers, water heaters, and unit heaters for maintaining the temperatures necessary to grow plants and to increase carbon dioxide (CO_2) levels to induce higher plant growth (Esen and Yuksel 2013). The high cost of heating a greenhouse with traditional fuel necessitates switching to low-cost, alternative fuels. The composition of digested sludge is about 67% carbon, 5% hydrogen, 25% oxygen, 2.2% nitrogen, and 0.8% Sulphur (Stasta et al. 2006). Dried digested sludge has a similar composition and calorific value (12.0-20.0 MJ kg^{-1}) to brown coal (14.6-26.7 MJ kg^{-1}) (Manara and Zabaniotou 2012, Stasta et al. 2006).

In addition, the bio-oil or biocrude converted from municipal sludge and biosolids via hydrothermal liquefaction (HTL) is another alternative. HTL is the process of heating and pressurizing an aqueous biomass slurry under 200 - 375°C and 15 - 22 MPa (2200-3200 psi) (Anthony 2015). The produced bio-oil contains higher portions of hydrogen and carbon than the initial feedstock, giving it a maximum heating value of 31.46 ± 0.37 MJ/kg with a conversion yield of 39.42 ± 1.4% that can be nearly as high as traditional crude oil (Anthony 2015). Moreover, HTL can mitigate the environmental impacts of sludge and biosolids by sterilizing pathogens, removing almost all heavy metals (Peterson et al. 2008), achieving dechlorination and denitrogenation, removing chemicals of emerging concerns (CECs), and reducing costs associated with anaerobic digestion and the transportation of biosolids (Anthony 2015).

2.5.2.5 Adsorbents for air purification in greenhouses

Biochar can be produced through biosolids pyrolysis (Collivignarelli et al. 2019, Smith et al. 2009). The produced biochar can be used as a low-cost adsorbent for air purification (Hadi et al. 2015). Typical usage examples include the adsorption of volatile organic compounds (Anfruns et al. 2011), NO_x (Pietrzak and Bandosz 2008), and H_2S (Bandosz and Block 2006) generated in greenhouse.

2.5.2.6 Bio-containers as plantable pots

Biosolids with an appropriate mix of additives can yield solid bio-containers that could be marketed based on end use characteristics (Stone 2017). In this application, transplant is not necessary because the bio-containers can degrade over time. This practice also reduces transplant shock, save the transplant time and cost, and avoids disposal of the containers (Nambuthiri et al. 2013). This can be advantageous for UA greenhouses and nurseries to begin growing their plants in a controlled environment, and then move the plant with container to the garden. Multiple mixes of biosolids, cardboard, cellulose, starch, polymer, and natural glue were developed to provide overall pot stability and structural strength (Stone 2017). The fiber additive could provide rigidity and help increase marketability as a legitimate commercial product. In all cases, plants grown in biocontainers made by biosolids and additives produced more biomass than plants grown in Peat Pots (Stone 2017).

2.5.3 Bioplastic production

The potential applications of bioplastics as replacement for petroleum-based plastics are gaining popularity in various fields involving packaging, coating, and construction materials useful for UA. Potential UA application include food wrapping, encapsulation of seeds, encapsulation of fertilizers for slow release, biodegradable plastic films for crop protection, and biodegradable containers for greenhouse facilities (Alcaraz Cercós 2015). There are current two pathways for bioplastic production from WRRFs, i.e., fat, oil and grease (FOG)-based and Polyhydroxyalkanoates (PHAs)-based bioplastic production.

Recent studies showed that the FOG in sewer systems can be recovered for bioplastic production (Michael et al. 2012). For example, the free fatty acids constituent of FOG can be used as a potential substrates for biopolymer synthesis, replacing plastics from petrochemical sources in many applications (Ruiz et al. 2014). Another constituent of FOG, namely crude glycerol, is also a viable feedstock for value-added conversion into biopolymers or biochemicals (Luo et al. 2016).

Cui et al. (2019) comprehensively reported the paths and mechanism of bioplastic synthesis from components of FOG such as fatty acid and crude glycerol.

PHAs are biodegradable polymers produced by many species of naturally occurring bacteria (Arcos-Hernández et al. 2015). Both pure and mixed culture PHA production strategies reduce production costs through the use of low-value carbon-rich raw material feedstocks like municipal and industrial wastewaters (Nikodinovic-Runic et al. 2013). Activated sludge utilized for PHA production is anticipated to be more cost-effectively advantageous than pure culture methods because reactor sterilization is not needed (Yadav et al. 2020). PHA production with municipal wastewater and sludge treatment occurs in four-stage process: (i) removal of readily biodegradable carbon from wastewater coupled to the selective growth of biomass with PHA storage capacity (Collivignarelli et al.), (ii) sludge acidogenic fermentation for the production of a VFA-rich liquid stream, (iii) PHA accumulation from the VFA-rich liquid stream using enriched biomass from step (i), and (iv) PHA recovery and characterization (Morgan-Sagastume et al. 2014). Morgan-Sagastume et al. (2014) reported the first pilot-scale system treating municipal wastewater and producing biomass with enhanced PHA storage capacity.

2.5.4 Phosphorus recovery as a fertilizer for UA

As a finite resource and an essential fertilizer element, the price of phosphorous (P) increased tenfold from 1950 to 2000. In 2007 alone, it grew by about 200% (Tan and Lagerkvist 2011). For these reasons, interests are drawn towards P recovery from obviously available but often unexploited P sources such as municipal wastewater (Cieślik and Konieczka 2017, Egle et al. 2016). Technically, P can be removed from municipal wastewater, sewage sludge, and sewage sludge ash from thermal disposal such as incineration.

Currently, the most widely used technologies for P recovery from WRRFs are those based on precipitation of phosphoric minerals from sludge or leachates (Cieślik and Konieczka 2017). Phosphoric minerals can be precipitated in the form of struvite ($NH_4MgPO_4 \cdot 6H_2O$), hydroxyapatites [$Ca_5(PO_4)_3(OH)$] or calcium phosphates [$Ca_3(PO_4)_2$]. Up to 85% of dissolved P can be recovery from digested supernatant by crystallization or instant precipitation (Egle et al.

2016). The most important advantage of this precipitation method is the ability to obtain high-quality phosphoric minerals, which can be applied in agriculture directly. Precipitated hydroxyapatite materials contain very low concentrations of heavy metals and are thus considered to be safe for the environment (Nakakubo et al. 2012). Furthermore, struvite is poorly soluble, represents a eco-friendly mean even with a high load of P (Kataki et al. 2016). Therefore, these high-quality phosphoric minerals can be recovered as excellent fertilizer in service for UA.

2.5.5 Biogas for UA

2.5.5.1 Sulfur recovery from biogas as a fertilizer

Raw biogas from sewage digesters mainly contains 55% to 65% methane (CH_4), 35% to 45% carbon dioxide (CO_2) and trace amounts of other components such as 0.005% to 2% hydrogen sulfide (H_2S) (Andriani et al. 2014, Rasi et al. 2007). H2S is harmful to the environment and corrosive to the metallic parts of engines, pumps, compressors, gas storage tanks and valves, and reduces the lifespan of process equipment (Huertas et al. 2011, Ryckebosch et al. 2011). THIOPAQ™ is a biotechnological process capable of absorbing H2S into a mild alkaline solution followed by the oxidation of the absorbed sulfide to elemental sulfur (S) by naturally occurring microorganisms such as Thiobacillus (Center 2004). The conversion efficiency of H2S to S is expected to be between 95-97% (Center 2004). The obtained S is an ideal slow-release S fertilizer. Although S is unavailable for plant uptake, it is oxidized to the plant available sulfate-S form by soil micro-organisms (Boswell and Friesen 1993). Therefore, S fertilizer produced from the technologies mentioned in this section can have a huge application potential in UA. Sulfur can be applied alone in the forms of dried pellets or particulates of different sizes, or can be mixed with superphosphate, bentonite clay, urea and other fertilizers to enhance fertilizer efficiency (Boswell and Friesen 1993).

2.5.5.2 Electricity and heat production from biogas

Wastewater treatment is the 8th largest anthropogenic source of CH_4 emissions (12.8 million metric tons of CO_2 equivalent) in the US (USEPA 2014). Therefore, efficient biogas production

and utilization at WRRFs can reduce the carbon footprint, minimize external energy requirements, and provide financial benefits for WRRFs (Agency et al. 2007, McCarty et al. 2011). Perhaps the most readily adaptable approach to reduce external energy requirements with existing treatment plants is to make full use of the CH4 produced from conventional anaerobic digesters through the use of combined heat and power (CHP) systems. CHP is the simultaneous production of electricity and heat from a single fuel source, such as biogas, natural gas, coal, or oil. CHP is not a single technology, but an energy system that can be modified depending on the needs of the energy end user. The electric power produced from CHP can offset all or most of a WRRF's power demand, and the surplus can be directly utilized by the equipment or facilities in UA. Likewise, the thermal energy produced by the CHP system can be used to meet digester heat loads and, in some cases, for space heating (Bastian et al. 2011) such as greenhouses and buildings.

2.5.5.3 Capture of carbon dioxide for utilization in UA

Raw biogas from sewage digesters or fume from CHP contains a large amount of CO_2 which has potential to be utilized in various UA scenarios. For example, gaseous CO_2 can be used for crop growth stimulation and pest control in greenhouses (Byrns et al. 2013, Song 2006), and for packaging gas of foodstuffs (Byrns et al. 2013, Song 2006). Liquid CO_2 can be used as cryogenic fluid in chilling or freezing operations or as dry ice for temperature control during the storage and distribution of foodstuffs.

The amount of CO_2 that can be produced and captured from municipal sludge anaerobic digesters is tremendous. Byrns et al. (2013) estimate that the annual biogas production in the UK is 342 million m^3 which contains 0.27 million tons of CO_2. The global market for merchant CO_2, measured by the amount of CO_2 sold in the market, which excludes in-plant CO_2 utilized by manufacturers, is estimated to be $3.2 billion/year back in 2003 (Gobina 2004). The CO_2 capture efficiency depend on the separation technologies which can be divided into physical, chemical, or biological methods. Examples include cryogenic, membrane, high-pressure water scrubbing, amine and alkaline absorption, and biofixation (Byrns et al. 2013). These technologies have been reported in detail by Khan et al. (2017) and De Hullu et al. (2008).

2.5.6 Life cycle assessment of the WRRF contribution to UA

Life Cycle Assessment (LCA) has been performed to evaluate the environmental impacts of using products recovered from WRRFs for UA. For irrigation using reclaimed water, LCA conducted by Pasqualino et al. (2011) based on the data from a WRRF located in Spain on the Mediterranean Coast showed that reclaimed water for irrigation with tertiary treatment has a lower environmental impact than the ocean discharge option in terms of all of the categories such as acidification potential, global warming potential, and eutrophication potential. Similarly, the results of LCA conducted by Romeiko (2019) indicted that replacing groundwater with reclaimed water as the irrigation source significantly decreased life cycle global warming, acidification, ozone depletion, smog formation, and respiratory impacts of corn, soybean and wheat systems in Northern China. The LCA conducted by Canaj et al. (2021) further revealed that tertiary reclaimed water as a supplementary source of irrigation water could reduce the net environmental impact by 23.8% due to lower consumption of irrigation water (-50%), electricity (-27.7%), and chemical fertilizers (-22.6%) compared to conventional groundwater irrigation system in Italy.

For using biosolids as solid amendment, LCA conducted by Peters and Rowley (2009) shows that the reuse of biosolids products can be environmentally beneficial but transportation distances can change the preferences between technologies, and drying biosolids using biogas produced in-situ in WRRFs rather than petrochemical methane could significantly improve environmental performance. Also, biosolids for kiln application such as bricks or cement production performs better than landfill, farmland application, composting, lime amending and heat-drying (Peters and Rowley 2009). LCA conducted by Sablayrolles et al. (2010) indicated that composted biosolids is more beneficial to the environment than heat-dried biosolids in terms of resource depletion, acidification, eutrophication, greenhouse effect, summer smog and ecotoxicity. LCA conducted by McDevitt et al. (2013) revealed that direct farmland application of biosolids has the least environmental impact than landfill, composting, and the amendment with biochar while biosolid composting has the most environmental impact. The results of the LCA by Mohajerani et al. (2018) further confirmed that the incorporation of biosolids into bricks is environmentally favorable and is a promising alternative approach with respect to most of the environmental impacts except water

depletion, which is mainly due to the higher water demand of biosolids-amended bricks during the shaping process.

For using biosolid as fuels, Mills et al. (2014) found that creating a solid fuel with post anaerobic digestion biosolids to displace coal was the most sustainable solution economically and environmentally in terms of LCA results. By converting raw sewage sludge to refinery-ready biocrude oil with hydrothermal liquefaction (HTL) technology nationwide, almost 4.5 million barrels of upgraded biocrude oil could be produced per year while about 330,000 metric tons of CO2 equivalent greenhouse gas emissions could be offset annually (Bond 2015). For adsorbents such as biochar production, Miller-Robbie et al. (2015) reported that the addition of biosolids biochar production adds little to the overall energy use but provides substantial (26%) reduction in greenhouse gas emissions for the national case in terms of LCA results, largely due to the recalcitrant carbon storage in biochar. In contrast, Thompson et al. (2016) reported that biosolids biochar adsorbent negatively affects environmental quality at the highest level than wood biochar and coal-based powdered activated carbon, attributing to energy consumption for biosolids drying, manufacture of mineral fertilizer to substitute biosolids applied for soil amendment, and the need for supplemental adsorbent.

For bioplastic production, Vogli et al. (2020) compared the LCA results of PHA-based biopolymers from anaerobically digested sewage sludge with other polymers. It can be noted that the PHA-based biopolymers tend to have both lower non-biogenic greenhouse gas (GHG) emissions and lower fossil energy demand values than the fossil-based polymers (Vogli et al. 2020). For P recovery, according to the LCA conducted by Bradford-Hartke et al. (2015), recovering P using struvite precipitation resulted in positive environmental impacts due to energy and chemical use being offset by operational savings and avoided mineral fertilizer production. In contrast, for Pradel and Aissani (2019), the overall assessment remains unfavorable for P recovery comparing to mineral P fertilizer use due to the low P yields, low P concentration in the sludge and the large amounts of energy and reactants needed to recover the P. For sulfur recovery from biogas, LCA by Cano et al. (2018) indicates that biological H2S scrubbing technologies are much more favorable than physical-chemical technologies in most environmental impact categories such as terrestrial

acidification, freshwater eutrophication, human toxicity, water depletion and photo-oxidant formation and, as expected, are more favorable than the non-treatment scenario.

For electricity and heat production from biogas, LCA by Singh et al. (2020) shows that biogas plant has negative GHG emissions (−0.2385 kg CO2 eq/m3) compared to coal-based electricity plant which indicates that sewage sludge-based biogas plant has beneficial impacts on the environment. For CO2 capture, Starr et al. (2012) evaluate the LCA of different technologies. The results show that alkaline absorption with regeneration technology had an 84% negative impact in all LCA categories than high pressure water scrubbing largely due to the energy intensive production of the alkaline reactants (Starr et al. 2012). For alkaline absorption with regeneration technology, it was determined that using NaOH instead of KOH improves its environmental performance by 34% (Starr et al. 2012).

2.5.7 Economic viability in leveraging WRRF for UA

Reclaimed water for irrigation has been widely accepted in developed countries (Organization 2006). For example, in Monterey County, California, more than 5,000 ha of raw-eaten food crops have been irrigated with reclaimed water for more than a decade (EPA 2012). Lv et al. (2021) developed a method to quantitatively analyze eco-economic benefits of urban reclaimed water for irrigation. The results show that the cost of using reclaimed water to irrigate urban green spaces was 46% of the cost of using tap water (Lv et al. 2021). The total benefit of using reclaimed water to irrigate green spaces was three times the benefit of using tap water (Lv et al. 2021). Yet, the cost of moving reclaimed water between centralized WRRFs and UA sites was not reported.

Limed and heat-dried biosolids have been commercialized. For example, in Australia, limed-biosolids blended with red clay has yielded a product known as Lime-amended BioClay (LaBC®) (Stamatelatou and Tsagarakis 2015). A heat-dried biosolid product known as Milorganite® produced in Milwaukee, Wisconsin, USA has also been commercialized in north America. Hydrochars from HTC of biosolids have been commercialized by enterprises in several developed countries such as AVA-CO_2 Schweiz AG in Switzerland and TerraNova Energy in Germany. Class A/EQ biosolids, amended and composted biosolids have also been widely accepted in developed

countries as fertilizers (Darvodelsky and Bridle 2012, Johnston et al. 2019). Similarly, biosolid-amended bricks and cement have also been commercialized (Collivignarelli et al. 2019, Johnson et al. 2014, Spinosa 2004).

Technological economics analysis (TEA) performed by Bond (2015) showed that economic impacts of biosolid-based bio-oil or biocrude production through a HTL project have the potential to be favorable. In the case of implementation at a local biosolid manage plant, this project could save the City of Austin on the scale of $32 million (Bond 2015). This technology has been commercialized by several utilities and companies. For example, Genifuel®, a company in Utah conducted biosolid HTL based on systems developed by the Pacific Northwest National Laboratory (PNNL), part of the US Department of Energy, which implements reactions at 350 °C and 200 bars, with residence times of approximately 45 min (Castello et al. 2018, Genifuel 2020). The whole system is even smaller than an anaerobic digester, which can convert biosolids with 20% total solids into biocrude oil and sterile water (Castello et al. 2018, Genifuel 2020). Biosolid-based adsorbents, bio-containers, and bioplastic production are still in lab or pilot scales, and the possibility of their commercialization is still under investigation. For example, a biosolid-based bioplastic production pilot plant has been operated in Sweden by Veolia subsidiary and project partner AnoxKaldnes (Bioplastic 2015). While its current production capacity is small, e.g., a few kilos per week, the idea is to scale this up to include the total treated wastewater volume and ultimately resulting in a production capacity of 2000 metric tons/year (Bioplastic 2015).

Currently, about 50 technologies have been developed to recover P from byproducts of WRRFs (e.g., digester supernatant, sewage sludge, sewage sludge ash) including crystallization, precipitation, wet chemical processes, and thermochemical processes (Egle et al. 2016). Many crystallization and precipitation processes have been commercialized including PhoStrip, PRISA, DHV Crystalactor, CSIR, Kurita, Ostara, Phosnix, Berliner Verfahren, and FIX-Phos (Mehta et al. 2015). For example, in 2016, Ostara and the Metropolitan Water Reclamation District of Greater Chicago opened the world's largest nutrient recovery facility with its Waste Activated Sludge Stripping to Remove Internal Phosphorus (WASSTRIP®) and Pearl® technologies (Ostara 2017). The technologies offer many benefits including a reduction in sludge production, up to 50% P removal, and a revenue stream with the sale of Crystal Green®, a slow release P fertilizer. As of

2017, the Ostara technology had 15 commercial installations located in the US, Canada, the Netherlands, Spain, and the United Kingdom (Ostara 2017). For P recovery as struvite from digested sludge, Life-Cycle Cost Analysis (LCCA) performed by Saerens et al. (2021) indicates that an overall positive economic result is observed in most scenarios as a result of the operational benefits (mainly from the improved dewaterability of the sludge) although struvite is currently undervalued.

After upgrading, biomethane were utilized for electricity and heat production through grid injection. All examined upgrading technologies (membrane separation, water scrubbing, chemical absorption with amine solvent, and pressure swing adsorption) have demonstrated substantial mitigation of the overall environmental and economic impacts (Ardolino et al. 2021). Membrane separation provides the best performances in terms of LCCA. Technology readiness level (TRL) for the production of biomethane by means of biogas upgrading reached a value equivalent to the market availability, which is the maximum level of development of a technology (Ardolino et al. 2021). For sulfur recovery from biogas, THIOPAQ™ and the Shell-Paques processes commercialized by Shell and Paques can remove up to 99% H_2S from biogas and convert it to elemental sulfur (Center 2004). The system application range is approximately 200 pounds to 40 tons of sulfur per day (Center 2004). However, the commercialization of carbon capture from biogas has rarely been reported.

2.6 Current understanding of the human health concerns

The human health concerns of utilizing reclaimed water for irrigation and biosolids for land application have to do with the presence of contaminants of emerging concerns (CECs) and trace metals. CECs comprise a diverse collection of chemicals, including pharmaceutical, personal care products (PCPs), surfactants such as Per- and polyfluoroalkyl substances (PFASs), polycyclic aromatic hydrocarbons (PAHs), flame retardants, metallic trace elements, pesticides, and endocrine disruptors (Daughton 1999, Samal et al. 2022). Majority of CECs used domestically are conveyed daily to WRRFs. The average wastewater retention time is generally shorter than the degradation half-lives of many organic CECs that enter a WRRF (Halling-Sørensen et al. 1998, Tchobanoglous 2003), resulting in their discharge via effluents and biosolids. Reported levels of

CECs and their degradation products in WRRF effluents ranged from ng/L to µg/L (Deblonde et al. 2011, Focazio et al. 2008, Loos et al. 2013, Pal et al. 2010) and in biosolids ranged from ng/kg to mg/kg (Boix et al. 2016, Clarke and Smith 2011, Daughton 1999, Halling-Sørensen et al. 1998, Heidler and Halden 2008, Kinney et al. 2006, Semblante et al. 2015, Tchobanoglous 2003, USEPA 2009, 2021a, Xia et al. 2005).

To date, there are no regulatory or recommended concentration limits for CECs in both WRRF effluent and biosolids (Samal et al. 2022). Land application of biosolids and WRRF effluent for agricultural production has been a widely accepted practice in the US and many other countries. The human health impacts of CECs associated with land application of biosolids and reclaimed water are considered to be de minimis according to Kuma (2017). In addition, some studies have shown that although some CECs can be taken up by plants (Al-Farsi et al. 2017, Liu et al. 2020, Miller et al. 2016, Reyes et al. 2021), human health impact due to consumption of food grown in biosolids- or reclaimed water- applied fields are considered to be negligible comparing to the daily household exposure to CECs (Hundal 2011, Kuma 2017).

In contrast to CECs, the health impacts of trace metals are much better understood (Briffa et al. 2020, He et al. 2005, Tchounwou et al. 2012). The USEPA Part 503 Biosolids Rule (USEPA 2018) has regulatory limits on a list of 10 trace metals for biosolids (USEPA 2021b) and requires that biosolids should be used in accordance with approved management practices including operational standards, monitoring, recordkeeping and reporting. Biosolids for farmland application, soil amendment and bio-containers are not allowed if the concentration of any of the 10 trace metals exceeds its celling concentration limit. The USEPA's guidelines for reclaimed water use for irrigation have recommended concentration limits for 17 trace elements (USEPA 2012). On the other hand, no health concerns were reported for the biosolid-based construction materials, fuels and adsorbents, recovered P fertilizer, and biogas utilization. As for bioplastics, its health concerns are similar to petroleum-based plastics, which have been documented elsewhere (Bernard 2014, Momani 2009).

2.7 Future directions and outlooks

Utilizing resources recovered from municipal wastewater for UA is still a controversial topic. On one hand, wastewater represents a new source of water, energy, nutrients, and renewable materials and thus should no longer be considered as waste but as a new resource to be handled in a circular economy-type loop. On the other hand, the use of recycled materials for UA may have an adverse impact on public health and the environment, depending on treatment and regulatory expectation. Current scientific knowledge in agronomic and environmental sciences, as well as in the economic and social sciences, can be integrated and used to lower the associated risk through the effective management and design of WRRFs. The following questions should be addressed in future works: (i) How to increase public acceptance of UA using WRRF materials for safe environmental reuse within an adapted risk assessment framework? (ii) What socio-economic models can render this integrated approach sustainable? (iii) What WRRF treatment systems can be used to ensure public health? And (iv) What economical methods should be developed to transport resources between centralized municipal WRRFs and decentralized UA sites.

2.8 References

Abelleira-Pereira, J.M., Perez-Elvira, S.I., Sanchez-Oneto, J., de la Cruz, R., Portela, J.R. and Nebot, E. (2015) Enhancement of methane production in mesophilic anaerobic digestion of secondary sewage sludge by advanced thermal hydrolysis pretreatment. Water Res 71, 330-340.

Aerts, R., Dewaelheyns, V. and Achten, W.M. (2016) Potential ecosystem services of urban agriculture: a review. PeerJ Preprints 4, e2286v2281.

Agency, U.E.P., Heat, C. and Partnership, P. (2007) Opportunities for and benefits of combined heat and power at wastewater treatment facilities. Eastern Research Group and Energy and Environmental Analysis; EPA-430/R-07-003.

Agustina, I. and Beilin, R. (2012) Community gardens: Space for interactions and adaptations. Procedia-social and Behavioral sciences 36, 439-448.

Al-Farsi, R.S., Ahmed, M., Al-Busaidi, A. and Choudri, B.S. (2017) Translocation of pharmaceuticals and personal care products (PPCPs) into plant tissues: A review. Emerging Contaminants 3(4), 132-137.

Al-Rajab, A.J., Sabourin, L., Lapen, D.R. and Topp, E. (2015) Dissipation of triclosan, triclocarban, carbamazepine and naproxen in agricultural soil following surface or sub-surface application of dewatered municipal biosolids. Science of the Total Environment 512-513, 480-488.

Alcaraz Cercós, E. (2015) Bioplastic production from wastes and wastewater, Bachelor thesis, Universitat de Barcelona, Barcelona

Alleman, J.E. and Berman, N.A. (1984) Constructive sludge management: biobrick. Journal of Environmental Engineering 110(2), 301-311.

Alvarenga, P., Mourinha, C., Farto, M., Santos, T., Palma, P., Sengo, J., Morais, M.-C. and Cunha-Queda, C. (2015) Sewage sludge, compost and other representative organic wastes as agricultural soil amendments: Benefits versus limiting factors. Waste management 40, 44-52.

Alvarez-Campos, O. and Evanylo, G.K. (2019) Biosolids Improve Urban Soil Properties and Vegetable Production in Urban Agriculture. Urban Agriculture & Regional Food Systems 4(1), 190002.

Andriani, D., Wresta, A., Atmaja, T.D. and Saepudin, A. (2014) A review on optimization production and upgrading biogas through CO 2 removal using various techniques. Applied biochemistry and biotechnology 172(4), 1909-1928.

Anfruns, A., Martin, M.J. and Montes-Morán, M.A. (2011) Removal of odourous VOCs using sludge-based adsorbents. Chemical engineering journal 166(3), 1022-1031.

Anthony, J.R. (2015) Hydrothermal liquefaction of municipal sludge and biosolids. Master Thesis, The University of Texas at Austin, Texas.

Arcos-Hernández, M., Montaño-Herrera, L., Murugan Janarthanan, O., Quadri, L., Anterrieu, S., Hjort, M., Alexandersson, T., Karlsson, A., Karabegovic, L. and Magnusson, P. (2015) Value-added bioplastics from services of wastewater treatment. Water Practice and Technology 10(3), 546-555.

Assembly, L. and Committee, E. (2006) A Lot to Lose: London's disappearing allotments, Greater London Authority, London.

Association, B.I. (2009) Sustainability and brick, Brick Industry Association, Brick Industry Association, Reston, Virginia.

Astee, L.Y. and Kishnani, N.T. (2010) Building integrated agriculture: Utilising rooftops for sustainable food crop cultivation in Singapore. Journal of Green Building 5(2), 105-113.

Aubry, C., Kebir, L., Pasquier, C., Traversac, J. and Petit, C. (2008) Transitions in peri-urban agriculture: how short supply chains evolutions question research. Examples and emerging researches in the Ile de France, The Netherlands.

Bailkey, M. and Nasr, J. (1999) From brownfields to greenfields: Producing food in North American cities. Community Food Security News, Fall 2000, 6.

Bandosz, T.J. and Block, K.A. (2006) Removal of hydrogen sulfide on composite sewage sludge-industrial sludge-based adsorbents. Industrial & engineering chemistry research 45(10), 3666-3672.

Banegas, V., Moreno, J., Moreno, J., Garcia, C., Leon, G. and Hernandez, T. (2007) Composting anaerobic and aerobic sewage sludges using two proportions of sawdust. Waste management 27(10), 1317-1327.

Bargmann, I., Rillig, M.C., Kruse, A., Greef, J.M. and Kücke, M. (2014) Effects of hydrochar application on the dynamics of soluble nitrogen in soils and on plant availability. Journal of plant nutrition and soil science 177(1), 48-58.

Basta, N.T., Busalacchi, D.M., Hundal, L.S., Kumar, K., Dick, R.P., Lanno, R.P., Carlson, J., Cox, A.E. and Granato, T.C. (2016) Restoring Ecosystem Function in Degraded Urban Soil Using Biosolids, Biosolids Blend, and Compost. Journal of Environmental Quality 45(1), 74-83.

Bastian, R., Cuttica, J., Fillmore, L., Hedman, B., Hornback, C., Levy, D. and Moskal, J. (2011) Opportunities for Combined Heat and Power at Wastewater Treatment Facilities: Market Analysis and Lessons from the Field. US Environmental Protection Agency Combined Heat and Power Partnership.

Bellows, A., Brown, K. and Smit, J. (2003) Health benefits of urban agriculture: Public health and food security, p. 4, Community Food Security Coalition, California.

Birkby, J. (2016) Vertical farming. ATTRA sustainable agriculture 12, IP386.

Blair, D., Giesecke, C.C. and Sherman, S. (1991) A dietary, social and economic evaluation of the Philadelphia urban gardening project. Journal of Nutrition Education 23(4), 161-167.

Blair, S.N. and Nichaman, M.Z. (2002) The public health problem of increasing prevalence rates of obesity and what should be done about it. Mayo Clinic Proceedings 77(2), 109-113.

Boix, C., Ibáñez, M., Fabregat-Safont, D., Morales, E., Pastor, L., Sancho, J.V., Sánchez-Ramírez, J.E. and Hernández, F. (2016) Behaviour of emerging contaminants in sewage sludge after anaerobic digestion. Chemosphere 163, 296-304.

Boswell, C. and Friesen, D. (1993) Elemental sulfur fertilizers and their use on crops and pastures. Fertilizer research 35(1-2), 127-149.

Briffa, J., Sinagra, E. and Blundell, R. (2020) Heavy metal pollution in the environment and their toxicological effects on humans. Heliyon 6(9), e04691.

Brown, K.H., Carter, A. and Bailkey, M. (2003) Urban agriculture and community food security in the United States: Farming from the city center to the urban fringe, Urban Agriculture Committee of the Community Food Security Coalition (CFSC), Portland, Oregon.

Brown, K.H. and Jameton, A.L. (2000) Public health implications of urban agriculture. Journal of public health policy 21(1), 20-39.

Brown, S., Ippolito, J.A., Hundal, L.S. and Basta, N.T. (2020) Municipal biosolids — A resource for sustainable communities. Current Opinion in Environmental Science & Health 14, 56-62.

Brown, S., Kurtz, K., Bary, A. and Cogger, C. (2011) Quantifying Benefits Associated with Land Application of Organic Residuals in Washington State. Environmental Science & Technology 45(17), 7451-7458.

Budaeva, A., Zoltoev, E., Tikhova, V. and Bodoev, N. (2006) Interaction of heavy metal ions with ammonium humates. Russian journal of applied chemistry 79(6), 920-923.

Bureau of Reclamation, I. (2010) North San Pablo bay restoration and reuse project (north bay water recycling program), California.

Butler, L.M. and Maronek, D.M. (2002) Urban and agricultural communities: Opportunities for common ground. CAST Task Force Report 138.

Byrns, G., Wheatley, A. and Smedley, V. (2013) Carbon dioxide releases from wastewater treatment: potential use in the UK, pp. 111-121, Thomas Telford Ltd.

Center, G.G.T. (2004) Test and Quality Assurance Plan: Paques THIOPAQ and Shell-Paques Gas Purification Technology. , U.S. EPA, North Carolina.

Cerón-Palma, I., Sanyé-Mengual, E., Oliver-Solà, J., Montero, J.-I. and Rieradevall, J. (2012) Barriers and opportunities regarding the implementation of Rooftop Eco. Greenhouses (RTEG) in Mediterranean cities of Europe. Journal of Urban Technology 19(4), 87-103.

Chang, A., Page, A. and Warneke, J. (1983) Soil conditioning effects of municipal sludge compost. Journal of Environmental Engineering 109(3), 574-583.

Cieślik, B. and Konieczka, P. (2017) A review of phosphorus recovery methods at various steps of wastewater treatment and sewage sludge management. The concept of "no solid waste generation" and analytical methods. Journal of Cleaner Production 142, 1728-1740.

Clarke, B.O. and Smith, S.R. (2011) Review of 'emerging' organic contaminants in biosolids and assessment of international research priorities for the agricultural use of biosolids. Environment International 37(1), 226-247.

Cluster, I.R.R. (2015) State of the art compendium report on resource recovery from water. IWA International Water Association: London, UK.

Coats, E.R. and Wilson, P.I. (2017) Toward nucleating the concept of the water resource recovery facility (WRRF): perspective from the principal actors. Environmental science & technology 51(8), 4158-4164.

Collivignarelli, M.C., Canato, M., Abba, A. and Miino, M.C. (2019) Biosolids: What are the different types of reuse? Journal of Cleaner Production 238, 117844.

Congress, G.C. (2020) JRC: 76.5% of world's population in urban areas as of 2015. https://www.greencarcongress.com/2020/02/20200208-jrc.html (Accessed 6/26)

Council, N.R. (2012) Water reuse: potential for expanding the nation's water supply through reuse of municipal wastewater, National Academies Press.

Craul, P.J. (1985) A description of urban soils and their desired characteristics. Journal of arboriculture 11(11), 330-339.

Crocker, R., Saint, C., Chen, G. and Tong, Y. (2018) Unmaking Waste in Production and Consumption: Towards the Circular Economy, Emerald Publishing Limited.

Cui, S., Borgemenke, J., Liu, Z. and Li, Y. (2019) Recent advances of "soft" bio-polycarbonate plastics from carbon dioxide and renewable bio-feedstocks via straightforward and innovative routes. Journal of CO2 Utilization 34, 40-52.

Dad, K., Wahid, A., Khan, A.A., Anwar, A., Ali, M., Sarwar, N., Ali, S., Ahmad, A., Ahmad, M., Khan, K.A., Ansari, M.J., Gulshan, A.B. and Mohammed, A.A. (2019) Nutritional status

of different biosolids and their impact on various growth parameters of wheat (Triticum aestivum L.). Saudi journal of biological sciences 26(7), 1423-1428.

Darvodelsky, P. and Bridle, T. (2012) Biosolids snapshot, Department of Sustainability, Environment, Water, Population and Communities, Northern Territory, Australia.

Daughton, C.G., Ternes, T. A. (1999) Pharmaceuticals and personal care products in the environment: agents of subtle change? Environ Health Perspect. 107, Suppl 6., 907-938.

De Bon, H., Parrot, L. and Moustier, P. (2010) Sustainable urban agriculture in developing countries. A review. Agronomy for sustainable development 30(1), 21-32.

De Hullu, J., Maassen, J., Van Meel, P., Shazad, S., Vaessen, J., Bini, L. and Reijenga, J. (2008) Comparing different biogas upgrading techniques. Eindhoven University of Technology, The Netherlands.

Deblonde, T., Cossu-Leguille, C. and Hartemann, P. (2011) Emerging pollutants in wastewater: A review of the literature. International Journal of Hygiene and Environmental Health 214(6), 442-448.

Defra (2011) June Survey of Agriculture and Horticulture, Cardiff, UK.

Despommier, D. (2011) The vertical farm: controlled environment agriculture carried out in tall buildings would create greater food safety and security for large urban populations. Journal für Verbraucherschutz und Lebensmittelsicherheit 6(2), 233-236.

Ebele, A.J., Abou-Elwafa Abdallah, M. and Harrad, S. (2017) Pharmaceuticals and personal care products (PPCPs) in the freshwater aquatic environment. Emerging Contaminants 3(1), 1-16.

Egle, L., Rechberger, H., Krampe, J. and Zessner, M. (2016) Phosphorus recovery from municipal wastewater: An integrated comparative technological, environmental and economic assessment of P recovery technologies. Science of the Total Environment 571, 522-542.

Elvidge, C.D., Milesi, C., Dietz, J.B., Tuttle, B.T., Sutton, P.C., Nemani, R. and Vogelmann, J.E. (2004) US constructed area approaches the size of Ohio. Eos, Transactions American Geophysical Union 85(24), 233-233.

Engelhard, B. (2010) Rooftop to tabletop: Repurposing urban roofs for food production, Master thesis University of Washington.

EPA (2012) 2012 guidelines for water reuse, US Agency for International Development Washington, DC.

Ervin E., A.B., and G. Evanylo (2013) Development and testing of EQ biosolids mixes for amending disturbed urban soils and improving tall fescue drought resistance, Long Beach, CA.

Escala, M., Zumbuhl, T., Koller, C., Junge, R. and Krebs, R. (2013) Hydrothermal carbonization as an energy-efficient alternative to established drying technologies for sewage sludge: a feasibility study on a laboratory scale. Energy & Fuels 27(1), 454-460.

Esen, M. and Yuksel, T. (2013) Experimental evaluation of using various renewable energy sources for heating a greenhouse. Energy and Buildings 65, 340-351.

Focazio, M.J., Kolpin, D.W., Barnes, K.K., Furlong, E.T., Meyer, M.T., Zaugg, S.D., Barber, L.B. and Thurman, M.E. (2008) A national reconnaissance for pharmaceuticals and other organic wastewater contaminants in the United States--II) untreated drinking water sources. Science of the Total Environment 402(2-3), 201-216.

Funke, A. and Ziegler, F. (2010) Hydrothermal carbonization of biomass: a summary and discussion of chemical mechanisms for process engineering. Biofuels, Bioproducts and Biorefining 4(2), 160-177.

Garnett, T. and Gillie, L. (1999) CityHarvest: The feasibility of growing more food in London, Sustain London.

Germer, J., Sauerborn, J., Asch, F., de Boer, J., Schreiber, J., Weber, G. and Müller, J. (2011) Skyfarming an ecological innovation to enhance global food security. Journal für Verbraucherschutz und Lebensmittelsicherheit 6(2), 237.

Getter, K.L. and Rowe, D.B. (2006) The role of extensive green roofs in sustainable development. HortScience 41(5), 1276-1285.

Gobina, E. (2004) Carbon dioxide utilization and recovery. BCC Report E-131, Business Communications Company, Norwalk, CT.

Goh, C., Short, M.D., Bolan, N.S. and Saint, C.P. (2018) Biosolids: the growing potential for use. Unmaking Waste in Production and Consumption: Towards the Circular Economy; Emerald Publishing Limited: Bingley, UK, 67-88.

Goldstein, B., Hauschild, M., Fernandez, J. and Birkved, M. (2016) Urban versus conventional agriculture, taxonomy of resource profiles: a review. Agronomy for sustainable development 36(1), 9.

Gottschall, N., Topp, E., Edwards, M., Russell, P., Payne, M., Kleywegt, S., Curnoe, W. and Lapen, D.R. (2010) Polybrominated diphenyl ethers, perfluorinated alkylated substances, and metals in tile drainage and groundwater following applications of municipal biosolids to agricultural fields. Science of the Total Environment 408(4), 873-883.

Gregory, J.H., Dukes, M.D., Jones, P.H. and Miller, G.L. (2006) Effect of urban soil compaction on infiltration rate. Journal of soil and water conservation 61(3), 117-124.

Guest, J.S., Skerlos, S.J., Barnard, J.L., Beck, M.B., Daigger, G.T., Hilger, H., Jackson, S.J., Karvazy, K., Kelly, L. and Macpherson, L. (2009) A new planning and design paradigm to achieve sustainable resource recovery from wastewater. Environmental science & technology 43(16), 6126-6130.

Hadi, P., Xu, M., Ning, C., Lin, C.S.K. and McKay, G. (2015) A critical review on preparation, characterization and utilization of sludge-derived activated carbons for wastewater treatment. Chemical engineering journal 260, 895-906.

Halling-Sørensen, B., Nors Nielsen, S., Lanzky, P.F., Ingerslev, F., Holten Lützhøft, H.C. and Jørgensen, S.E. (1998) Occurrence, fate and effects of pharmaceutical substances in the environment- A review. Chemosphere (Oxford) 36(2), 357-393.

Halweil, B. (2002) Home grown: the case for local food in a global market, Worldwatch Institute, Washington, DC

Hamilton, A.J., Burry, K., Mok, H.-F., Barker, S.F., Grove, J.R. and Williamson, V.G. (2014) Give peas a chance? Urban agriculture in developing countries. A review. Agronomy for sustainable development 34(1), 45-73.

He, Z.L., Yang, X.E. and Stoffella, P.J. (2005) Trace elements in agroecosystems and impacts on the environment. Journal of Trace Elements in Medicine and Biology 19(2), 125-140.

Heidler, J. and Halden, R.U. (2008) Meta-Analysis of Mass Balances Examining Chemical Fate during Wastewater Treatment. Environmental Science & Technology 42(17), 6324-6332.

Heimlich, R.E. and Barnard, C.H. (1997) Agricultural adaptation to urbanization: Farm types and agricultural sustainability in US Metropolitan Areas. Rural sustainable development in America, 283-303.

Heinemann, E., Prato, B. and Shepherd, A. (2011) Rural poverty report 2011. International Fund for Agricultural Development (IFAD), Rome.

Hodgson, K., Campbell, M.C. and Bailkey, M. (2011) Urban agriculture: Growing healthy, sustainable places, American Planning Association, Chicago, Illinois.

Honeyman, M.K. (1992) Vegetation and stress: a comparison study of varying amounts of vegetation in countryside and urban scenes. The role of horticulture in human well-being and social development, 143-145.

Hou, J., Johnson, J.M. and Lawson, L.J. (2009) Greening Cities, Growing Communities: Learning from Seattle's Urban Community Gardens, Landscape Architecture Foundation, Washington, DC.

Huertas, J., Giraldo, N. and Izquierdo, S. (2011) Removal of H2S and CO2 from Biogas by Amine Absorption. Mass Transfer in Chemical Engineering Processes, 133-150.

Hundal, L., Kumar, K., Basta, N. and Cox, A. (2011) Evaluating exposure risk to trace organic chemicals in biosolids. Biocycle 52(4), 31-36.

Hunger, H.S.C.o. (1990) Food Security in the United States, US Government Printing Office Washington, DC.

Hynes, H.P. and Howe, G. (2002) Urban horticulture in the contemporary United States: personal and community benefits, pp. 171-181.

Johnson, O.A., Napiah, M. and Kamaruddin, I. (2014) Potential uses of waste sludge in construction industry: a review. Research Journal of Applied Sciences, Engineering and Technology 8(4), 565-570.

Johnston, J. and Baker, L. (2005) Eating outside the box: FoodShare’s good food box and the challenge of scale. Agriculture and human values 22(3), 313-325.

Johnston, T.E., Stephens, A.B., Challenger, L.C., Elliott, H.A., Brandt, R.C., Taylor, M., Zurek, L., Evanylo, G., Felton, G. and Toffey, W.E. (2019) High Quality Biosolids from Wastewater.

Kaill-Vinish, P. (2009) Toronto green roof policy and roof top food production. Plan Canada 49(2), 39-41.

Kambo, H.S. and Dutta, A. (2014) Strength, storage, and combustion characteristics of densified lignocellulosic biomass produced via torrefaction and hydrothermal carbonization. Applied Energy 135, 182-191.

Kaplan, R. and Kaplan, S. (1990) Restorative experience: The healing power of nearby nature. The Meaning of Gardens. MIT Press, Cambridge, 238-243.

Karnjanapiboonwong, A., Suski, J.G., Shah, A.A., Cai, Q., Morse, A.N. and Anderson, T.A. (2011) Occurrence of PPCPs at a Wastewater Treatment Plant and in Soil and Groundwater at a Land Application Site. Water, Air, & Soil Pollution 216(1), 257-273.

Kataki, S., West, H., Clarke, M. and Baruah, D.C. (2016) Phosphorus recovery as struvite: Recent concerns for use of seed, alternative Mg source, nitrogen conservation and fertilizer potential. Resources, Conservation and Recycling 107, 142-156.

Khan, I.U., Othman, M.H.D., Hashim, H., Matsuura, T., Ismail, A., Rezaei-DashtArzhandi, M. and Azelee, I.W. (2017) Biogas as a renewable energy fuel–A review of biogas upgrading, utilisation and storage. Energy Conversion and Management 150, 277-294.

Kinney, C.A., Furlong, E.T., Zaugg, S.D., Burkhardt, M.R., Werner, S.L., Cahill, J.D. and Jorgensen, G.R. (2006) Survey of Organic Wastewater Contaminants in Biosolids Destined for Land Application. Environmental Science & Technology 40(23), 7207-7215.

Kortright, R. and Wakefield, S. (2011) Edible backyards: a qualitative study of household food growing and its contributions to food security. Agriculture and human values 28(1), 39-53.

Kumar, K., Hundal, L.S., Bastian, R.K. and Davis, B. (2017) Land Application of Biosolids: Human Health Risk Assessment Related to Microconstituents, Water Environment Federation, Virginia.

Kümmerer, K. (2008) Pharmaceuticals in the Environment, pp. 3-21, Springer, Berlin.

Lamptey, B., Barron, E. and Pollard, D. (2005) Impacts of agriculture and urbanization on the climate of the Northeastern United States. Global and Planetary Change 49(3-4), 203-221.

Lapen, D.R., Topp, E., Metcalfe, C.D., Li, H., Edwards, M., Gottschall, N., Bolton, P., Curnoe, W., Payne, M. and Beck, A. (2008) Pharmaceutical and personal care products in tile drainage following land application of municipal biosolids. Science of the Total Environment 399(1–3), 50-65.

LeBlanc, R.J., Matthews, P. and Richard, R.P. (2009), p. 605, United Nations Human Settlements Programme (UN-HABITAT), Kenya.

Libra, J.A., Ro, K.S., Kammann, C., Funke, A., Berge, N.D., Neubauer, Y., Titirici, M.-M., Fühner, C., Bens, O. and Kern, J. (2011) Hydrothermal carbonization of biomass residuals: a comparative review of the chemistry, processes and applications of wet and dry pyrolysis. Biofuels 2(1), 71-106.

Liu, X., Liang, C., Liu, X., Zhao, F. and Han, C. (2020) Occurrence and human health risk assessment of pharmaceuticals and personal care products in real agricultural systems with long-term reclaimed wastewater irrigation in Beijing, China. Ecotoxicology and Environmental Safety 190, 110022.

Lohrberg, F., Lička, L., Scazzosi, L. and Timpe, A. (2016), pp. 19-24, Jovis, Berlin.

Loos, R., Carvalho, R., António, D.C., Comero, S., Locoro, G., Tavazzi, S., Paracchini, B., Ghiani, M., Lettieri, T., Blaha, L., Jarosova, B., Voorspoels, S., Servaes, K., Haglund, P., Fick, J., Lindberg, R.H., Schwesig, D. and Gawlik, B.M. (2013) EU-wide monitoring survey on emerging polar organic contaminants in wastewater treatment plant effluents. Water Research 47(17), 6475-6487.

Lovell, S.T. (2010) Multifunctional urban agriculture for sustainable land use planning in the United States. Sustainability 2(8), 2499-2522.

Lu, D. and Weng, Q. (2006) Use of impervious surface in urban land-use classification. Remote Sensing of Environment 102(1-2), 146-160.

Lu, Y., Silveira, M.L., Vendramini, J.M.B., Erickson, J.E. and Li, Y. (2020) Biosolids and biochar application effects on bahiagrass herbage accumulation and nutritive value. Agronomy Journal 112(2), 1330-1345.

Luo, X., Ge, X., Cui, S. and Li, Y. (2016) Value-added processing of crude glycerol into chemicals and polymers. Bioresource technology 215, 144-154.

Manara, P. and Zabaniotou, A. (2012) Towards sewage sludge based biofuels via thermochemical conversion–a review. Renewable and Sustainable Energy Reviews 16(5), 2566-2582.

Mantovi, P., Baldoni, G. and Toderi, G. (2005) Reuse of liquid, dewatered, and composted sewage sludge on agricultural land: effects of long-term application on soil and crop. Water Research 39(2-3), 289-296.

McCarty, P.L., Bae, J. and Kim, J. (2011) Domestic wastewater treatment as a net energy producer–can this be achieved? Environmental science & technology 45(17), 7100–7106.

McIvor, K., Cogger, C. and Brown, S. (2012) Effects of Biosolids Based Soil Products on Soil Physical and Chemical Properties in Urban Gardens. Compost Science & Utilization 20(4), 199-206.

Melo, T.M., Bottlinger, M., Schulz, E., Leandro, W.M., de Oliveira, S.B., de Aguiar Filho, A.M., El-Naggar, A., Bolan, N., Wang, H. and Ok, Y.S. (2019) Management of biosolids-derived

hydrochar (Sewchar): Effect on plant germination, and farmers' acceptance. Journal of environmental management 237, 200-214.

Miccoli, S., Finucci, F. and Murro, R. (2016) Feeding the cities through urban agriculture the community esteem value. Agriculture and Agricultural Science Procedia 8, 128-134.

Michael, C., Dirk, C., Harald, K., Jan, R. and Joachim, V. (2012) Policy paper on bio-based economy in the EU: level playing field for bio-based chemistry and materials., nova-Institut, Germany.

Miller, E.L., Nason, S.L., Karthikeyan, K.G. and Pedersen, J.A. (2016) Root Uptake of Pharmaceuticals and Personal Care Product Ingredients. Environmental Science & Technology 50(2), 525-541.

Mogk, J.E., Wiatkowski, S. and Weindorf, M.J. (2010) Promoting urban agriculture as an alternative land use for vacant properties in the city of Detroit: Benefits, problems and proposals for a regulatory framework for successful land use integration. Wayne L. Rev. 56, 1521.

Mok, H.-F., Williamson, V.G., Grove, J.R., Burry, K., Barker, S.F. and Hamilton, A.J. (2014) Strawberry fields forever? Urban agriculture in developed countries: a review. Agronomy for sustainable development 34(1), 21-43.

Møller, J., Boldrin, A. and Christensen, T.H. (2009) Anaerobic digestion and digestate use: accounting of greenhouse gases and global warming contribution. Waste management & research 27(8), 813-824.

Morgan-Sagastume, F., Valentino, F., Hjort, M., Cirne, D., Karabegovic, L., Gerardin, F., Johansson, P., Karlsson, A., Magnusson, P. and Alexandersson, T. (2014) Polyhydroxyalkanoate (PHA) production from sludge and municipal wastewater treatment. Water Science and Technology 69(1), 177-184.

Mougeot, L.J. (1996) Introduction: an improving domestic and international environment for African urban agriculture. African Urban Quarterly 11(2-3), 137-152.

Mougeot, L.J. (2000) Urban Agriculture: Definition, Presence, Potentials and Risks, and Policy Challenges. Cities Feeding People Series, Report 31. International Development Research Centre (IDCR), Canada.

Nakakubo, T., Tokai, A. and Ohno, K. (2012) Comparative assessment of technological systems for recycling sludge and food waste aimed at greenhouse gas emissions reduction and phosphorus recovery. Journal of Cleaner Production 32, 157-172.

Nambuthiri, S., Schnelle, R., Fulcher, A., Geneve, R., Koeser, A., Verlinden, S. and Conneway, R. (2013) Alternative containers for a sustainable greenhouse and nursery crop production, Univeristy of Kentucky Cooperative Extension Service, Kentucky.

Nikodinovic-Runic, J., Guzik, M., Kenny, S.T., Babu, R., Werker, A. and Connor, K.E. (2013) Advances in applied microbiology, pp. 139-200, Elsevier, The Netherlands.

Nilsen, E., Smalling, K.L., Ahrens, L., Gros, M., Miglioranza, K.S.B., Picó, Y. and Schoenfuss, H.L. (2019) Critical review: Grand challenges in assessing the adverse effects of contaminants of emerging concern on aquatic food webs. Environmental Toxicology and Chemistry 38(1), 46-60.

Organization, W.H. (2006) WHO guidelines for the safe use of wasterwater excreta and greywater, p. 25, World Health Organization, Switzerland.

Orsini, F., Kahane, R., Nono-Womdim, R. and Gianquinto, G. (2013) Urban agriculture in the developing world: a review. Agronomy for sustainable development 33(4), 695-720.

Ozores-Hampton, M., Stansly, P.A. and Salame, T.P. (2011) Soil chemical, physical, and biological properties of a sandy soil subjected to long-term organic amendments. Journal of Sustainable Agriculture 35(3), 243-259.

Pabi, S., Amarnath, A., Goldstein, R. and Reekie, L. (2013) Electricity use and management in the municipal water supply and wastewater industries, Electric Power Research Institute, Palo Alto, California.

Pagliai, M. and Antisari, L.V. (1993) Influence of waste organic matter on soil micro-and macrostructure. Bioresource technology 43(3), 205-213.

Pal, A., Gin, K.Y.-H., Lin, A.Y.-C. and Reinhard, M. (2010) Impacts of emerging organic contaminants on freshwater resources: Review of recent occurrences, sources, fate and effects. Science of the Total Environment 408(24), 6062-6069.

Paramashivam, D., Clough, T.J., Carlton, A., Gough, K., Dickinson, N., Horswell, J., Sherlock, R.R., Clucas, L. and Robinson, B.H. (2016) The effect of lignite on nitrogen mobility in a low-fertility soil amended with biosolids and urea. Science of the Total Environment 543, 601-608.

Paramashivam, D., Dickinson, N.M., Clough, T.J., Horswell, J. and Robinson, B.H. (2017) Potential environmental benefits from blending biosolids with other organic amendments before application to land. Journal of environmental quality 46(3), 481-489.

Patel, M., Kumar, R., Kishor, K., Mlsna, T., Pittman, C.U. and Mohan, D. (2019) Pharmaceuticals of Emerging Concern in Aquatic Systems: Chemistry, Occurrence, Effects, and Removal Methods. Chemical Reviews 119(6), 3510-3673.

Paxton, A. (1994) The Food Miles Report: the Dangers of Long Distance Food Transport; Safe Alliance: London, 1994, Safe Alliance, London.

Peterson, A.A., Vogel, F., Lachance, R.P., Fröling, M., Antal Jr, M.J. and Tester, J.W. (2008) Thermochemical biofuel production in hydrothermal media: a review of sub-and supercritical water technologies. Energy & environmental science 1(1), 32-65.

Pietrzak, R. and Bandosz, T.J. (2008) Interactions of NO2 with sewage sludge based composite adsorbents. Journal of hazardous materials 154(1-3), 946-953.

Plakias, A.C. (2016) The farm on the roof: What Brooklyn Grange taught us about entrepreneurship, community, and growing a sustainable business, Penguin Publishing Group, New York.

Punshon, T., Adriano, D.C. and Weber, J.T. (2002) Restoration of drastically eroded land using coal fly ash and poultry biosolid. Science of the Total Environment 296(1-3), 209-225.

Rasi, S., Veijanen, A. and Rintala, J. (2007) Trace compounds of biogas from different biogas production plants. Energy 32(8), 1375-1380.

Reyes, N.J.D.G., Geronimo, F.K.F., Yano, K.A.V., Guerra, H.B. and Kim, L.-H. (2021) Pharmaceutical and Personal Care Products in Different Matrices: Occurrence, Pathways, and Treatment Processes. Water 13(9), 1159.

Ruetten, J., Birkhoff, J., Darr, K., Drewes, J., Flatt, J., Kelso, D., McDaniel, M. and Noble, D. (2004) Best Practices for Developing Indirect Potable Reuse Project: Phase 1 Report, WateReuse Foundation Alexandria, Virginia.

Ruiz, C., Kenny, S., Walsh, M. and O'Connor, K. (2014) Production of biodegradable plastic by bacteria using waste resources. Science & Solutions for a Sustainable Environment 9(1), 509.

Ryckebosch, E., Drouillon, M. and Vervaeren, H. (2011) Techniques for transformation of biogas to biomethane. Biomass and bioenergy 35(5), 1633-1645.

Saldivar-Tanaka, L. and Krasny, M.E. (2004) Culturing community development, neighborhood open space, and civic agriculture: The case of Latino community gardens in New York City. Agriculture and human values 21(4), 399-412.

Sanyé-Mengual, E., Oliver-Solà, J., Montero, J.I. and Rieradevall, J. (2015) An environmental and economic life cycle assessment of rooftop greenhouse (RTG) implementation in Barcelona, Spain. Assessing new forms of urban agriculture from the greenhouse structure to the final product level. The International journal of life cycle assessment 20(3), 350-366.

Semblante, G.U., Hai, F.I., Huang, X., Ball, A.S., Price, W.E. and Nghiem, L.D. (2015) Trace organic contaminants in biosolids: Impact of conventional wastewater and sludge processing technologies and emerging alternatives. Journal of Hazardous materials 300, 1-17.

Shanmugam, S., Abbott, L.K. and Murphy, D.V. (2014) Clay addition to lime-amended biosolids overcomes water repellence and provides nitrogen supply in an acid sandy soil. Biology and fertility of soils 50(7), 1047-1059.

Shaun, R.B. and Williams, B.E. (2017) Biosolids Promote Similar Plant Growth and Quality Responses as Conventional and Slow-release Fertilizers. HortTechnology hortte 27(6), 794-804.

Simmler, M., Ciadamidaro, L., Schulin, R., Madejón, P., Reiser, R., Clucas, L., Weber, P. and Robinson, B. (2013) Lignite reduces the solubility and plant uptake of cadmium in pasturelands. Environmental science & technology 47(9), 4497-4504.

Smith, K., Fowler, G., Pullket, S. and Graham, N.J.D. (2009) Sewage sludge-based adsorbents: a review of their production, properties and use in water treatment applications. Water research 43(10), 2569-2594.

Song, C. (2006) Global challenges and strategies for control, conversion and utilization of CO2 for sustainable development involving energy, catalysis, adsorption and chemical processing. Catalysis today 115(1-4), 2-32.

Spinosa, L. (2004) From sludge to resources through biosolids. Water Science and Technology 50(9), 1-9.

Spokas, K., Koskinen, W., Baker, J. and Reicosky, D. (2009) Impacts of woodchip biochar additions on greenhouse gas production and sorption/degradation of two herbicides in a Minnesota soil. Chemosphere 77(4), 574-581.

Stamatelatou, K. and Tsagarakis, K.P. (2015) Sewage treatment plants: Economic evaluation of innovative technologies for energy efficiency, IWA Publishing, London.

Stasta, P., Boran, J., Bebar, L., Stehlik, P. and Oral, J. (2006) Thermal processing of sewage sludge. Applied Thermal Engineering 26(13), 1420-1426.

Stoffella, P.J., Ozores-Hampton, M., Roe, N.E., Li, Y. and Obreza, T.A. (2001) Compost utilization in vegetable crop production systems, pp. 125-128.

Stone, P.F. (2017) Evaluation of Biosolids for Use in Biodegradable Transplant Containers. Doctoral dissertation, Virginia Tech, Virginia.

Stuart, T. (2009) Waste: Uncovering the global food scandal, WW Norton & Company, New York.

Sydnor, M. and Redente, E. (2002) Reclamation of high-elevation, acidic mine waste with organic amendments and topsoil. Journal of environmental quality 31(5), 1528-1537.

Takashi, A., Franklin, B. and Harold, L. (2007) Water reuse: Issues, technologies, and applications, McGraw-Hill Education, New York.

Tan, Z. and Lagerkvist, A. (2011) Phosphorus recovery from the biomass ash: A review. Renewable and Sustainable Energy Reviews 15(8), 3588-3602.

Tasca, A.L., Nessi, S. and Rigamonti, L. (2017) Environmental sustainability of agri-food supply chains: An LCA comparison between two alternative forms of production and distribution of endive in northern Italy. Journal of Cleaner Production 140, 725-741.

Taylor, J.R. and Lovell, S.T. (2012) Mapping public and private spaces of urban agriculture in Chicago through the analysis of high-resolution aerial images in Google Earth. Landscape and urban planning 108(1), 57-70.

Tchobanoglous, G.L.F., H. Burton, and D. Stensel. (2003) Wastewater engineering : treatment and reuse, McGraw-Hill, Boston.

Tchounwou, P.B., Yedjou, C.G., Patlolla, A.K. and Sutton, D.J. (2012) Heavy metal toxicity and the environment. Experientia supplementum (2012) 101, 133-164.

Tian, H., Lu, C., Pan, S., Yang, J., Miao, R., Ren, W., Yu, Q., Fu, B., Jin, F.-F. and Lu, Y. (2018) Optimizing resource use efficiencies in the food–energy–water nexus for sustainable agriculture: From conceptual model to decision support system. Current Opinion in Environmental Sustainability 33, 104-113.

Tilman, D., Fargione, J., Wolff, B., D'Antonio, C., Dobson, A., Howarth, R., Schindler, D., Schlesinger, W.H., Simberloff, D. and Swackhamer, D. (2001) Forecasting agriculturally driven global environmental change. science 292(5515), 281-284.

Timmons, D. and Wang, Q. (2010) Direct food sales in the United States: evidence from state and county-level data. Journal of Sustainable Agriculture 34(2), 229-240.

Topp, E., Monteiro, S.C., Beck, A., Coelho, B.B., Boxall, A.B.A., Duenk, P.W., Kleywegt, S., Lapen, D.R., Payne, M., Sabourin, L., Li, H. and Metcalfe, C.D. (2008) Runoff of pharmaceuticals and personal care products following application of biosolids to an agricultural field. Science of the Total Environment 396(1), 52-59.

Uchimiya, M., Lima, I.M., Thomas Klasson, K., Chang, S., Wartelle, L.H. and Rodgers, J.E. (2010) Immobilization of heavy metal ions (CuII, CdII, NiII, and PbII) by broiler litter-derived biochars in water and soil. Journal of agricultural and food chemistry 58(9), 5538-5544.

Ulrich, R.S. (1992) Influences of passive experiences with plants on individual well-being and health. The role of horticulture in human well-being and social development, 93-105.

USEPA (1990) Title 40, Code of Federal Regulations. https://www.epa.gov/laws-regulations/regulations#cfr (Accessed 6/29/2020)

USEPA (2008) Contaminants of Emerging Concern including Pharmaceuticals and Personal Care Products. https://www.epa.gov/wqc/contaminants-emerging-concern-including-pharmaceuticals-and-personal-care-products (accessed 02/20/0219).

USEPA (2009) Targeted National Sewage Sludge Survey Sampling and Analysis Technical Report EPA 822-R-08-016. U.S. Environmental Protection Agency Office of Water. https://www.epa.gov/biosolids/sewage-sludge-surveys#2009 (Accessed 2/20/2019).

USEPA (2014) Inventory of US greenhouse gas emissions and sinks: 1990–2012. https://www.epa.gov/ghgemissions/inventory-us-greenhouse-gas-emissions-and-sinks-1990-2012 (Accessed 5/4/2020).

USEPA (2018) Part 503 - Standards for the use or disposal of sewage sludge. https://www.govinfo.gov/content/pkg/CFR-2018-title40-vol32/xml/CFR-2018-title40-vol32-part503.xml (Accessed 2/20/2019).

USEPA (2021a) Biosolids Biennial Report No 8 (Reporting Period 2018-2019) https://www.epa.gov/biosolids/biennial-report-no-8-reporting-period-2018-2019 (Accessed 12/12/2021).

USEPA (2021b) Regulatory Determinations for Pollutants in Biosolids. https://www.epa.gov/biosolids/regulatory-determinations-pollutants-biosolids (Accessed 12/12/2021).

Valderrama, C., Granados, R. and Cortina, J.L. (2013) Stabilisation of dewatered domestic sewage sludge by lime addition as raw material for the cement industry: understanding process and reactor performance. Chemical engineering journal 232, 458-467.

Vandermeer, J., Smith, G., Perfecto, I., Quintero, E., Bezner-Kerr, R., Griffith, D., Ketcham, S., Latta, S., Lin, B. and MacMichaels, P. (2009) Effects of industrial agriculture on global warming and the potential of small-scale agroecological techniques to reverse those effects. New World Agriculture and Ecology Group.

Vietor, D., Schnell, R., Munster, C., Provin, T. and White, R. (2010) Biosolid and alum effects on runoff losses during turfgrass establishment. Bioresource technology 101(9), 3246-3252.

Wang, H., Lin, K., Hou, Z., Richardson, B. and Gan, J. (2010) Sorption of the herbicide terbuthylazine in two New Zealand forest soils amended with biosolids and biochars. Journal of Soils and Sediments 10(2), 283-289.

Washington, K. (2000) Growing food in cities: Urban agriculture in North America, Community Food Security News, New York.

Xia, K., Bhandari, A., Das, K. and Pillar, G. (2005) Occurrence and Fate of Pharmaceuticals and Personal Care Products (PPCPs) in Biosolids. Journal of Environmental Quality 34(1), 91-104.

Xia, K., Hundal, L.S., Kumar, K., Armbrust, K., Cox, A.E. and Granato, T.C. (2010) Triclocarban, triclosan, polybrominated diphenyl ethers, and 4-nonylphenol in biosolids and in soil receiving 33-year biosolids application. Environmental Toxicology and Chemistry 29(3), 597-605.

Yadav, B., Pandey, A., Kumar, L.R. and Tyagi, R.D. (2020) Bioconversion of waste (water)/residues to bioplastics-A circular bioeconomy approach. Bioresource technology 298, 122584.

Yu H., G.E., and K. Haering (2013) Comparisons of exceptional quality biosolids amendments as disturbed soil amendments. Poster 3010, Tampa, FL.

Zasada, I. (2011) Multifunctional peri-urban agriculture—A review of societal demands and the provision of goods and services by farming. Land use policy 28(4), 639-648.

Zhang, J.-h., LIN, Q.-m. and ZHAO, X.-r. (2014) The hydrochar characters of municipal sewage sludge under different hydrothermal temperatures and durations. Journal of Integrative Agriculture 13(3), 471-482.

Chapter 3 Effects of Nitrate Recycle on the Sludge Densification in Plug-Flow Bioreactors Fed with Real Domestic Wastewater

(This chapter has been published as "Wang, J., An, Z., Zhang, X., Angelotti, B., Brooks, M., and Wang, Z.W. (2023), Effects of Nitrate Recycle on the Sludge Densification in Plug-Flow Bioreactors Fed with Real Domestic Wastewater, Processes, DOI: https://doi.org/10.3390/pr11071876)

3.1 Abstract

The impact of adding a modified Ludzack–Ettinger (MLE) configuration with Nitrate Recycle (NRCY) on continuous-flow aerobic granulation has yet to be explored. The potential negative effects of MLE on sludge densification include that: (1) bioflocs brought by NRCY could compete with granules in feast zones; and (2) carbon addition to anoxic zones could increase the system organic loading rates and lead to higher feast-to-famine ratios. Two pilot-scale plug flow reactor (PFR) systems fed with real domestic wastewater were set up onsite to test these hypotheses. The results showed that MLE configuration with NRCY could hinder the sludge granulation, but the hindrance could be alleviated by the NRCY location change which to some extent also compensates for the negative effect of higher feast-to-famine ratios due to carbon addition in MLE. This NRCY location change can be advantageous to drive sludge densification without a radical washout of the sludge inventory, and had no effects on the chemical oxygen demand (COD) and nitrogen removal efficiencies. The PFR pilot design for the MLE process with a modified NRCY location tested in this study could be developed as an alternative to hydrocyclones for full-scale, greenfield, continuous sludge densification applications.

3.2 Keywords

NRCY; MLE; granular sludge; PFR startup

3.3 Introduction

Process intensification through the employment of advanced cell immobilization techniques such as activated sludge densification via aerobic granulation provides an economical option to expand the treatment capacity of wastewater resource recovery facilities (WRRFs) with low capital, land, and maintenance investment (Kent et al., 2018). To achieve aerobic granulation, hydraulic selection pressure has always been utilized as a driving force to selectively return better settling sludge to the feast zone or phase of either plug flow reactors (PFRs) or sequencing batch reactors (SBRs). This mode of operation selectively favors coaggregation of microbial sludge into aerobic granules by washing out their diffuse flocculent sludge counterpart (Kent et al., 2018). As a result, the transition from flocculent sludge to densified sludge often came at the cost of substantial sludge washout over the course of the reactor startup. This in turn directly resulted in the loss of treatment capacity until the granular sludge inventory within the reactor was slowly re-established (Sun et al., 2019). However, in full-scale applications, WRRFs cannot withstand such a treatment interruption, even if it is temporary, and have to comply with discharge permit limits all the time. Therefore, a strategy is needed to drive densified sludge formation by selectively separating granules and bioflocs while also safeguarding the effluent quality throughout the reactor startup period without treatment degradation or interruption.

Hydrocyclones have been employed in most of the WRRFs to provide such a selection pressure; however, their relatively low hydraulic capacity (e.g. 120-3360 m^3 d^{-1}) limits their application in large systems to sidestream return activated sludge (RAS) where only a small portion, e.g., 5-7%, of the RAS flow can be processed for physical selection (Avila et al., 2021; Partin, 2019; Regmi et al., 2022). This low strength selection pressure plus the high suspended solids content in RAS, e.g., 5000 mg L^{-1}, compromised the physical selection efficiency of hydrocyclones for sludge densification (Ford et al., 2016). As a result, a prolonged startup phase perhaps as long as a year was required to observe significant sludge settleability improvements in full-scale continuous flow reactors in which densified sludge formation is still a challenge (Ford et al., 2016; Kent et al., 2018; Roche et al., 2022; Welling et al., 2015; Wett et al., 2015). For this reason, an alternative strategy should be developed to provide sufficient selection strength to promote successful continuous flow sludge densification while maintaining the startup treatment performance required for large full-

scale applications. To this end, An et al. (2021a) demonstrated a new strategy by continuously returning the sludge in the underflow and overflow of an SBR gravity selector to the feast and famine zones of a plug flow reactor, respectively, which can effectively drive a smoother transition from flocculent activated sludge to granular sludge without dramatic sludge concentration and effluent quality decline during reactor startup. However, this strategy was only proven successful in conventional activated sludge pilot without biological nitrogen removal (BNR) (An et al., 2021a). Its application in a modified Ludzack–Ettinger (MLE) configuration with Nitrate Recycle (NRCY) has yet to be explored. The potential challenges for this could be: 1) NRCY could bring bioflocs to feast zone to compete with granules; 2) carbon addition to anoxic zones could lift the system organic loading rates and result in higher feast-to-famine ratios. Our hypotheses are that by changing the NRCY location, bioflocs could be largely separated from densified sludge which makes the sludge densification achievable. Meanwhile, the higher organic loading rates (OLRs) and feast-to-famine ratios in MLE systems with NRCY caused by carbon addition could hinder the full granulation process. But the hindrance might be compensated to some extent by the NRCY location change.

Thus, two PFR pilots fed with real domestic wastewater were set up onsite to test the hypotheses (Figure 3.1). Compared to the configuration in the study by An et al. (2021a), a NRCY system along with an equalization tank was added, and the SBR gravity selector was modified to a continuous upflow selector, which will be discussed in detail in the following sections. Continuous upflow selectors could be developed using clarifier-like structures with high surface overflow rates (SOR), e.g., 10 m h^{-1}, which was proposed to overcome the practical size limitations of SBR selectors or hydrocyclone in full-scale applications. The results from this study would shed light on how to drive sludge densification through granulation in an MLE process while safeguarding effluent quality during reactor startup and provide a novel approach to enable full-scale application of continuous flow sludge densification technology with reasonable infrastructure modifications.

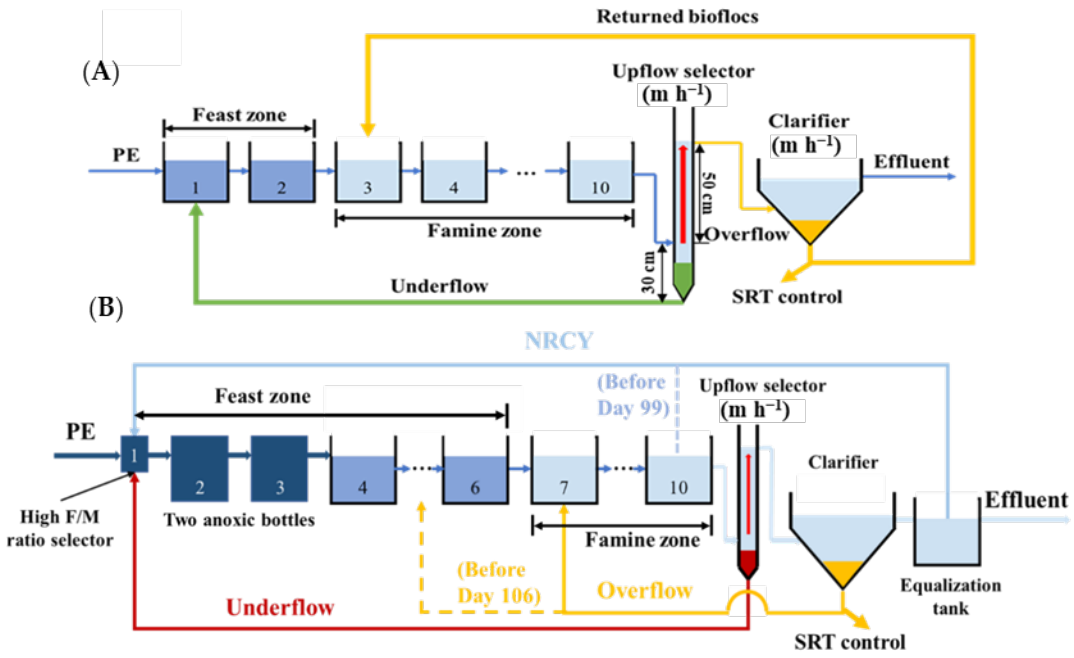

Figure 3.1 Illustrative design of the PFR systems equipped without NRCY (A) and with NRCY (B).

3.4 Material and methods

3.4.1 Reactor setup and operation

Two granulation PFR pilot trains were set up as illustrated in Figure 3.1, and operated in situ by feeding real primary effluent (PE) at the Upper Occoquan Service Authority (UOSA), a WRRF in Centreville, VA, USA. The startup strategy of a conventional activated sludge process was tested using the PFRs configured in Figure 3.1 A and compared to the MLE PFRs with NRCY configurations in Figure 3.1 B. Each PFR pilot with a 140 L total working volume was made of 10 identical completely mixed chambers connected in a series to create feast/famine conditions along the flow direction. The hydraulic retention time of each pilot was controlled at 6.5 h, similar to that of the full-scale secondary process at UOSA. All chambers in Figure 3.1 A and Chambers 4 to 10 in Figure 3.1 B were aerated at a flow rate of 3 L min^{-1} through aeration stones to ensure dissolved oxygen (DO) > 2 mg L^{-1} and maintain homogenous mixing conditions in each chamber. In contrast, the first three chambers in Figure 3.1 B (MLE system with NRCY) were airtight and

kept anoxic by purging nitrogen gas at the beginning and recirculating headspace gas in each chamber afterward. Methanol was added to the first chamber as a carbon source for denitrification. As shown in Figures 3.1 A and B, a continuous upflow column with an internal diameter of 8 cm and a total working height of 80 cm was installed at the end of the PFR to mimic a high-rate clarifier. The column inflow, i.e., the mixed liquor from the PFR effluent, continuously entered at a height of 30 cm from the column bottom and then flowed up for 50 cm before overflowing from the top of the upflow column (Figures 3.1 A and B). The upflow velocity of this column, which is equivalent to the surface overflow rate (SOR) of a clarifier, was set at 10 m h^{-1} based on the flow rate and column cross-section area, to separate the sludge particles based on their settling velocity. Theoretically, only those particles with a settling velocity greater than 10 m h^{-1} can be retained within the underflow of the velocity selector and returned to the first feast zone chamber of the PFR (Figures 3.1 A and B). The unsettled bioflocs in the overflow were sent to another clarifier designed with a more typical SOR of 1 m h^{-1}. A portion of bioflocs settled under this low SOR was wasted on a daily basis for solids retention time (SRT) control (Figures 3.1 A and B). The remainder of the flocculent sludge was returned to the first famine zone of the PFR. The flow rate ratio of the selector overflow to underflow was set at about 1.6. An airlifting method described in a previous study was used to return sludges in Figures 3.1 A and B (Sun et al., 2019). In addition, an equalization tank with an HRT of about 1 h was added to the MLE system after the clarifier (Figure 3.1 B). NRCY in Figure 3.1 B was achieved through a peristaltic pump (Masterflex® L/S, Cole-Parmer, Vernon Hills, IL, USA), and its flow rate to the inflow rate was set at a ratio of 2. The NRCY location was changed from Chamber 10 to the equalization tank on Day 99.

3.4.2 Analytical methods

The chemical oxygen demand (COD), nitrate, nitrite and ammonia concentrations were analyzed using TNTplus® 820, 835, 839 and 840 vials in a spectrophotometer (Hach, Loveland, CO, USA). Nitrate, nitrite, ammonia, and soluble COD (sCOD) samples were measured with the filtrate from 0.45 μm syringe filters (EZFlow®, Old Saybrook, CT, USA). The total inorganic nitrogen (TIN) concentration was calculated by summing nitrate, nitrite and ammonia nitrogen concentrations. DO was measured using an HQ40D meter (Hach, Loveland, CO, USA). The sludge volume index (SVI), zone settling velocity (V_{ZS}), mixed liquor suspended solids (MLSS), mixed liquor volatile

suspended solid (MLVSS), as well as the carbonaceous and nitrogenous specific oxygen uptake rates (SOURs) were analyzed according to standard methods (Baird and Bridgewater, 2017). The 5 min and 30 min SVI were measured using a standard 2 L settle meter and recorded as SVI_5 and SVI_{30}, respectively. It is noteworthy that SVI herein was measured after the dilution of mixed liquor samples to total suspended solids (TSS) concentrations of 1000 mg/L to avoid hindered settling (Baird and Bridgewater, 2017).

3.5 Results

3.5.1 Negative impacts of NRCY on granulation

Figure 3.2 allows a comparison of the settleability improvement in the last chamber of the two PFRs in Figures 3.1 A and B. One (Figures 3.1 A) is a conventional activated sludge process without BNR and the other (Figure 3.1 B) is an MLE process with NRCY and external carbon (methanol) addition. The former appeared to achieve better granulation than the latter. Figure 3.2 A shows that after 141-day operation, SVI30 of the systems without and with NRCY dropped to around 74 mL/g and 100 mL/g, respectively. It can be seen from Figure 3.2 A that SVI_{30} of the system without NRCY somehow started at 153 mL/g which was much higher than that of the system with NRCY (114 mL/g). In addition, SVI_{30} surges in the system without NRCY were observed on Days 36 and 71 due to accidental sludge loss events (Figure 3.2 A). Despite all of those, SVI_{30} of the system without NRCY still dropped to a lower level than that of the system with NRCY after 113-day operation, which indicated that NRCY facilities might hinder the sludge settleability. Meanwhile, SVI_5/SVI_{30} evolution in Figure 3.2 B demonstrated that system without NRCY had lower values than the system with NRCY. For example, after about 140-day operation, SVI_5/SVI_{30} of the system without NRCY plummeted to around 1.5 while the one with NRCY stayed around 2.1. It was reported that SVI_5/SVI_{30} of successful granulation should approximate 1 (Sun et al., 2019). Thus, the system without NRCY likely achieved more granulation than the other with NRCY. This could also be evidenced by the zone velocity (V_{ZS}) profiles in Figure 3.2 C. It can be seen that after around 140-day operation, V_{ZS} of the system without NRCY rose to 5.4 m/h which was 42% higher than that of the system with NRCY.

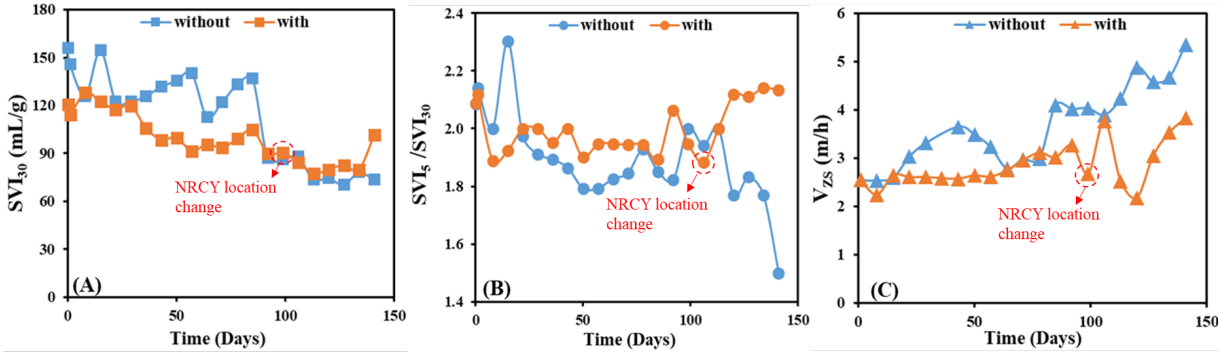

Figure 3.2 Profiles of (A) SVI_{30}, (B) SVI_5/SVI_{30} and (C) V_{zs} measured in the last chamber of the PFR with and without NRCY.

As discussed above, the system could achieve better granulation and thus, better sludge settleability when NRCY was not employed. In other words, the NRCY configuration could be disadvantageous to the aerobic granulation. The potential reasons for this were twofold. Firstly, NRCY located at the end of aerobic zone could bring bioflocs to the feast zone competing with the granules, which defeated the purpose of pilot design. The pilot design herein can take advantage of feast/famine conditions in PFRs to provide biological selection internal to the bioreactors by redirecting the underflow and overflow of the physical velocity selector to the feast and famine zones of the treatment train, respectively (An et al., 2021b). Therefore, the introduction of bioflocs to feast zones might be responsible for the inferior sludge settleability. This challenge was addressed by changing the NRCY location from the last aerobic chamber containing significant MLSS biomass to an equalization tank after biomass separation in the clarifier on Day 99 as shown in Figure 3.1 B. The hypothesis of recirculating flocculent biomass to the feast zone will be tested and discussed in the following sections. Even so, sludge settleability in the system with NRCY was still inferior to the one without NRCY. This could be ascribed to a second reason, i.e., the higher OLRs and feast-to-famine ratios caused by carbon addition. To denitrify NO_3^--N brought by NRCY in the anoxic zone, external carbon (methanol) was added to the first anoxic chamber as shown in Figure 3.1 B, which led to a higher OLR than the one without NRCY (Figure 3.1 A). According to Zhang et al. (2019), decreased OLR enhances the formation and stability of aerobic granular sludge because granular sludge cultivated under decreased OLR maintain the good balance between polysaccharides and protein in the extracellular polymeric substances (EPS) content. Similarly, Ghangrekar et al. (2005) reported that for reactors started at higher OLR, the

SVI of the sludge became higher even if the SVI of inoculum was lower. In addition, average sCOD concentrations in each chamber of two systems were shown in Figure 3.3. One can see that without NRCY, majority of the readily biodegradable sCOD (rbsCOD) was removed in the first two chambers, leaving mostly refractory sCOD in downstream chambers. A feast-to-famine duration ratio of 0.25, as estimated from Figure 3.3, was deemed to be beneficial to aerobic granulation in PFRs (An et al., 2021b). In contrast, with the NRCY configuration and external carbon addition, rbsCOD was not consumed until the Chambers 5 (before NRCY relocation) and 7 (after NRCY relocation), resulting in a feast-to-famine duration ratio of 0.67 and 1.50, respectively, which were considered less favorable for successful granulation (An et al., 2021b). Therefore, the higher organic loading rates and feast-to-famine ratios in MLE system with NRCY (Figure 3.1 B) could explain its inferior granulation process to the one without NRCY (Figure 3.1 A).

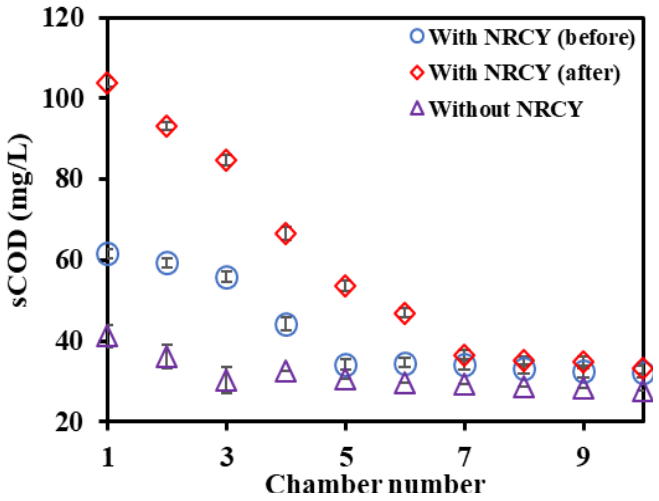

Figure 3.3 Average sCOD concentration profiles of the PFR pilot without NRCY (using data from Days 120 to 134), with NRCY and before its location change (using data from Days 43 to 57), and after its location change (using data from Days 120 to 134).

3.5.2 Effects of NRCY location on solid concentrations

As mentioned in the previous section, it is hypothesized that introduction of bio-flocs to the feast zone by NRCY could be avoided by relocating NRCY from the last aerobic chamber to an

equalization tank after the clarifier. This hypothesis was tested, and the results were revealed in the following sections.

From Day 1 to 98, NCRY was located at the 10th aerobic chamber, which was similar to the full-scale MLE process as shown in Figure 3.1 B. Day 1 to 36 was benchmarked as startup period as shown in Figure 3.4. After the startup, MLVSS profiles of each chamber stabilized (Figure 3.4) during Day 37 to 98 under the combined effects of NRCY and sludge inventory redistribution. Along with NO_3^--N, a huge amount of flocculent biomass in the NRCY stream was returned to the first feast chamber, namely Chamber 1. It is well-known that bioflocs are very competitive in utilizing readily available substrates for a number of reasons. They can outcompete granules because of their looser structure and higher specific surface area that promotes fast substrate diffusion and utilization (Tay et al., 2002). Therefore, returning both flocculent and granular sludges in the NRCY to the same feast zone, as is conventionally practiced, is counterproductive to the progression and stabilization of continuous flow sludge densification. After realizing this, the NRCY location was changed to the equalization tank after the clarifier on Day 99 (Figure 3.1 B). There were very little suspended solids in the equalization tank after the clarifier. Thus, almost no flocs were returned to the feast zone after the location change. Consequently, a substantial drop of MLVSS in all feast chambers was observed as shown in Figure 3.4. For example, average MLVSS concentration in Chamber 1 (C1) plummeted from 1403 to 498 mg/L after the location change. Conversely, MLVSS concentrations in the famine chambers were not subjected to the NRCY location change and thus, barely changed. This was because a large amount of bioflocs from the clarifier were returned to the first famine chamber, namely Chamber 7, by internal sludge inventory redistribution shown in Figure 3.1 B regardless of NRCY location change.

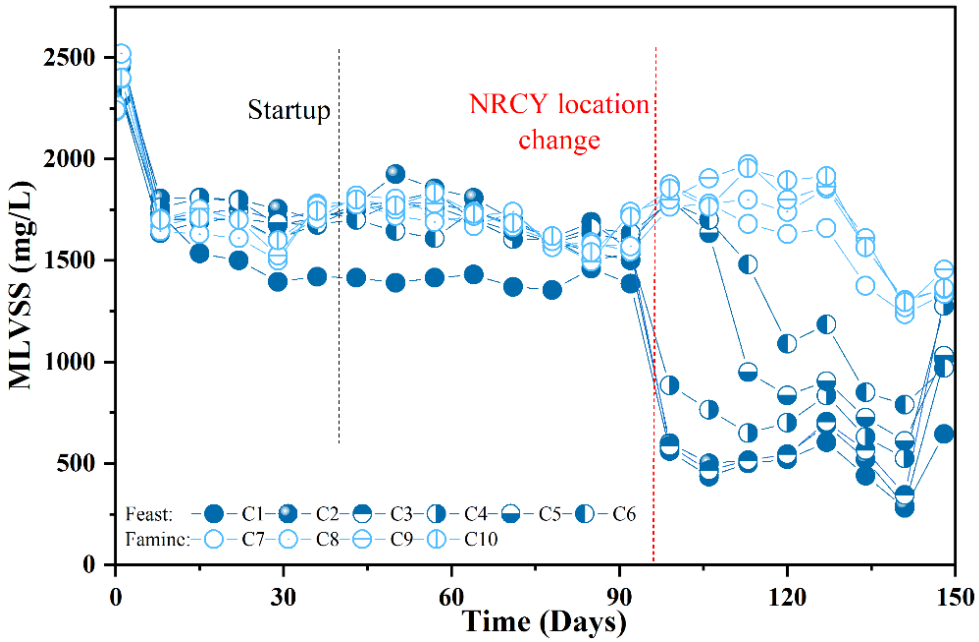

Figure 3.4 MLVSS profiles in different chambers over the course of the pilot operation with NRCY.

With all this being said, sludge concentrations in the entire PFR actually decreased after the switch to the new NRCY source location. This was ascribed to effluent solid concentrations (TSS and VSS) increase (Figure 3.5 A) and an actual SRT decrease (Figure 3.5 B). When NRCY was relocated from the last aerobic chamber to the equalization tank (Figure 3.1 B), the surface overflow rate (SOR) of the clarifier rose from 1 to 1.7 m/h because the additional recycle flow went through the clarifier. Given this, it was anticipated that effluent TSS concentrations would increase. The degree of which was not well accounted for, from 27 mg/L (Day 106) to 73 mg/L (Day 148) after NRCY location change (Figure 3.5 A). SRT was being calculated based only on the waste activated sludge (WAS) being purposely discharged while the actual SRT is impacted by the sludge lost in the clarifier effluent. In retrospect, when SOR of the clarifier was small ($\leq$ 1 m/h), WAS was deemed as the only significant sludge leaving the system, but with the NRCY location change and the increase of SOR, the sludge loss through the effluent ramped up considerably, dropping the actual SRT after Day 99 to as low as 3 days on Day 141 (Figure 3.5 B). Similar to the clarifier, the upflow velocity of the upflow selector also increased from 10 to 17 m/h with the NRCY location change Figure 3.1 B. Less densified sludge was retained in the underflow and more flocs were washed out, which caused the drop of MLVSS concentrations in the underflow of

the upflow selector (Figure 3.6 A). As a result, dry mass ratios of underflow over overflow also declined (Figure 3.6 B).

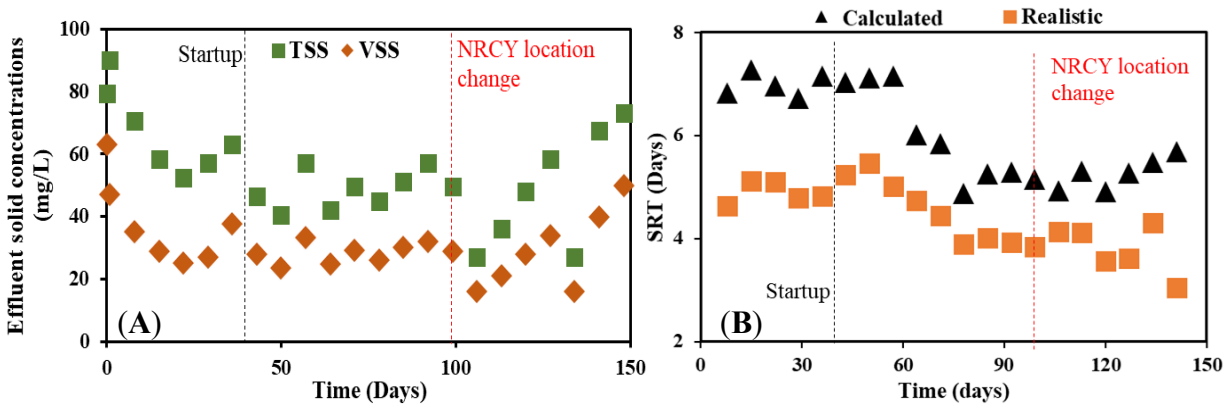

Figure 3.5 (A) Effluent TSS and VSS profiles, and (B) the calculated and realistic SRT profiles.

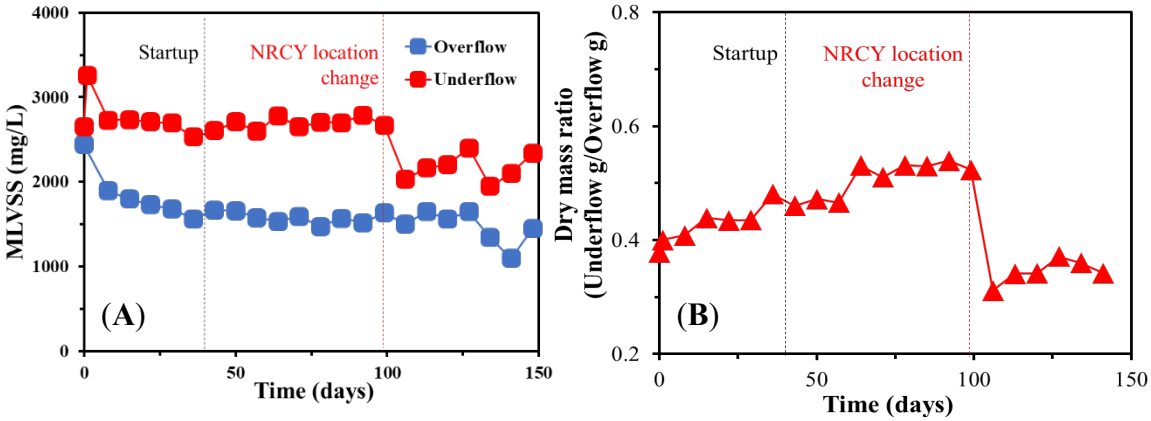

Figure 3.6 (A) MLVSS profiles in overflow and underflow of the upflow selector; (B) Effects of NRCY location changes on the biomass ratio in the underflow and overflow of the upflow selector.

3.5.3 Effects of the NRCY Location on Mixed Liquor Settleability

As mentioned in the previous section, NRCY relocation facilitated the separation and redistribution of heavier densified sludge and lighter bioflocs to the feast and famine zones, respectively. Biofloc out-selection was further boosted by subjecting bio-flocs to low substrate availability. As a result, an improvement of sludge settleability especially in feast chambers was observed after the NRCY location change.

As shown in Figure 3.7, SVI_{30} of all the chambers dropped after the NRCY location change on Day 99. Among those, SVI_{30} of the feast chambers dropped more than that of the famine chambers. For example, SVI_{30} values of Chambers 2, 3 and 4 (C2, C3 & C4) dropped from 73, 74 and 90 mL/g to around 51, 49 and 54 mL/g, respectively, around 50 days after the NRCY location change (Figure 3.7). Kent et al. (2018) suggested an upper limit of 60 mL/g SVI_{30} for successful sludge densification or granulation. With that being said, successful sludge densification has been achieved in the feast chambers such as C2 and C3, which demonstrated the effectiveness of the upflow selector and sludge redistribution system. Similarly, the drops of SVI_5/SVI_{30} values in feast chambers were also observed (Figure 3.8). For example, SVI_5/SVI_{30} of C2, C3, and C4 dropped from 2, 2, and 1.8 to 1.6, 1.3, and 1.5 mL/g, respectively, 50 days after the NRCY location change. It should be pointed out that these SVI_5/SVI_{30} values were still away from 1 which is a theoretical value when successful aerobic granulation was achieved (Schwarzenbeck et al., 2004), indicating the incomplete sludge granulation process. The improved settleability was also evidenced by VZS profiles in Figure 3.9. It can be seen that V_{ZS} of the sludge in all the feast zones increased substantially. Among those, the values of V_{ZS} in C1, C2, C5 and C6 became greater or equal to the upflow velocity of the selector (17 m/h) 50 days after the NRCY location change, which indicated that sludges in these feast chambers were adapted to the reactor's gravity selection pressure.

In contrast, the improvement of sludge settleability in the famine chambers after the NRCY location change was very limited in terms of SVI_{30} (Figure 3.7), SVI_5/SVI_{30} (Figure 3.8) and VZS (Figure 3.9), which indicated that only part of the sludge inventory was densified through the granulation unlike the system without NRCY mentioned in Section 3.1. It appears that the system was headed in the right direction but as a result of unfavorable conditions for entire system granulation, more time would have been needed to nurture the granular sludge formation and weed out the flocculent sludge from the system. One of the bottlenecks is the high feast-to-famine duration ratio due to supplemental carbon addition in the MLE system with NRCY (Figure 3.3).

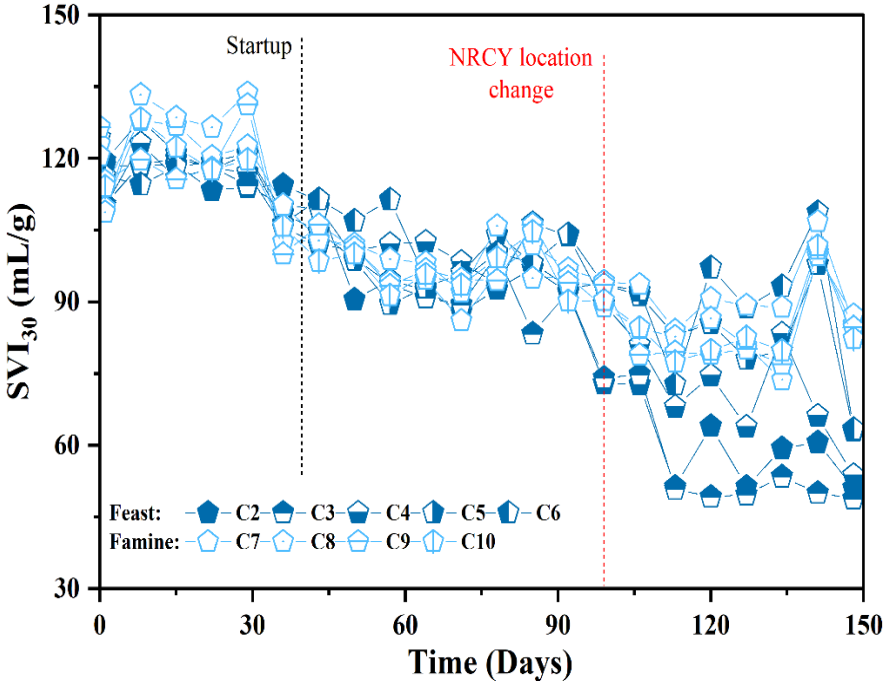

Figure 3.7 SVI_{30} profiles in different chambers over the course of pilot operation

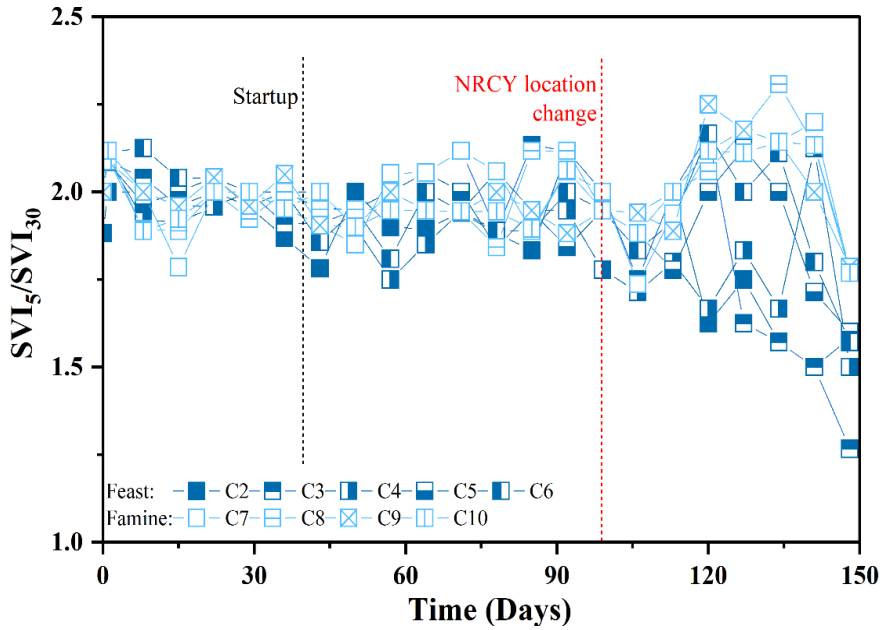

Figure 3.8 SVI_5 /SVI_{30} profiles in different chambers over the course of pilot operation

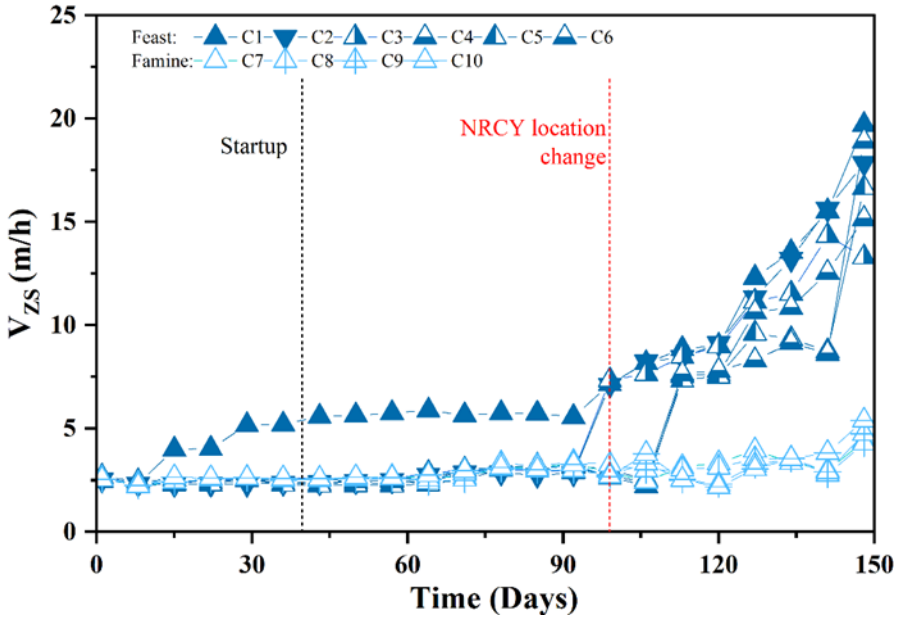

Figure 3.9 SVI_5 /SVI_{30} profiles in different chambers over the course of pilot operation

3.5.4 Effects of NRCY Location on COD and Nitrogen Removal

As discussed in the previous section, after the change of NRCY location, better sludge settleability was observed especially in the feast chambers. However, limited sludge settleability improvement was achieved in the famine zone, which indicated that only part of the sludge inventory was densified through granulation. The potential reason for this could be the relative higher feast and famine ratios of the system after the NRCY location change (Figure 3.1 B). As shown in Figure 3.3, before the NRCY reloca-tion, the majority of the rbsCOD was removed in the first four chambers leaving most-ly refractory sCOD in downstream chambers, which resulted in a feast-to-famine du-ration ratio of 0.67. After the NRCY relocation, MLVSS of the first several chambers declined substantially as mentioned in Section 3.2. Consequently, under the same OLR, rbsCOD was not used up until the seventh chamber after the change of NRCY location, which led to a feast-to-famine duration ratio of 1.5 (Figure 3.3). It was reported by An et al. (2021b) that to achieve successful continuous sludge densification in PFRs, a feast-to-famine duration ratio should be equal to or less than 0.6 in addition to an ad-equate external gravity selection pressure. With this being said, feast-to-famine dura-tion ratios of 0.67 and 1.5 before and after NRCY relocation, respectively, were both considered unfavorable to successful sludge densification in PFRs.

However, the change of NRCY location promoted the sludge densification especially in feast chambers in terms of sludge settleability despite the unfavorable feast-to-famine duration ratio. One can see that biological selection internal to the reactor imposed by separately returning heavier densified sludge and lighter bioflocs to the feast and famine zones with the aid of NRCY relocation, and the increased gravity selection pressure in terms of the upflow velocity in the selector could compensate for the increase of feast-to-famine duration ratios to some extent.

Influent tCOD and sCOD removal efficiencies remained around 75% and 65%, respectively, and they were uninterrupted throughout the entire operation (Figure 3.10). Similarly, ammonia removal efficiencies also remained stable (Figure 3.10) regardless of NRCY location change excluding some fluctuations from Days 71 to 92 due to SRT alteration (Figure 3.5 B), which indicated the good nitrification performance over the course of the operation. These could be explained by the fact that floc recirculation from the bottom of the clarifier allowed the retention of an adequate amount of sludge inventory. Figure 3.11 A and B show the nitrogen profiles on Day 57 (before NRCY location change) and Day 127 (after NRCY location change), respectively. The NRCY location change seemed to have no effect on system total inorganic nitrogen (TIN) removal as both locations resulted in around 70% TIN removal and met the discharge limit of TIN < 10 mg/L. Specifically, system TIN removals mainly relied on the methanol-driven denitrification in the anoxic chambers, especially in C3 (Figures 3.11 A and B). As shown in Figure 3.12, DO concentrations were above 1 mg/L in C1 and C2 but dropped to around 0.6 mg/L in C3 on both Days 57 and 127. In other words, the chambers did not turn strictly anoxic until C3 although methanol was added in C1, and aeration was not employed in the first three chambers. DO concentrations in C1 were even higher than the influent. This could be explained by the fact that NRCY and granule recirculation streams to the C1 were entrained with large amounts of DO. As mentioned in Section 2, these air-uplifted granule streams from the underflow of the upflow selector contained lots of air. The DO was not consumed by ordinary hetero-trophic organisms (OHOs) until the third chamber (C3). As a result, most of the denitrification took place in C3 as shown in Figures 3.11 A and B. The TIN drop in C1 could be ascribed to the dilution caused by the mix of influent, NRCY, and granule recirculation. Nitrification started as the aeration began in C4 and basically, all of the NH4+-N residuals were oxidized to NO_3^--N before C9.

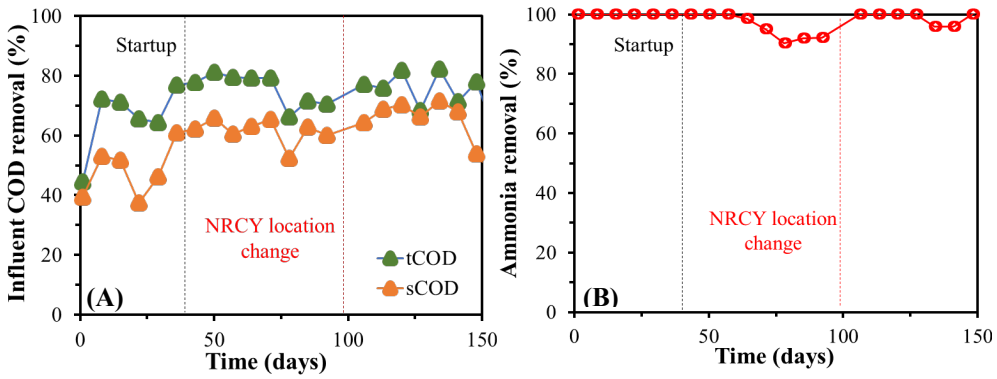

Figure 3.10 Profiles of influent COD and ammonia removal efficiencies over the course of pilot operation.

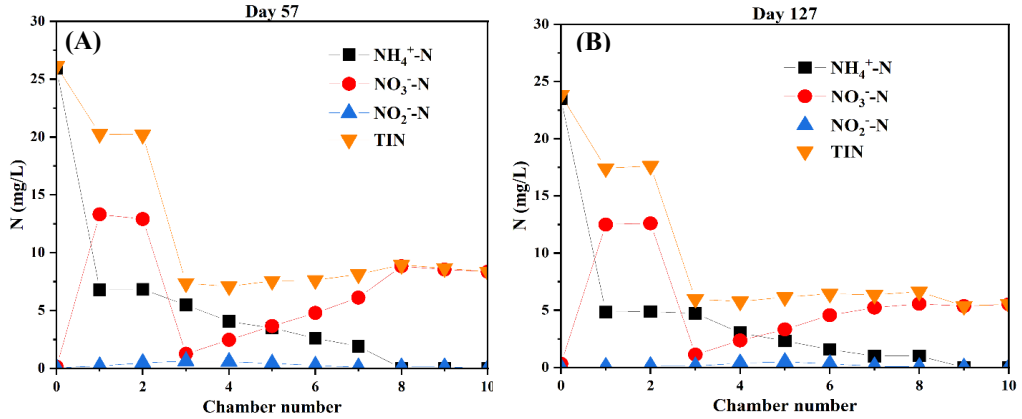

Figure 3.11 Nitrogen concentration profiles in different chambers on Day 57 (A) and Day 127 (B). Chamber 0 refers to influent.

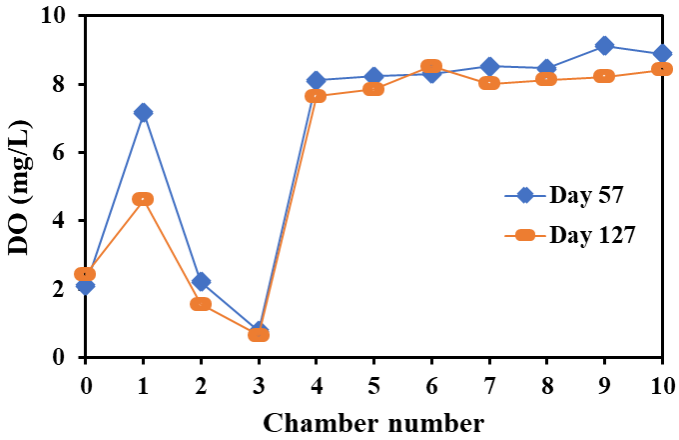

Figure 3.12 DO concentration profiles in different chambers on Day 57 (A) and Day 127 (B). Chamber 0 refers to influent.

3.6 Discussion

3.6.1 The synergy between physical and biological selection pressures

Granulated cells were not able to compete with dispersed cells (biofocs) for the limited substrate availability because bioflocs have looser structure and higher specific surface area that promotes fast substrate diffusion and utilization (Tay et al., 2002). There is consensus that sludge densification is normally driven by physical selection pressure that selectively reduces the persistence of bioflocs in a bioreactor (Kent et al., 2018). For this reason, extremely low SRTs, e.g. 0.3-0.4 days, had to be employed with such a conventional approach to rid the biomass inventory of bioflocs in a radical way (Cofré et al., 2018; Sun et al., 2019) because SRTs of dense granules and bioflocs were not able to be differentiated in previous granulation studies. As an undesirable consequence, the MLVSS in a bioreactor subjected to such a radically short SRT will also have a dramatic reduction in performance resulting in poor effluent quality (Cofré et al., 2018; Sun et al., 2019). This performance loss resulting from the drastic physical out-selection pressure could be resolved by incorporating a strategy that manages to separate flocculent sludge and granule SRTs while incorporating reactor internal bio-logical selection through controlling feast and famine regimes for the distinctly differ-ent sludge morphologies, i.e., selective densified and biofloc returns to feast and famine zones, respectively. As shown in Figure 3.1 B, an upflow selector with selection velocity of 10 ~ 17 m/h offered the possibility for SRT deviation of densified and flocculant sludge. It is noteworthy that other than loss of solids in the final clarifier effluent, bio-floc wasting from the bottom of the clarifier through SRT control is the only outlet for bioflocs to be removed from the PFR system (Figure 3.1 B), and bioflocs were the only type of sludge wasted. The short SRT of bioflocs realized significant outselection of this type of biomass while retention and recirculation of densified sludge resulted in their persistence and dominance in the sludge bed of feast chambers as mentioned in Section 3.3. In contrast to the physical selection provided by the upflow selector external to the bioreactors, biological selection internal to the reactor imposed by separately returning heavier densified sludge and lighter bioflocs to the feast and famine zones further boosted biofloc outselection by subjecting bioflocs to low substrate availability. To this end, an innovation on the NRCY location of an MLE process in a PFR pilot train was conducted in this study as mentioned in the previous sections, i.e., returning ni-trate-rich mix liquor from the

equalization tank after the clarifier instead of the aera-tion tank to avoid returning bioflocs to the feast chambers. This is a novel application of internally biological selection pressure that can boost a continuous flow sludge den-sification and has not been widely accepted in full-scale applications. Consequently, the densified sludge MLSS gradually built up in the PFR, obtaining the advantage from their growth in the feast zone while bioflocs were steadily starved out.

3.6.2 Implications on full-scale application

At present, the most popular continuous flow selectors employed in MLE processes in WRRFs are hydrocyclones which are currently limited to sidestream wasting ap-plications due to technology sizing limitations and associated costs (Partin, 2019; Wett et al., 2015). UOSA has also employed hydrocyclones to successfully enhance its full-scale activated sludge settleability. As designed, only 5% of the RAS was processed through the hydrocyclones. Consequently, only moderate sludge settleability im-provement was observed over 23 months of operation. In contrast, in this study, it only took 148 days to achieve sludge densification in C2, C3, and C4 as indicated by SVI_{30} profiles in Figure 3.7. SVI_{30} of C2, C3, and C4 dropped to below 60 mL/g on Day 148 while SVI30 of the rest of chambers still kept above 60 mL/g (Figure 3.7). If we assume that biomass in C2, C3, and C4 with $SVI_{30} < 60$ mL/g was densified sludge and biomass in other chambers (C5 to C10) was bioflocs as suggested by Kent et al. (2018), then around 32% sludge inventory was densified in terms of MLVSS in Figure 3.4. According to Roche et al. (2022), pursuing full granulation in full-scale application is unnecessary, and only a smaller quantity of aerobic granular sludge proportion, as low as 20%, is sufficient to maintain SVI below 100 mL/g, and could solve a lot of operational problems for plants suffering acute recurring seasonal bulking or subjected to hydraulic overloading beyond original clarifier design while subjected to storm induced peak events. If more time was available for the experiment, it may have been possible to continue to outselect the bioflocs by more aggressively wasting down the SRT of the flocculant biomass and thus not returning those to the feast section in the RAS.

In addition, the design of upflow selector and an equalization tank incorporated in Figure 3.1 B is achievable in WRRFs. For example, the upflow selector mimics a conventional clarifier with a very high SOR so there may, in some cases, be the flexibility to fit upflow physical selector

structures within WRRFs. Therefore, the PFR pilot design (Figure 3.1 B) for MLE process with modified NRCY location tested in this study could be developed as an alternative to hydrocyclones for full-scale, greenfield, continuous sludge densification applications. However, the effluent TSS increase and sludge loss issues mentioned in Section 3.2 after the NRCY location change should be further addressed in future studies.

3.7 Conclusions

The following concluding remarks can be drawn from this study:

1) MLE configuration with NRCY could hinder the sludge granulation but the hindrance could be alleviated by the NRCY location change from the aerobic chamber to the equalization tank after the clarifier.
2) MLE configuration tended to have higher feast-to-famine ratios. But the negative effects of which on the sludge densification could be compensated by NRCY location change to some extent.
3) The NRCY location change in conjunction with floc recirculation and continuous upflow selection can be advantageous to drive sludge densification without radical washout of sludge inventory.
4) The NRCY location change had no effects on COD and nitrogen removal efficiencies.
5) Higher feast-to-famine ratios of the MLE system with NRCY could be the bottleneck for full sludge granulation processes.
6) Future testing of a scenario like this requiring anaerobic or anoxic zones should consider using recycle methods that do not introduce dissolved oxygen. In other words, should not use air lift type pumping.
7) Similarly, mixing of the chamber that houses the source of NRCY should not be mixed with diffused aeration and should use some other form of low shear mixing.

3.8 References

An, Z., Bott, C.B., Angelotti, B., Brooks, M. and Wang, Z.-W. 2021a. Leveraging feast and famine selection pressure during startup of continuous flow aerobic granulation systems to manage treatment performance. Environmental Science: Water Research & Technology 7(9), 1622-1629.

An, Z., Sun, Y., Angelotti, B., Brooks, M. and Wang, Z.-W. 2021b. Densification dependence in continuous flow and sequential batch granulation systems on reactor feast-to-famine duration ratio. Journal of Water Process Engineering 40, 101800.

Avila, I., Freedman, D., Johnston, J., Wisdom, B. and McQuarrie, J. 2021. Inducing granulation within a full-scale activated sludge system to improve settling. Water Science and Technology 84(2), 302-313.

Baird, R.B. and Bridgewater, L. (2017) Standard methods for the examination of water and wastewater, American Public Health Association, Washington, DC, USA.

Cofré, C., Campos, J.L., Valenzuela-Heredia, D., Pavissich, J.P., Camus, N., Belmonte, M., Pedrouso, A., Carrera, P., Mosquera-Corral, A. and Val del Río, A. 2018. Novel system configuration with activated sludge like-geometry to develop aerobic granular biomass under continuous flow. Bioresource technology 267, 778-781.

Ford, A., Rutherford, B., Wett, B. and Bott, C.B. 2016. Implementing hydrocyclones in mainstream process for enhancing biological phosphorus removal and increasing settleability through aerobic granulation. Proceedings of the Water Environment Federation 2016(9), 2809-2822.

Ghangrekar, M., Asolekar, S. and Joshi, S. 2005. Characteristics of sludge developed under different loading conditions during UASB reactor start-up and granulation. Water research 39(6), 1123-1133.

Kent, T.R., Bott, C.B. and Wang, Z.-W. 2018. State of the art of aerobic granulation in continuous flow bioreactors. Biotechnology advances 36(4), 1139-1166.

Partin, A.K. (2019) Hydrocyclone implementation at two wastewater treatment facilities to promote overall settling improvement (Master's Thesis), Virginia Tech, Blacksburg, VA.

Regmi, P., Sturm, B., Hiripitiyage, D., Keller, N., Murthy, S. and Jimenez, J. 2022. Combining continuous flow aerobic granulation using an external selector and carbon-efficient nutrient

removal with AvN control in a full-scale simultaneous nitrification-denitrification process. Water Research 210, 117991.

Roche, C., Donnaz, S., Murthy, S. and Wett, B. 2022. Biological process architecture in continuous-flow activated sludge by gravimetry: Controlling densified biomass form and function in a hybrid granule–floc process at Dijon WRRF, France. Water Environment Research 94(1), e1664.

Schwarzenbeck, N., Erley, R. and Wilderer, P. 2004. Aerobic granular sludge in an SBR-system treating wastewater rich in particulate matter. Water Science and Technology 49(11-12), 41-46.

Sun, Y., Angelotti, B. and Wang, Z.-W. 2019. Continuous-flow aerobic granulation in plug-flow bioreactors fed with real domestic wastewater. Science of the Total Environment 688, 762-770.

Tay, J.H., Liu, Q.S. and Liu, Y. 2002. Characteristics of aerobic granules grown on glucose and acetate in sequential aerobic sludge blanket reactors. Environmental Technology 23(8), 931-936.

Welling, C., Kennedy, A., Wett, B., Johnson, C., Rutherford, B., Baumler, R. and Bott, C.B. 2015. Improving settleability and enhancing biological phosphorus removal through the implementation of hydrocyclones. Proceedings of the Water Environment Federation 2015(17), 6171-6179.

Wett, B., Podmirseg, S.M., Gómez-Brandón, M., Hell, M., Nyhuis, G., Bott, C.B. and Murthy, S. 2015. Expanding DEMON sidestream deammonification technology towards mainstream application. Water Environment Research 87(12), 2084-2089.

Zhang, Z., Qiu, J., Xiang, R., Yu, H., Xu, X. and Zhu, L. 2019. Organic loading rate (OLR) regulation for enhancement of aerobic sludge granulation: Role of key microorganism and their function. Science of The Total Environment 653, 630-637.

Chapter 4 Carbon efficient nutrients removal from real municipal wastewater under conditions of highly variable influent quality and low temperature

(This chapter is ready for submission to a peer-reviewed journal)

4.1 Abstract

In order to achieve carbon efficient nutrient removal of real primary effluent under the conditions of highly variable influent quality and low temperature, this study integrated partial nitrification, endogenous denitrification, partial denitrification-anammox, and enhanced biological phosphorus removal into one advanced pilot design. The pilot system has been operated for 212 days and was able to handle highly variable conditions with the aid of automatic feedback and feedforward controllers nested in secondary and tertiary treatment, respectively. Comparing to the case when full nitrification and full dentification technologies were used to meet the effluent requirement of total inorganic nitrogen (TIN) ≤ 3 mg/L and orthophosphate phosphorus (OP) ≤ 0.1 mg/L, the pilot results showed that 100% carbon and 55.5% oxygen could be saved in the secondary process and another 45.2% carbon could be saved in the tertiary process. More savings can be achieved when a higher TIN discharge level is allowed. To achieve effluent TIN ≤3 mg/L, 44.5% influent TIN was removed through endogenous denitrification in the secondary treatment with another 39.5% TIN polished by partial denitrification-anammox in tertiary treatment. Because there was almost no NO_X-N left at the beginning of each SBR cycle, it was concluded that the mixed liquor recirculation that was popular in traditional design for pre-anoxic zone denitrification can be eliminated to save even more energy. The mechanism of carbon savings was analyzed, and the limitation of the study was also discussed. The outcome of this study should be interesting to engineers and scientists seeking innovative technologies for carbon reduction in wastewater treatment plants.

4.2 Keywords

Partial nitrification, endogenous denitrification, partial denitrification-anammox, enhanced biological phosphorus removal, mainstream treatment

4.3 Introduction

Municipal wastewater treatment performed by conventional activated sludge processes faces challenges of intensive energy and external carbon consumption for biological nutrient removal (BNR), which contributes to significant greenhouse gas (GHG) emissions, hindering the achievement of carbon neutrality (Du et al., 2022). It was reported that 3~4% energy produced in the U.S. was spent on wastewater treatment (Gao et al., 2014; Molinos-Senante and Maziotis, 2022), and approximately 1.6% of global GHG emissions were from wastewater treatment processes (Lu et al., 2018). Nowadays, major energy consumers and GHG producers in wastewater treatment plants (WWTPs) include mixed liquor recirculation (MLR) pumping for pre-anoxic denitrification, aeration for chemical oxygen demand (COD) removal and nitrification, and external carbon addition for discharge nutrient polishing (Maktabifard et al., 2023). For instance, Falk et al. (2013) reported that MLR pumping, nitrification, and denitrification account for around 7.5%, 14.4%, and 15.8% of the total GHG emission of WWTPs, respectively.

To leverage influent organic carbon for denitrification, usually a MLR flow rate four times the primary effluent (PE) flowrate is required (Grady Jr et al., 2011). Pumping such a high MLR flow rate not only is energy consuming but also poses the risk of bringing dissolved oxygen (DO) to the pre-anoxic zone and diluting the influent readily biodegradable COD (rbCOD) (Kim et al., 2015; Pelaz et al., 2018), leading to low reaction rates and in turn increased tank size. Technically, MLR-enabled pre-anoxic denitrification can be replaced by the post-anoxic denitrification which is realized by transporting extracellular rbCOD in the form of intracellular carbon from a pre-anaerobic zone to a post anoxic zone (Bauhs et al., 2022). This intracellular carbon can be either in the form of cell mass or carbon storage such as polyhydroxyalkanoates (PHA) and glycogen. In contrast to the exogenous denitrification enabled by MLR, this study categorizes the intracellular carbon-enabled denitrification as endogenous denitrification (ED). In literature, there were two

lab-scale studies, published from the same research team, focusing on MLR elimination by using post-ED to transport influent organic carbon to the anoxic tank right after nitrification zone for denitrification with no need of MLR (Zhang et al., 2018; Zhao et al., 2018). It should be pointed out that both studies relied on nitritation to reduce the energy consumption and also incorporated enhanced biological phosphorus removal (EBPR) for biologically phosphorus removal (Zhang et al., 2018; Zhao et al., 2018). Both studies achieved effluent TIN of ≤ 3 mg/L and orthophosphate (OP) of < 0.5 mg/L, indicating the validity of using post-ED to replace MLR. However, these studies were performed in laboratory environment with relatively stable influent quality, e.g., soluble COD (sCOD)/N ratios, for provision of sufficient influent rbCOD for ED and EBPR. These studies were also conducted under room temperature (22~26 °C) to facilitate the suppression of nitrite oxidizing bacteria (NOB) for achieving nitritation but not nitrification. It is broadly accepted that nitritation is not applicable for mainstream wastewater treatment in WWTPs located in temperate zones, and the post-ED and EBPR are also known to be sensitive to the variable influent quality (Qiu et al., 2021).

In treatment trains using post ED to replace MLR, a low sCOD/N ratio (e.g. < 6 g/g) in influent could lead to insufficient internal carbon storge by phosphorus accumulating organisms (PAOs) and glycogen accumulating organisms and denitrifying glycogen accumulating organisms (D/GAOs), and in turn a low nutrient removal efficiency (Zhao et al., 2018). On the other hand, an extremely high sCOD/N ratio in influent could lead to either insufficient nitrification or depletion of internal carbon as a result of over-aeration if it is not feedback controlled (Wang et al., 2020). In addition, it was also reported that the optimal sCOD/N ratios for activated sludge settleability was 8~10 g/g, and fluctuating sCOD/N ratios could worsen the sludge settleability (Wang et al., 2019; Ye et al., 2011).

The highly variable influent quality and cold temperatures (10~20 °C) are two major challenges in full-scale application of advanced BNR technologies. A low mainstream temperature (e.g. < 20 °C) could cause ineffective NOB suppression and in turn lead to a failure of nitritation (Qiu et al., 2021). Besides, nitrifying bacteria was reported to be more sensitive to temperature drop than heterotrophs, which could result in decreased nitrification rate and extended aerobic hydraulic retention times (HRTs) (Yuan et al., 2018). Meanwhile, the denitrification rate was also reported

to be 10 times lower with every 50% temperature drop (Erdal, 2002), leading to increased external carbon demand in anoxic zone (Kanda et al., 2017). A dramatic temperature drop could also lead to EBPR performance loss because PAOs are more sensitive to low temperature than D/GAOs, which could make D/GAOs outcompete PAOs on rbCOD utilization (Cavaliere and Baulch, 2019).

Partial denitrification-anammox (PdNA) is a proven technology that can be applied in mainstream wastewater treatment in temperate zones (Campolong, 2019; Huaguang et al., 2023). It was our hypothesis that a synergistic integration of ED with PdNA into a novel system shown in Figure 4.1 can reconcile the aforementioned challenges in achieving carbon-effective BNR. This is because both ED and PdNA require precise feedback and feedforward control, which are naturally advantageous in coping with the highly variable influent quality. In addition, the synergy between ED and PdNA may also bring other advantages that help address the technology applicability concerns. For example, successful ED requires a substantial reduction of aeration intensity and duration for partial nitrification, which not only reduce GHG but also are required conditions for enabling downstream PdNA (Campolong, 2019; Huaguang et al., 2023). Anammox (AMX) is a well-known technology for carbon and GHG reduction because it utilzies ammonia to reduce nitrite to nitrogen gas without external carbon addition. So far, the only mainstream applicable AMX technology to low temperature environment (e.g., < 20 °C) is PdNA because it does not require NOB suppression (Huaguang et al., 2023). Although implementing AMX through PdNA does not eliminate 100% external carbon addition as can be achieved in sidestream partial nitritation anammox (Huaguang et al., 2023), it could still theoretically result in up to 60% reduction in aeration and an 80% reduction in supplemental carbon compared to conventional nitrification/denitrification processes (Sharp et al., 2020). In order to achieve PdNA, only a portion of influent ammonia needs to be nitrified (partial nitrification), and NOB suppression is not required anymore. Hence, aeration can be reduced accordingly, which in turn save internal carbon from excessive aeration (Zhang et al., 2018; Zhao et al., 2018). This means more influent carbon can be allocated for ED when PdNA is applied. Besides, ED is known to be more adaptable to the highly variable, low temperature environment (e.g., < 15°C) than exogenous denitrification (Peng et al., 2023). This is because ED system had less microbial dynamics and sludge morphology changes than exogenous denitrification in response to sudden temperature drop (Peng et al., 2023). Moreover, microorganisms good at intracellular carbon storing, such as that PAO and D/GAOs,

are also known to be denser than ordinary heterotrophic organisms (OHO) (Kent et al., 2018) and thus may compensate the settleability loss caused by fluctuating sCOD/N ratios.

Usually, PdNA is implemented in biofilm reactors for AMX bacteria retention (Campolong, 2019; Huaguang et al., 2023). Both secondary integrated fixed film activated sludge (IFAS) system and tertiary moving bed biofilm reactors (MBBR) have been employed for realizing PdNA at low temperatures of 13~20 °C (Campolong, 2019; Ladipo-Obasa et al., 2022; Macmanus et al., 2022). In this study, we prefer to implement PdNA in a tertiary MBBR (Figure 4.1) because secondary IFAS configurations have disadvantages such as media clogging by suspended growth and compression of the tankage space for PAO proliferation (Grady Jr et al., 2011; Waqas et al., 2023). While tertiary MBBR does not require clarifiers and is directly compatible with downstream filtration processes, which can be employed without major retrofitting of the secondary process. It is also noteworthy that we only utilize the tertiary MBBR as a polishing process with minimum external carbon addition to safeguard the effluent TIN targets. In contrast, we expect majority of the influent TIN to be removed through ED for replacing MLE. To our knowledge, this is the very first study integrating ED and PdNA for TIN removal with the least external carbon input using real municipal wastewater under conditions of highly variable influent quality and low temperature.

Placing PdNA in a tertiary MBBR requires a much higher level of NO_X residue in the secondary effluent, which inevitably elevates the NO_X level in returned activated sludge (RAS). Since the RAS flow rate is usually equal to that of the PE, we are aware that recirculating this high level of NO_X into the pre-anaerobic chamber may negatively impact the performance of EBPR. In order to counteract this side-effect from tertiary PdNA integration, two special designs (Figure 4.1) were made in this study, i.e., i) ED was encouraged in secondary clarifier to remove NO_X as much as possible; and ii) another RAS anoxic zone was added to polish the residual NO_X as did in Johannesburg design to protect the anaerobic zone from taking in NOX through RAS.

To simplify the experimental design, this pilot work used a sequential batch reactor (SBR) to mimic a secondary treatment train capable of EBPR, partial nitrification, secondary clarifier ED, and RAS ED. As for the question whether MLR can be totally eliminated, the answer depends on the level of NO_X to be measured at the end of each SBR cycle, i.e., if majority of NO_X can be removed by

ED without entering the anaerobic phase, we can conclude that MLR can be eliminated. Following the secondary SBR, a tertiary MBBR is added to perform PdNA for effluent polishing. This two-reactor-integrated system has been operated onsite in a local WWTP for 212 days for treating real PE with highly variable influent quality (e.g., 195.9% coefficient of variance (CV) for daily sCOD/N changes) and low temperature (17.9 ± 3.1°C). The operation of the two reactors (SBR and MBBR) were automatically controlled by a synergistic feedback and feedforward control system to smartly cope with the fluctuating influent quality and low temperature. The potential savings and principles underpinning the system were analysed and revealed. The outcome of this study should be interesting to engineers and scientists seeking innovative technologies for carbon reduction in WWTPs.

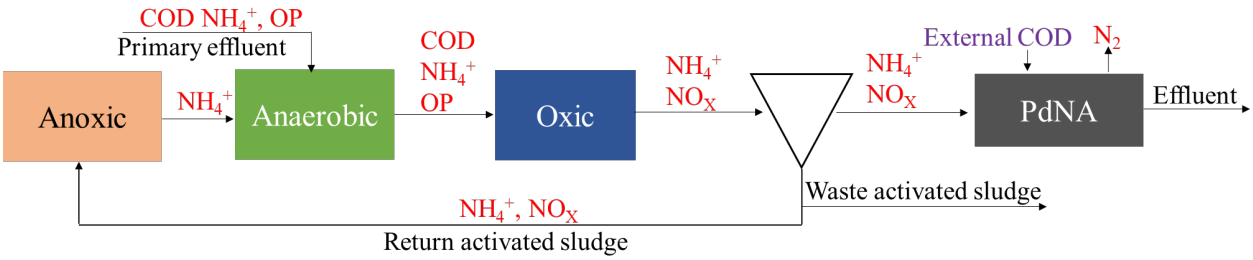

Figure 4.1 Flow chart of the low carbon wastewater treatment system innovated with ED and PdNA integration for MLE elimination

4.4 Material and methods

4.4.1 Reactor setup

The pilot treatment train was housed at Everett WWTP, WA. A SBR with working volume of 26 L and an exchange ratio of 50% was seeded with the BNR sludge for achieving partial nitrification, EBPR and ED. The cycle time of the SBR was four hours, comprising a 10-min feeding phase, a 40-min anaerobic phase, a 80~150-min aeration phase feedback controlled by a NO_x-N/NH_4^+-N ratio setpoint, a 30 min settling phase, a 10 min decant phase, and an idle phase depending on the actual length of the aeration phase regulated by the feedback controller (Figure 4.2a). The anoxic tertiary MBBRs with working volume of 12 L were seeded with a mixture of K5 media (specific surface area of 800 m^2/m^3) established with AMX bacteria and IDI ActiveCell 450 media (specific

surface area of 400 m^2/m^3) established with OHOs with a volumetric ratio of 1:1. The volumetric media filling ratio of the MBBR was 50%. The HRT of the MBBR was 2 hours. The external COD in the form of glycerol (20% v/v) was dosed into the anoxic MBBR by a feedforward controller based on an effluent nitrate setpoint to achieve PdNA. An equalization tank (EQ) was placed between the SBR and MBBR to address two artifact problems incurred by the size of this pilot system, i.e., 1) it equalized the SBR batch effluent into continuous flow feeding for the MBBR as shown in Figure 4.2a; and 2) it prevented the lab-scale NO_X and DO probes from suspended solid interference. This EQ tank is unnecessary in the full-scale continuous flow reactors when industrial scale probes are used because of their good tolerance of suspended solids.

4.4.2 System automation, operation, and sampling procedure

The pilot system was automated by a Python script (Spyder, Python 3.8) in a PC placed onsite and connected to the internet via a hotspot. The input to the Python script was real-time signals from probes for feedback and feedforward control (Figure 4.2a). For feedback control as shown in Figure 4.2b, an ammonium probe (AmmoLyt Plus 700 IQ, Xylem Inc., OH) placed in the SBR and a NO_x & DO probe (EXO NitraLED, Xylem Inc., OH) placed in the EQ tank were used to provide a feedback control loop to ensure the minimum aeration time for achieving the designated NO_x-N/NH_4^+-N ratios. Whenever the NO_x-N/NH_4^+-N ratio reached the setpoint value, the Python program immediately shut off the aeration pump to stop oxygen supply. In the course of 212-day operation, three different SBR effluent NO_x-N/NH_4^+-N ratio setpoints were used in three different operational phases, namely 1.2 ± 0.9 g/g, 2.4 ± 1.2 g/g, and 2.7 ± 0.6 g/g. These increasing NO_x-N/NH_4^+-N ratio setpoints were employed to enhance the downstream TIN removal in MBBR for meet more stringent effluent TIN target. In addition, the solid retention time (SRT) of the SBR was controlled at around 12 days via a peristaltic pump (Masterflex, PA) through mixed liquor discharge.

For feedforward control, the NO_X & DO probes in the EQ tank (Figure 4.2a) were used in a feedforward control loop to control carbon dosing. Real-time NO_x & DO data of the SBR effluent were sent to the Python program. An Ismatec Reglo ICC Digital Pump (Cole-Parmer, IL, USA) receiving signals from the Python program precisely dosed the desired amount of glycerol to the

MBBR according to a feedforward controller as defined in Eq. 4.1. The operation of the pilot was monitored via webcams and online control panels in the Python program. There was a mechanical breakdown during day 88 to 134, during which samples were not taken.

$$COD_{feed} = a\left(NO_{3inf}^{-} - NO_{3\,eff,setpoint}^{-}\right) + bDO_{inf} \quad (4.1)$$

in which $NO_{3\,inf}^{-}$ and DO_{inf} denote real-time NO_3^--N and DO concentrations in the MBBR influent, $NO_{3\,eff,setpoint}^{-}$ denotes residual NO_3^--N concentration (0.5~2.3 mg/L) targeted in the MBBR effluent, a is an empirical value of COD/NO_3^--N ratio which was 4 as adapted from the study by Zhang et al. (2020), b is another empirical value of COD/DO ratio which was 3 as was used in previous pilot studies conducted by our team.

4.4.3 Analytical methods

OP, NO_3^--N, NO_2^--N, NH_4^+-N, and sCOD were analyzed with Hach TNT® 843, 835, 839, 830 and 820 vials, respectively, in a spectrophotometer (DR 3900, Hach, Loveland, CO, USA) after 0.45 μm syringe filter (MilliporeSigma, MD, USA) filtration according to the standard method (Rice et al., 2012). Total inorganic nitrogen (TIN) in this study was defined as the sum of NO_3^--N, NO_2^--N, and NH_4^+-N concentrations. The sludge volume index (SVI) and mixed liquor suspended solid (MLSS) concentrations were also analyzed according to standard methods (Rice et al., 2012). Time-lapse SVI was calculated and recorded over a 30-min period.

4.4.4 Denitrification and anammox activity determination

Both ex-situ denitrification and anammox batch tests were conducted in 2 L working volume bottles filled with 1 L biofilm media and 1 L supernatant from the MBBR. DO was monitored by a HQ30d Portable Multi-Parameter Meter (Hach Company, Colorado, USA). The batch test did not start until DO had been depleted by OHOs. Denitrification tests were conducted by dosing 20 mg/L NO_3^--N in the form of sodium nitrate and COD in the form of 10% v/v glycerol. Aqueous samples were grabbed at various time intervals for a duration of 150 minutes. Likewise, ex-situ AMX activity batch tests were conducted by dosing 10 mg/L NH_4^+-N in the form of ammonium chloride and 10~15 mg/L NO_2^--N in the form of sodium nitrite. Samples were grabbed at various

time intervals for a duration of 200~240 minutes. NO_3^--N, NO_2^--N, NH_4^+-N, and sCOD of each sample were analyzed as described in Section 2.3.

4.4.5 DNA extraction and 16S rRNA sequencing analysis

DNA was extracted using a Qiagen DNeasy PowerBiofilm Kit (Qiagen, Hilden, Germany) following the manufacturer's protocol. DNA was measured for concentration using Quibit4 (Invitrogen, Waltham, MA) and stored at -20 °C until further analysis. The V4-V5 region of the 16S rRNA gene was amplified by PCR for next generation sequencing using 515F-Y/926R primers (Parada et al., 2016). Library preparation and next generation sequencing were performed by GENEWIZ (Seattle) (Genewiz, Seattle, WA). 2x250 bp paired-end sequencing data generated by an Illumina Miseq platform were received from the sequencing facility. Bioinformatic analysis of the sequencing data was performed with QIIME2 (Bolyen et al., 2019). Quality trimming, denoising, paired-end read merging, chimera removal, and dereplication was performed with DADA2 (Callahan et al., 2016). The amplicon sequencing variants (ASVs) were taxonomically classified according to the SILVA database release 132 (Quast et al., 2012) using the scikit-learn classifier (Pedregosa et al., 2011).

4.4.6 Calculation methods

TIN removal by AMX can be estimated by Eq. 4.2,

$$\Delta \mathrm{TIN}_{AMX} = (1 + 1.32 - 0.26) \times (NH_{4\,inf}^{+} - NH_{4\,Eff}^{+} - NH_{4\,assimilated}^{+}) \quad (4.2)$$

in which 1.32 and 0.26 are based on the stoichiometry of the AMX reaction: $NH_4^+ + 1.32NO_2^- + 0.066HCO_3^- + 0.13H^+ \rightarrow 1.02N_2 + 0.26NO_3^- + 0.066CH_2O_{0.5}N_{0.15} + 2.03H_2O$ reported in a previous study (Ma et al., 2016); $NH_{4\,inf}^{+}$ and $NH_{4\,Eff}^{+}$ stand for NH_4^+- N concentrations in the MBBR influent and effluent, respectively; $NH_{4\,assimilated}^{+}$ stands for the NH_4^+- N assimilated by the OHOs for growth, which can be estimated by Eq. 4.3:

$$NH_{4\,assimilated}^{+} = \mathrm{Y} \times \mathrm{C} \times (sCOD_{inf} - sCOD_{eff}) \quad (4.3)$$

in which $sCOD_{inf}$ and $sCOD_{eff}$ stand for sCOD concentrations in MBBR influent and effluent, respectively; Y is the observed growth yield (0.2 mg biomass COD/mg substrate COD consumed);

C is the biomass nitrogen content (0.07 mg N/mg biomass) based on results reported by Grady Jr et al. (2011).

Nitrite accumulation ratio (NAR) can be calculated by the concentration ratio of NO_2^--N/ NO_x^--N. COD consumption by EBPR was estimated based on the stoichiometry reported by Grady Jr et al. (2011), i.e., each gram of PO_4^{3-}-P removal requires eight grams of sCOD consumption. For endogenous denitrification, each gram of TIN removal requires 3.58 gram of sCOD consumption (Henze et al., 2006). The COD removed in addition to the consumption by EBPR and ED was categorized as 'other', which refers to the fraction of COD that was oxidized by excessive aeration without contribution to BNR.

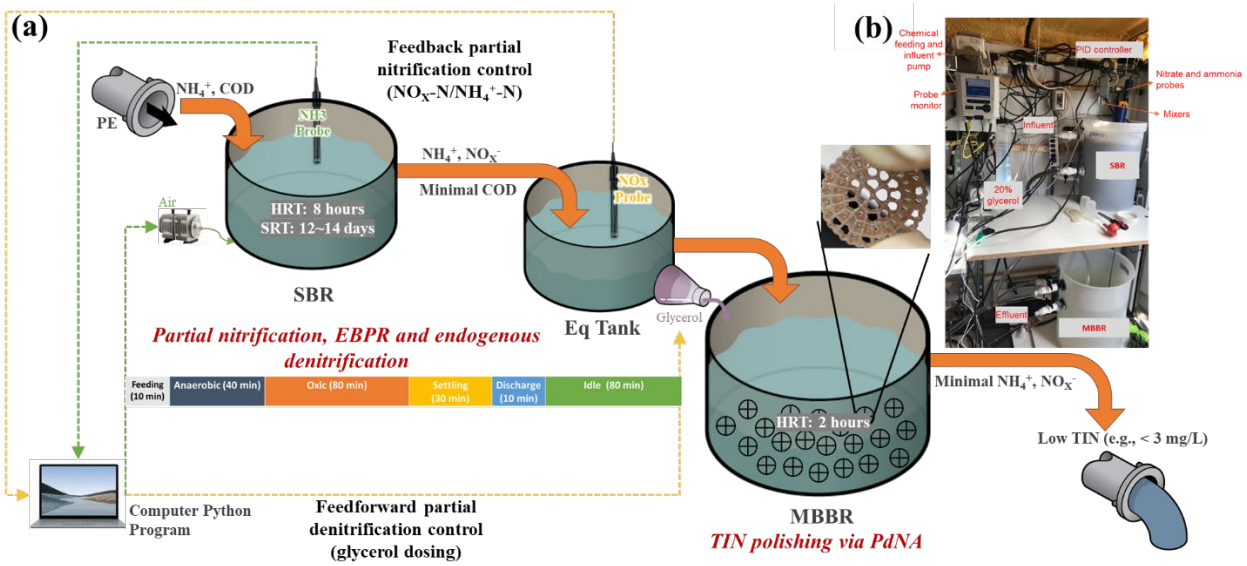

Figure 4.2 (a) Schematic illustration and (b) actual setup of the pilot system

4.5 Results

4.5.1 Influent quality and temperature variation

The variation of the influent TIN, OP, and sCOD concentration as well as the temperature of PE used in this study are summarized in Table 4.1. In general, a data set could be considered highly variable when its CV is > 30% (Aronhime et al., 2014). As can be seen in Table 4.1, CV of % daily

change of all parameters was > 130%, indicating all influent characteristic parameters are highly variable. Many key parameters such as sCOD/N and sCOD/OP even varied with CV of % daily change > 200%. It was reported that the optimal sCOD/N ratio in the municipal wastewater for biological nitrogen removal should be in the ranges of 6~12.5 g/g (Sun et al., 2010). The upper limit of the sCOD/N used in this study (12.3 g/g) was within this optimal range; however, the lower limit (3.9 g/g) was way under it, indicating insufficient influent carbon source for denitrification, which justifies the use of AMX in this study. Yet, the CV of sCOD/N daily change was around 196%, adding greater challenges to biological nitrogen removal for such great substrate fluctuation. What is more challenging is the temperature fluctuation from 2.5 to 31.2 °C, and a high CV of temperature daily change around 150.8% (Table 4.1). Figure 4.3 exhibited the temperature profiles and distribution over the 212 days of operational period. It is noteworthy that 84% of the time were with temperature < 20 °C which is considered too low to suppress NOB growth (Qiu et al., 2021). Hence, the chance to achieve successful nitritation under such low temperature is slim.

Table 4.1 PE characteristics and variations over the course of the 212 days of operational period (±: standard deviation; CV: Coefficient of variation)

Parameters	Average value	Min.-Max.	%Daily change	CV of %Daily change
TIN (mg/L)	20.2 ± 5.6	4.3-35.2	25.3 ± 33.1	131.2
OP (mg/L)	6.1 ± 3.6	1.03-37.4	35.3 ± 73.6	208.2
sCOD (mg/L)	163.2 ± 85.3	24.0-679.0	39.9 ± 80.4	201.3
sCOD/N (g/g)	8.2 ± 3.2	3.9-12.3	24.0 ± 47.0	195.9
sCOD/OP (g/g)	28.3 ± 10.3	2.8-69.8	29.6 ± 61.7	208.8
Temperature (°C)	17.9 ± 3.1	2.5 ± 31.2	5.5 ± 8.2	150.8

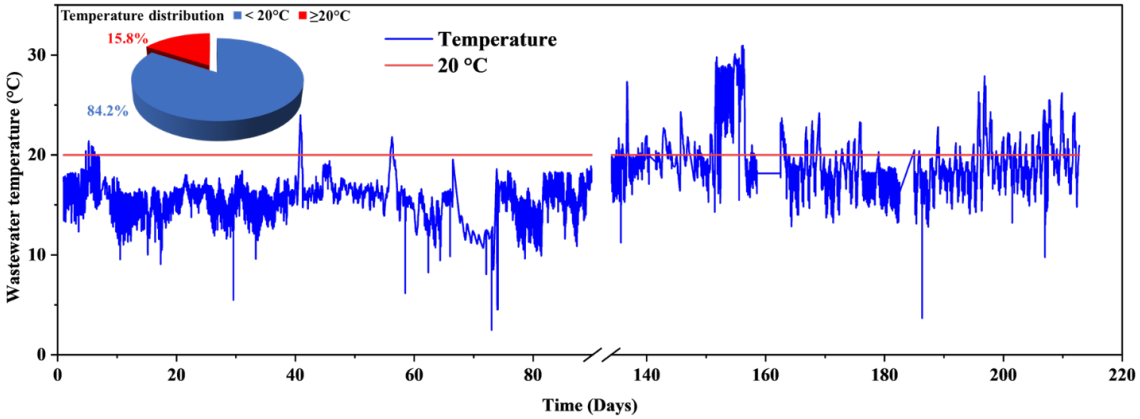

Figure 4.3 Profile and distribution of wastewater temperature

4.5.2 Nitrogen removal performance

As mentioned previously, the pilot system was composed of a SBR performing partial nitrification, EBPR, and ED, and an anoxic MBBR performing PdNA. In this section, the 212-day operational period of the pilot can be divided into three phases in terms of different SBR effluent NO_x-N/NH_4^+-N ratio setpoints in preparation of the influent for MBBR. The average values showing the performance of SBR and MBBR during each phase were summarized in Table 4.2 and discussed below. The high standard deviation of all these values are results from the high influent quality variation shown in Table 4.1.

Table 4.2 Pilot effluent quality and removal efficiencies during three operational periods (±: standard deviation)

Parameters	Phase 1 (Days 1 to 87)	Phase 2 (Days 135 to 180)	Phase 3 (Days 181 to 212)
SBR effluent NO_x-N/NH_4^+-N (g/g)	1.2 ± 0.9	2.4 ± 1.2	2.7 ± 0.6
SBR effluent TIN (mg/L)	9.9 ± 2.8	11.4 ± 3.6	9.2 ± 2.5
MBBR effluent TIN (mg/L)	6.4 ± 3.6	5.8 ± 3.3	2.8 ± 1.7
% TIN removal by SBR	48.0 ± 14.1	48.2 ± 11.2	44.5 ± 13.4
% TIN removal by the MBBR	25.8 ± 13.6	28.0 ± 17.6	39.5 ±15.3
%TIN removal by AMX in the MBBR	19.3 ± 22.0	11.5 ± 2.5	12.5 ± 8.9
%TIN removal by denitrification in the MBBR	6.3 ± 10.2	16.2 ± 10.1	23.8 ± 10.5
MBBR ΔNH_4^+-N (mg/L)	2.8 ± 2.3	1.6 ± 0.8	1.09 ± 0.25
MBBR effluent NO_3^--N (mg/L)	2.3 ± 2.2	2.0 ± 1.3	0.5 ± 0.3
MBBR ΔsCOD/ΔTIN (g/g)	2.9 ± 0.9	3.4 ± 2.1	3.5 ± 0.6
SBR effluent NO_2^--N (mg/L)	0.3 ± 0.2	1.8 ± 0.7	1.5 ± 0.2
SBR effluent NAR (%)	7.2 ± 7.5	29.7 ± 22.1	23.7 ± 2.8
Effluent OP-P (mg/L)	0.6 ± 0.6	0.1 ± 0.16	Undetectable (< 0.1)
OP removal efficiency (%)	91.6 ± 9.2	98.4 ± 2.03	>98.6%

Figure 4.4a shows the TIN concentration profiles in the PE, SBR effluent, and MBBR effluent. In Phase 1 when NO_x-N/NH_4^+-N setpoint in the SBR effluent was feedback controlled at its lowest level, namely 1.2 ± 0.9 g/g, 48.0 ± 14.1% of influent TIN (Table 4.2 and Figure 4.4a) was removed in the SBR without any external carbon addition. Besides that, another 19.3 ± 22.0% and 6.3 ± 10.2% were removed by AMX and full denitrification in MBBR, respectively, leaving an average effluent TIN of 6.4 ± 3.6 mg/L in Phase 1 (Table 4.2 and Figure 4.4a). Specifically, concentration profiles of NH_4^+-N, NO_3^--N, and NO_2^--N in the PE, SBR effluent, and MBBR effluent were shown in Figure 4.4 b, c, and d, respectively. Influent NH_4^+-N (Figure 4.4b), which was the major component of PE TIN, was partially nitrified to NO_x-N in the aerobic phase of the SBR (Figure 4.4 b, c and d) through the feedback controller to prepare a mix of NH_4^+-N and NO_X-N for downstream PdNA with no need of NOB suppression. 7.2% of the NO_X-N in the SBR effluent was NO_2^--N in Phase 1 (Table 4.2 and Figure 4.4 d). As shown in Figure 4.5, Nitrosomonas as a typical ammonia oxidizing bacteria (AOB) and *Nitrospira* as a most widely-spread NOB were detected in the SBR with the relative abundance of 0.11% and 0.18%, respectively (Ferguson et al., 2007). The NARs of 7.2~29.7% in the SBR effluent (Table 4.2) were achieved via the synergy between *Nitrosomonas* and *Nitrospira*. In this study, partial nitrification is followed by a PdNA process. NO_3^--N in the NO_x-N was then reduced to NO_2^--N (Figure 4.4 c and d) through partial denitrification (PdN) for AMX utilization in the MBBR with feedforward-controlled glycerol dosing (Eq. 4.1). The feedforward controller aimed to achieve the designated effluent TIN setpoint by precisely dosing glycerol. As a result, average effluent NO_3^--N of 2.3 ± 2.2 mg/L was achieved in Phase 1 (Table 4.2 and Figure 4.4c). This great standard deviation is a result of the influent quality fluctuation. It was previously reported that a certain amount of nitrate residual is essential for the achievement of PdN (Campolong, 2019; Le et al., 2019). The anoxic NH_4^+-N removal of 2.8 ± 2.3 mg/L was achieved in the MBBR in Phase 1, which can be ascribed to AMX activities (Table 4.2 and Figure 4.4b). *Candidatus Brocadia* as one of the mostly found AMX bacteria in the WWTPs and large-scale AMX reactors was detected in the MBBR (Figure 4.5) with the relative abundance of 0.02%, evidencing the existence of AMX.

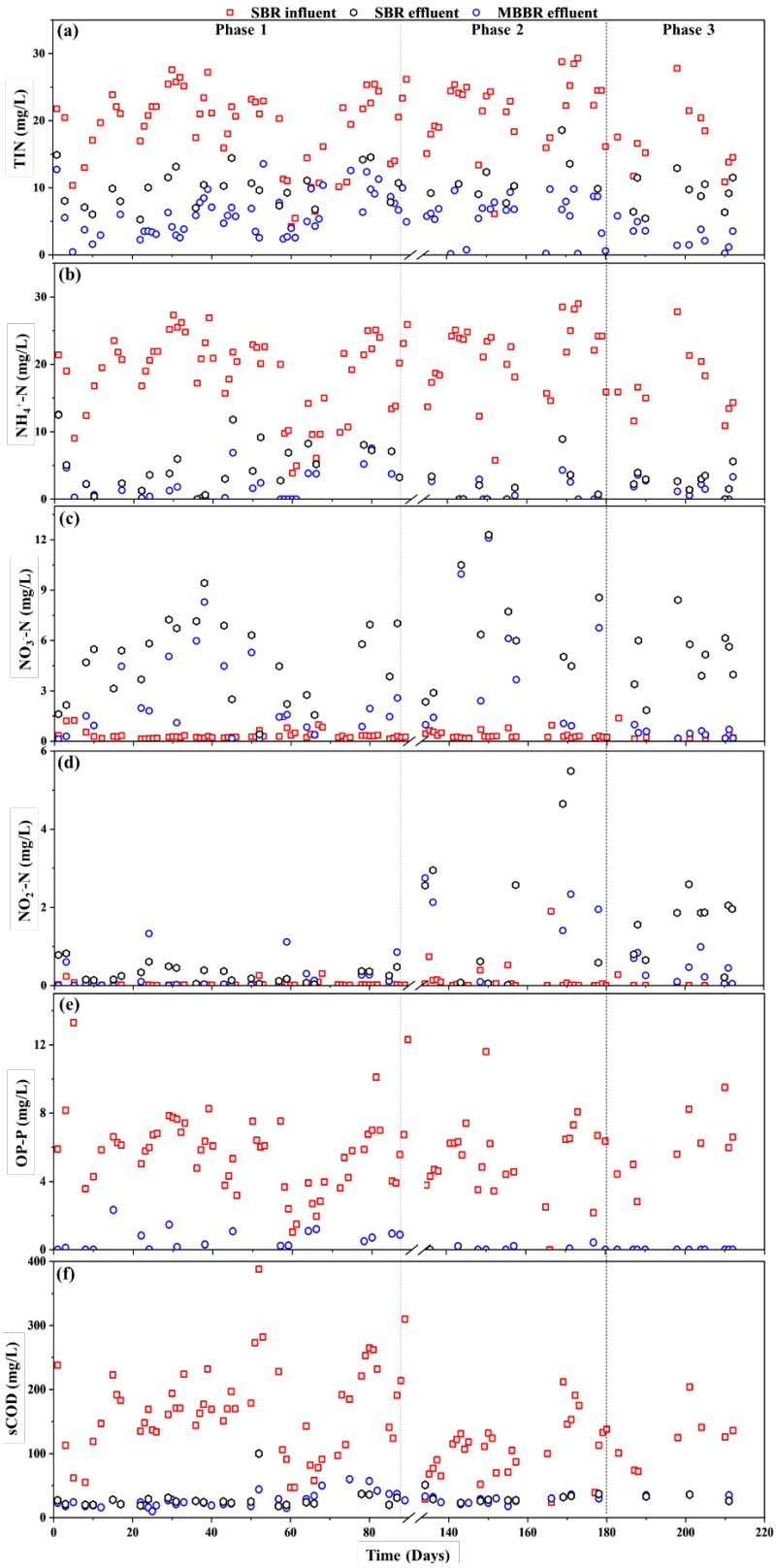

Figure 4.4 Concentration profiles of (a) TIN, (b) NH_4^+-N, (c) NO_3^--N, (d) NO_2^--N , (e) OP-P, and (f) sCOD in the SBR influent, SBR effluent, and MBBR effluent

In phase 2 operation, in order to reduce the effluent TIN to an even lower level, NO_x-N/NH_4^+-N setpoint in the SBR effluent was increased from 1.2 ± 0.9 g/g to 2.4 ± 1.2 g/g in the feedback controller (Table 4.2), and the effluent NO_3^--N setpoint was reduced from 2.3 to 2.0 mg/L (Table 4.2) in the feedforward controller (Eq. 4.1) to encourage more denitrification in MBBR given the limited AMX capacity. Consequently, influent TIN removal by MBBR slightly increased from 25.8 ± 13.6% to 28.0 ± 17.6% in Phase 2, leaving an average effluent TIN of 5.8 ± 3.3 mg/L (Table 4.2 and Figure 4.4a), which was still higher than the effluent TIN target of 3 mg/L. Meanwhile, AMX contributions to influent TIN removal and anoxic NH_4^+-N removal in MBBR in Phase 2 dropped from 19.3 ± 22.0% to 11.5 ± 2.5% and from 2.8 ± 2.3 mg/L to 1.6 ± 0.8 mg/L, respectively (Table 4.2 and Figure 4.4b).

In phase 3, in order to further reduce the effluent TIN, the NO_x-N/NH_4^+-N setpoint in the SBR effluent was further increased from 2.4 ± 1.2 g/g to 2.7 ± 0.6 g/g in the feedback controller (Table 4.2), along with the further increase of glycerol addition into the MBBR by decreasing the effluent NO_3^--N setpoint to 0.5 mg/L (Table 4.2) in the feedforward controller (Eq. 4.1). This led to an increase in denitrification contribution to influent TIN removal in MBBR from 16.2 ± 10.1% to 23.8 ± 10.5%. Consequently, influent TIN removal by MBBR increased from 28.0 ± 17.6% to 39.5 ±15.3%, leaving an average effluent TIN of 2.8 ± 1.7 mg/L (Table 4.2 and Figure 4.4a), which met the effluent TIN target of ≤ 3 mg/L. Meanwhile, AMX contributions to influent TIN removal almost remained the same as that in the Phase 2 (Table 4.2).

The increase of TIN removal along with the increase of NO_X-N/NH_4^+-N setpoints in phases 1 to 3 suggested that full denitrification has to be leveraged when a very low effluent TIN concentration (e.g. ≤ 3 mg/L) is desired. This is because a residual NO_3^--N level in bulk solution, e.g., 1~2 mg/L, is required for enabling PdNA (Campolong, 2019; Le et al., 2019). It is presumable that this bulk NO_3^--N level created a rate differential between denitratation and denitritation, which produced NO_2^--N for anammox utilization. Hence, it is not difficult to understand that decreasing the bulk NO_3^--N level in the effluent led to decreased AMX activity which can be seen from the anoxic ammonia utilization decrease from 2.8 ± 2.3 mg/L to 1.09 ± 0.25 mg/L in Table 4.2. PdN efficiency as high as 88.5% in terms of ΔNO_2^--N/ΔNO_3^--N was measured in the denitrification batch tests

when the bulk NO_3^--N level was as high as around 5 mg/L (Figure 4.6a), confirming the effectiveness of glycerol in supporting PdN process at high bulk NO_3^--N residue. Hence, rate differential could have provided NO_2^--N for AMX to grow. Therefore, it can be concluded from Table 4.2 that AMX activity had to be scarified when an extremely low effluent NO_3^--N level was targeted. To verify the AMX activities in the MBBR, ex-situ batch tests were conducted as mentioned in Section 2.4, and the results were shown in Figure 4.6. As can be seen, an ammonia removal rate of 0.1 g NH_4^+-N/m^2/day was achieved in the batch test indicating the existence of AMX activities in the MBBR. This value was comparable to the ammonia removal rates of 0.08~0.17 g NH_4^+-N/m^2/day in continuous-flow MBRRs reported by Macmanus et al. (2022).

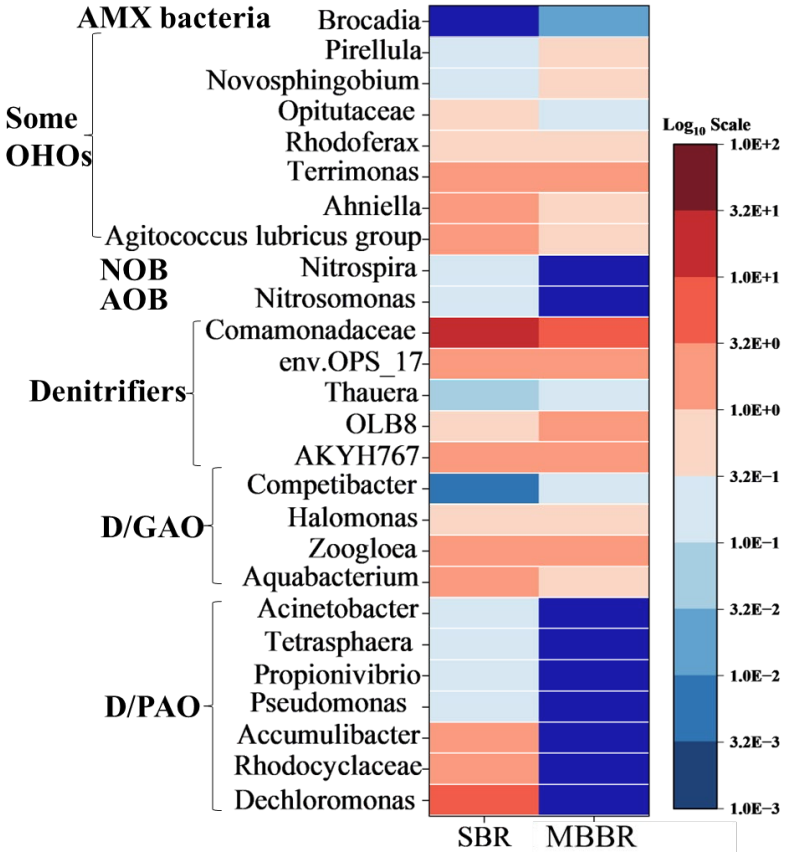

Figure 4.5 Heatmaps of bacterial community composition at genus level in activated sludge cultivated in SBR and in biofilms cultivated on MBBR media. Sample collected on the 210th day of operation.

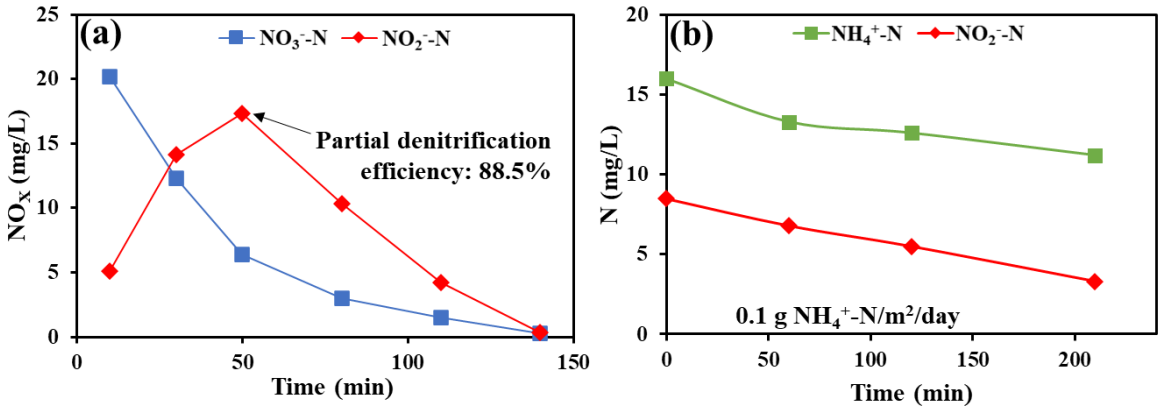

Figure 4.6 Results of ex-situ (a) partial denitrification and (b) AMX activity batch tests conducted on Days 203 and 212 in Phase 3, respectively

4.5.3 OP and rbCOD removal performance

OP removal efficiencies > 90% were achieved throughout all three phases (Table 4.2 and Figure 4.4e). In Phase 3, OP concentrations in the SBR effluent even dropped to undetectable level (< 0.1 mg/L). The phosphorus accumulating organism (PAO) such as *Accumulibacter* (1.19%), *Pseudomonas* (0.27%), and *Tetrasphaera* (0.12%), as well as denitrifying PAO (DPAO) such as *Dechloromonas* (3.30%), *Rhodocyclaceae* (1.75%), and *Propionivibrio* (0.22%) were detected in the SBR (Figure 4.5), which have been considered to be responsible for EBPR process (Albertsen et al., 2016; Ferguson et al., 2007; Han et al., 2018; Zhang and Kinyua, 2020). The excellent EBPR performance has to do with the RAS anoxic zone designed in Figure 4.1. In addition, sCOD levels in effluent were consistent during the entire operational period, which indicated that nearly all the rbsCOD in the PE was removed after the aerobic phase, leaving around 30 mg/L recalcitrant COD in the effluent (Figure 4.4f).

4.5.4 SBR cyclic performance ffluent quality

An SBR cycle comprises 5 phases, namely idle, feed, anaerobic, aerobic, and settling phases, respectively. Taking a representative cycle during Phase 3 as an example, Figure 4.7 a, b, and c show the cyclic profiles of bulk N, OP mass, and DO concentrations. Figure 4.7d shows the fractions of influent rbCOD utilized by EBPR, ED, and other in this cycle, respectively. We are

going to use the data analyzed from this representative cycle to understand the mechanism of TIN and OP removal in the secondary SBR.

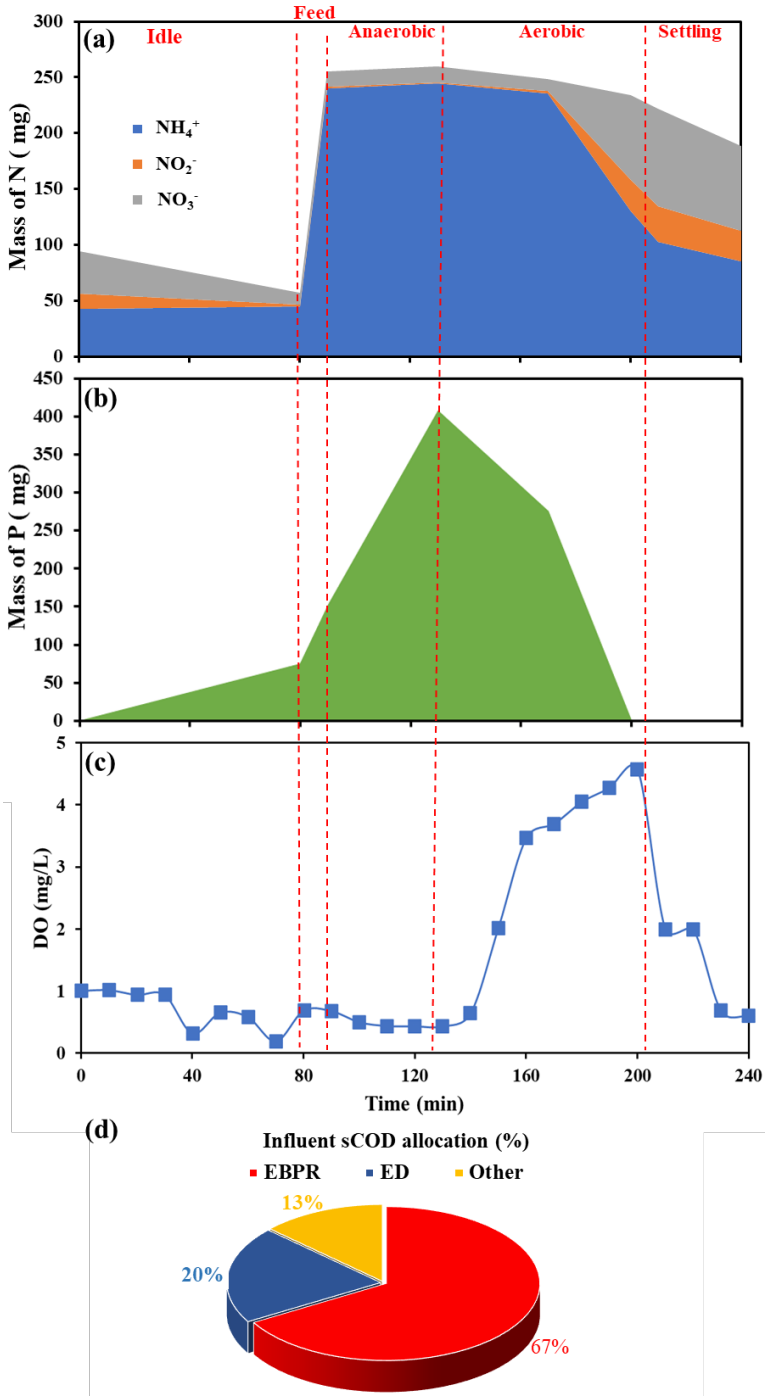

Figure 4.7 SBR cyclic concentration profiles of (a) N species, (b) OP, and (c) DO, as well as (d) influent rbCOD allocation for EBPR, ED, and other within a representative SBR cycle on Day 186 in Phase 3.

At the end of the settling, 50% of the NO_x-N and NH_4^+-N mass was decanted from the SBR to MBBR (Figure 4.2), and the other 50% mingled with the sludge settled at the bottom of SBR. This sludge going through the subsequent idle phase could be considered as RAS being conditioned in an anoxic tank as indicated by the low DO concentrations (<1 mg/L DO) during the idle phase (Figure 4.7c). A NO_X removal efficiency of 80% was achieved during the idle phase (Figure 4.7a), leaving only 11.2 mg (or 0.5 mg/L) NOx by the end of the idle phase. A specific denitrification rate (SDNR) of 0.86 mg N/g MLVSS/h was observed. Since nearly all the readily rbCOD was removed in the aerobic phase of the previous SBR cycle (Figure 4.4f), it can be concluded that this TIN removal during the idle phase was achieved through ED. However, there was no NH_4^+-N releasing during the idle phase (Figure 4.7a), indicating minor biomass decay. In general, there are two types of ED, namely sludge decay-driven or carbon storage-driven ED (Bauhs et al., 2022). For sludge decay-driven ED, rbCOD produced from the sludge decay was used as the electron donor for NO_X reduction, which is accompanied by elevated ammonium concentrations due to the decomposition of proteins in the decayed sludge (Jönsson and Jansen, 2006). The SDNRs of sludge decay-driven ED is usually in the range of 0.2-0.6 mg N/g MLVSS/h (Coats et al., 2011). For carbon storage-driven ED, it is usually performed by D/GAOs using internal carbon storage such as PHA as electron donors for NO_X reduction (He et al., 2017), with typical SDNRs in the range of 0.69-2.9 mg N/g MLVSS/h (Bauhs et al., 2022; Coats et al., 2011; Qin et al., 2005). The GAO and D/GAOs such as *Aquabacterium* (1.95%)*, Zoogloea, Halomonas* (0.45%), and *Competibacter* (0.01%) were detected in the SBR (Figure 4.5), which were reported to be responsible for carbon storage-driven ED (Lin et al., 2019; Lopez-Vazquez et al., 2009; Senderovich and Halpern, 2013). Although GAOs can be considered as the main competitors for PAOs as they can also anaerobically assimilate rbCOD without contributing to the P removal, their coexistence in the same reactor has been reported previously (Hong et al., 2023; Lopez-Vazquez et al., 2009). In view of the SDNR range and the lack of NH_4^+-N releasing, as well as the microbial community analysis results, it can be concluded that ED occurring during the idle time can be most likely attributed to carbon storage-driven ED. It was this complete ED that has prevented NOx impact on the subsequent EBPR in the anaerobic zone in Figure 4.1. In fact, a slight OP release has already been observed in the idle phase (Figure 4.7b), indicating the SBR was turning from anoxic to anaerobic during this idle phase. This anaerobic condition extended into the feed phase where a surge of bulk NH_4^+-N and

OP-P level and an even faster OP release were observed (Figure 4.7 a and b). Such strict anaerobic condition was maintained during the subsequent anaerobic phase where majority of the OP was released. In total, 329.4 mg (or 12.7 mg/L) OP was release during the idle and anaerobic phases (Figure 4.7b), evidencing the sufficient anaerobic condition has been provided even when 75.9 mg (or 5.8 mg/L) NO_X residue was intentionally left for PdNA (Figure 4.7a), which again can be ascribed to the ED contribution.

In the following aerobic phase, DO concentrations gradually increased to around 4.8 mg/L along with the partial nitrification feedback controlled by the NO_x-N/NH_4^+-N setpoint, and OP assimilation. At the end of aerobic phase, barely any OP was left (Figure 4.7b). It is interesting to see that a fraction of NOx (37.8%) formed at end of the aerobic phase was actually the NO_2^--N, which was unexpected. Referring to Figure 4.4d, this NO_2^--N residue fluctuate around 2~3 mg/L throughout the Phases 2 and 3 of the 212 days of operation.

During the settling phase, DO dropped to below 1 mg/L within the first 10 minutes (Figure 4.7c). The mass of TIN decreased by 32.8 mg with the SDNR of 1.0 mg N/g MLVSS/h. There were neither rbCOD available nor NH_4^+-N release during the settling phase (Figure 4.7a). Hence, the TIN removal could be again attributed to the carbon storage-driven ED. This settling phase of the SBR could be considered as a secondary clarifier in full-scale applications (Figure 4.1). The carbon storage-driven ED in secondary clarifiers has been observed in several full-scale settings (Lee, 2022; Li et al., 2022; Siegrist et al., 1995). For example, Li et al. (2022) reported that the secondary sedimentation tank had more contributions (15.3 ± 1.4%) to the total nitrogen removal than post-anoxic zone (10.5 ± 3.1%) in an anaerobic-anoxic-oxic-post-anoxic-post-oxic (AAO-AO) process. This was because the microbial sludge was concentrated in the clarifier after supernatant being discharged, which offers an expedited ED rate (Lee, 2022; Li et al., 2022).

In sum, 99.9% OP and 52.3% TIN were removed during the SBR cycle. It is noteworthy that there was no external carbon addition during the SBR operation, which means both ED and EBPR were achieved with the influent rbCOD. However, it should be also pointed out that the NO_X formed during the aeration phase did not have a chance to meet the influent rbCOD before removal, which is equivalent to the MLE elimination in Figure 4.1. Hence, majority of the TIN removal was

through ED by utilizing internal carbon storage. A mass balance calculation of the influent rbCOD allocation based on the stoichiometry of ED and EBPR is shown in Figure 4.7d. There were about 67% and 20% of the influent rbCOD allocated for EBPR and ED in this representative SBR cycle while only 13% were consumed by aeration without contribution to P and N removal (Figure 4.7d). Despite the highly variable influent quality, such an efficient utilization of carbon storage during secondary process significantly eased the burden on the tertiary treatment.

4.5.5 SBR sludge settleability

Although it was reported that the optimal sCOD/N ratios for activated sludge settleability was 8-10 g/g, and fluctuating sCOD/N ratios could worsen the sludge settleability (Wang et al., 2019), activated sludge in the SBR of this study behaved differently. The SVI profile in Figure 4.8 indicated that after around 180-day operation, SVI of the SBR mix liquor dropped from 150 mL/g in the seed sludge to 56 mL/g in the steady state sludge, which was even below the SVI of 60 mL/g suggested by Kent et al. (2018) for successful sludge densification or granulation. Moreover, it only took about 10 min for the sludge to settle to the level of 80 mL/g, indicating excellent settleability (Figure 4.8). With that being said, successful sludge densification has been achieved in the SBR regardless of the fluctuating sCOD/N ratios (Table 4.1). One of the potential reasons for this could be the enrichment of PAO and D/GAO with the relative abundance of 6.85% and 2.41%, respectively (Figure 4.5). It is well-known that PAO and D/GAO dominated sludge has high density and thus tend to have better settleability (Kent et al., 2018). In addition, cyclic anoxic, anaerobic, and aerobic phases also tend to suppress filamentous organisms and improve sludge settleability (Kent et al., 2018). Meanwhile, the alternation of feast and famine conditions in terms of substrate concentrations in SBR was also essential for the successful densification (Kent et al., 2018).

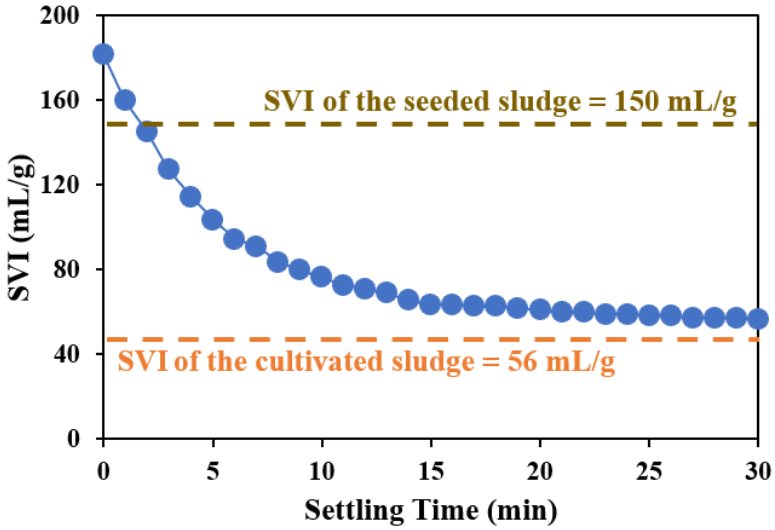

Figure 4.8 SVI profile measured on Day 200 in Phase 3

4.5.6 TIN and COD flow

Technically, TIN has four pathways to go through once entered the treatment system in Figure 4.1, i.e., 1) reduced by intracellular COD into N_2 through ED, 2) turned into N_2 by AMX through PdNA, 3) reduced by extracellular COD into N_2 through exogenous denitrification, or 4) remain in the effluent as the residue. Figure 4.9a demonstrated the fractions of TIN flow among the four pathways. Throughout the three phases of the 212 days of operation, ED was the No.1 contributor to TIN removal regardless of the level of the SBR influent quality variation and effluent NO_x-N/NH_4^+-N setpoints, accounting for about 44.5~48.2% TIN removal, which explains why we believe MLE can be eliminated. In contrast, AMX was the second largest contributor only during the Phase 1 when NO_x-N/NH_4^+-N setpoint was low because this setpoint prioritize AMX for low external carbon addition in tertiary MBBR. As a result, the TIN removal through exogenous denitrification was the least but the effluent TIN was the highest (6.4 ± 3.6 mg/L) among the three pathways during this phase (Table 4.2). When achieving a low effluent TIN level was prioritized during the Phases 2 and 3 operation, more TIN was removed through exogenous denitrification than though the AMX in the MBBR because the setpoints of NO_x-N/NH_4^+-N was adjusted to higher levels of 2.4 ± 1.2 g/g and 2.7 ± 0.6 g/g during these two phases to encourage more exogenous denitrification. Thus can be seen, the higher the setpoints are, the more TIN flows

towards the exogenous denitrification in tertiary MBBR, which means more external carbon consumption.

In terms of carbon efficiency, influent organic carbon utilization by TIN and OP removal were prioritized. Figure 4.9b exhibits the COD consumption by EBPR, ED, and PdNA, respectively. Since external carbon was only dosed into the tertiary MBBR, all COD utilized by EBPR and ED was from PE. In contrast, all COD utilized by PdNA was glycerol dosed through feedforward controller (Eq. 4.1). The difference between the influent COD entered the treatment system and the COD utilized by EBPR, ED, and PdNA can be regarded as the COD that reacted with the excessive aeration, which is categorized as 'other' in this study. OHOs which were responsible for aeration consumption such as *Ahniella* (1.19%), *Terrimonas* (1.19%), *Rhodoferax* (0.58%), and *Opitutaceae* (0.52%), etc., were detected in the SBR (Figure 4.5). In Phase 1 when average sCOD/N ratio in the PE was as high (e.g. 8.3 ± 2.1 g/g), relatively low fractions of COD (e.g. 28.9 ± 17.1% and 24.4 ± 12.9%) were allocated for EBPR and ED, leaving majority of the system COD (42.5 ± 23.6%) for 'other' (e.g., aeration oxidation). This represents the scenario when influent COD was in excess. As a consequence, the extra influent COD has to be first depleted by aeration to enable partial nitrification to occur.

Because the influent COD was more than sufficient in Phase 1 (Figure 4.9b), and the SBR effluent NO_x-N/NH_4^+-N setpoint was the lowest, the fraction of external carbon addition for PdNA in tertiary treatment (e.g. 7.7 ± 5.9%) was also the lowest in this phase. In contrast, in Phase 2 when PE had a lowest average sCOD/N ratio of 4.7 ± 1.0 g/g, the COD allocations for EBPR and ED increased from 28.9 ± 17.1% to 38.6 ± 22. 9% and from 24.4 ± 12.9% to 37.4 ± 8.8%, respectively. This represents a scenario when influent COD was insufficient. As a consequence, the pilot system prioritized COD consumption by EBPR and ED by reducing the 'other' consumption from 42.5 ± 23.6% to 8.3 ± 9.6%. Besides the insufficient influent COD, a higher NO_x-N/NH_4^+-N ratio setpoint in Phase 2 aggravated external carbon demand in the tertiary MBBR by increasing its fraction from 7.7 ± 5.9% to 27.3 ± 8.7%. In Phase 3 when the average sCOD/N ratios in PE resumed to 8.0 ± 1.8 g/g, namely an influent COD excessive scenario again, the excessive COD that has to be depleted by aeration increased from 8.3 ± 9.6% to 30.5 ± 14.5%. In response, the COD allocation for ED and PdNA decreased from 37.4 ± 8.8% to 19.8 ± 10.0%, and from 27.3 ± 8.7% to 13.4 ±

4.4%, respectively. However, the fraction of COD allocated for EBPR barely changed (e.g. 36.4 ± 10.1%). Meanwhile, the fraction of external carbon consumption in tertiary MBBR reduced from 27.3 ± 8.7% to 13.4 ± 4.4% because of the increased average influent sCOD/N ratios in Phase 3 than Phase 2.

The effect of influent sCOD/N ratio observed in Figure 4.9c has to do with the sequence of influent COD utilization in Figure 4.9b and also the rate-limiting reactants. When sCOD/N ratios were ≤ 6 g/g, rbCOD was first assimilated by PAO and D/GAO in the anaerobic zone as internal carbon for EBPR and ED. Because rbCOD availability becomes a limiting factor at a low influent sCOD/N ratio, it is expected to observe a strong correlation of sCOD/N ratios to EBPR and ED in Figure 4.9c. However, when influent sCOD/N ratios were > 6 g/g, rbCOD in the PE became more than sufficient for EBPR and ED in the anaerobic zone, the limiting factors for rbCOD assimilation became polyphosphate availability in PAO and glycogen availability in D/GAO. Because partial nitrification would not occur until rbCOD is depleted (Grady Jr et al., 2011), extensive aeration has to be used to oxidize excessive COD if any. Therefore, when influent sCOD/N ratios were high, the increase of influent sCOD/N ratios had little effects on the COD consumption by EBPR and ED but led to an increase in aeration consumption, namely 'other' in Figure 4.9c. For the external COD addition to the MBBR, it was feedforward controlled (Eq. 4.1) by the NO_x-N/NH_4^+-N ratio setpoints and effluent NO_3^--N setpoints but not by the influent sCOD/N ratios. Thus, COD consumption by MBBR was not affected by influent sCOD/N ratios regardless of the influent quality fluctuation.

To sum up, when influent sCOD/N ratios were low (e.g. < 6 g/g), the influent rbCOD availability becomes a limiting factor and thus sCOD/N ratios exhibited a good correlation with COD allocations for EBPR and ED, respectively (Figure 4.9c). However, when sCOD/N ratios in PE were high enough (e.g. > 6 g/g), rbCOD availability was not a rate-limiting factor for EBPR and ED anymore. Hence, sCOD/N ratios lost correlation with the COD consumption by EBPR and ED (Figure 4.9c).

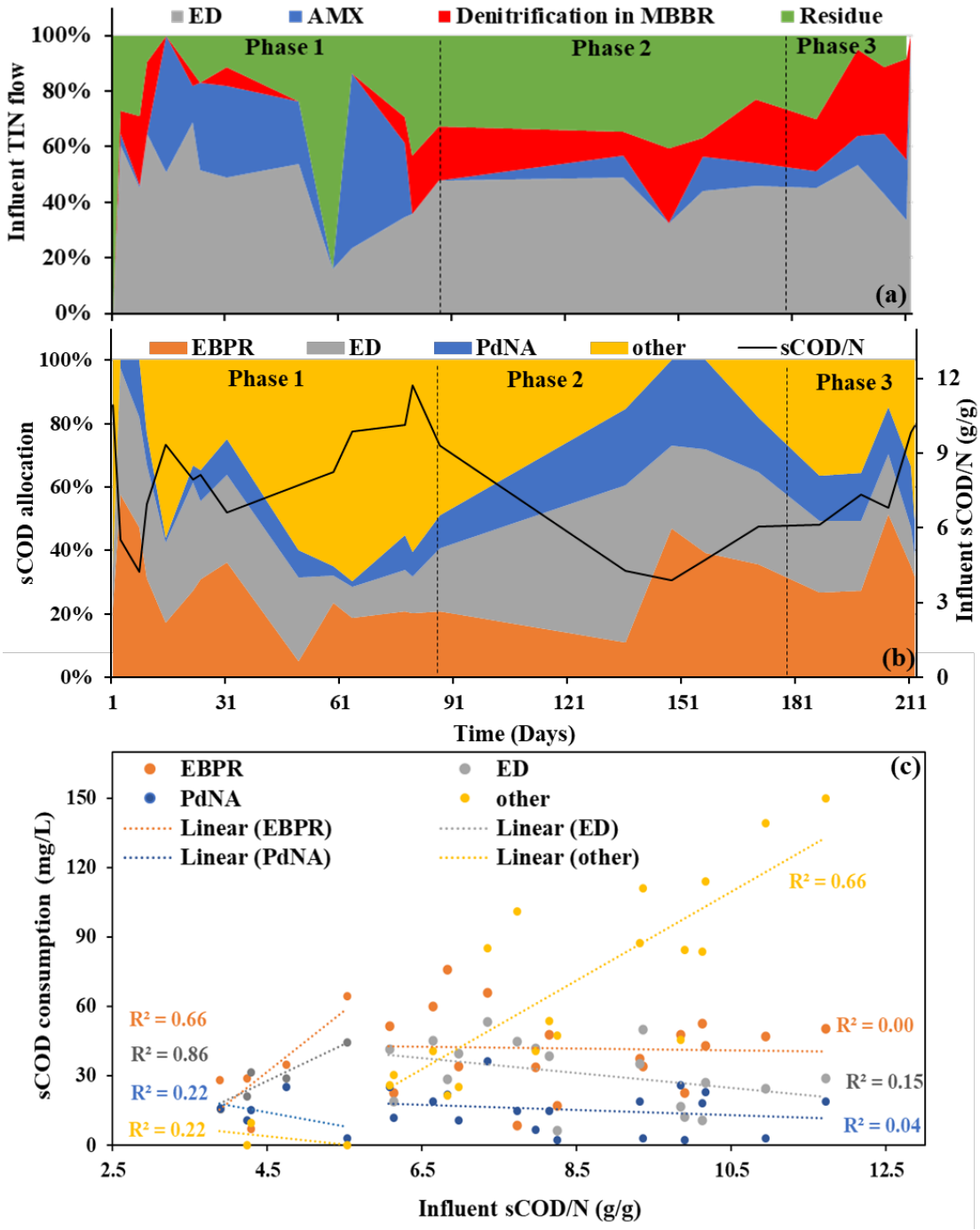

Figure 4.9 (a) Percent of TIN flow to ED, AMX, denitrification in MBBR, and effluent residue over the experimental duration; (b) Percent of sCOD allocation for EBPR, ED, other in SBR, and PdNA along with influent sCOD/N ratio over the experimental duration; and (c) Correlations between influent sCOD/N ratios and sCOD consumption for EBPR, ED, other in SBR, and PdNA in MBBR.

4.6 Discussion

To our best knowledge, this study was the first that have integrated partial nitrification, EBPR, ED, and PdNA in one system using real PE under conditions of highly variable influent quality and low temperature to meet effluent TIN ≤ 3 mg/L and OP ≤ 0.1 mg/L.

4.6.1 Carbon saving and implications for full-scale application

The fact that there was almost no NO_x-N left at the beginning of the SBR cycle proved that MLR elimination can be eliminated in this configuration (Figure 4.1), which alone could reduce 7.1%-21.4% of total energy and carbon emission in WWTPs (Silva and Rosa, 2022) depending on the MLR ratios. MLR as an essential configuration for nitrogen removal has been used for about 50 years (Grady Jr et al., 2011). Its elimination could be attributed to a synergy between successful ED in settling (secondary clarifier) and idling phases (anoxic RAS conditioning tank). Specifically, 44.5~48.2% of influent TIN was removed with internal carbon-driven ED in the secondary SBR (Figure 4.9a), and 7.2~19.3% of influent TIN was reduced by AMX in the tertial MBBR, leaving only 9.3%~23.8% removal by external carbon-driven full denitrification (Figure 4.9a). An added benefit of ED that MLE does not have is its capacity of safeguarding anaerobic zone from RAS NO_X-N disturbance, especially when AMX is incorporated in tertiary treatment as was done in Figure 4.1. This is obvious to be seen in Figure 4.7a, i.e., although NO_X-N level as high as 51.9 mg (or 4.0 mg/L) blended in RAS recirculating toward the anoxic zone, the discharge OP level still can be maintained as low as 0.1 mg/L or undetectable. This is because ED was able to deplete NO_X-N during RAS preparation and transportation. It was reported that NO_X-N removal in RAS could be critical for EBPR when high NO_X-N concentrations was in the effluent for downstream AMX process (Guerrero et al., 2013; Zeng et al., 2014; Zeng et al., 2017). This study provided a perfect solution to the conflicts between EBPR and tertiary PdNA.

Phases 3, i.e., when a stringent effluent TIN below 3 mg/L was set, can be considered as a high-performance benchmark for future full-scale application. During Phase 3, instead of oxidizing all influent NH_4^+-N via the conventional nitrification, an average of 27.0% influent NH_4^+-N shortcut

secondary SBR into tertiary MBBR with no need of oxidation. Besides, another average of 17.3% influent NH_4^+-N was converted to NO_2^--N in the SBR effluent in Phase 3 (Table 4.2). Substituting these numbers into the stoichiometries of full and partial nitrification in Eqs. 4.4 and 4.5 (Faskol and Racoviţeanu, 2021; Zhang et al., 2019), it can be estimated that 55.5% oxygen could be saved in the SBR (mainstream secondary treatment) in comparison with conventional full nitrification.

$$NH_4^+ + 1.83O_2 + 1.98HCO_3^- \rightarrow 0.021C_5H_7O_2N + 0.98NO_3^- + 1.041H_2O + 1.88H_2CO_3^- \quad (4.4)$$

$$NH_4^+ + 1.37O_2 + 0.08CO_2 + 0.02HCO_3^- \rightarrow 0.98NO_2^- + 0.02C_5H_7O_2N + 0.97H_2O + 1.96H^+ \quad (4.5)$$

On the other hand, it should be also pointed out that external carbon consumption in the tertiary MBBR depended on effluent TIN requirement given the limited AMX capacity in the low nitrogen polishing process. For example, ΔsCOD/ΔTIN increased from 2.9 ± 0.9 mg/L to 3.5 ± 0.6 mg/L, means 20% more external carbon was needed, when the targeted effluent TIN level was reduced from 6.4 ± 3.6 to 2.8 ± 1.7 mg/L (Table 4.2). For WWTPs in the U.S. required to meet the TIN discharge target of 6~8 mg/L (Falk et al., 2013), 54.7% carbon could be saved in the tertiary MBBR compared to the theoretical value (6.4 g/g) of full denitrification when glycerol was used as the carbon source (Campolong, 2019). Even for the WWTPs required to meet discharge TIN ≤ 3 mg/L (Falk et al., 2013), 45.2% external carbon still can be reduced with the same calculation.

4.6.2 Tolerance of highly variable influent quality and low temperature

Despite the dramatic fluctuation of influent quality and low temperature, the pilot system designed in Figure 4.1 managed to achieve the target effluent quality with substantially less energy and carbon inputs. This can be attributed to at least five novelties of the design. First, the smart feedback control system employed in the secondary process avoided the risk of either over or under aeration resulting from sCOD/N ratio fluctuation. When influent sCOD/N ratios were high (e.g., > 6 g/g), the feedback controller with preset NO_x-N/NH_4^+-N ratios (1.2~2.7 g/g) in the aerobic zone can tell the aeration pump to automatically extend the aeration time for completing both excessive sCOD depletion and partial nitrification and in turn avoided the risk of insufficient nitrification when influent sCOD was high. When influent sCOD/N ratios were low (e.g., ≤ 6 g/g), smart feedback control system automatically shortened the aeration time to the length that was just enough for partial nitrification targeted by the NO_x-N/NH_4^+-N ratio setpoints. This exact aeration time prevented intracellular carbon loss from over aeration and in turn ensured sufficient TIN

removal through ED during the secondary process. Similarly, Bauhs et al. (2022) reported that a shorter aeration time led to better ED in the post-anoxic zone than the longer aeration time did because more internal carbon can be left. Second, the partial nitrification strategy compensated nitrifiers' activity loss under low temperature. Although low temperature slowed down all bacterial activity including those of AOB and NOB (Barnard et al., 2005; Kanda et al., 2017), the workload expected for AOB and NOB to do was actually discounted under the concept of partial nitrification. For example, only 50~70% NH_4^+-N needs to be nitrified when the PE average temperature was as low as 17.9 ± 3.1°C. Third, the employment of PdNA allowed AMX to be applicable at temperature < 20 °C to achieve more energy and carbon savings. PdNA has been successfully full-scale applied in the secondary process. This study extended its application in the tertiary process where another smart feedforward-controller was used to safeguard the effluent TIN target despite the fluctuating influent sCOD/N ratios. Fourth, compared to exogenous denitrification, ED was reported to be more capable of adapting to low temperature (Peng et al., 2023). Therefore, replacing MLE with ED should have conferred more low temperature tolerance on the TIN removal capacity of the secondary process. Last but not the least, the excellent settleability of the secondary sludge allowed the sludge blankets to be well thickened during the settling phase. For example, had a high MLSS concentration of RAS was determined as 9000-15000 mg/L. Such a high bacterial concentration had accelerated the denitrification rate in the anoxic phase and in turn compensated the denitrification rate loss for the low temperature. Similar high bacterial concentration-enhanced ED rate was also reported elsewhere (Lee, 2022; Li et al., 2022).

4.6.3 Limitation and future work

It is a pity that 7.7~27.3% external carbon still needs to be added to polish the effluent TIN to a desired low level, even when 8.3~42.5% influent sCOD had to be depleted by aeration to enable partial nitrification to occur. Technically, this external carbon dose still has room to be minimized by directly shortcutting a portion of influent carbon into the tertiary MBBR to encourage more exogenous full denitrification besides PdNA. This is especially important when the influent sCOD/N ratio was > 6 g/g. This approach is worth being explored further in the future study. This is because it allows not only endogenous carbon but also exogenous carbon to be utilized in post anoxic zones for TIN removal and thus further void the need of MLE. Even when sCOD/N ratio

was < 6 g/g, the actual influent COD resource that can be shortcut into tertiary MBBR could be even more in that this study did not consider particulate and colloidal COD. Theoretically, there should be more particular and colloidal COD than sCOD in PE. Therefore, taking advantage of these extra influent COD has the potential to bring even more carbon savings to the proposed system.

4.7 Conclusions

The following conclusions can be drawn from this pilot study:

1) This study for the first time integrated partial nitrification, EBPR, ED, and PdAN in one system treating real PE under conditions of highly variable influent quality and low temperature to meet effluent TIN ≤ 3 mg/L and OP ≤ 0.1 mg/L.
2) It was estimated that 100% carbon and 55.5% oxygen were saved in the secondary process and another 45.2% carbon was saved in the tertiary process, depending on the expected effluent quality. In general, more savings had to be sacrificed when a lower discharge level, e.g., TIN ≤ 3 mg/L, is expected.
3) Most of the influent TIN (44.5~48.2%) can be removed through ED in the secondary treatment with another 25.8~39.5% polished by PdNA in tertiary treatment.
4) Experimental results demonstrated that the MLR which has been used for decades in convention WWTPs can be eliminated because almost all NOx- can be removed through post-anoxic ED.
5) The pilot system was able to handle highly variable influent quality and low temperature with the aid of automatic feedback and feedforward controllers nested in secondary and tertiary treatment, respectively.
6) The proposed system allocated influent rbCOD in priority to EBPR and ED, leaving only 7.7~27.3% external rbCOD demand for polishing in tertiary treatment.

4.8 References

Albertsen, M., McIlroy, S.J., Stokholm-Bjerregaard, M., Karst, S.M. and Nielsen, P.H. 2016. "*Candidatus Propionivibrio aalborgensis*": a novel glycogen accumulating organism abundant in full-scale enhanced biological phosphorus removal plants. Frontiers in Microbiology 7, 1033.

Aronhime, S., Calcagno, C., Jajamovich, G.H., Dyvorne, H.A., Robson, P., Dieterich, D., Isabel Fiel, M., Martel-Laferriere, V., Chatterji, M. and Rusinek, H. 2014. DCE-MRI of the liver: effect of linear and nonlinear conversions on hepatic perfusion quantification and reproducibility. Journal of Magnetic Resonance Imaging 40(1), 90-98.

Barnard, R., Leadley, P.W. and Hungate, B.A. 2005. Global change, nitrification, and denitrification: a review. Global biogeochemical cycles 19(1), GB1007.

Bauhs, K.T., Gagnon, A.A. and Bott, C.B. 2022. Investigating the use of anaerobically stored carbon in post-anoxic denitrification. Water Environment Research 94(6), e10749.

Bolyen, E., Rideout, J.R., Dillon, M.R., Bokulich, N.A., Abnet, C.C., Al-Ghalith, G.A., Alexander, H., Alm, E.J., Arumugam, M. and Asnicar, F. 2019. Reproducible, interactive, scalable and extensible microbiome data science using QIIME 2. Nature biotechnology 37(8), 852-857.

Callahan, B.J., McMurdie, P.J., Rosen, M.J., Han, A.W., Johnson, A.J.A. and Holmes, S.P. 2016. DADA2: High-resolution sample inference from Illumina amplicon data. Nature methods 13(7), 581-583.

Campolong, C.J. (2019) Bioaugmentation and retention of anammox granules to a mainstream deammonification bio-oxidation pilot with a post polishing anoxic partial denitrification/anammox moving bed biofilm reactor, (Master thesis) Virginia Tech.

Cavaliere, E. and Baulch, H.M. 2019. Winter nitrification in ice-covered lakes. PLoS One 14(11), e0224864.

Coats, E.R., Mockos, A. and Loge, F.J. 2011. Post-anoxic denitrification driven by PHA and glycogen within enhanced biological phosphorus removal. Bioresource technology 102(2), 1019-1027.

Du, R., Li, C., Liu, Q., Fan, J. and Peng, Y. 2022. A review of enhanced municipal wastewater treatment through energy savings and carbon recovery to reduce discharge and CO2 footprint. Bioresource Technology, 128135.

Erdal, U.G. (2002) The effects of temperature on system performance and bacterial community structure in a biological phosphorus removal system, (Master thesis) Virginia Tech.

Falk, M.W., Reardon, D.J., Neethling, J., Clark, D.L. and Pramanik, A. 2013. Striking the balance between nutrient removal, greenhouse gas emissions, receiving water quality, and costs. Water Environment Research 85(12), 2307-2316.

Faskol, A. and Racoviţeanu, G. 2021 Effect of DO, alkalinity and pH on nitrification using three different sunken materials types in biological aerated filter BAFs (Conference Proceedings), p. 012079.

Ferguson, S.J., Richardson, D.J. and Van Spanning, R.J. (2007) Biology of the nitrogen cycle, pp. 209-222, Elsevier.

Gao, H., Scherson, Y.D. and Wells, G.F. 2014. Towards energy neutral wastewater treatment: methodology and state of the art. Environmental science: Processes & impacts 16(6), 1223-1246.

Grady Jr, C.L., Daigger, G.T., Love, N.G. and Filipe, C.D. (2011) Biological wastewater treatment, CRC press.

Guerrero, J., Flores-Alsina, X., Guisasola, A., Baeza, J.A. and Gernaey, K.V. 2013. Effect of nitrite, limited reactive settler and plant design configuration on the predicted performance of simultaneous C/N/P removal WWTPs. Bioresource technology 136, 680-688.

Han, Y.-H., Fu, T., Wang, S.-S., Yu, H.-T., Xiang, P., Zhang, W.-X., Chen, D.-L. and Li, M. 2018. Efficient phosphate accumulation in the newly isolated *Acinetobacter junii strain LH4*. 3 Biotech 8, 1-12.

He, Q., Zhang, W., Zhang, S. and Wang, H. 2017. Enhanced nitrogen removal in an aerobic granular sequencing batch reactor performing simultaneous nitrification, endogenous denitrification and phosphorus removal with low superficial gas velocity. Chemical engineering journal 326, 1223-1231.

Henze, M., Gujer, W., Mino, T. and Van Loosedrecht, M. (2006) Activated sludge models ASM1, ASM2, ASM2d and ASM3, IWA Publishing.

Hong, S., Winkler, M.-K., Wang, Z. and Goel, R. 2023. Integration of EBPR with mainstream anammox process to treat real municipal wastewater: process performance and microbiology. Water Research, 119758.

Huaguang, L., Wenyi, D., Zilong, Z., Hongjie, W., Zilong, H., Yanchen, L., Shuo, C. and Diwen, X. 2023. Anammox-based technologies for municipal sewage nitrogen removal: Advances in implementation strategies and existing obstacles. Journal of Water Process Engineering 55, 104090.

Jönsson, K. and Jansen, J.l.C. 2006. Hydrolysis of return sludge for production of easily biodegradable carbon: effect of pre-treatment, sludge age and temperature. Water Science and Technology 53(12), 47-54.

Kanda, R., Kishimoto, N., Hinobayashi, J., Hashimoto, T., Tanaka, S. and Murakami, Y. 2017. Influence of temperature and COD loading on biological nitrification–denitrification process using a trickling filter: an empirical modeling approach. International Journal of Environmental Research 11, 71-82.

Kent, T.R., Bott, C.B. and Wang, Z.-W. 2018. State of the art of aerobic granulation in continuous flow bioreactors. Biotechnology advances 36(4), 1139-1166.

Kim, S., Bae, W., Kim, M., Kim, J.-O. and Chung, J. 2015. Evaluation of denitrification–nitrification biofilter systems in treating wastewater with low carbon: nitrogen ratios. Environmental technology 36(8), 1035-1043.

Ladipo-Obasa, M., Forney, N., Riffat, R., Bott, C., DeBarbadillo, C. and De Clippeleir, H. 2022. Partial denitrification–anammox (PdNA) application in mainstream IFAS configuration using raw fermentate as carbon source. Water Environment Research 94(4), e10711.

Le, T., Peng, B., Su, C., Massoudieh, A., Torrents, A., Al-Omari, A., Murthy, S., Wett, B., Chandran, K. and deBarbadillo, C. 2019. Nitrate residual as a key parameter to efficiently control partial denitrification coupling with anammox. Water Environment Research 91(11), 1455-1465.

Lee, B. 2022. Comparison of Effluent Suspended Solid Concentrations from Two Types of Rectangular Secondary Clarifiers. Water 14(10), 1577.

Li, J., Wang, Y., Liu, J., Peng, Y., Zhang, L. and Lin, J. 2022. Intensified nitrogen removal by endogenous denitrification in a full-scale municipal wastewater treatment plant. Environmental Research 205, 112564.

Lin, Z., Wang, Y., Huang, W., Wang, J., Chen, L., Zhou, J. and He, Q. 2019. Single-stage denitrifying phosphorus removal biofilter utilizing intracellular carbon source for advanced nutrient removal and phosphorus recovery. Bioresource technology 277, 27-36.

Lopez-Vazquez, C.M., Hooijmans, C.M., Brdjanovic, D., Gijzen, H.J. and van Loosdrecht, M.C. 2009. Temperature effects on glycogen accumulating organisms. water research 43(11), 2852-2864.

Lu, L., Guest, J.S., Peters, C.A., Zhu, X., Rau, G.H. and Ren, Z.J. 2018. Wastewater treatment for carbon capture and utilization. Nature Sustainability 1(12), 750-758.

Ma, B., Wang, S., Cao, S., Miao, Y., Jia, F., Du, R. and Peng, Y. 2016. Biological nitrogen removal from sewage via anammox: recent advances. Bioresource technology 200, 981-990.

Macmanus, J., Long, C., Klaus, S., Parsons, M., Chandran, K., De Clippeleir, H. and Bott, C. 2022. Nitrogen removal capacity and carbon demand requirements of partial denitrification/anammox MBBR and IFAS processes. Water Environment Research 94(8), e10766.

Maktabifard, M., Al-Hazmi, H.E., Szulc, P., Mousavizadegan, M., Xu, X., Zaborowska, E., Li, X. and Mąkinia, J. 2023. Net-zero carbon condition in wastewater treatment plants: A systematic review of mitigation strategies and challenges. Renewable and Sustainable Energy Reviews 185, 113638.

Molinos-Senante, M. and Maziotis, A. 2022. Evaluation of energy efficiency of wastewater treatment plants: The influence of the technology and aging factors. Applied Energy 310, 118535.

Parada, A.E., Needham, D.M. and Fuhrman, J.A. 2016. Every base matters: assessing small subunit rRNA primers for marine microbiomes with mock communities, time series and global field samples. Environmental microbiology 18(5), 1403-1414.

Pedregosa, F., Varoquaux, G., Gramfort, A., Michel, V., Thirion, B., Grisel, O., Blondel, M., Prettenhofer, P., Weiss, R. and Dubourg, V. 2011. Scikit-learn: Machine learning in Python. the Journal of machine Learning research 12, 2825-2830.

Pelaz, L., Gómez, A., Letona, A., Garralón, G. and Fdz-Polanco, M. 2018. Nitrogen removal in domestic wastewater. Effect of nitrate recycling and COD/N ratio. Chemosphere 212, 8-14.

Peng, Z., Zhang, Q., Li, X., Wang, S. and Peng, Y. 2023. Exploring and comparing the impacts of low temperature to endogenous and exogenous partial denitrification: the nitrite supply, transcription mechanism, and microbial dynamics. Bioresource Technology 370, 128568.

Qin, L., Liu, Y. and Tay, J.-H. 2005. Denitrification on poly-β-hydroxybutyrate in microbial granular sludge sequencing batch reactor. Water research 39(8), 1503-1510.

Qiu, S., Li, Z., Hu, Y., Shi, L., Liu, R., Shi, L., Chen, L. and Zhan, X. 2021. What's the best way to achieve successful mainstream partial nitritation-anammox application? Critical Reviews in Environmental Science and Technology 51(10), 1045-1077.

Quast, C., Pruesse, E., Yilmaz, P., Gerken, J., Schweer, T., Yarza, P., Peplies, J. and Glöckner, F.O. 2012. The SILVA ribosomal RNA gene database project: improved data processing and web-based tools. Nucleic acids research 41(D1), D590-D596.

Rice, E.W., Baird, R.B., Eaton, A.D. and Clesceri, L.S. (2012) Standard methods for the examination of water and wastewater (23rd Version), American public health association Washington, DC.

Senderovich, Y. and Halpern, M. 2013. The protective role of endogenous bacterial communities in chironomid egg masses and larvae. The ISME journal 7(11), 2147-2158.

Sharp, R., Khunjar, W., Daly, D., Perez-Terrero, J., Chandran, K., Niemiec, A. and Pace, G. 2020. Nitrogen removal from water resource recovery facilities using partial nitrification, denitratation-anaerobic ammonia oxidation (PANDA). Science of The Total Environment 724, 138283.

Siegrist, H., Krebs, P., Bühler, R., Purtschert, I., Rock, C. and Rufer, R. 1995. Denitrification in secondary clarifiers. Water Science and Technology 31(2), 205-214.

Silva, C. and Rosa, M.J. 2022. A comprehensive derivation and application of reference values for benchmarking the energy performance of activated sludge wastewater treatment. Water 14(10), 1620.

Sun, S.-P., Nàcher, C.P.i., Merkey, B., Zhou, Q., Xia, S.-Q., Yang, D.-H., Sun, J.-H. and Smets, B.F. 2010. Effective biological nitrogen removal treatment processes for domestic wastewaters with low C/N ratios: a review. Environmental Engineering Science 27(2), 111-126.

Wang, X., Chen, Z., Shen, J., Zhao, X. and Kang, J. 2019. Impact of carbon to nitrogen ratio on the performance of aerobic granular reactor and microbial population dynamics during aerobic sludge granulation. Bioresource technology 271, 258-265.

Wang, Y., Singh, R.P., Geng, C. and Fu, D. 2020. Carbon-to-nitrogen ratio influence on the performance of bioretention for wastewater treatment. Environmental Science and Pollution Research 27, 17652-17660.

Waqas, S., Harun, N.Y., Sambudi, N.S., Abioye, K.J., Zeeshan, M.H., Ali, A., Abdulrahman, A., Alkhattabi, L. and Alsaadi, A.S. 2023. Effect of operating parameters on the performance of integrated fixed-film activated sludge for wastewater treatment. Membranes 13(8), 704.

Ye, F., Ye, Y. and Li, Y. 2011. Effect of C/N ratio on extracellular polymeric substances (EPS) and physicochemical properties of activated sludge flocs. Journal of hazardous materials 188(1-3), 37-43.

Yuan, J., Dong, W., Sun, F. and Zhao, K. 2018. Low temperature effects on nitrification and nitrifier community structure in V-ASP for decentralized wastewater treatment and its improvement by bio-augmentation. Environmental science and pollution research 25, 6584-6595.

Zeng, W., Bai, X., Zhang, L., Wang, A. and Peng, Y. 2014. Population dynamics of nitrifying bacteria for nitritation achieved in Johannesburg (JHB) process treating municipal wastewater. Bioresource technology 162, 30-37.

Zeng, W., Wang, A., Li, C., Guo, Y. and Peng, Y. 2017. Population dynamics of "*Candidatus Accumulibacter phosphatis*" under the modes of complete nitrification and partial nitrification (nitritation) in domestic wastewater treatment system. Biochemical engineering journal 124, 69-77.

Zhang, M., Wang, S., Ji, B. and Liu, Y. 2019. Towards mainstream deammonification of municipal wastewater: Partial nitrification-anammox versus partial denitrification-anammox. Science of the Total Environment 692, 393-401.

Zhang, T., Cao, J., Zhang, Y., Fang, F., Feng, Q. and Luo, J. 2020. Achieving efficient nitrite accumulation in glycerol-driven partial denitrification system: Insights of influencing factors, shift of microbial community and metabolic function. Bioresource Technology 315, 123844.

Zhang, T., Wang, B., Li, X., Zhang, Q., Wu, L., He, Y. and Peng, Y. 2018. Achieving partial nitrification in a continuous post-denitrification reactor treating low C/N sewage. Chemical Engineering Journal 335, 330-337.

Zhang, Y. and Kinyua, M.N. 2020. Identification and classification of the *Tetrasphaera* genus in enhanced biological phosphorus removal process: a review. Reviews in Environmental Science and Bio/Technology 19, 699-715.

Zhao, J., Wang, X., Li, X., Jia, S. and Peng, Y. 2018. Combining partial nitrification and post endogenous denitrification in an EBPR system for deep-level nutrient removal from low carbon/nitrogen (C/N) domestic wastewater. Chemosphere 210, 19-28.

Chapter 5 Kinetic mechanism of methanol-fed partial denitrification anammox in tertiary moving bed biofilm reactors fed with real secondary effluent

(This chapter is ready for submission to a peer-reviewed journal)

5.1 Abstract

A pilot-scale tertiary moving bed biofilm reactor (MBBR) treatment train was operated onsite for 417 days in a local municipal wastewater treatment plant (WWTP) to understand the effectiveness and mechanisms of methanol-fed partial denitrification anammox (PdNA). This MBBR train was able to achieve effluent total inorganic nitrogen (TIN) ≤ 3 mg/L under normal loading operation and ≤ 4 mg/L under peak loading operation. Remarkably, the process enabled a 46.3% reduction in methanol usage and projected a significant oxygen saving of 1.1 to 1.6 tons per day for the WWTP. The research unravelled two coexisting mechanisms, i.e., in low strength wastewater treatment such as tertiary polishing where bulk COD ≤ 8 mg/L and bulk NO_3^--N ≤ 4 mg/L, NO_2^--N sink by anammox bacteria was found to be a dominant mechanism enabling partial denitrification (PdN); while in high strength wastewater treatment, the PdN mechanism shifted to the reliance on rate differential between denitratation and denitritation. This research advanced our understanding of methanol-enabled PdNA, elucidating the impact of operational conditions on the mechanisms and performance. Additionally, it offered a valuable framework for designing and optimizing full-scale methanol-fed PdNA processes, promoting low carbon nitrogen removal.

5.2 Keywords

Partial denitrification; anammox; MBBR; feedforward; BNR

5.3 Introduction

Moving bed biofilm reactors (MBBRs) have been commonly used as a polishing process for biological nitrogen removal to meet the stringent effluent total inorganic nitrogen (TIN) target, e.g., ≤ 3 mg/L. In these applications, supplemental carbon such as methanol, which has low market price, low biomass yield, and low environmental impacts (Badia et al., 2021; Purtschert and Gujer, 1999), has been widely used for denitrification (Bill et al., 2009; Ginige et al., 2009). However, conventional denitrification in these polishing processes is carbon-intensive and stoichiometrically consumes methanol for unit TIN removal at ≥ 4.8 g ΔCOD/g ΔTIN (Campolong, 2019).

Technically, a coupling of partial denitrification (PdN) with anammox (AMX) process can reduce aeration and methanol demands and in turn lead to tankage, chemical, and energy savings (Zhang et al., 2020). This is because AMX as an autotrophic process can directly convert NH_4^+-N and NO_2^--N into N_2 without external carbon utilization. AMX also can reduce aeration requirements as only a portion of NH_4^+-N needs to be oxidized into NO_X-N (Xu et al., 2020). However, methanol has been deemed as an undesirable carbon source for PdNA compared to glucose, glycerol and acetate (Zhang et al., 2020), and the reasons behind it remain unknown. As methanol is most widely used in the U.S., it would be convenient and cost-effective if the existing methanol storage and dosing facilities can be directly leveraged to perform partial denitrification anammox (PdNA). Therefore, studies on methanol-driven PdN sprung up in recent years (Campolong, 2019; Le et al., 2019a; Macmanus et al., 2022).

Since the supply of NO_2^--N is a key to achieve AMX, there are two hypotheses explaining the access of AMX to NO_2^--N when methanol was used as a carbons source. Hypothesis 1 assumes there is a NO_2^--N sink provided by AMX, i.e., AMX outcompetes denitritation in NO_2^--N utilization (Campolong, 2019; Le et al., 2019a). In this hypothesis, NO_2^--N is utilized by AMX as soon as it is produced from denitratation and thus NO_2^--N accumulation is usually unseen (Campolong, 2019; Le et al., 2019a). Hence, in this hypothesis, AMX enhances PdN because PdN deteriorates without AMX. In contrast, Hypothesis 2 assumes there is a rate differential between denitratation and denitritation regardless of the AMX involvement, i.e., neither AMX nor denitritation is fast enough to catch up the denitratation rate, and thus NO_2^--N accumulation is

usually observed (Al-Omari et al., 2021; Si et al., 2018; Zhang et al., 2020). In this hypothesis, PdN performance mainly depends on the denitratation rate rather than AMX rate. It should be pointed out that the mechanistic discrepancy between these two hypotheses have not been reconciled in literature.

Besides the lack of mechanistic understanding, the applicability of methanol-fed PdNA for meeting the stringent effluent TIN target of ≤ 3 mg/L is also unknown. This is important because the effluent TIN limits of 3 mg/L or less are common in regions such as the Chesapeake Bay watershed, coastal areas of North Carolina, mid-Colorado and Okanagan Lake area of British Columbia, Canada, and increasingly stringent effluent discharge limits will surely be imposed in the near future (Moore, 2010). In line with this low effluent TIN level requirement, the capacity of attenuating the effluent TIN to ≤ 4 mg/L under peak loading condition is also essential for proving the applicability of the technology (Moore, 2010). Hence, the validity of the Hypotheses 1 and 2 in normal and peak loading environments should be tested in real wastewater application for better understanding of the full-scale application potential of the technology.

To fill these knowledge gaps, a pilot MBBR treatment train receiving real secondary effluent and dosed with methanol as a supplement carbon source was set up and operated onsite at a local wastewater treatment plant (WWTP), namely Noman Cole pollution control plant (NCPCP), for 417 days. The MBBR performance and mechanism behind were analysed, which was anticipated to provide insights and guidance for future full-scale application of the methanol-fed PdNA technology.

5.4 Materials and methods

5.4.1 Reactor setup

The MBBR setup used in this study is illustrated in Figure 5.1a. Briefly, two 14 L working volume anoxic MBBRs, namely Cell A and Cell B, filled with polyethylene K1 media (Veolia, NJ, USA) at a volumetric fraction of 45%, were connected in sequence and followed by an 8 L working volume oxic MBBR, namely Cell C, which was filled with K1 media at a volumetric fraction of

32%. This MBBR treatment train mimics the full-scale MBBR design used in the same WWTP (Figure 5.1b). K1 media with established methylotrophs were collected from the full-scale MBBRs. The Cell A and Cell B were mechanically mixed with motor-driven paddles (McMaster-Carr, NJ, U.S.) at a rotating speed of 60 rpm. Cell C was fully aerated by an air pump (Simple Deluxe, CA, U.S.).

During startup, 1.5 L of suspended AMX biomass was seeded into each anoxic MBBR in Figure 5.1a, and the system was operated in an integrated fixed film activated sludge (IFAS) mode with the aid of a clarifier to recirculate suspended sludge for AMX bacterial colonization on the media. 30 days after seeding, suspended AMX biomass was washed out, and the system shifted to the MBBR mode. The designed hydraulic retention time (HRTs) of each anoxic MBBR (namely Cell A and Cell B) and the aerobic MBBR (namely Cell C) in Figure 5.1 were 19 min and 10 min, respectively. Thereby, Cell A and Cell B performed PdN or PdNA while Cell C polished residual NH_4^+-N coming out the Cell B if any (Figure 5.1b).

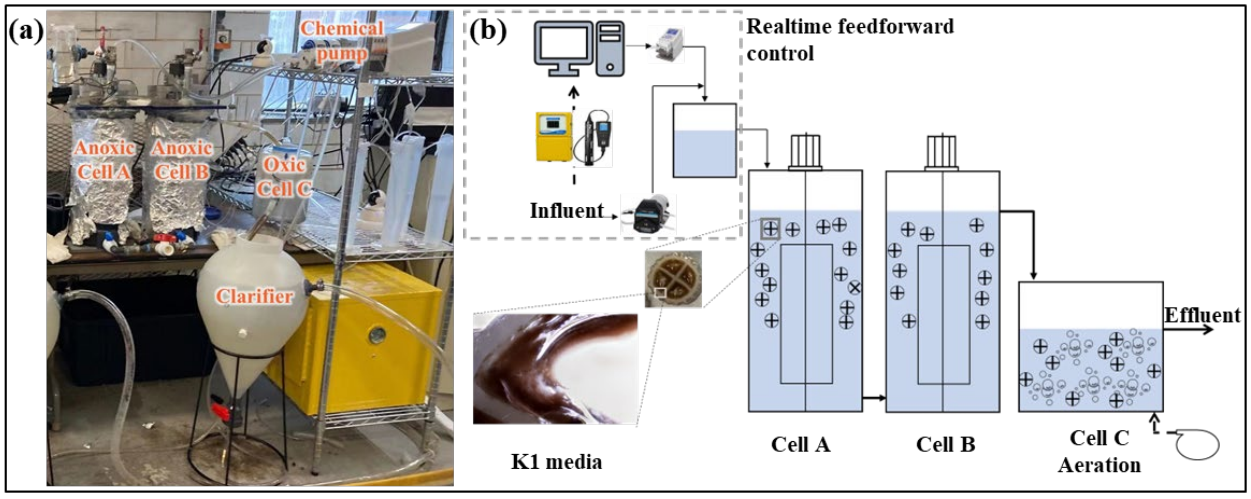

Figure 5.1 (a) real and (b) schematic view of the pilot MBBRs stationed at NCPCP.

5.4.2 Automatic control

Real-time NO_3^--N, NO_2^--N, NH_4^+-N, and dissolved oxygen (DO) concentration data of secondary effluent was measured by a Chemscan real-time analyser (ChemScan Inc., Wisconsin, USA) and a ProDSS Multiparameter Digital Water Quality Meter (YSI Incorporated, OH, USA). These data

were sent to a process control program written in Python 3.8 on a PC (Figure 5.1b). The PC in turn sent signals to an Ismatec Reglo ICC Digital Pump (Cole-Parmer, IL, USA) to precisely dose NH_4Cl and methanol to the Cell A according to the controller formulas set in Eqs. 5.1 and 5.2. The purpose of NH_4Cl addition is to mimic the NH_4^+-N residue to be produced from partial nitrification in the future full-scale secondary treatment process,

$$NH_{4\,feed}^{+} = NO_{3\,inf}^{-} \quad \text{or selected setpoints} \tag{5.1}$$

$$COD_{feed} = a \times \left(NO_{3\,inf}^{-} - NO_{3\,eff,setpoint}^{-}\right) + b \times DO_{inf} \tag{5.2}$$

in which $NO_{3\,inf}^{-}$ and DO_{inf} are real-time influent NO_3^--N and DO concentrations. $NH_{4\,feed}^{+}$ and COD_{feed} are concentrations of NH_4^+-N and COD dosed into Cell A. $NO_{3\,eff,setpoint}^{-}$ is the NO_3^--N concentration targeted in the Cell B effluent, which was set as 1~1.5 mg/L. Three $NH_{4\,feed}^{+}$ levels were used in this study, i.e., $NH_{4\,feed}^{+}$ was set equal to $NO_{3\,inf}^{-}$ from Days 1 to 132 and decreased to 4 mg/L from Days 133 to 199, and then further decreased to 2 mg/L from Days 200 to 417, respectively. 'a' in Eq. 5.2 is a coefficient used to adjust influent COD for achieving $NO_{3\,eff,setpoint}^{-}$. 'b' in Eq. 5.2 represents the COD consumption per unit DO removal when methanol is used as a carbon source. Hence, 'a' and 'b' values were set as 4 g/g and 2 g/g in this study, respectively. It should be noted that the DO_{inf} was around 3 mg/L in this study because of the intrinsic turbulence in secondary effluent flow in this particular WWTP. With these being said, COD_{feed} was composed of COD consumed for PdN and DO removal. For monitoring the chemical dose accuracy, a small chemical mixing tank with a HRT of 2 ~ 3 min was added in front of the Cell A (Figure 5.1b), where influent samples after chemical dosing could be grabbed. Grab samples from the influent, Cell A, Cell B, and Cell C were analyzed 3 ~ 4 times a week.

5.4.3 Chemical and statistical analysis methods

The concentrations of NO_3^--N, NO_2^--N, NH_4^+-N, and sCOD after 0.45 μm syringe filter (MilliporeSigma, MD, USA) filtration were analysed with Hach TNT® 835, 839, 830, and 820 vials, respectively, in a spectrophotometer (DR 3900, Hach, Loveland, CO, USA) according to the standard method (Rice et al., 2012). The readily biodegradable soluble COD (rbsCOD) was calculated by subtracting the MBBR effluent sCOD from the influent sCOD. Spearman correlation analysis was performed in GraphPad Prism 10 (Dotmatics, MA, USA).

5.4.4 Model development

Kinetics of PdN can be simplified to the competition between denitratation (NO_3^--N → NO_2^--N) and denitritation (NO_2^--N → N_2) according to Glass and Silverstein (1998). The specific NO_3^--N uptake rate of denitratation (q_{DNA}) can be described by Eq. 5.3 according to Activated Sludge Model NO. 1 (Henze et al., 2000). Similarly, the specific NO_2^--N uptake rate of denitritation (q_{DNI}) can be described by Eq. 5.4. Likewise, the specific NO_2^--N uptake rate of AMX bacteria can be described by Eq. 5.5. Definitions and values of all kinetic parameters used in these equations are listed in Table 5.1.

$$q_{DNA} = \frac{\mu_m^{Da}}{Y_{NO3}^{Da}} \frac{S_{COD}}{K_{COD}+S_{COD}} \frac{S_{NO_3^-}}{K_{NO3}^{Da}+S_{NO_3^-}} \tag{5.3}$$

$$q_{DNI} = \frac{\mu_m^{Di}}{Y_{NO2}^{Di}} \frac{S_{COD}}{K_{COD}+S_{COD}} \frac{S_{NO_2^-}}{K_{NO2}^{Di}+S_{NO_2^-}} \tag{5.4}$$

$$q_{AMX} = \frac{\mu_m^{AN}}{Y_{NO2}^{AN}} \frac{S_{NH3}}{K_{NH3}^{AN}+S_{NH3}} \frac{S_{NO_2^-}}{K_{NO2}^{AN}+S_{NO_2^-}} \tag{5.5}$$

Table 5.1 Monod kinetic parameters for Eqs. 5.3, 5.4, and 5.5

Symbol	Definition	Value	References
Methylotrophic denitratation and denitritation (20 °C value)			
μ_m^{Da}	Maximum specific growth rate of denitratation bacteria (/d)	1	Her and Huang (1995)
μ_m^{Di}	Maximum specific growth rate of denitritation bacteria (/d)	0.89	Her and Huang (1995)
K_{NO3}^{Da}	Half saturation constant for NO_3^--N (mg/L)	3	Al-Omari et al. (2021)
K_{NO2}^{Di}	Half saturation constant for NO_2^--N (mg/L)	1.5	Al-Omari et al. (2021)
K_{COD}	Half saturation constant for COD (mg/L)	15	Al-Omari et al. (2021)
Y_{NO2}^{Di}	Biomass growth yield on NO_2^--N (g/g)	0.58	Campolong (2019)
Y_{NO3}^{Da}	Biomass growth yield on NO_3^--N (g/g)	0.38	Campolong (2019)
Anammox (20 °C value)			
μ_m^{AN}	Maximum specific growth rate of AMX (/d)	0.08	Bi et al. (2015)
K_{NO2}^{AN}	Half saturation constant for nitrite (mg/L)	0.55	Bi et al. (2015)
K_{NH3}^{AN}	Half saturation constant for ammonia (mg/L)	0.73	Bi et al. (2015)
Y_{NO2}^{AN}	Biomass yield on nitrite (g/g)	0.11	Bi et al. (2015)

S_{COD}	Concentration of biodegradable soluble COD in the bulk liquid (mg/L)
$S_{NO_3^-}$	Concentration of NO_3^--N in the bulk liquid (mg/L)
$S_{NO_2^-}$	Concentration of NO_2^--N in the bulk liquid (mg/L)
S_{NH3}	Concentration of NH_4^+-N in the bulk liquid (mg/L)

5.4.5 Calculation methods

PdN efficiency, namely the percent of NO_3^--N that was only denitrified to NO_2^--N but not further denitrified to N_2 by organic reducers, was determined in Eq. 5.6,

$$PdN\ \% = \frac{NO_{2\,eff}^- - NO_{2\,inf}^- + 1.32 \times (NH_{4\,inf}^+ - NH_{4\,eff}^+ - NH_{4\,assmilated}^+)}{NO_{3\,inf}^- - NO_{3\,eff}^- + 0.26 \times (NH_{4\,inf}^+ - NH_{4\,eff}^+ - NH_{4\,assimilated}^+)} \quad (5.6)$$

in which $NO_{2\,inf}^-$, $NO_{3\,inf}^-$, and $NH_{4\,inf}^+$ are the influent concentrations of NO_2^--N, NO_3^--N and NH_4^+-N. $NO_{2\,eff}^-$, $NO_{3\,eff}^-$, and $NH_{4\,eff}^+$ are effluent concentrations. 1.32 and 0.26 are based on the stoichiometries of AMX reaction in Eq. 5.7 according to a previous study (Ma et al., 2016), i.e.,

$$NH_4^+ + 1.32NO_2^- + 0.066HCO_3^- + 0.13H^+ \rightarrow 1.02N_2 + 0.26NO_3^- + 0.066CH_2O_{0.5}N_{0.15} + 2.03H_2O \quad (5.7)$$

$NH_{4\,assimilated}^+$ represents the NH_4^+-N assimilated by the heterotrophic organisms for growth and was estimated by Eq. 5.8,

$$NH_{4\,assimilated}^+ = \mathrm{Y} \times \mathrm{C} \times (sCOD_{inf} - sCOD_{eff}) \quad (5.8)$$

in which $sCOD_{inf}$ and $sCOD_{eff}$ are the sCOD concentrations in the influent and effluent. Y is observed growth yield of heterotrophic organisms, namely 0.2 mg biomass COD/mg rbsCOD consumed, and C is biomass nitrogen content, namely 0.07 mg N/mg Biomass, based on the study by Grady Jr et al. (2011). Hence, NO_2^--N utilization by AMX can be calculated in Eq. 5.9,

$$\Delta NO_{2\,AMX}^- = 1.32 \times (NH_{4\,inf}^+ - NH_{4\,eff}^+ - NH_{4\,assmilated}^+) \quad (5.9)$$

TIN concentration in this study was defined as the sum of NO_3^--N, NO_2^--N, and NH_4^+-N concentrations. AMX contribution to TIN removal, namely $\Delta TIN_{AMX}/\Delta TIN$, was calculated by Eq. 5.10,

$$\Delta \mathrm{TIN}_{AMX}/\Delta \mathrm{TIN} = \frac{(1+1.32-0.26) \times (NH_{4\,inf}^+ - NH_{4\,eff}^+ - NH_{4\,assimilated}^+)}{\mathrm{TIN}_{inf} - \mathrm{TIN}_{eff}} \quad (5.10)$$

in which 1, 1.32 and 0.26 were derived from Eq. 5.7. TIN_{inf} and TIN_{eff} represent TIN concentrations in the influent and effluent of Cell A and Cell B, respectively.

NO_2^--N utilization rates of AMX (V_{AMX}) and denitritation (V_{DNI}) in the Cell A were calculated with Eqs. 5.11 and 12

$$V_{AMX} = \frac{1.32\times(NH_4^+{}_{inf} - NH_4^+{}_{eff} - NH_4^+{}_{assimilated})}{HRT} \quad (5.11)$$

$$V_{DNI} = \frac{NO_3^-{}_{inf} - NO_3^-{}_{eff} + NO_2^-{}_{inf} - NO_2^-{}_{eff} - (1.32-0.26)\times(NH_4^+{}_{inf} - NH_4^+{}_{eff} - NH_4^+{}_{assimilated})}{HRT} \quad (5.12)$$

in which HRT represents the hydraulic retention time (namely, 20 minutes) of Cell A.

5.4.6 qPCR analysis

Quantitative polymerase chain reaction (qPCR) was performed to quantify the copy numbers of total bacterial 16S ribosomal RNA (rRNA) gene, the 16S rRNA of *Candidatus* Kuenenia, hydrazine synthase subunit A *(hzsA)* and B *(hzsB)* genes on a QuantStudio 3 thermocycler (Applied Biosystems, Waltham, MA). Each 20-μL qPCR reaction mixture contained 10 μL of 2× SYBR™ Green PCR Master Mix with ROX (Life Technologies, Carlsbad, CA), 1 μL each of forward and reverse primers (0.2 μM), 7 μL molecular-grade water (Sigma-Aldrich, St. Louis, MO) and 1 μL DNA template. The thermal cycling conditions for qPCR amplification were as follow: 95 ℃ for 2 min, 40 cycles at 95 ℃ for 15 s, 60 ℃ for 15 s, 72 ℃ for 20 s, melt-curve for 45 s (95 ℃ for 15 s, 60 ℃ for 15 s and 95 ℃ for 15 s). All qPCR runs had an efficiency between 90% and 110% with an $R^2 > 0.95$. Each gene was quantified in triplicate with a standard curve and negative control (with water as template). Results were reported as relative abundance in terms of gene copies per 16S gene copies.

5.5 Results

5.5.1 System performance

The entire MBBR operation can be divided into three stages, namely startup, normal loading operation, and peak loading operation made of a peak flow test and a peak concentration test

(Figure 5.2). During the normal loading operation, 47.2 ± 12.2%, 12.2 ± 5.1%, and 0.4 ± 0.7% of influent TIN were removed in Cell A (anoxic), Cell B (anoxic), and Cell C (oxic), respectively (Figure 5.2a), achieving around 59.8% total TIN removal regardless of the influent quality and temperature fluctuation, which can be ascribed to the effectiveness of automatic feedforward control system incorporated in the study (Figure 5.1b). In contrast, during the peak flow test when the inflow rate was doubled, TIN removal efficiency was reduced from 47.2 ± 12.2% to 25.8 ± 4.2% in Cell A but increased from 12.2 ± 5.1% to 27.4 ± 3.4% and from 0.4 ± 0.7% to 5.0 ± 3.3% in Cell B and Cell C, respectively (Figure 5.2a), giving the total TIN removal of 58.2%, which is only slightly lower than that during normal loading operation. The slight TIN removal increase in the oxic Cell C during the peak flow test can be ascribed to the cell assimilation (Figure 5.2a). It is interesting to observe that the sum of TIN removal in Cell A and Cell B during the peak flow test was approximately the same as that in Cell A alone during the normal loading operation. This is because after doubling the inflow rate, the total HRT of Cell A and Cell B was equal to the individual HRT of Cell A during normal flow (Figure 5.2a). Therefore, Cell B took on more TIN removal burden when the loading rate exceeded Cell A capacity, evidencing the good buffering capacity from the system redundancy (Figure 5.1). During the normal loading operation, 38.2% of TIN removal was contributed by AMX (Figure 5.2b). Specifically, AMX in Cell A and Cell B contributed 28.2 ± 9.7% and 10.0 ± 5.4% TIN removal, respectively, indicating greater AMX activity in Cell A over that in Cell B. During the peak flow and peak concentration tests, AMX contribution in Cell A dramatically decreased from 28.2 ± 9.7% to 9.1 ± 2.0% and 13.4 ± 5.1%, respectively (Figure 5.2b), but AMX contribution in Cell B to the total TIN removal barely changed. This was because more complete denitrification occurred in Cell A as a result of bulk rbsCOD concentration surge in Cell A but not in Cell B during the peak loading operation (Figure 5.2c). For example, bulk rbsCOD concentrations in Cell A increased from 4.3 ± 2.3 mg/L in normal loading operation to 17.4 ± 2.5 mg/L and 12.5 ± 4.8 mg/L during peak flow and peak concentration tests, respectively, while rbsCOD concentrations in Cell B only slightly increased from 1.0 ± 1.3 mg/L to 5.3 ± 1.4 mg/L and 3.9 ± 2.0 mg/L, respectively, due to the rbsCOD utilization in Cell A (Figure 5.2c).

In addition, some NO_3^--N residue was intentionally maintained in Cell B (Figure 5.2d) with the aid of the feedforward controller (Eq. 5.2) for enabling PdN. For example, average NO_3^--N residue

of 1-1.5 mg/L was maintained in Cell B from Day 190 forward. It was reported that a certain level of NO_3^--N residue is essential for achieving PdN (Campolong, 2019; Le et al., 2019b). In addition, influent NH_4^+-N (Figure 5.2e) was dosed at the same concentration as the real-time influent NO_3^--N concentration through the feedforward controller (Eq. 5.1) to facilitate the growth and colonization of AMX bacteria according to its stoichiometry in Eq. 5.7 during the startup (Days 1 to 120). However, because of the limited AMX capacity in MBBR, total anoxic NH_4^+-N removal in both Cell A and Cell B was only ≤ 2 mg/L by day 200 (Figure 5.2e), leading to high levels of NH_4^+-N breakthrough which increased the effluent TIN level (Figure 5.2f). This observation means any unused NH_4^+-N will become part of the effluent TIN. For this regard, NH_4^+-N dose was reduced to 2 mg/L from Day 200 onward regardless of influent NO_3^--N. As can be seen from Figure 2e, average anoxic NH_4^+-N removal of 1.3 ± 0.4 mg/L was achieved during the normal loading operation, which can be attributed to AMX activities. Specifically, more NH_4^+-N removal was achieved in Cell A (1.0 ± 0.3 mg/L) than in Cell B (0.3 ± 0.2 mg/L) during the normal loading operation (Figure 5.2e). Accordingly, qPCR results in Figure 5.3 also detected a higher level of AMX in Cell A than in Cell B in terms of anammox bacteria (*Candidatus Kuenenia*), hydrazine synthase subunit A *(hzsA),* and B *(hzsB)*. It should be pointed out that a minor baseline level of AMX was also detected in the full-scale MBBRs where was without PdN control. This baseline level of AMX indicates that full-scale application of the PdNA technology might be achieved without AMX bacteria inoculation.

After NH_4^+-N dosing adjustment, an average effluent TIN of 2.6 ± 0.6 mg/L was achieved during the rest of the normal loading operation time from Days 200 to 372 as shown in Figure 5.2f, which met the strict discharge TIN limit of ≤ 3 mg/L. Even during the peak flow and peak concentration tests, an average effluent TIN of 3.4 ± 1.3 mg/L and 3.6 ± 0.9 mg/L was also achieved, respectively, which met the peak loading TIN discharge target of ≤ 4 mg/L (Figure 5.2f). With the aid of autotrophic nitrogen removal by AMX activities, ΔsCOD/ΔTIN of the system was stabilized around 2.5 ± 0.6 g COD/g N (Figure 5.2g), which was 46.3% lower than full-scale MBBR value, namely 4.7 g COD/g N, when only full denitrification was used. It is noteworthy that these values were obtained after influent DO was deducted. This carbon reduction could directly save a fortune for the utility given the current methanol price. ΔsCOD/ΔTIN of this study was in the same range as those of 1.7 ~ 3.3 g/g reported by Campolong (2019) and Macmanus et al. (2022), who also

performed PdNA using methanol as the carbon source in tertiary MBBRs or IFAS, respectively. Meanwhile, instead of oxidizing all influent NH_4^+-N, around 1~1.5 mg/L influent NH_4^+-N could shortcut the secondary train into tertiary MBBRs with no need of nitrification (Figure 5.2e). Thus, according to the stoichiometry of nitrification in Eq. 5.13 (Faskol and Racovițeanu, 2021), 1.1 ~1.6 tons O_2 per day can be saved in this WWTP with a flow rate of 69 million gallon per day. Consequently, both aeration energy and tankage volume can be reduced by employing the PdNA.

$$NH_4^+ + 1.83O_2 + 1.98HCO_3^- \rightarrow 0.021C_5H_7O_2N + 0.98NO_3^- + 1.041H_2O + 1.88H_2CO_3^- \quad (5.13)$$

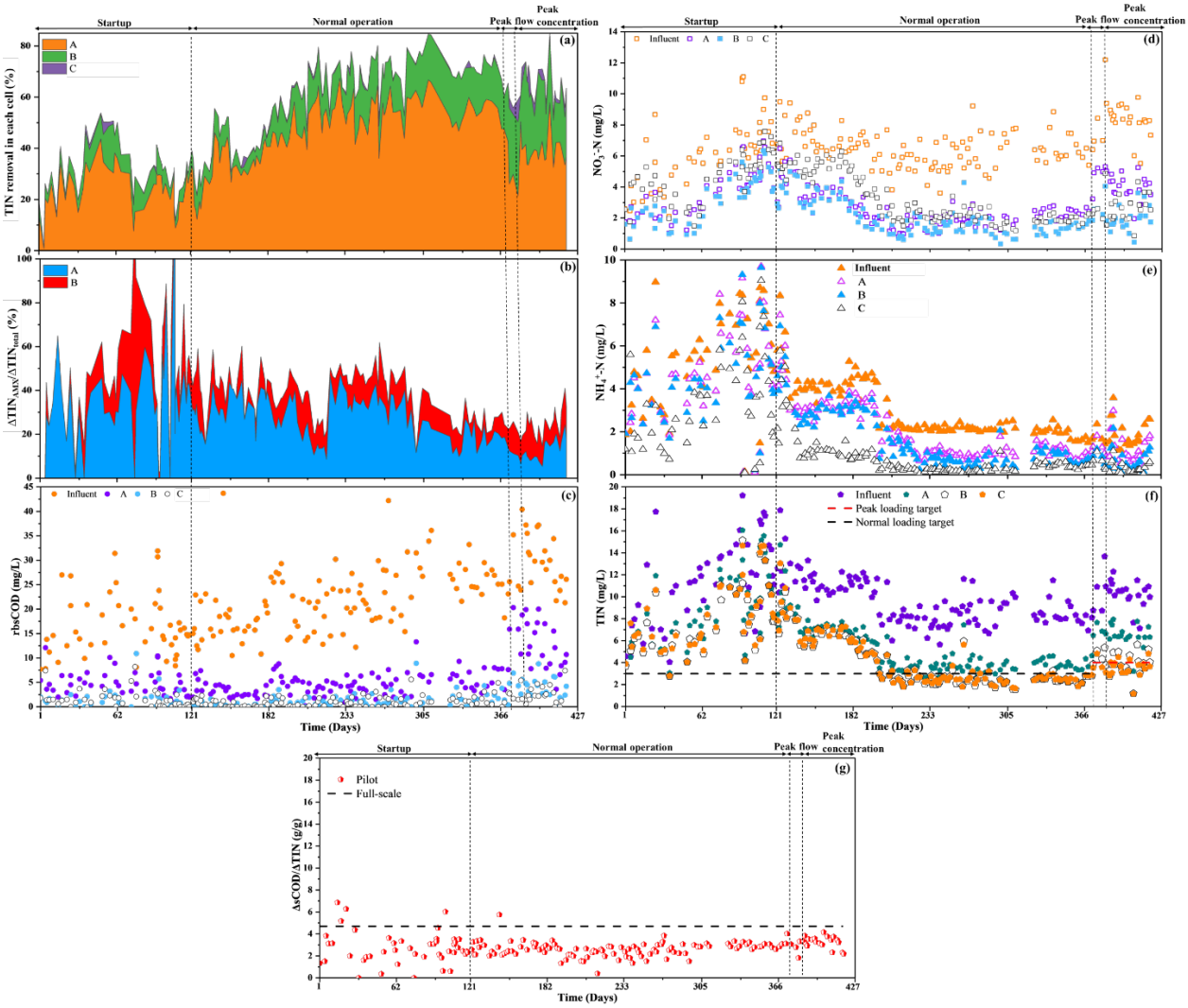

Figure 5.2 (a) Stacked profiles of influent TIN removal efficiency in each cell; (b) Stacked profiles of AMX contribution in Cell A and Cell B to total TIN removal; Profiles of (c) rbsCOD, (d) NO_3^--N, (e) NH_4^+-N, and (f) TIN concentrations in the influent, Cell A, Cell B, and Cell C; (g) Profiles of ΔsCOD/ΔTIN and its comparison with counterpart full-scale value. Note: ΔsCOD values are after influent DO deduction

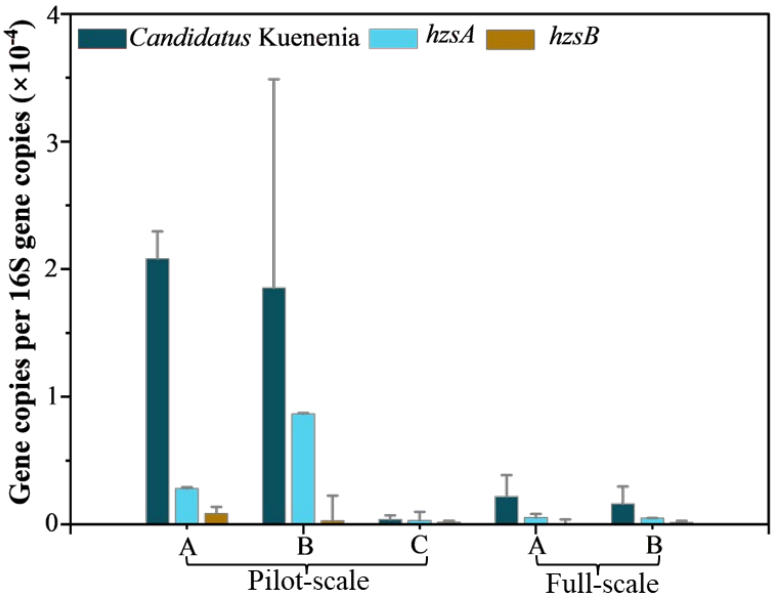

Figure 5.3 Relative abundance of anammox bacteria (*Candidatus Kuenenia*) and hydrazine synthase subunit A *(hzsA)* and B *(hzsB)* gene copies in the Cell A, Cell B, and Cell C of the pilot-scale MBBR and in Cell A and Cell B of full-scale MBBR (on Day 380).

5.5.2 Fate of nitrite during normal and peak loading operation

The success of autotrophic nitrogen removal through AMX depends on the availability of NO_2^--N for AMX utilization. Theoretically, NO_2^--N has three destinations after formation in anoxic reactors, i.e., denitrifier reduction, AMX utilization, or effluent NO_2^--N residue. Since the last two destinations belong to the scope of PdN, monitoring the NO_2^--N flow towards these two destinations helps test the aforementioned Hypotheses 1 and 2.

Figure 5.4 shows PdN efficiencies and NO_2^--N flow in Cell A and Cell B. During normal loading operation, PdN efficiency in Cell A was stabilized around 39.2 ± 9.5% for the most time (from Days 122 to 311) but slightly decreased to around 25.8 ± 5.7% from Days 326 to 372 due to the operational hiccups (Figure 5.4a). PdN efficiency resumed to 32.0 ± 7.2% during the peak flow test with a double inflow rate (from Days 373 to 380). And this PdN efficiency further resumed to 35.4 ± 9.8% during the peak concentration test (from Days 383 to 418) as shown in Figure 5.4a. It is noteworthy that, during the normal loading operation, majority of NO_2^--N produced from PdN was utilized by AMX, leaving only a small residue of NO_2^--N (0.6 ± 0.2 mg/L) in Cell A (Figure

5.4a), which belongs to the scope of Hypothesis 1. In contrast, NO_2^--N produced from PdN during the peak concentration test seemed to be more than sufficient for AMX utilization, thus leaving a much greater residue of NO_2^--N (1.1 ± 0.5 mg/L) in Cell A. Given the saturation of AMX capacity in Cell A, this NO_2^--N accumulation indicates a rate differential between denitratation and denitritation, which belongs to the scope of Hypothesis 2.

In Cell B, although the average PdN efficiency was only around 11.4 ± 15.3% during the normal loading operation, it increased to 27.1 ± 15.3% during the peak concentration test (Figure 5.4b), which was due to the more available rbCOD and NO_3^--N overflow from Cell A. However, the improved PdN did not lead to better NO_2^--N utilization by AMX in Cell B, leaving much more NO_2^--N residue (1.0~1.2 mg/L) in the bulk liquid during the peak loading operation (Figure 5.4b). The reason might have to do with the limited AMX capacity in Cell B because PdN in Cell B has been at a minimum level during normal loading operation (Figure 5.4b).

To sum up, the fraction of NO_2^--N flow to AMX or residue is a major difference between normal (less NO_2^--N residue) and peak loading operation (more NO_2^--N residue), which implied a potential PdN mechanism shift from Hypothesis 1 to Hypothesis 2.

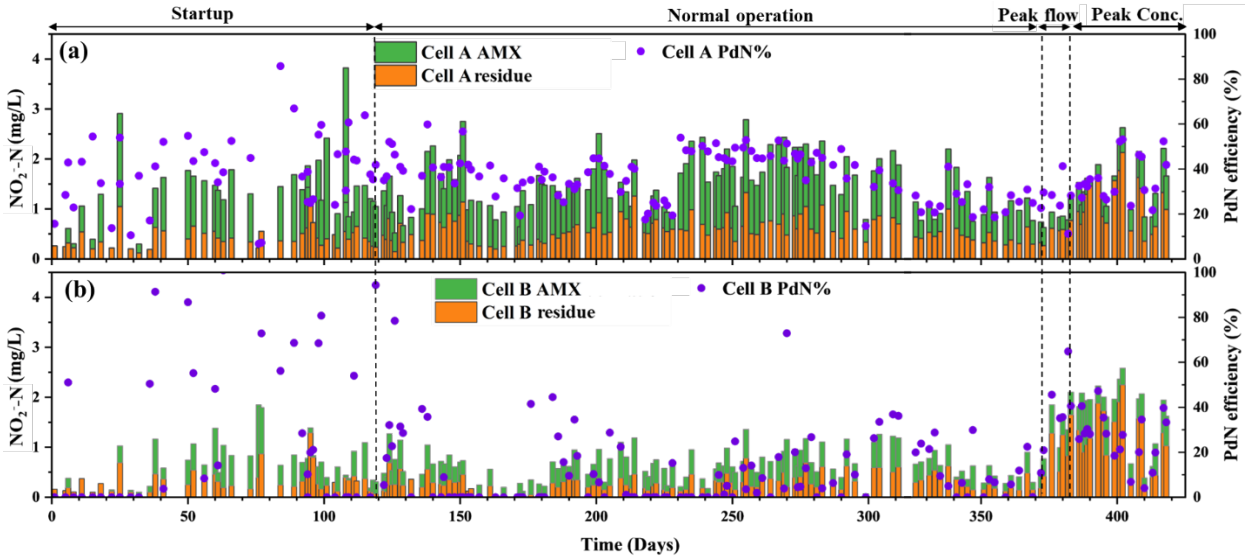

Figure 5.4 PdN efficiency and NO_2^--N flow in (a) Cell A and (b) Cell B

5.5.3 PdN efficiency versus AMX contribution in Cell A and Cell B

Figure 5.5 a and b plotted PdN efficiency against AMX contribution to TIN removal ($\Delta TIN_{AMX}/\Delta TIN$) at various bulk rbsCOD and NO_3^--N concentrations in Cell A and Cell B, respectively. For this kind of plot, three scenarios exist. In scenario 1, if most experimental data fell 'on' the diagonal, Hypothesis 1 holds true because it means AMX utilized all NO_2^--N produced from PdN and thus might have played a role in PdN performance. In scenario 2, if most experimental data fell within the region above the diagonal, Hypothesis 2 may hold true because AMX only can utilize a small portion of the NO_2^--N produced by PdN and thus was unlikely to dictate PdN. In this scenario, PdN performance depends on the rate differential between denitratation and denitritation. In scenario 3, if the experimental data fell within the region below the diagonal, then AMX contribution to TIN removal exceeded that of the PdN efficiencies, which means that high NO_2^--N concentrations pre-existed in the influent, and thus AMX could occur even without PdN. Figure 5.5a shows that PdN efficiency and AMX contribution were almost equal for most data of Cell A under normal loading operation, which belongs to the scenario 1. Only during peak loading operation when higher rbsCOD and NO_3^--N showed up in the bulk liquid of Cell A, PdN efficiency tended to be greater than AMX contribution (Figure 5.5a), indicating high rbsCOD and NO_3^--N concentrations enabled rate differential as predicted in the scenario 2. This observation evidenced that the PdN mechanism shifted from Hypothesis 1 to Hypothesis 2 under different substrate loading conditions. In Cell B where only minor PdN was achieved due to the lack of rbsCOD and NO_3^--N availability (Figure 5.5b), AMX contribution even exceeded PdN efficiency due to the NO_2^--N overflow from Cell A, which belongs to the scenario 3.

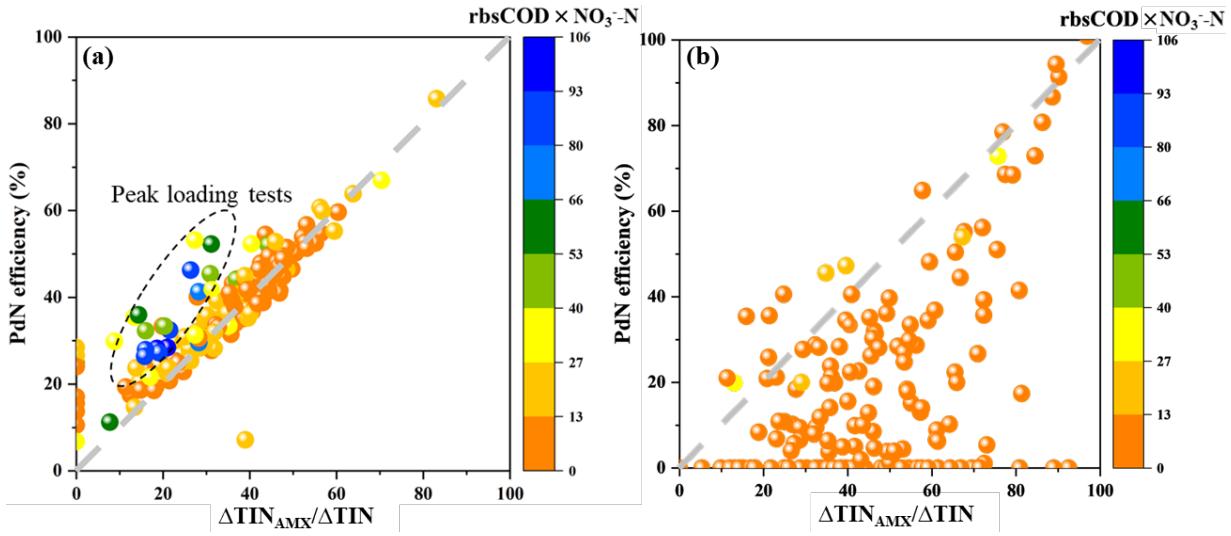

Figure 5.5 PdN efficiency v.s. AMX contribution to TIN removal ($\Delta TIN_{AMX}/\Delta TIN$) in Cells A and B in response to the product of rbsCOD and NO_3^--N

5.5.4 Statistical correlations between PdN efficiencies and other controllable parameters

In order to further reveal the PdN mechanism shift from Hypothesis 1 to Hypothesis 2 under different substrate loading conditions, statistical correlations between PdN efficiency and controllable parameters such as influent concentrations of rbsCOD, NO_3^--N, NH_4^+-N, and NO_3^--N residue were statistically analyzed using Spearman correlations. Results in Table 5.2 show that during normal loading operation, only influent rbsCOD and NH_4^+-N concentrations in Cell A were highly correlated with PdN efficiency with *p*-values (< 0.05). Specifically, PdN efficiency in Cell A was positively correlated to influent NH_4^+-N concentrations ($r = 0.34$, $p < 0.05$), indicating that NO_2^--N sink by AMX (Hypothesis 1) played an important role in PdN during the normal loading operation, which is in line with observation in Figure 5.4 and Figure 5.5. Meanwhile, PdN efficiency in Cell A was negatively correlated to influent rbsCOD ($r = -0.23$, $p < 0.05$), indicating an increase in influent rbsCOD concentration led to a decrease in PdN efficiency. This is because rbsCOD can help denitrifiers outcompete AMX bacteria over NO_2^--N utilization, leading to lower AMX activities and thus a lower PdN efficiency, which agrees with the observation in Figure 5.2 b and c. In contrast, PdN efficiency in Cell B during the normal loading operation showed no correlations ($p > 0.05$) with other operational parameters in Table 5.2. This is because PdN efficiencies in Cell B were at negligible levels for most of the normal loading operation period

(Figure 5.4), due to the extremely low rbsCOD and NO_3^--N concentrations in Cell B (Figures 5.2 c and d).

During the peak loading operation (Table 5.2), PdN efficiency in Cell A had no correlation with influent NH_4^+-N concentration anymore ($p > 0.05$). Instead, it started to show positive corelation with NO_3^--N concentrations in the influent (r = 0.37, $p < 0.05$) and in Cell A bulk liquid (r = 0.38, $p < 0.05$) (Table 5.2), evidencing the shift of PdN mechanisms from Hypothesis 1 (NO_2^--N sink) to Hypothesis 2 (rate differential) in the peak loading operation. Similar results were also observed in Cell B during the peak loading operation except that PdN efficiency in Cell B was also found to be positively correlated with influent rbsCOD concentration (Table 5.2). This is because rbsCOD concentrations in Cell B influent were at the minimum level during the normal loading operation (Figure 5.2c), and thus PdN in Cell B has been carbon-limited.

Table 5.2 Spearman correlations between the operational parameters and PdN efficiency (PdN%) during the normal and peak loading tests in Cell A and Cell B

Parameters	PdN% v.s. rbsCOD influent	PdN% v.s. NO_3^--N influent	PdN% v.s. NH_4^+-N influent	PdN% v.s. NO_3^--N residue
Normal loading operation in Cell A				
Spearman r	-0.23	-0.01	0.34	0.15
P (two-tailed)	1.30×10^{-3}	0.90	1.20×10^{-5}	0.06
Normal loading operation in Cell B				
Spearman r	0.13	0.09	0.12	-0.05
P (two-tailed)	0.11	0.30	0.14	0.58
Peak loading in Cell A				
Spearman r	0.23	0.37	0.17	0.38
P (two-tailed)	0.14	0.02	0.27	0.01
Peak loading in Cell B				
Spearman r	0.69	0.62	0.28	0.31
P (two-tailed)	2.53×10^{-7}	1.14×10^{-5}	0.07	0.04

5.5.5 Role of AMX in PdN

In order to evaluate the role of AMB in PdN, NH_4^+-N dosing was intentionally paused on Days 95, 96 and 104 during normal loading operation as shown in Figure 5.6. Hypothetically, if PdN is mainly dependent on the rate differential between denitratation and denitritation as described by Hypothesis 2, arresting AMX activity by pausing NH_4^+-N feed should not affect PdN efficiency. If otherwise, it means AMX was involved in PdN (Hypothesis 1). Results in Figure 5.6 showed that whenever AMX activity was arrested by stopping NH_4^+-N dosing, PdN efficiency dramatically dropped from 40~60% to below 20%. It is noteworthy that NO_2^--N residue in Cell A almost doubled without AMX utilization, but the total NO_2^--N produced by PdN was much lower than that during the time with AMX utilization (Figure 5.6). These data suggested that AMX activity augmented the rate differential, which is relevant to Hypothesis 1.

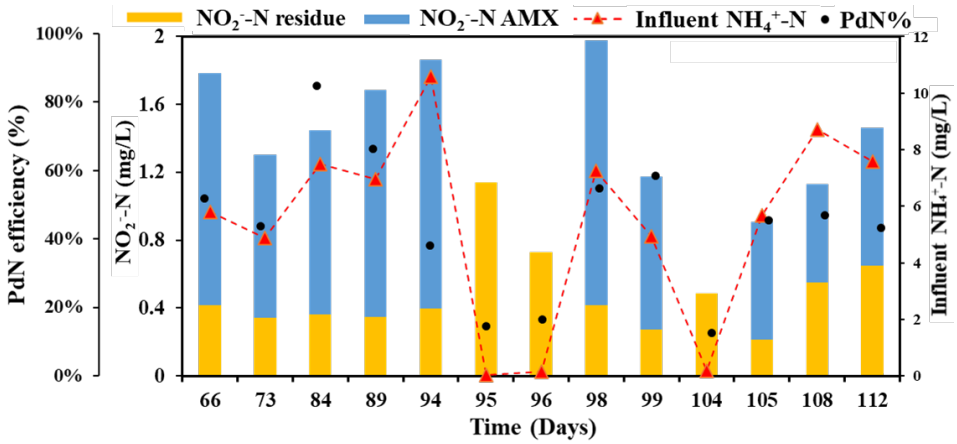

Figure 5.6 PdN efficiency with and without NH_4^+-N addition in Cell A

5.6 Discussion

5.6.1 Kinetic interpretation of the PdN augmentation by AMX

Technically, the rate differential between denitratation and denitritation can be calculated by the ratio of q_{DNA}/q_{DNI} which can be calculated by substituting kinetic parameters listed in Table 5.1 into Eqs. 5.3 and 5.4 and plotted in Figure 5.7. In general, it can be seen that this ratio increases with bulk NO_3^--N and decreases with bulk NO_2^--N concentration. This is because the difference

between q_{DNA} and q_{DNI} is mainly dependent on bulk NO_3^--N and NO_2^--N concentrations when the same sCOD and K_{COD} are shared between Eqs. 5.3 and 5.4. As mentioned in Figure 5.6, without AMX utilization, bulk NO_2^--N concentration would have been almost doubled, and the existence of AMX activities led to a much lower NO_2^--N concentration. Therefore, according to the model results in Figure 5.7, it was the NO_2^--N sink created by AMX that has led to a much lower bulk NO_2^--N concentration which resulted in a much higher q_{DNA}/q_{DNI} ratio augmenting the PdN performance. Overlaying experimental data of Cell A in Figure 5.7 shows that all data fell within the region where $q_{DNA}/q_{DNI} > 1$, indicating there was always a rate differential between denitratation and denitritation ($q_{DNA} > q_{DNI}$) regardless of the normal or peak loading operation. It was the magnitude of this rate differential that depends on the bulk NO_3^--N and NO_2^--N concentrations.

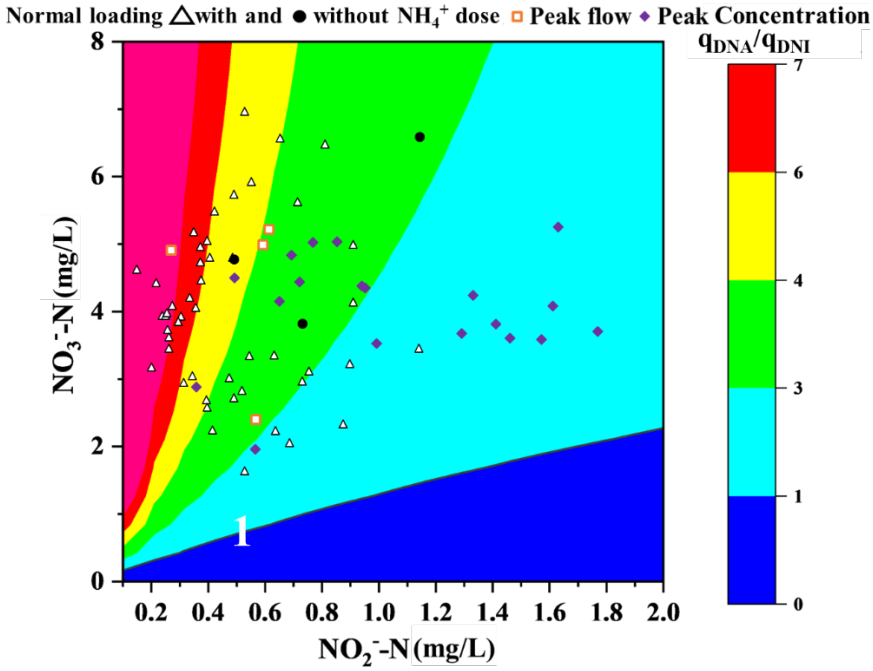

Figure 5.7 Heatmap model simulation and experimental data of q_{DNA}/q_{DNI} ratios as a function of NO_3^--N and NO_2^--N in Cell A during normal loading with and without NH_4^+-N dose, peak flow test, and peak concentration test

5.6.2 Kinetic interpretation of the PdN mechanism shift between normal and peak loading conditions

As discussed above, the mechanisms of PdN shifted from NO_2^--N sink by AMX (Hypothesis 1) during the normal loading operation to the rate differential (Hypothesis 2) during the peak loading operation. The key difference between these two mechanisms is whether AMX has the ability to outcompete denitritation. According to Eqs. 5.4 and 5.5, NO_2^--N is a common substrate for both AMX and denitritation. Moreover, bulk NH_4^+-N concentration barely changed from Day 200 onward (Figure 5.2e). Therefore, it was hypothetically the rbsCOD concentration difference between the normal and peak loading operation that has become a major influencer uncoupling the denitritation rate from AMX rate. To test this hypothesis, the ratio of NO_2^--N utilization rate by AMX to that by denitritation, namely V_{AMX}/V_{DNI}, were calculated with Eqs. 5.11 and 5.12 and plotted against Cell A bulk rbsCOD concentrations in Figure 5.8. It can be seen that the V_{AMX}/V_{DNI} ratios measured during the peak loading operation with much higher bulk rbsCOD concentrations were significantly lower ($p < 0.05$) than those measured during normal operation with much lower bulk rbsCOD. This experimental observation evidenced that it was the bulk rbsCOD concentration difference between the normal and peak loading operation that have shifted the PdN mechanism from the NO_2^--N sink in the former to the rate differential in the latter.

To sum up, during normal loading operation when bulk rbsCOD were low (e.g., rbsCOD ≤ 8 mg/L), Hypothesis 1 holds true. The kinetic mechanism unraveled in this study evidenced that NO_2^--N sink has been a dominant mechanism when methanol was used as a carbon source in low strength wastewater. In contrast, during peak loading operation, when bulk rbsCOD concentrations were high, e.g., rbsCOD ≥ 8 mg/L, Hypothesis 2 holds true. Hence, it was the rbsCOD loading conditions that determines which PdN mechanism dominates.

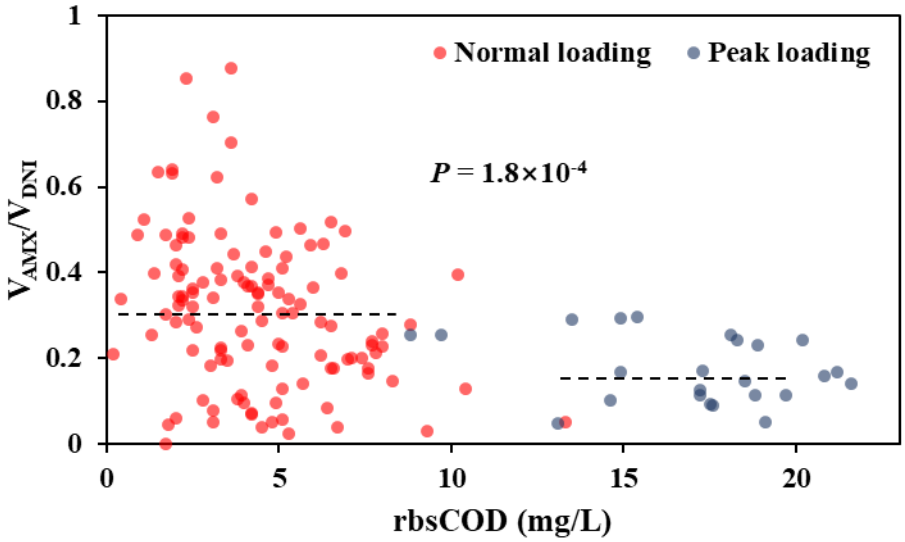

Figure 5.8 Effect of rbsCOD concentrations on the ratios of NO_2^--N utilization rates by AXM (V_{AMX}) to that by denitritation (V_{DNI}) in Cell A during normal and peak loading operation

5.6.3 Kinetic interpretation of the difference between methanol and other types of carbon sources in driving PdN

Theoretically, the maximum rate differential between denitratation (q_{DNA}) and denitritation (q_{DNI}) could be calculated as $(\frac{\mu_m^{Da}}{y_{NO3}^{Da}} - \frac{\mu_m^{Di}}{y_{NO2}^{Di}})$ according to Eqs. 5.3 and 5.4. When methanol was used as a carbon source, this value turned out to be 1.1 g/g/d as can be calculated with the parameters in Table 5.1. This value appears to be much lower than counterpart values, e.g., 3.1 to 5.4 g/g/d, when glucose, glycerol, or acetate was used as the carbon source as can be calculated with the parameters reported in respective studies (Al-Omari et al., 2021; Campolong, 2019; Peng et al., 2021). This dramatically lower maximum rate differential value of methanol than those of other types of carbon sources provides a reasonable explanation why methanol has been deemed as an undesirable carbon source for PdN (Le et al., 2019a; Zhang et al., 2020), i.e., the room for rate differential to increase is limited by the kinetic nature of methanol.

Although methanol is not a good rate differential carbon source, this study showed that it is actually good at NO_2^--N sink in low strength wastewater. This is because methylotrophic denitrifiers possess a NO_2^--N half-saturation constant (K_{NO2}^{Di}) of 1.5 mg/L (Table 5.1) which is much greater than counterpart K_{NO2}^{Di} values (0.2~1.0 mg/L) when glucose, glycerol, and acetate were used as

carbon sources (Al-Omari et al., 2021; Henze et al., 2000). This greater K_{NO2}^{Di} value of methylotrophic denitrifiers put themselves in an inferior position to compete with AMX bacteria for NO_2^--N, which offers a fundamental explanation for the preference of NO_2^--N sink when methanol was used in low strength wastewater such as tertiary influent (Campolong, 2019; Macmanus et al., 2022). Another relevant explanation has to do with the lower COD half-saturation constant (K_{COD}) of methanol than those of the counterpart values when glucose, glycerol, and acetate were used as carbon sources (Bill et al., 2009; Cherchi et al., 2009; Le et al., 2019a). According to Eq. 5.3, when K_{COD} of methanol is low, a lower bulk COD concentration is necessary to achieve the same NO_3^--N denitrification rate as that of the other types of carbon with high K_{COD}. This explains why a lower bulk COD concentration tended to promote a higher V_{AMX}/ V_{DNI} ratio as shown in Figure 5.8. Hence, methanol naturally triggers NO_2^--N sink in low bulk COD concentration (Hypothesis 1), which also explains the similar phenomena reported in previous studies (Campolong, 2019; Le et al., 2019a; Macmanus et al., 2022).

5.7 Conclusions

The following conclusions can be drawn from this study, which are anticipated to provide insights and guidance for full-scale application of methanol-driven PdNA:

1) The long-term (417 days) operational results in this study revealed that it was feasible to achieve low concentration nitrogen polishing in tertiary MBBRs via methanol-driven PdNA. Effluent TIN concentration of 2.6 ± 0.6 mg/L was achieved during normal loading operation. During peak loading operation, the effluent TIN concentration still can meet the peak loading discharge target of ≤ 4 mg/L.
2) 46.3% methanol saving can be achieved in the tertiary MBBRs with another 1.1 ~1.6 tons O_2 per day can be saved, assuming a flow rate of 69 million gallon per day.
3) It was the bulk rbsCOD concentrations that determines whether it was the NO_2^--N sink or rate differential that governs the mechanism of PdN when methanol was used as a carbon source.
4) In low strength wastewater such as the tertiary polishing in Figure 5.1 (e.g., bulk rbCOD ≤ 8 mg/L), it was the NO_2^--N sink created by AMX that has led to a much lower bulk NO_2^--N concentration which resulted in PdN augmentation.

5) In high strength wastewater such as the secondary treatment or peak loading operation (e.g., bulk rbCOD > 8 mg/L), the rate differential between denitratation and denitritation became a dominant mechanism enabling PdN.
6) It was the special metabolic kinetics of methylotrophs in terms of the maximum rate differential value, the NO_2^--N half-saturation constant, and the COD half-saturation constant that confer methanol with different PdN mechanism from other types of carbon sources.

5.8 References

Al-Omari, A., De Clippeleir, H., Ladipo-Obasa, M., Klaus, S., Bott, C., McCullough, K., Fofana, R., Wadhawan, T., Murthy, S. and Fevig, S. 2021 Modelling partial heterotrophic denitrification in mainstream nitrogen removal processes–model development and evaluation, pp. 67-71.

Badia, A., Kim, M. and Dagnew, M. 2021. Nitrite denitrification using biomass acclimatized with methanol as complementary carbon source: long-term performance and kinetics study. Environmental Science: Water Research & Technology 7(1), 93-106.

Bi, Z., Takekawa, M., Park, G., Soda, S., Zhou, J., Qiao, S. and Ike, M. 2015. Effects of the C/N ratio and bacterial populations on nitrogen removal in the simultaneous anammox and heterotrophic denitrification process: mathematic modeling and batch experiments. Chemical Engineering Journal 280, 606-613.

Bill, K.A., Bott, C. and Murthy, S. 2009. Evaluation of alternative electron donors for denitrifying moving bed biofilm reactors (MBBRs). Water Science and Technology 60(10), 2647-2657.

Campolong, C.J. (2019) Bioaugmentation and retention of anammox granules to a mainstream deammonification bio-oxidation pilot with a post polishing anoxic partial denitrification/anammox moving bed biofilm reactor, (Master thesis) Virginia Tech.

Cherchi, C., Onnis-Hayden, A., El-Shawabkeh, I. and Gu, A.Z. 2009. Implication of using different carbon sources for denitrification in wastewater treatments. Water Environment Research 81(8), 788-799.

Faskol, A. and Racovițeanu, G. 2021 Effect of DO, alkalinity and pH on nitrification using three different sunken materials types in biological aerated filter BAFs (Conference Proceedings), p. 012079.

Ginige, M.P., Bowyer, J.C., Foley, L., Keller, J. and Yuan, Z. 2009. A comparative study of methanol as a supplementary carbon source for enhancing denitrification in primary and secondary anoxic zones. Biodegradation 20(2), 221-234.

Glass, C. and Silverstein, J. 1998. Denitrification kinetics of high nitrate concentration water: pH effect on inhibition and nitrite accumulation. Water research 32(3), 831-839.

Grady Jr, C.L., Daigger, G.T., Love, N.G. and Filipe, C.D. (2011) Biological wastewater treatment, CRC press.

Henze, M., Gujer, W., Mino, T. and van Loosdrecht, M.C. (2000) Activated sludge models ASM1, ASM2, ASM2d and ASM3, IWA publishing.

Her, J.J. and Huang, J.S. 1995. Denitrifying kinetics involving the distributed ratio of reductases. Journal of Chemical Technology & Biotechnology: International Research in Process, Environmental AND Clean Technology 62(3), 261-267.

Le, T., Peng, B., Su, C., Massoudieh, A., Torrents, A., Al-Omari, A., Murthy, S., Wett, B., Chandran, K. and DeBarbadillo, C. 2019a. Impact of carbon source and COD/N on the concurrent operation of partial denitrification and anammox. Water Environment Research 91(3), 185-197.

Le, T., Peng, B., Su, C., Massoudieh, A., Torrents, A., Al-Omari, A., Murthy, S., Wett, B., Chandran, K. and deBarbadillo, C. 2019b. Nitrate residual as a key parameter to efficiently control partial denitrification coupling with anammox. Water Environment Research 91(11), 1455-1465.

Ma, B., Wang, S., Cao, S., Miao, Y., Jia, F., Du, R. and Peng, Y. 2016. Biological nitrogen removal from sewage via anammox: recent advances. Bioresource technology 200, 981-990.

Macmanus, J., Long, C., Klaus, S., Parsons, M., Chandran, K., De Clippeleir, H. and Bott, C. 2022. Nitrogen removal capacity and carbon demand requirements of partial denitrification/anammox MBBR and IFAS processes. Water Environment Research 94(8), e10766.

Moore, G.T. 2010. Nutrient control design manual. US Environmental Protection Agency, Washington, DC.

Peng, Z., Lou, T., Jiang, K., Niu, N., Wang, J. and Liu, A. 2021. Characteristics of nutrients removal under partial denitrification initiated by different initial nitrate concentration. Bioprocess and Biosystems Engineering 44(10), 2051-2059.

Purtschert, I. and Gujer, W. 1999. Population dynamics by methanol addition in denitrifying wastewater treatment plants. Water science and technology 39(1), 43-50.

Rice, E.W., Baird, R.B., Eaton, A.D. and Clesceri, L.S. (2012) Standard methods for the examination of water and wastewater (23rd Version), American public health association Washington, DC.

Si, Z., Peng, Y., Yang, A., Zhang, S., Li, B., Wang, B. and Wang, S. 2018. Rapid nitrite production via partial denitrification: pilot-scale operation and microbial community analysis. Environmental Science: Water Research & Technology 4(1), 80-86.

Xu, X., Ma, B., Lu, W., Feng, D., Wei, Y., Ge, C. and Peng, Y. 2020. Effective nitrogen removal in a granule-based partial-denitrification/anammox reactor treating low C/N sewage. Bioresource technology 297, 122467.

Zhang, Z., Zhang, Y. and Chen, Y. 2020. Recent advances in partial denitrification in biological nitrogen removal: From enrichment to application. Bioresource Technology 298, 122444.

Chapter 6 Mechanistic understanding of the performance difference between methanol- and glycerol-fed partial denitrification anammox in tertiary moving bed biofilm reactors treating real secondary effluent

(This chapter is ready for submission to a peer-reviewed journal)

6.1 Abstract

Two pilot-scale tertiary moving bed biofilm reactor (MBBR) treatment trains were operated onsite for 371 days in a local wastewater treatment plant (WWTP) to compare their treatment performance and mechanistic difference when methanol and glycerol were used as carbon sources, respectively. Both trains were able to meet the stringent effluent total inorganic nitrogen (TIN) requirement of ≤ 3 mg/L while saving 46.3% methanol and 43.8% glycerol, respectively. However, very different nitrite provision mechanism was found between the two types of carbon sources, i.e., nitrite sink was the major source of nitrite provision for anammox bacteria when methanol was used as a carbon; while rate differential between denitratation and denitritation was the major nitrite source when glycerol was used as a carbon. The cause of this mechanistic discrepancy can be ascribed to the dramatic different half-saturation constants between the two types of carbon sources. This study provided fundamental understandings that can be used to reconcile the controversy over whether methanol is suitable for PdNA in low strength wastewater treatment.

6.2 Keywords

Partial denitrification; glycerol; methanol; anammox; MBBR;

6.3 Introduction

Moving bed biofilm reactors (MBBRs) have been used as a polishing process for biological nitrogen removal to meet the stringent effluent total inorganic nitrogen (TIN) target, e.g., ≤ 3 mg/L. However, conventional nitrification and denitrification used in these processes are energy-intensive with high external carbon consumption. Technically, a coupling of partial denitrification

(PdN) with anammox (AMX) process can reduce aeration and external carbon demands and in turn lead to tankage, chemical, and energy savings if properly applied in tertiary MBBR (Zhang et al., 2020b). This is because AMX as an autotrophic process can directly convert NH_4^+-N and NO_2^--N into N_2 without external carbon. AMX also can reduce aeration requirements as only a portion of influent NH_4^+-N needs to be oxidized by aeration when AMX is used (Xu et al., 2020).

Multiple approaches to promoting PdN have been reported previously (Ma et al., 2016; Zhang et al., 2020b). Among those, a selection of the right type of external carbon source was rated the most important factor for enabling PdN. As the most widely used carbon source in the U.S., methanol has a low market price, low biomass yield, and low environmental impacts (Badia et al., 2021; Purtschert and Gujer, 1999). Therefore, it would be convenient and cost-effective if the existing methanol storage and dosing facilities can be directly leveraged to perform partial denitrification anammox (PdNA). On the other hand, glycerol as a byproduct of biodiesel (Zhang et al., 2022), is reproducible and environmental-friendly, which is the second cheapest carbon source after methanol in Mid-Atlantic region of the U.S. (Fofana et al., 2023; Zhang et al., 2020b). Additionally, its noncorrosive and nonflammable characteristics simplify the full-scale storage requirements (Uprety, 2013). Therefore, studies on methanol- and glycerol-driven PdN or PdNA have sprung up recently (Fofana et al., 2023; Klaus et al., 2023; Le et al., 2019a; Macmanus et al., 2022; Zhang et al., 2020a; Zhang et al., 2022). In comparison with glycerol, methanol has been considered a less favorable carbon source for achieving PdNA for a long time due to its lower PdN efficiency especially in high strength wastewater treatment such as the secondary treatment (Ma et al., 2016; Zhang et al., 2020b). However, lately, it was reported that when low strength wastewater was used such as in tertiary treatment, the performance of methanol-driven PdNA could somehow be comparable to that of glycerol (Fofana et al., 2023; Klaus et al., 2023). Understanding the mechanisms behind these observations could advance the application of methanol or glycerol in tertiary PdNA process, which is however, still in their early stages.

Since the supply of NO_2^--N is a key to achieve PdNA, there are two hypotheses explaining the access of AMX to NO_2^--N when methanol and glycerol were used as carbon sources. Hypothesis 1 assumes there is a NO_2^--N sink provided by AMX, i.e., AMX outcompetes denitritation in NO_2^--N utilization (Campolong, 2019; Le et al., 2019a). In this hypothesis, AMX was capable of

competing with NO_2^--N denitrifiers for NO_2^--N utilization, and thus NO_2^--N accumulation is usually unseen (Campolong, 2019; Le et al., 2019a). Hence, in this hypothesis, AMX plays an essential role in enhancing PdN because PdN would deteriorate without AMX. In contrast, Hypothesis 2 assumes there is a rate differential between denitratation and denitritation regardless of the AMX involvement, i.e., neither AMX nor denitritation is fast enough to catch up the denitratation rate, and thus NO_2^--N accumulation is usually observed (Al-Omari et al., 2021; Si et al., 2018; Zhang et al., 2020b). In this hypothesis, PdN performance mainly depends on the faster denitratation rate rather than AMX. It should be pointed out that the mechanistic discrepancy between these two hypotheses has neither been understood nor reconciled in literature. Specifically, in the context of the low nitrogen polishing process, where the influent NO_3^--N was as low as 6.1 ± 1.1 mg/L as practiced in tertiary treatment, the mechanism responsible for methanol- and glycerol-driven denitrification remains unclear.

Besides the lack of mechanistic understanding, the applicability of methanol- and glycerol-fed PdNA in tertiary MBBRs for meeting the stringent effluent TIN target of ≤ 3 mg/L is also unknown. This knowledge is important because the effluent TIN limits of 3 mg/L or less are common in regions such as the Chesapeake Bay watershed, coastal areas of North Carolina, mid-Colorado and Okanagan Lake area of British Columbia, Canada, and increasingly stringent effluent discharge limits will surely be imposed in the near future (Moore, 2010). To sum up, this study aims to explore and compare the differences between methanol- and glycerol-driven PdNA in terms of: (1) their effectiveness in achieving rigorous effluent TIN target of ≤ 3 mg/L and cost savings in low-nitrogen polishing MBBRs; and (2) their mechanistic difference in achieving PdN if any. To this end, two parallel MBBR treatment trains were set up and operated onsite at a local wastewater treatment plant (WWTP), namely Noman Cole pollution control plant (NCPCP), for 371 days. These two treatment trains receive real secondary effluent with methanol and glycerol added as external carbon sources, respectively. The outcome of this study was anticipated to provide valuable insights and guidance for carbon source selection in future full-scale application of PdNA technology.

6.4 Materials and methods

6.4.1 Reactor setup

Two parallel MBBR treatment trains were set up as illustrated in Figure 6.1. Briefly, in each train, two 14 L working volume anoxic MBBRs, namely Cell A and Cell B, were filled with polyethylene K1 media (Veolia, NJ, USA) at a volumetric fraction of 45%. Cell A and Cell B were connected in sequence and followed by an 8 L working volume oxic MBBR, namely Cell C, which was filled with K1 media at a volumetric fraction of 32%. The MBBR treatment trains mimic the full-scale MBBR design used in the same WWTP (Figure 6.1). K1 media established with methylotrophs were collected from the full-scale MBBRs. The Cells A and B were mixed with motor-driven paddles (McMaster-Carr, NJ, U.S.) at a rotating speed of 60 rpm. Cell C was fully aerated by an air pump (Simple Deluxe, CA, U.S.). During startup, 1.5 L of suspended AMX biomass was seeded into each anoxic MBBR in Figure 6.1, and the system was operated in an integrated fixed film activated sludge (IFAS) mode with the aid of a clarifier to recirculate suspended sludge for AMX bacterial colonization on the media. 30 days after seeding, suspended AMX biomass was washed out, and then the system shifted to the MBBR mode. For methanol train, the designed hydraulic retention time (HRT) of each anoxic MBBR (namely Cell A and Cell B) and the aerobic MBBR (namely Cell C) in Figure 6.1 were 19 min and 10 min, respectively. For glycerol train, the HRTs of Cell A and Cell B were in the range of 19~38 min, and the HRT of Cell C was in the ranges of 10~20 min. Thereby, Cell A and Cell B performed PdN or PdNA while Cell C polished residual NH_4^+-N coming out the Cell B if any (Figure 6.1).

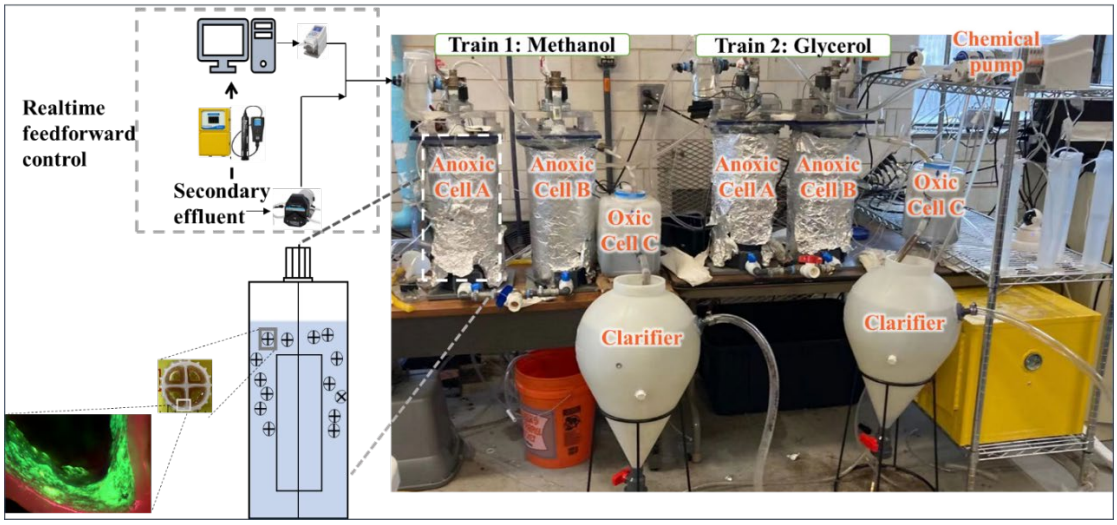

Figure 6.1 Schematic and real view of the pilot MBBRs setup at NCPCP

6.4.2 Automatic control

Real-time NO_3^--N, NO_2^--N, NH_4^+-N, and dissolved oxygen (DO) data of secondary effluent was measured by a Chemscan real-time analyser (ChemScan Inc., Wisconsin, USA) and a ProDSS Multiparameter Digital Water Quality Meter (YSI Incorporated, OH, USA). These data were sent to a process control program written in Python 3.8 on a PC (Figure 6.1). The PC in turn sent signals to an Ismatec Reglo ICC Digital Pump (Cole-Parmer, IL, USA) to precisely dose NH_4Cl and methanol or glycerol to the Cell A according to the controller formulas set in Eqs. 6.1 and 6.2. The purpose of NH_4Cl addition was to mimic the NH_4^+-N residue bleeding from the partial nitrification process to be installed in the future secondary treatment.

$$NH_{4\,feed}^{+} = NO_{3\,inf}^{-} \text{ or selected setpoints} \tag{6.1}$$

$$COD_{feed} = a \times \left(NO_{3\,inf}^{-} - NO_{3\,eff,setpoint}^{-}\right) + b \times DO_{inf} \tag{6.2}$$

in which $NO_{3\,inf}^{-}$ and DO_{inf} are real-time influent NO_3^--N and DO concentrations. $NH_{4\,feed}^{+}$ and COD_{feed} are concentrations of NH_4^+-N and COD in the form of methanol and glycerol fed into Cell A. $NO_{3\,eff,\ setpoint}^{-}$ is the NO_3^--N concentration targeted in the Cell B effluent, which was set as 0.5~1.5 mg/L. Three $NH_{4\,feed}^{+}$ levels were used in this study. $NH_{4\,feed}^{+}$ was set equal to $NO_{3\,inf}^{-}$ from Days 1 to 132 and decreased to 4 mg/L from Days 133 to 199, and then further decreased to 2 mg/L from Days 200 to 417, respectively. 'a' in Eq. 6.2 is a coefficient used to

adjust influent COD for achieving $NO_{3\ eff,setpoint}^{-}$. 'b' in Eq. 6.2 represents the COD consumption per unit DO removal. Hence, 'a' value was set as 4 g/g for both methanol and glycerol trains, and 'b' value was set as 2 g/g and 3 g/g for methanol and glycerol trains, respectively. It should be noted that the DO_{inf} was always around 3 mg/L in this study because of the intrinsic turbulence in secondary effluent flow in this particular WWTP. With these being said, COD_{feed} was composed of COD consumed for nitrogen and DO removal. For monitoring the chemical dose accuracy, a small chemical mixing tank with an HRT of 2~3 min was added in front of the Cell A, where influent after chemical dosing can be grabbed. Grab samples from the influent, Cell A, Cell B, and Cell C were analyzed 3~4 times a week.

6.4.3 Model development

Kinetics of PdN can be simplified as the competition between denitratation (NO_3^--N → NO_2^--N) and denitritation (NO_2^--N → N_2) according to Glass and Silverstein (1998). The specific NO_3^--N uptake rate of denitratation (q_{DIA}) can be described by Eq. 6.3 according to Activated Sludge Model NO. 1 (Henze et al., 2000). Similarly, the specific NO_2^--N uptake rate of denitritation (q_{DNI}) can be described by Eq. 6.4. Definitions and values of all kinetic parameters used in these equations are listed in Table 6.1. For tertiary treatment where substrate concentration was low, and biofilm was thin, it is a reasonable assumption that these Monod equations (Eqs. 6.3 and 6.4) can be directly applied by ignoring the mass diffusion limitation of thin biofilm.

$$q_{DNA} = \frac{\mu_m^{Da}}{y_{NO3}^{Da}} \frac{S_{COD}}{K_{COD}+S_{COD}} \frac{S_{NO_3^-}}{K_{NO3}^{Da}+S_{NO_3^-}} \tag{6.3}$$

$$q_{DNI} = \frac{\mu_m^{Di}}{y_{NO2}^{Di}} \frac{S_{COD}}{K_{COD}+S_{COD}} \frac{S_{NO_2^-}}{K_{NO2}^{Di}+S_{NO_2^-}} \tag{6.4}$$

Table 6.1 Monod kinetic parameters

Symbol	Definition	Value	References
Glycerol denitratation and denitritation (20 °C value)			
μ_m^{Da}	Maximum specific growth rate of denitratation culture (/d)	3.2	(Al-Omari et al., 2021)
μ_m^{Di}	Maximum specific growth rate of denitritation culture (/d)	1.1	(Al-Omari et al., 2021)
K_{NO3}^{Da}	Half saturation constant for nitrate (mg/L)	4.5	(Al-Omari et al., 2021)
K_{NO2}^{Di}	Half saturation constant for nitrite (mg/L)	0.2	(Henze et al., 2000)
K_{COD}	Half saturation constant for COD (mg/L) in denitratation and denitritation	25.0	(Henze et al., 2000)
y_{NO2}^{Di}	Biomass yield on nitrite (g/g)	1.2	(Campolong, 2019)
y_{NO3}^{Da}	Biomass yield on nitrate (g/g)	0.8	(Campolong, 2019)
Methylotrophic denitratation and denitritation (20 °C value)			
μ_m^{Da}	Maximum specific growth rate of denitratation culture (/d)	1.0	Her and Huang (1995)
μ_m^{Di}	Maximum specific growth rate of denitritation culture (/d)	0.9	Her and Huang (1995)
K_{NO3}^{Da}	Half saturation constant for nitrate (mg/L)	3.0	(Al-Omari et al., 2021)
K_{NO2}^{Di}	Half saturation constant for nitrite (mg/L)	1.5	(Al-Omari et al., 2021)
K_{COD}	Half saturation constant for COD (mg/L) in denitratation and denitritation	15.0	(Al-Omari et al., 2021)
y_{NO2}^{Di}	Biomass yield on nitrite (g/g)	0.6	(Campolong, 2019)
y_{NO3}^{Da}	Biomass yield on nitrate (g/g)	0.4	(Campolong, 2019)
S_{COD}	Concentration of rbsCOD in the bulk liquid (mg/L)		
$S_{NO_3^-}$	Concentration of NO_3^--N in the bulk liquid (mg/L)		
$S_{NO_2^-}$	Concentration of NO_2^--N in the bulk liquid (mg/L)		
S_{NH3}	Concentration of NH_4^+-N in the bulk liquid (mg/L)		

6.4.4 Calculation methods

PdN efficiency, namely the percent of NO_3^--N that was only denitrified to NO_2^--N but not to N_2, was determined using Eq. 6.5,

$$PdN\ \% = \frac{NO_{2\,eff}^{-} - NO_{2\,inf}^{-} + 1.32 \times (NH_{4\,inf}^{+} - NH_{4\,eff}^{+} - NH_{4\,assmilated}^{+})}{NO_{3\,inf}^{-} - NO_{3\,eff}^{-} + 0.26 \times (NH_{4\,inf}^{+} - NH_{4\,eff}^{+} - NH_{4\,assimilated}^{+})} \quad (6.5)$$

in which $NO_2^-{}_{inf}$, $NO_3^-{}_{inf}$, and $NH_4^+{}_{inf}$ are the influent NO_2^--N, NO_3^--N and NH_4^+-N concentrations. $NO_2^-{}_{eff}$, $NO_3^-{}_{eff}$, and $NH_4^+{}_{eff}$ are their effluent concentrations. 1.32 and 0.26 are based on the stoichiometries of AMX reaction in Eq. 6.6 according to a previous study (Ma et al., 2016),

$$NH_4^+ + 1.32NO_2^- + 0.066HCO_3^- + 0.13H^+ \rightarrow 1.02N_2 + 0.26NO_3^- + 0.066CH_2O_{0.5}N_{0.15} + 2.03H_2O \quad (6.6)$$

$NH_4^+{}_{assimilated}$ represents the NH_4^+-N assimilated by the heterotrophic organisms for growth and was calculated by Eq. 6.7,

$$NH_{4\,assimilated}^+ = \mathrm{Y} \times \mathrm{C} \times (sCOD_{inf} - sCOD_{eff}) \quad (6.7)$$

in which $sCOD_{inf}$ and $sCOD_{eff}$ are the sCOD concentrations in the influent and effluent. Y is observed growth yield of heterotrophic organisms, namely 0.2 mg biomass COD/mg rbsCOD (readily biodegradable soluble COD) consumed, and C is biomass nitrogen content, namely 0.07 mg N/mg biomass, based on the study by Grady Jr et al. (2011). Hence, NO_2^--N utilization by AMX can be calculated in Eq. 6.8,

$$\Delta NO_{2\,AMX}^- = 1.32 \times (NH_{4\,inf}^+ - NH_{4\,eff}^+ - NH_{4\,assmilated}^+) \quad (6.8)$$

TIN concentration in this study was defined as the sum of NO_3^--N, NO_2^--N, and NH_4^+-N concentrations. The AMX contribution to TIN removal ($\Delta TIN_{AMX}/\Delta TIN$) was calculated by Eq. 6.9,

$$\Delta \mathrm{TIN}_{AMX}/\Delta \mathrm{TIN} = \frac{(1+1.32-0.26)\times(NH_{4\,inf}^+ - NH_{4\,eff}^+ - NH_{4\,assimilated}^+)}{\mathrm{TIN}_{inf} - \mathrm{TIN}_{eff}} \quad (6.9)$$

in which 1, 1.32 and 0.26 were derived from Eq. 6.6. TIN_{inf} and TIN_{eff} represent TIN concentrations in the influent and effluent of Cell A and Cell B, respectively.

NO_3^--N utilization rate of denitratation (V_{DNA}) and NO_2^--N utilization rates of denitritation (V_{DNI}) and AMX (V_{AMX}) in the Cell A were calculated with Eqs. 6.10, 6.11, and 6.12.

$$\mathrm{V}_{DNA} = \frac{NO_{3\,inf}^- - NO_{3\,eff}^-}{HRT} \quad (6.10)$$

$$\mathrm{V}_{DNI} = \frac{NO_{3\,inf}^- - NO_{3\,eff}^- + NO_{2\,inf}^- - NO_{2\,eff}^- - (1.32-0.26)\times(NH_{4\,inf}^+ - NH_{4\,eff}^+ - NH_{4\,assimilated}^+)}{HRT} \quad (6.11)$$

$$\mathrm{V}_{AMX} = \frac{1.32\times(NH_{4\,inf}^+ - NH_{4\,eff}^+ - NH_{4\,assimilated}^+)}{HRT} \quad (6.12)$$

HRT represents hydraulic retention time in Cell A of both treatment trains. TIN removal rate by AMX, namely $\Delta \mathrm{TIN}_{AMX}/\mathrm{HRT}$, in the Cell A was calculated by Eq. 6.13

$$\Delta \mathrm{TIN}_{AMX}/\mathrm{HRT} = \frac{(1+1.32-0.26)\times(NH_{4\,inf}^+ - NH_{4\,eff}^+ - NH_{4\,assimilated}^+)}{\mathrm{HRT}} \quad (6.13)$$

6.4.5 qPCR analysis

Quantitative polymerase chain reaction (qPCR) was performed to quantify the copy numbers of total bacterial 16S ribosomal RNA (rRNA) gene, the 16S rRNA of *Candidatus* Kuenenia, hydrazine synthase subunit A *(hzsA)* and B *(hzsB)* genes on a QuantStudio 3 thermocycler (Applied Biosystems, Waltham, MA). Each 20-µL qPCR reaction mixture contained 10 µL of 2× SYBR™ Green PCR Master Mix with ROX (Life Technologies, Carlsbad, CA), 1 µL each of forward and reverse primers (0.2 µM), 7 µL molecular-grade water (Sigma-Aldrich, St. Louis, MO) and 1 µL DNA template. The thermal cycling conditions for qPCR amplification were as follows: 95 ℃ for 2 min, 40 cycles at 95 ℃ for 15 s, 60 ℃ for 15 s, 72 ℃ for 20 s, melt-curve for 45 s (95 ℃ for 15 s, 60 ℃ for 15 s and 95 ℃ for 15 s). All qPCR runs had an efficiency between 90% and 110% with an $R^2 > 0.95$. Each gene was quantified in triplicate with a standard curve and negative control (with water as template). Results were reported as gene copies per 16S gene copies.

6.4.6 Chemical and statistical analysis methods

NO_3^--N, NO_2^--N, NH_4^+-N and sCOD after 0.45 µm syringe filter (MilliporeSigma, MD, USA) filtration were analyzed with Hach TNT® 835, 839, 830, and 820 vials, respectively, in a spectrophotometer (DR 3900, Hach, Loveland, CO, USA) according to the standard method (Rice et al., 2012). The rbsCOD was calculated by subtracting the MBBR effluent sCOD from the influent sCOD.

6.5 Results

6.5.1 System performance

Over the course of 371-day operation, most of the TIN removal was achieved in Cell A (Figure 6.2 a-1 and b-1) for both methanol and glycerol trains. Specifically, for methanol train, 47.2 ± 12.2%,

12.2 ± 5.1%, and 0.4 ± 0.7% of influent TIN were removed in Cell A (anoxic), Cell B (anoxic), and Cell C (oxic), respectively, achieving around 59.8% total TIN removal (Figure 6.2 a-1), out of which 38.2% of TIN removal in methanol train was contributed by AMX (Figure 6.2 a-2). In particular, AMX in Cell A and Cell B contributed 28.2 ± 9.7% and 10.0 ± 5.4% TIN removal, respectively, indicating greater AMX activities in Cell A over that in Cell B of the methanol train. For glycerol train, 37.4 ± 10.8%, 23.5 ± 8.4%, and 1.1 ± 1.5% of influent TIN were removed in Cell A, Cell B, and Cell C, respectively, achieving around 62.1% total TIN removal (Figure 6.2 b-1), out of which 25.1% of TIN removal in glycerol train was contributed by AMX (Figure 6.2 b-2). In particular, AMX in Cell A and Cell B contributed 15.3 ± 9.1% and 9.8 ± 7.5% TIN removal, respectively, also indicating greater AMX activities in Cell A over that in Cell B (Figure 6.2 b-2). Hence, good TIN removal efficiencies were achieved in both methanol and glycerol trains regardless of the influent quality fluctuation (Figure 6.2 a-1 and b-1), which can be ascribed to the effectiveness of automatic feedforward control system incorporated in the study (Figure 6.1). However, methanol train appeared to have higher AMX activities than glycerol train did in terms of the AMX contribution to the total TIN removal (Figure 6.2 a-2 and b-2). This was also confirmed by the qPCR results in Figure 6.3 that higher levels of AMX bacteria were detected in methanol train than in glycerol train in terms of AMX bacteria *Candidatus Kuenenia*. The plausible reason seems related to the higher bulk rbsCOD concentrations in the glycerol train (Table 6.2), which will be further analyzed in the following sections. In addition, Cell A of methanol train contributed much more TIN removal (47.2 ± 12.2%) than that of glycerol train (37.4 ± 10.8%), but the total TIN removal of two trains was almost equal (Figures 6.2 a-1 and a-2). It seemed that glycerol Cell B took on more TIN removal burdens than methanol Cell B. This was because rbsCOD level in glycerol Cell A effluent almost doubled that in methanol Cell A (Table 6.2). Some NO_3^--N residue was intentionally maintained in Cell B (Table 6.2) of both methanol and glycerol trains with the aid of the feedforward controller (Eq. 6.2) for enabling PdN. Specifically, an average NO_3^--N residue of 1~1.5 mg/L and 0.5~1.0 mg/L was maintained in Cell B of methanol and glycerol trains, respectively. It was reported previously that leaving a certain amount of NO_3^--N residue was essential for the achievement of PdN (Campolong, 2019; Le et al., 2019b).

In addition, influent NH_4^+-N was dosed at the same concentration as the real-time influent NO_3^--N concentration through the feedforward controller (Eq. 6.1) to facilitate the growth and

colonization of AMX bacteria according to its stoichiometry during startup (Days 1 to 120). However, because of the limited AMX capacity in MBBRs, total anoxic NH_4^+-N removal in both Cell A and Cell B was ≤ 2 mg/L by day 200, leading to high levels of NH_4^+-N breakthrough and thus increased effluent TIN level. This observation means any unutilized NH_4^+-N will become part of the effluent TIN. For this regard, NH_4^+-N dosage was reduced to a setpoint of 2 mg/L (Table 6.2) from Day 200 onward regardless of influent NO_3^--N. Both methanol and glycerol trains achieved average anoxic NH_4^+-N removal of around 1.3 mg/L after the startup (Table 6.2). Given the fact that methanotrophs have lower biomass yield than glycerol utilizing bacteria (Table 6.1), methanol actually had more AMX NH_4^+-N removal than glycerol according to Eq. 6.7, which aligned with the observation in Figures 2 a-2 and b-2. After the adjustment of influent NH_4^+-N dosage on Day 200, both methanol and glycerol trains met the strict discharge TIN limit of ≤ 3 mg/L (Figures 6.2 a-3 and b-3). Specifically, average effluent TIN of 2.6 ± 0.6 and 2.5 ± 0.7 mg/L were achieved in methanol and glycerol trains, respectively (Figures 6.2 a-3 and b-3, and Table 6.2). With the aid of autotrophic nitrogen removal by AMX activities, ΔsCOD/ΔTIN of the methanol train was stabilized around 2.5 ± 0.6 g COD/g N (Figure 6.2c and Table 6.2), which was 46.3% lower than the theoretical methanol full denitrification value, namely 4.7 g COD/g N (Grady Jr et al., 2011). ΔsCOD/ΔTIN of the glycerol train was stabilized around 3.6 ± 1.0 g/g (Figure 6.2c and Table 6.2), which was 43.8% lower than the theoretical glycerol full denitrification value of 6.4 g/g from the literature (Campolong, 2019). It is noteworthy that these values were obtained after influent DO was deducted. The comparison between experimental and theoretical full denitrification ΔsCOD/ΔTIN values of each carbon source indicated remarkable amount of carbon savings for both methanol and glycerol trains. However, methanol appeared to be more economical. The price of methanol and glycerol in the Mid-Atlantic region of the U.S. were about 0.32 and 0.48 $/kg COD, respectively (Campolong, 2019). Hence, the costs of methanol and glycerol to removal per kilogram TIN in this study were calculated as 0.8 and 1.7 $/ kg N (Table 6.2). Therefore, methanol was more economical than glycerol, which has to do with the higher AMX activities and lower biomass yield in methanol train. Meanwhile, instead of oxidizing all influent NH_4^+-N, around 1.3 mg/L NH_4^+-N could shortcut the secondary train into tertiary MBBRs without nitrification in both methanol and glycerol trains (Table 6.2). Thus, according to the stoichiometry of nitrification in Eq. 6.14 (Faskol and Racoviţeanu, 2021), 1.6 tons O_2 per day can be saved for

each train in the WWTP assuming a flow rate of 69 million gallon per day. Consequently, both aeration energy and tankage volume can be reduced by employing the PdNA.

$$NH_4^+ + 1.83O_2 + 1.98HCO_3^- \rightarrow 0.021C_5H_7O_2N + 0.98NO_3^- + 1.041H_2O + 1.88H_2CO_3^- \quad (6.14)$$

Table 6.2 Influent characteristics and performance of methanol and glycerol trains ('±' means standard deviation; Average values were calculated with data from Days 200 to 371)

	Methanol	**Glycerol**
Influent		
NO_3^--N (mg/L)	6.1 ± 1.1	6.1 ± 1.1
NO_2^--N (mg/L)	$3.0\times10^{-2} \pm 3.0\times10^{-2}$	$3.0\times10^{-2} \pm 3.0\times10^{-2}$
NH_4^+-N (mg/L)	2.2 ± 0.6	2.2 ± 0.6
rbsCOD (mg/L)	22.4 ± 6.5	32.8 ± 6.6
Cell A		
NO_3^--N (mg/L)	2.0 ± 0.5	2.3 ± 0.9
NO_2^--N (mg/L)	0.6 ± 0.2	1.5 ± 1.0
NH_4^+-N (mg/L)	1.2 ± 0.6	1.3 ± 0.5
rbsCOD (mg/L)	4.3 ± 2.3	8.1 ± 5.3
PdN efficiency (%)	35.1 ± 11.3	42.6 ± 19.6
$\Delta TIN_{AMX}/\Delta TIN_{total}$ (%)	28.2 ± 9.7	15.3 ± 9.1
HRT (min)	20.0	30.0
Cell B		
NO_3^--N (mg/L)	1.4 ± 0.4	0.8 ± 0.4
NO_2^--N (mg/L)	0.3 ± 0.1	0.8 ± 0.6
NH_4^+-N (mg/L)	0.9 ± 0.6	0.9 ± 0.5
rbsCOD (mg/L)	1.0 ± 1.3	0.8 ± 2.6
PdN efficiency (%)	11.4 ± 15.3	9.1 ± 17.7
$TIN_{AMX}/\Delta TIN_{total}$ (%)	10.0 ± 5.4	9.8 ± 7.5
HRT (min)	20.0	30.0
Cell C		
TIN (mg/L)	2.6 ± 0.6	2.5 ± 0.7
HRT (min)	10.0	10.0
System		

ΔCOD/ΔTIN (g/g)	2.5 ± 0.6	3.6 ± 1.0
Carbon saving (%)	46.3	43.8
Aeration saving (tons O_2 per day)	1.6	1.6
Denitrification costs ($/ kg N)	0.8	1.7

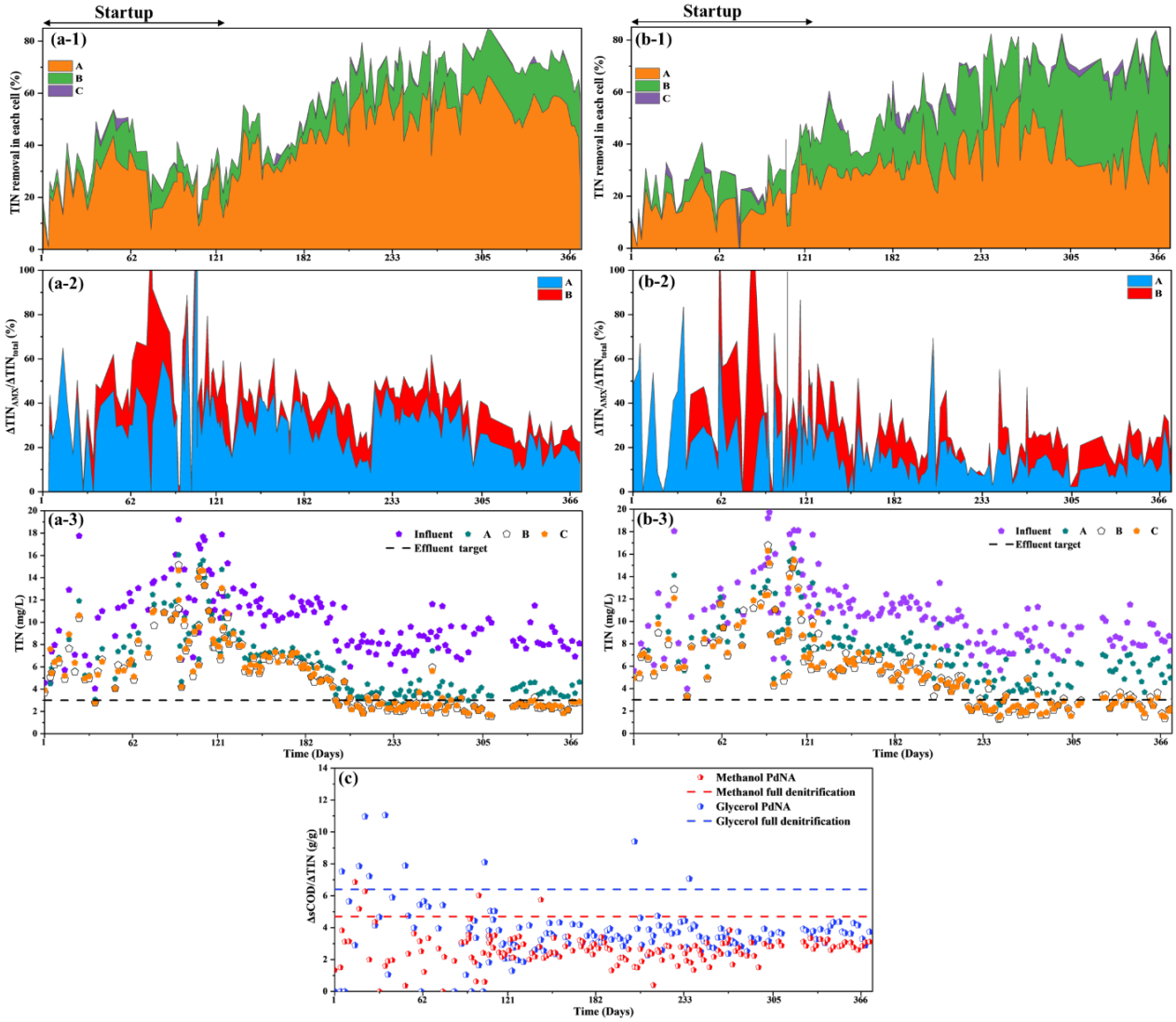

Figure 6.2 Stacked profiles of influent TIN removal efficiency in methanol (a-1) and glycerol (b-1) trains; Stacked profiles of AMX contribution in Cell A and Cell B to total TIN removal of methanol (a-2) and glycerol (b-2) MBBRs; Profiles of TIN concentrations in the influent, Cell A, Cell B, and Cell C of methanol (a-3) and glycerol (b-3) trains; (c) Profiles of ΔsCOD/ΔTIN of methanol and glycerol trains under PdNA and full denitrification conditions. Note: ΔsCOD values are after influent DO deduction

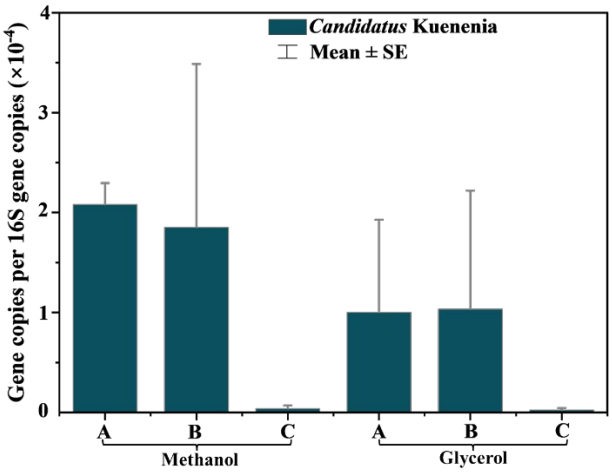

Figure 6.3 Gene copies per 16S gene copies of AMX bacteria (*Candidatus Kuenenia*) in the Cell A, Cell B, and Cell C of methanol and glycerol trains (on Day 380). SE denotes standard errors.

6.5.2 Fate of nitrite

The success of autotrophic nitrogen removal through AMX depends on the availability of NO_2^--N for AMX utilization. Theoretically, NO_2^--N has three destinations after the formation in anoxic reactors, i.e., denitrifier reduction, AMX utilization, or effluent NO_2^--N residue. Since the last two destinations belong to the scope of PdN, monitoring the NO_2^--N flow towards these two destinations helped test the aforementioned Hypotheses 1 and 2.

Figure 6.4 shows PdN efficiencies and NO_2^--N flows in Cell A of methanol and glycerol trains over the course of the entire operational period. After startup, PdN efficiency of methanol train stabilized around 35.1 ± 11.3% (Figure 6.4a), which was lower than that of glycerol train (42.6 ± 19.6%) in Figure 6.4b. Similar observations were also reported in tertiary MBBRs and IFAS by Macmanus et al. (2022) and Klaus et al. (2023). It is noteworthy that in methanol train, majority of NO_2^--N produced from PdN was utilized by AMX, leaving only a small residue of NO_2^--N (0.6 ± 0.2 mg/L) in Cell A effluent (Figure 6.4a). This observation indicated that NO_2^--N sink provided by AMX might have existed in methanol train, which belongs to the scope of Hypothesis 1. Conversely, in glycerol rain, only around 30% of NO_2^--N produced from PdN was utilized by AMX, leaving the majority of NO_2^--N (1.5 ± 1.0 mg/L) as residue in the effluent (Figure 6.4b). This NO_2^--N accumulation in glycerol train indicated a rate differential between denitratation and denitritation, which belonged to the scope of Hypothesis 2.

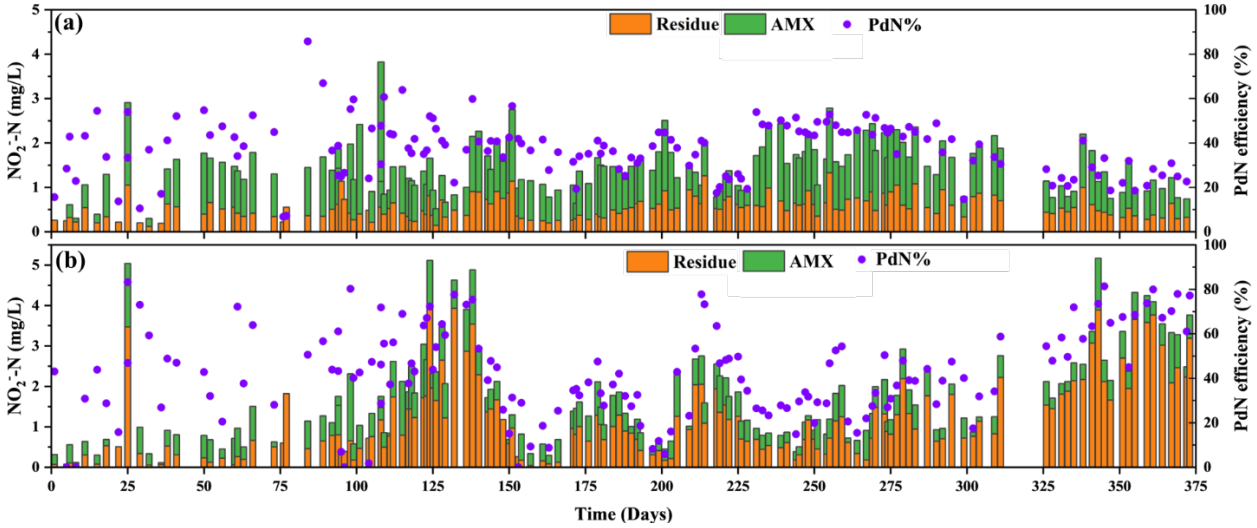

Figure 6.4 NO_2^--N flow and PdN efficiency in Cell A of methanol (a) and glycerol (b) trains

6.5.3 Statistical understanding of PdN mechanisms in methanol and glycerol trains

In order to further understand the mechanisms behind PdN in methanol and glycerol trains, its correlations with the rate differential between denitratation and denitritation (V_{DNA}-V_{DNI}) calculated by Eqs. 6.10 and 6.11, and TIN removal rate by AMX (ΔTIN_{AMX}/HRT) calculated by Eq. 6.13 were plotted in Figure 6.5 a and b for methanol and glycerol trains, respectively. PdN efficiency of glycerol train exhibited a stronger positive correlation (R^2 = 0.79) with the rate differential (V_{DNA}-V_{DNI}) than that of the methanol train (R^2 = 0.33) in Figure 6.5a but had a weaker correlation (R^2 = 0.41) with the TIN removal rate by AMX (ΔTIN_{AMX}/HRT) than that of the methanol train (R^2 = 0.58) in Figure 6.5b. This statistical results suggested that the glycerol-driven PdN was mainly dependent on the rate differential between denitratation and denitritation (Hypothesis 2) but not the AMX activities. Conversely, methanol-driven PdN was more relevant to the AMX activity (Hypothesis 1) but not by the rate differential, which aligned with the observation in Figure 6.4.

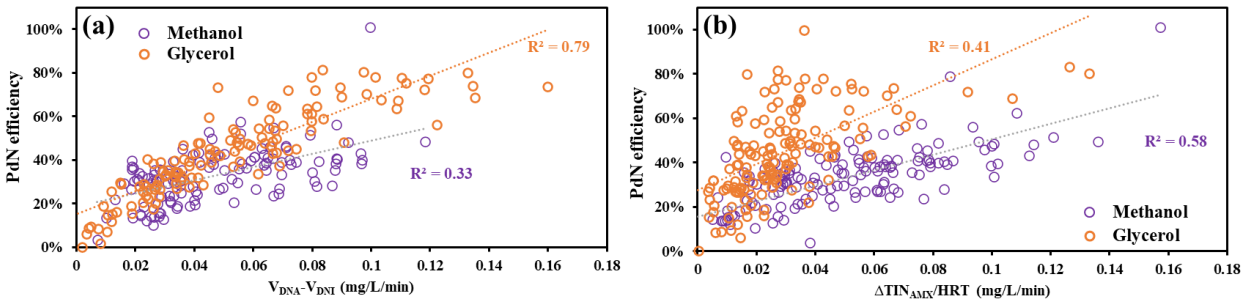

Figure 6.5 Statistical correlations between PdN efficiency and rate differential between denitratation and denitritation ($V_{DNA} - V_{DNI}$), and TIN removal rate by AMX ($\Delta TIN_{AMX}/HRT$) in (a) methanol and (b) glycerol trains

6.5.4 PdN efficiency versus AMX contribution in Cell A and Cell B

Figure 6.6 a and b plotted PdN efficiencies against AMX contributions to TIN removal ($\Delta TIN_{AMX}/\Delta TIN$) at various rbsCOD and NO_3^--N concentrations in methanol and glycerol Cell A, respectively. For this kind of plot, three scenarios exist. In scenario 1, if most experimental data fell 'on' the diagonal, Hypothesis 1 holds true because it means AMX utilized all NO_2^--N produced from PdN and thus are more likely the driving force of PdN. In scenario 2, if most experimental data fell within the region above the diagonal, Hypothesis 2 may hold true because AMX only can utilize a small portion of the NO_2^--N produced by PdN and thus unlikely act as the driving force of PdN. In this scenario, the rate differential between denitratation and denitritation might function as the driving force. In scenario 3, if the experimental data fell within the region below the diagonal, then AMX contribution to TIN removal exceeded that of the PdN efficiencies, which means that high NO_2^--N concentrations might have pre-existed in the influent, and thus AMX could occur even without PdN.

Figure 6.6a shows that majority of the data in methanol train fell 'on' the diagonal, which indicated that PdN efficiency and AMX contribution were almost equal for most time, which belonged to scenario 1. This aligned with the observation in Figure 6.4 a and Figure 6.5 b that NO_2^--N sink by AMX might have existed in the methanol train, and Hypothesis 1 held true. On the contrary, in glycerol train, PdN efficiency was greater than AMX contribution which belongs to the scenario 2. This aligned with the observation in Figure 6.4 and Figure 6.5 a, i.e., NO_2^--N accumulation in glycerol train was resulted from the rate differential between denitratation and denitritation, and

the weak AMX activities cannot catch up the NO_2^--N production, which belonged to the scope of Hypothesis 2.

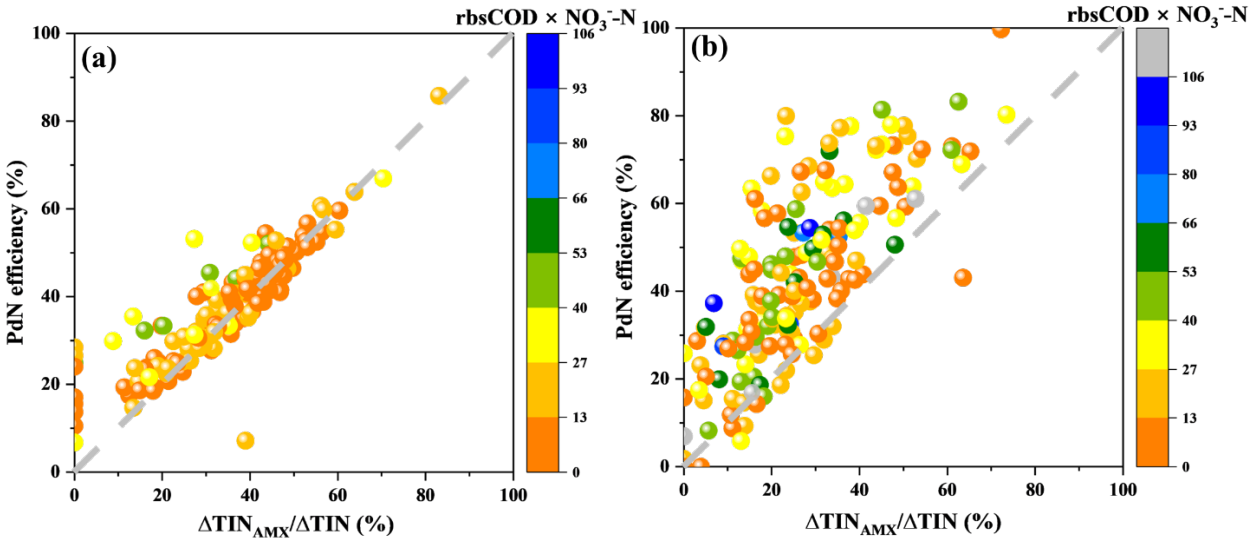

Figure 6.6 PdN efficiency v.s. AMX contribution to TIN removal ($\Delta TIN_{AMX}/\Delta TIN$) in response to the product of rbsCOD and NO_3^--N in methanol (a) and glycerol (b) trains.

6.6 Discussion

6.6.1 Bulk rbsCOD and its impacts on PdNA mechanisms

All experimental results presented above indicated that the two types of carbon sources might have triggered two types of PdNA mechanisms described in Hypotheses 1 and 2. Since the essence of PdNA is a competition of AMX with denitritation for NO_2^--N, the ratio of V_{AMX}/V_{DNI} for all experimental data were calculated from Eqs. 6.11 and 6.12 and plotted against their corresponding bulk rbsCOD in Figure 6.7a. It is obvious to see that the experiential data collected from the methanol and glycerol trains naturally separated from each other in Figure 6.7a with *p*-value of 7.6×10^{-4}. This is because the bulk rbsCOD values in the glycerol train were much greater than those in the methanol train with an average rbsCOD value of 8.1 ± 5.3 and 4.3 ± 2.3 in the former and latter (Figure 6.7a and Table 6.2). Since it was the denitritation but not AMX that depends on the rbsCOD (Eqs. 6.4 and 6.6), V_{AMX}/V_{DNI} naturally deceased with the increase of bulk rbsCOD because higher rbsCOD facilitated denitritation to compete with AMX. As a consequence, both the

AMX bacteria abundance and AMX contribution to TIN removal were much lower in glycerol train than that in the methanol train (Figures 6.2 a-2, b-2, and Figure 6.3, and Table 6.2).

As for the reason why glycerol train tended to have much higher bulk rbsCOD than methanol train did (Figure 6.7a), it has to do with the difference in their kinetics. To shed light on this aspect, the kinetic relationships between bulk rbsCOD concentrations (S_{COD}) and denitratation rates (V_{DNA}) in methanol and glycerol trains are plotted in Figure 6.7b. S_{COD} values were predicted from Eq. 6.3 by substituting the following parameters into Eq. 6.3, i.e., kinetic parameters listed in Table 6.1; $S_{NO_3^-}$ of 2 mg/L, an average values adopted from Table 6.2; and q_{DNA} values calculated by ratio of V_{DNA} to the biomass concentration in Cell A. The biomass concentration in Cell A was estimated by the ratio of V_{DNA} in Eq. 6.10 to q_{DNA} in Eq. 6.3 using the experimentally measured S_{COD} and V_{DNA} data marked on the model profiles in Figure 6.7b. As can be seen from Figure 6.7b, S_{COD} required to achieve the same V_{DNA} was always much higher when glycerol was used than when methanol was used as a substrate. This kinetic discrepancy was determined by their different half-saturation constants. In general, glycerol has a much higher K_{COD} (25 mg/L) than methanol K_{COD} (15 mg/L) as shown in Table 6.1. Le et al. (2019a) also hypothesized that the COD affinity for glycerol might be much lower than that for methanol. It is generally believed that the same K_{COD} is shared between denitratation and denitritation kinetics (Al-Omari et al., 2021; Henze et al., 2000). To achieve the same denitratation rate, namely V_{DNA}, which is controlled by the effluent NO_3^--N setpoint in Eq. 6.2 and HRT in Eq. 6.10, the bulk rbsCOD (S_{COD}) in glycerol has to be higher than that in the methanol train because of the lower COD affinity of glycerol according to Figure 6.7b. This high S_{COD} is also shared by denitritation kinetics in Eq. 6.4, which means the denitritation rate (V_{DIN}) was indirectly boosted by the high rbsCOD required for denitratation. Consequently, nitrite denitrifiers in glycerol train had a better chance to outcompete AMX bacteria, which explains the lower AMX bacteria abundance (Figure 6.3) and also lower AMX contribution to TIN removal (Figures 6.2 a-2 and b-2) when glycerol was used as a carbon source.

These being said, the mechanism discrepancy between methanol (Hypothesis 1) and glycerol (Hypothesis 2) trains shown in Figure 6.5, Figure 6.6 and Figure 6.7 was a result of their disparate bulk rbsCOD. It was the high COD affinity of methylotrophs that has played down the bulk rbsCOD concentration which in turn put NO_2^--N denitrifiers in an inferior position to compete

with AMX bacteria when methanol was used as a substrate. It was this advantage of AMX over denitritation at low bulk rbsCOD that has created a NO_2^--N sink resulting in an increased PdN efficiency in methanol train shown in Figure 6.5b, which provided a theoretical basis in support of Hypothesis 1. In contrast, when glycerol was used as a carbon source, its low COD affinity required a much higher bulk rbsCOD concentration to achieve a same effluent NO_3^--N setpoint (Figure 6.7b), which put AMX bacteria in an inferior position to compete with nitrite denitrifers for NO_2^--N, leading to higher NO_2^--N residue in the effluent (Figure 6.4b). In this case, AMX activities cannot catch up with the rate differential between denitratation and denitritation, which is line with Hypothesis 2.

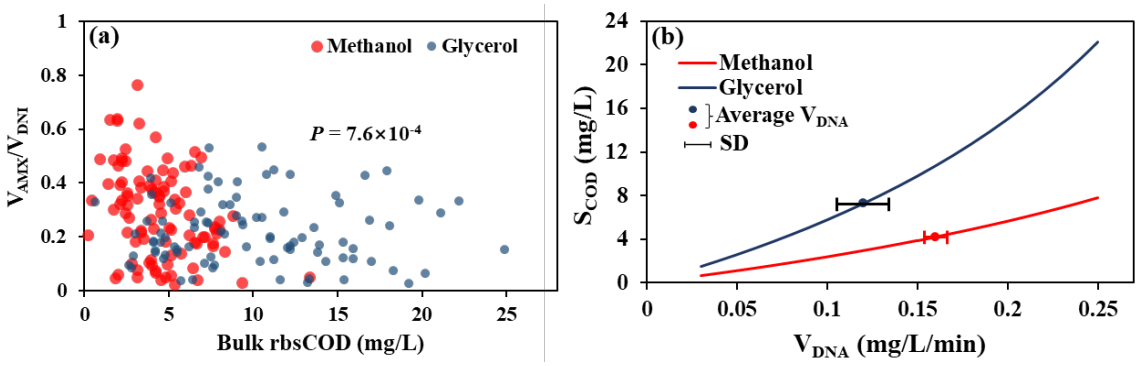

Figure 6.7 (a) Ratios of NO_2^--N utilization rates by AXM (V_{AMX}) to denitritation rate (V_{DNI}) against bulk rbsCOD concentrations in Cell A of methanol and glycerol trains; (b) Bulk rbsCOD concentrations (S_{COD}) simulated in methanol and glycerol trains at different denitratation rates (V_{DNA}) and an average bulk NO_3^--N concentration of 2 mg/L adopted from Table 6.2. SD denotes standard deviation.

6.6.2 Kinetic interpretation of the difference between methanol and glycerol in driving PdN

Theoretically, the maximum rate differential between denitratation (q_{DNA}) and denitritation (q_{DNI}) could be calculated as $(\frac{\mu_m^{Da}}{y_{NO3}^{Da}} - \frac{\mu_m^{Di}}{y_{NO2}^{Di}})$ according to Eqs. 6.3 and 6.4. When methanol was used as a carbon source, this value turned out to be 1.1 g/g/d, which appears to be much smaller than its counterpart value (3.2 g/g/d) when glycerol was used as a carbon source according to parameters in Table 6.1. The dramatically lower maximum rate differential value of methanol than glycerol suggested that the room for rate differential to increase in methanol train is limited by the kinetic nature of methanol. This provides a reasonable explanation for why the rate differential (V_{DNA} −

V_{DNI}) in glycerol train can be much higher than that in the methanol train as shown in Figure 6.5a, and also why methanol has been deemed less favorable for PdN in high strength wastewater (Le et al., 2019a; Zhang et al., 2020b).

Although methanol is not a good rate differential carbon source, this study showed that it is actually good at NO_2^--N sink in low strength wastewater. As listed in Table 6.2, methanol has a lower K_{COD} (15 mg/L) than glycerol (25 mg/L). When K_{COD} is low, only a lower bulk rbsCOD concentration is needed to achieve the same denitratation rate (Figure 6.7b). This lower bulk rbsCOD concentration simultaneously facilitated AMX bacteria to compete for more NO_2^--N utilization (Figure 6.7a). Another relevant reason could be that AMX bacteria also possess a lower NO_2^--N half-saturation constant (K_{NO2}^{Di}) of 1.5 mg/L than counterpart value of 0.2 mg/L of methylotrophic denitrifiers (Table 6.1). This greater K_{NO2}^{Di} value of methylotrophic denitrifiers put themselves in an inferior position to compete with AMX bacteria for NO_2^--N, which offers a fundamental explanation for the preference of NO_2^--N sink when methanol was used in low strength wastewater polishing processes such as tertiary treatment (Campolong, 2019; Macmanus et al., 2022). Hence, when methanol was used for tertiary PdNA, its kinetic characteristics should naturally trigger NO_2^--N sink (Hypothesis 1) which also explains the similar phenomena reported in other studies (Campolong, 2019; Le et al., 2019a; Macmanus et al., 2022).

6.7 Conclusions

The following conclusions can be drawn from this study, which are anticipated to provide insights into carbon source selection for future full-scale applications of PdNA:

1) The long-term (371 days) operational results in this study revealed that it was feasible to achieve low concentration nitrogen polishing in tertiary MBBRs via either methanol- or glycerol-fed PdNA. Effluent TIN concentration of < 3 mg/L can be achieved with both types of carbon sources.
2) 46.3% and 43.8% carbon saving can be achieved in the methanol and glycerol trains, respectively, plus another 1.6 tons O_2 savings per day assuming a flow rate of 69 million gallon per day.

3) Methanol was more economical than glycerol in unit nitrogen removal, which can be ascribed to its lower price, lower biomass yield of methylotrophic bacteria, and the kinetic advantage of AMX in competing with methylotrophic denitrifiers for NO_2^--N.
4) NO_2^--N sink by AMX dominated the PdN performance in methanol train; while the rate differential between denitratation and denitritation was the major mechanism of NO_2^--N provision when glycerol was used as a carbon source.
5) The disparate mechanism between methanol- and glycerol-fed PdN can be attributed to the different rbsCOD levels resulted from the half-saturation constant difference between the two types of carbon sources.
6) It was the lower rbsCOD in methanol train that has facilitated AMX to outcompete denitritation for NO_2^--N utilization, which explains higher abundance of AMX bacteria and also higher contribution of AMX to TIN removal in the methanol train over glycerol train.

6.8 References

Al-Omari, A., De Clippeleir, H., Ladipo-Obasa, M., Klaus, S., Bott, C., McCullough, K., Fofana, R., Wadhawan, T., Murthy, S. and Fevig, S. 2021 Modelling partial heterotrophic denitrification in mainstream nitrogen removal processes–model development and evaluation, pp. 67-71.

Badia, A., Kim, M. and Dagnew, M. 2021. Nitrite denitrification using biomass acclimatized with methanol as complementary carbon source: long-term performance and kinetics study. Environmental Science: Water Research & Technology 7(1), 93-106.

Campolong, C.J. (2019) Bioaugmentation and retention of anammox granules to a mainstream deammonification bio-oxidation pilot with a post polishing anoxic partial denitrification/anammox moving bed biofilm reactor, (Master thesis) Virginia Tech.

Faskol, A. and Racoviţeanu, G. 2021 Effect of DO, alkalinity and pH on nitrification using three different sunken materials types in biological aerated filter BAFs (Conference Proceedings), p. 012079.

Fofana, R., Parsons, M., Bachmann, M., Jones, K., Vela, J.D., Akyon, B., Liu, W., Klaus, S., deBarbadillo, C. and Bott, C. 2023. Robustness of partial denitrification-anammox

(PdNA) in filters with methanol and glycerol as carbon sources. Environmental Science: Water Research & Technology 9(4), 1124-1136.

Glass, C. and Silverstein, J. 1998. Denitrification kinetics of high nitrate concentration water: pH effect on inhibition and nitrite accumulation. Water research 32(3), 831-839.

Grady Jr, C.L., Daigger, G.T., Love, N.G. and Filipe, C.D. (2011) Biological wastewater treatment, CRC press.

Henze, M., Gujer, W., Mino, T. and van Loosdrecht, M.C. (2000) Activated sludge models ASM1, ASM2, ASM2d and ASM3, IWA publishing.

Her, J.J. and Huang, J.S. 1995. Denitrifying kinetics involving the distributed ratio of reductases. Journal of Chemical Technology & Biotechnology: International Research in Process, Environmental AND Clean Technology 62(3), 261-267.

Klaus, S., Campolong, C., Rosenthal, A., Sabba, F., Baideme, M., Wells, G., De Clippeleir, H., Chandran, K. and Bott, C. 2023. Comparison of carbon sources in a partial denitrification/anammox MBBR using glycerol, acetate, and methanol. Environmental Science: Water Research & Technology 9(4), 1041-1052.

Le, T., Peng, B., Su, C., Massoudieh, A., Torrents, A., Al-Omari, A., Murthy, S., Wett, B., Chandran, K. and DeBarbadillo, C. 2019a. Impact of carbon source and COD/N on the concurrent operation of partial denitrification and anammox. Water Environment Research 91(3), 185-197.

Le, T., Peng, B., Su, C., Massoudieh, A., Torrents, A., Al-Omari, A., Murthy, S., Wett, B., Chandran, K. and deBarbadillo, C. 2019b. Nitrate residual as a key parameter to efficiently control partial denitrification coupling with anammox. Water Environment Research 91(11), 1455-1465.

Ma, B., Wang, S., Cao, S., Miao, Y., Jia, F., Du, R. and Peng, Y. 2016. Biological nitrogen removal from sewage via anammox: recent advances. Bioresource technology 200, 981-990.

Macmanus, J., Long, C., Klaus, S., Parsons, M., Chandran, K., De Clippeleir, H. and Bott, C. 2022. Nitrogen removal capacity and carbon demand requirements of partial denitrification/anammox MBBR and IFAS processes. Water Environment Research 94(8), e10766.

Moore, G.T. 2010. Nutrient control design manual. US Environmental Protection Agency, Washington, DC.

Purtschert, I. and Gujer, W. 1999. Population dynamics by methanol addition in denitrifying wastewater treatment plants. Water science and technology 39(1), 43-50.

Rice, E.W., Baird, R.B., Eaton, A.D. and Clesceri, L.S. (2012) Standard methods for the examination of water and wastewater (23rd Version), American public health association Washington, DC.

Si, Z., Peng, Y., Yang, A., Zhang, S., Li, B., Wang, B. and Wang, S. 2018. Rapid nitrite production via partial denitrification: pilot-scale operation and microbial community analysis. Environmental Science: Water Research & Technology 4(1), 80-86.

Uprety, K. (2013) Evaluation of glycerol and waste alcohol as supplemental carbon sources for denitrification, (Master Thesis) Virginia Tech.

Xu, X., Ma, B., Lu, W., Feng, D., Wei, Y., Ge, C. and Peng, Y. 2020. Effective nitrogen removal in a granule-based partial-denitrification/anammox reactor treating low C/N sewage. Bioresource technology 297, 122467.

Zhang, T., Cao, J., Zhang, Y., Fang, F., Feng, Q. and Luo, J. 2020a. Achieving efficient nitrite accumulation in glycerol-driven partial denitrification system: Insights of influencing factors, shift of microbial community and metabolic function. Bioresource Technology 315, 123844.

Zhang, T., Cao, J., Zhu, Q., Fu, B., Yang, E., Fang, F., Feng, Q. and Luo, J. 2022. Revealing the characteristics and formation mechanisms of partial denitrification granular sludge for efficient nitrite accumulation driven by glycerol. Chemical Engineering Journal 428, 131195.

Zhang, Z., Zhang, Y. and Chen, Y. 2020b. Recent advances in partial denitrification in biological nitrogen removal: From enrichment to application. Bioresource Technology 298, 122444.

Chapter 7 Unblocking the rate-limiting step of the municipal sludge anaerobic digestion

(This chapter has been published as "Wang, J., Sun, Y., Zhang, D., Broderick, T., Strawn, M., Santha, H., Pallansch, K., Denies, A. and Wang, Z.W. (2022), Unblocking the rate-limiting step of the municipal sludge anaerobic digestion., Water Environment Research, e10793, DOI: https://doi.org/10.1002/wer.10793")

7.1 Abstract

Anaerobic digestion stabilizes municipal sludge through total solids reduction and biogas production. It is generally accepted that hydrolysis accounts for the rate-limiting step of municipal sludge anaerobic digestion, impacting the overall rates of solids reduction and methane production. Technically, the sludge hydrolysis rate can be enhanced by the application of thermal hydrolysis pretreatment (THP) and is also affected by the total solids concentration, temperature, and solids retention time used in the anaerobic digestion. This study systematically analyzed and compared ways to take these four factors into the consideration of modern anaerobic digestion system for achieving the maximum solid reduction. Results showed that thermophilic anaerobic digestion was superior to mesophilic anaerobic digestion in terms of solids reduction but vice versa in terms of the methane production when integrated with THP. This difference has to do with the intermediate product accumulation and inhibition when hydrolysis outpaced methanogenesis in THP-enhanced thermophilic anaerobic digestion, which can be mitigated by adjusting the solids retention time.

7.2 Keywords

Mesophilic; Thermophilic; Hydrolysis; Anaerobic; Sludge; SRT

7.3 Introduction

Anaerobic digestion is a biological process commonly used in water resources recovery facilities (WRRFs) for reducing the mass and volume of the primary and secondary sludge produced during wastewater treatment (Mills et al., 2014) and, in turn, saves the cost of biosolids transportation and disposal in the landfills or on the farmlands. Along with this solid reduction, the organic fraction of the sludge also can be biologically converted to biogas that can be utilized as a type of renewable energy for generating heat, electricity, and even vehicle fuel (Tian et al., 2021). Similar to the solids fermentation processes used in other fields (Chilakamarry et al., 2022; Liu et al., 2020), the rate of solids hydrolysis is usually the limiting step constraining the overall rate of the anaerobic digestion processes consisting of hydrolysis, acidogenesis, acetogenesis, and methanogenesis (Appels et al., 2008; Wang et al., 2011). Therefore, the purpose of this study is to develop a strategy that can substantially improve the municipal sludge hydrolysis rate, which is highly desired in industrial practices to unblock this rate-limiting step for upgrading the capacity of existing anaerobic digesters. Technically, the sludge hydrolysis rate is affected by the total solids concentration (TS) (Di Capua et al., 2020; Xu et al., 2021), the solids retention time (SRT) (Appels et al., 2008; Ge et al., 2011; Jain et al., 2015; Pilli et al., 2015; Zhen et al., 2017), and the temperature (e.g., mesophilic or thermophilic) used in anaerobic digestion (AD) processes (Müller, 2000). In recent years, thermal hydrolysis pretreatment (THP) has also been increasingly used to further enhance the sludge hydrolysis rate (Appels et al., 2008; Ge et al., 2011; Jain et al., 2015; Pilli et al., 2015; Zhen et al., 2017). To date, these measures have not been investigated in a systematic manner to explore the extent to which the sludge hydrolysis rate can be maximized through the process integration and optimization. To this end, this study is aimed to determine the enhancement these four measures can possibly bring to the municipal sludge AD. It is anticipated that the outcomes from this study are able to provide engineering guidance for WRRFs to maximize the capacity of existing anaerobic digesters.

7.4 Material and methods

7.4.1 THP setup

THP was performed in a 2 L pressure vessel (No. 4602, Parr Instrument, Moline, IL) (Figure 7.1a) heated in a muffle furnace at 170 °C and 890 kPa for 2.5 h to ensure sufficient heat penetration. The THP temperature was selected based on the specification of full-scale Cambi THP process (Appels et al., 2008), which was also suggested by previous studies (Di Capua et al., 2020; Zhang et al., 2021) in terms of the extents of sludge solubilization and subsequent biogas production to be achieved under such conditions. We are aware that this lab-scale THP time (2.5 h) is much longer than the 0.5 h commonly used in full-scale THP, which uses hot stream for quick heat penetration. Due to the lab-scale setup limitation, we chose to make this necessary compromise as was practiced in many other similar lab-scale studies (Zhang et al., 2021). As a result, the outcome from this study is expected to overestimate the THP effects. The sludge processed in this lab-scale THP was then fed to the lab-scale anaerobic digesters shown in Figure 7.1b. The feed sludge characteristics before and after THP are shown in Table 7.1. More detailed information about the lab-scale THP setup can be found in the study by Zhang et al. (2021)

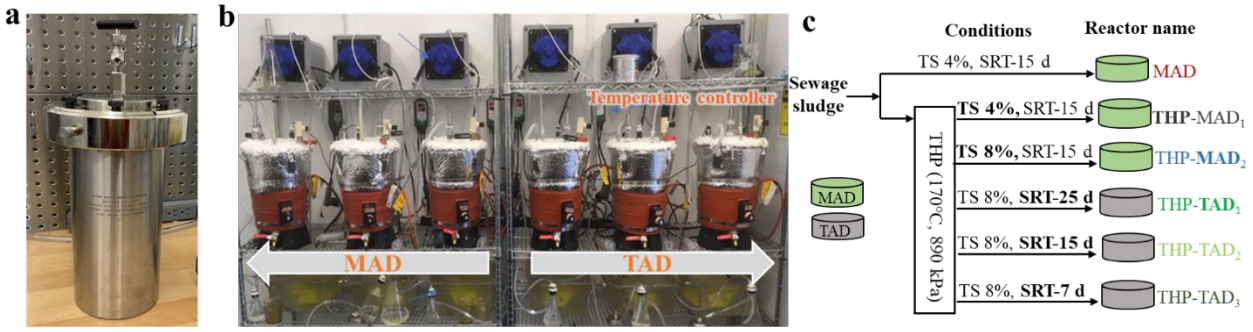

Figure 7.1 Experimental design: a, THP; b, anaerobic digesters; c, summary of experimental design

Table 7.1 Feed sludge characteristics before and after THP

	Raw sludge	**After THP**
TS (wt %)	4.0 ± 0.1	4.0 ± 0.1
VS (wt %)	78.0 ± 0.58	78.0 ± 0.80
tCOD (mg L^{-1})	41843 ± 488	42303 ± 1464
sCOD (mg L^{-1})	3494 ± 81	9074 ± 117
Alkalinity (mg $CaCO_3$ L^{-1})	742 ± 19	1419 ± 21
VFAs (mg Acetate L^{-1})	987 ± 49	2496 ± 77
Soluble protein (mg L^{-1})	1671 ± 37	2678 ± 62
Soluble carbohydrate (mg L^{-1})	424 ± 50	3779 ± 7
pH	7.03 ± 0.0	7.11 ± 0.0

Abbreviations: sCOD, soluble chemical oxygen demand; tCOD, total chemical oxygen demand; THP, thermal hydrolysis pretreatment; TS, total solids concentration; VFAs, volatile fatty acid; VS, volatile solids concentration.

7.4.2 Anaerobic digester setup

A total of six stainless steel anaerobic digesters with the design described in a previous study was employed in this research (Zhang et al., 2020a). Referring to Figure 7.1b, each digester came with a working volume of 5 L was completely mixed via biogas recirculation at a flow rate of 0.5 L min^{-1} from the headspace to the conical bottom. The temperature of these digesters was maintained with insulation layers and heating blankets (50-425F, Cole-Parmer, Vernon Hills, IL) via feedback temperature controllers (ITC-308, Inkbird Tech, Shenzhen, China). The biogas production was monitored using calibrated tipping-bucket meters coupled with automatic data loggers (HOBO Pendant®, Bourne, MA Archae Press, Nashville, TN). The mesophilic digesters were inoculated with digestate from a full-scale mesophilic anaerobic digester in a local WRRF, and the thermophilic digesters were inoculated with digestate from a lab-scale thermophilic digester that has been stabilized for 280 days (Zhang et al., 2020a). The dewatered sludge cake fed into these digesters was collected from another local WRRF and contains 20.0 % TS made of primary and secondary sludge blended in a dry mass ratio of 31:19. Distilled water was used to dilute the cake to 4% or 8% TS according to the experimental design in Figure 7.1c. Briefly, three digesters were

operated under mesophilic (35 ± 0.3 °C) conditions while the other three were operated under thermophilic (55 ± 0.3 °C) conditions. A one-factor-at-a-time approach was taken to understand the effect of a factor and then integrate the better level of the factor for the next factor optimization. Therefore, a single variable experiment was designed to evaluate the contribution of each of the four factors to the hydrolysis rate enhancement and methane production. Briefly, in order to evaluate the effect of THP on hydrolysis rate, sludges with and without THP were fed into two identical mesophilic anaerobic digesters (MADs) to compare their digestibility. Likewise, the post THP sludge with 4.0 % and 8.0 % TS were fed into two identical MADs, respectively, to understand the TS effect. A thermophilic anaerobic digester (TAD) was also compared to a MAD to understand the digester temperature effect. In the end, three TADs operated with the SRTs of 7, 15, and 25 days were also operated in parallel to understand the SRT effect (Figure 7.1c).

7.4.3 Chemical analysis

Gas samples from the headspace of the digesters were measured for methane contents, using a gas chromatograph (GC) equipped with a thermal conductivity detector and a flame photometric detector (Shimadzu, Columbia, MD). The pH, TS, and volatile solids concentration (VS) were analyzed according to the standard method (APHA, 2012). Alkalinity, volatile fatty acid (VFA) concentration, and VFA-to-Alkalinity ratio were quantified using an auto-titrator (Hanna Instruments, Woonsocket, RI). Sludge samples were filtered through a 0.45 μm PTFE filter (MilliporeSigma, Burlington, MA) to measure the total ammonia, soluble chemical oxygen demand (sCOD), a well as protein and carbohydrate contents using Hach test kits of TNT 832, Hach TNT plus Vial, modified Lowry protein assay kits (Pierce™, Rockford, IL), and the phenol-sulfuric acid method (Nielsen, 2010), respectively. Total chemical oxygen demand (tCOD) was measured using Hach TNT plus Vial according to the standard method (APHA, 2012). The free ammonia nitrogen (FAN) concentration was calculated using the ideal equilibrium equation from the study by Emerson et al. (1975). The volatile solid reduction (VSR) ratios were calculated using the equation from the study by Mei et al. (2016). The volumetric methane production rate (L L^{-1} d^{-1}) was calculated by dividing daily methane production volume by the working volume of the digester. The volumetric solids reduction rate (g L^{-1} d^{-1}) was calculated by dividing daily mass of solids destroyed by the working volume of the digester.

7.4.4 Statistical analysis

Microsoft Excel was used to tabulate data and perform simple statistics such as mean, standard deviation, and T test. T tests were used to determine if the mean difference between two variables was statistically significant ($p < 0.05$). The AD steady states were also determined by T tests of random monitoring data sampled from the daily pH and volumetric methane production rate profiles presented in Figure 7.3; that is, experimental data collected after the time behind the dash lines in Figure 7.3 are with $p > 0.05$ and thus can be regarded as steady state data. The data from THP-TAD_3 in Figure 7.1c did not have a steady state because of the failure in methane production.

7.5 Results

7.5.1 Effect of THP on sludge hydrolysis

The effect of 170 °C THP for 2.5 hours on sludge hydrolysis was studied in a MAD operated at an SRT of 15 days. Table 7.1 shows that the THP itself did not change TS, VS, pH, and tCOD of the sludge. However, THP has substantially increased all the soluble metrics. For example, sCOD, alkalinity, VFAs, as well as soluble protein and carbohydrate concentrations have increased for 0.6 to 7.9 folds as a result of THP (Table 7.1), which indicates the effectiveness of THP in hydrolyzing the municipal sludge solids.

The higher VFA availability in the effluent of THP (Table 7.1) is expected to grow more methanogens in the THP-MAD_1 which can be reflected by its significantly greater volumetric methane production rate over that of the MAD without THP measured at the steady state (Table 7.2 and Figure 7.2a). In contrast, an insignificant difference of volumetric solids reduction rate between MAD and THP-MAD_1 was measured in Table 7.2 and Figure 7.2a, suggesting that the microbial hydrolysis in MAD can be as good as that of the THP at such a low TS content of 4%. This conclusion can be supported by the similar VSR values measured in the two digesters (Table 7.2). It is also noteworthy that not much difference was found in the VFA-to-Alkalinity ratio between MAD and THP-MAD_1 at the steady state either (Table 7.2). Since VFAs are the intermediate products between hydrolysis and methanogenesis assuming acidification and

acetification are not the rate-limiting step, this VFA-to-Alkalinity ratio can be used an indicator of whether methanogenesis rate can catch up with the hydrolysis rate because the ratio would have substantially increased, and the pH would have dropped if otherwise (Lossie and Pütz, 2008). The similar VFA concentrations and neutral pH values in the two digesters' effluent suggest that the methanogenesis has paced well with the hydrolysis with or without THP. Again, the reason might have to do with the low TS loaded into both MADs because microbial hydrolysis apparently has handled such a low TS as well as that of the THP. This hypothesis was tested in the subsequent TS effect study.

7.5.2 Effects of TS on sludge hydrolysis

The TS that can be effectively mixed with biogas recirculation in these lab-scale anaerobic digesters is below 8% (Figure 7.1b). Therefore, two MADs fed with 4% and 8% TS sludge were compared side-by-side to understand the TS effect on sludge hydrolysis when all other parameters such as THP, SRTs, and AD temperatures were kept the same. Results in Table 3.2 showed that the VSR declined for 13.0% as a result of doubling the TS in the feed sludge. As a matter of fact, it is expected to see this hydrolysis efficiency decrease because the solids loading applied on the THP-MAD_2 has doubled. Accordingly, the volumetric solids reduction and methane production rates in THP-MAD_2 has also doubled over the THP-MAD_1 operated with half solids loading (Table 7.2 and Figure 7.2 b). This proportional increase in hydrolysis and methanogenesis rates along with the solids loading rate increase suggests that the methanogenesis was still able to keep up with the pace of the hydrolysis increase along with the TS increase and was subjected to minor inhibition from the accumulation of the intermediate products such as VFAs and FAN. Results in Table 7.2 showed that the VFAs and FAN did increase from 1228.1 mg Acetate L^{-1} and 26.8 mg L^{-1} to 3849.6 mg Acetate L^{-1} and 35.1 mg L^{-1}, respectively, as a result of doubling the influent TS. The uncompromised rates of solids hydrolysis and methane production just revealed that these levels of intermediate product accumulation were not severe enough to impede the high-TS MAD performance and thus should be pursued in full-scale application for better use of the MAD volumetric capacity.

7.5.3 Effects of AD temperature on sludge hydrolysis

To understand the effects of AD temperature on the sludge hydrolysis, a MAD and a TAD were operated with an SRT of 15 days in parallel with all other parameters kept the same. Results in Table 7.2 showed that the VSR have substantially increased from 44.1% in THP-MAD_2 to 51.2% in THP-TAD_2 as a result of the AD temperature increase from 35 °C to 55 °C, evidencing the essential role of AD temperature in governing the sludge hydrolysis rate even with THP applied. As a result of this microbial hydrolysis enhancement, the volumetric solids reduction rate has significantly increased for 31.5% in THP-TAD_2 over the THP-MAD_2 (Figure 7.2 c); however, the volumetric methane production rate has dropped for 53.8% in the THP-TAD2 over that in the THP-MAD_2 (Figure 7.2 c). This sharp decline in methanogenesis rate has to do with the inhibition from the intermediate-product accumulation. Table 7.2 shows that the VFA-to-Alkalinity ratio and FAN have substantially increased for 54.8% and 689.1% in THP-TAD_2 over THP-MAD_2, respectively. Obviously, this intermediate product accumulation can be explained by the inability of methanogenesis to keep up with the pace of hydrolysis in THP-TAD_2. The fact that TAD has been used for municipal sludge stabilization for decades without the intermediate product accumulation problem implies that this out-of-the-pace between hydrolysis and methanogenesis has to do with the THP integration (Figure 7.1 a). A literature review in Table 7.3 shows that the volumetric methane production rate has been low in all previous THP-TAD integrations even though the VSR has been very high, indicating that an integration of two high-rate processes such as THP and TAD has accelerated the hydrolysis rate to the extent that the methanogenesis cannot keep up with anymore. As a consequence, the VFAs and FAN of THP-TAD_2 have been dramatically accumulated to the levels of 5733.6 mg Acetate L-1 and 276.9 mg L-1, respectively (Table 7.2). Therefore, feeding 8% TS of THP-processed sludge to a TAD operated at a 15-day SRT is not a very good choice for methane production even though doing so can substantially improve the sludge hydrolysis performance in terms of VSR and volumetric solids reduction rate as compared to the THP-MAD_2 operated under the same conditions (Table 7.2 and Figure 7.2 c).

7.5.4 Effects of SRTs on THP-TAD

Knowing the THP-TAD_2 operation at a 15-day SRT has already increased the hydrolysis rate to the extent that methanogenesis rate cannot keep up with anymore, the SRT was investigated as a single variable in this experiment to understand whether it can be manipulated to moderate the

paces between hydrolysis and methanogenesis. Theoretically, increasing SRT allows more methanogens to be enriched and thus offers higher methanogenesis rate. Meanwhile, increasing SRT should also enhance VSR for the longer digestion time and thus produce lower TS in the digester effluent. This prediction is in line with the experimental results measured in Table 7.2, i.e., increasing the SRT of TAD from 7 to 15 and then to 25 days has significantly improved the volumetric methane production rates from 0.28 to 0.80 and then to 1.03 L L-1 d-1 as a result of the more methanogen retention with the SRT increase (Figure 7.2 d). Likewise, the VSR also increased from 41.0, to 51.2, and then to 63.4% along with the SRT increase (Table 7.2). It is noteworthy that the volumetric solids reduction rate actually decreased along with this VSR increase, and such a VSR increase was proportional to the decrease of volumetric solids reduction rate (Table 7.2). This can be explained by the first-order microbial hydrolysis rate that has been recognized in AD (Batstone et al., 2002), i.e., the solid hydrolysis rate is supposed to be proportional to the in-situ TS in the AD. Hence, a high VSR has attenuated the in-situ TS to such a low level that the volumetric solids reduction rate proportional to it according to the first-order reaction kinetics has also become low (Batstone et al., 2002).

It is noteworthy that the volumetric methane production rate in the THP-TAD_2 operated at a 15-day SRT was still significantly lower than that in the THP-MAD_2 operated at the same SRT despite the significantly higher volumetric hydrolysis achieved in the former (Figure 7.2 c). Results in Table 7.2 show that the VFA-to-Alkalinity ratio and FAN in the THP-TAD_2 were both substantially greater than that in the THP-MAD_2, indicating that the inhibitor accumulation might be the reason responsible for compromised volumetric methane production in THP-TAD_2. This inference is supported by the significantly improved volumetric methane production rate in the THP-TAD_1 operated at an SRT of 25 days because both the VFA level and the VFA-to-Alkalinity ratio have declined for 29.7% and 16.7% (Table 7.2) with the SRT increase because more time has been offered to methanogens to convert more VFAs to methane gas. Yet, the volumetric methane production rate achieved at such a long SRT (25 days) in THP-TAD_1 still did not exceed that in the THP-MAD_2 operated at a much shorter SRT of 15 days. The ultimate inhibitory factor has to do with the FAN as it is an end product of AD and thus cannot be removed through methanogenesis like VFAs do. FAN inhibition levels to TAD were reported to vary from 45 to 297 mg L^{-1} depending on the microbial communities and acclimation (Capson-Tojo et al., 2020; Rajagopal et al., 2013).

The FAN level of 349.4 mg L^{-1} measured in the THP-TAD_1 apparently has exceeded this inhibitory range as a result of the greatest VSR of 63.4% achieved (Table 7.2). This result just suggested that the FAN inhibition might be the ultimate bottleneck limiting the AD capacity when the rate-limitation on the sludge hydrolysis is unblocked.

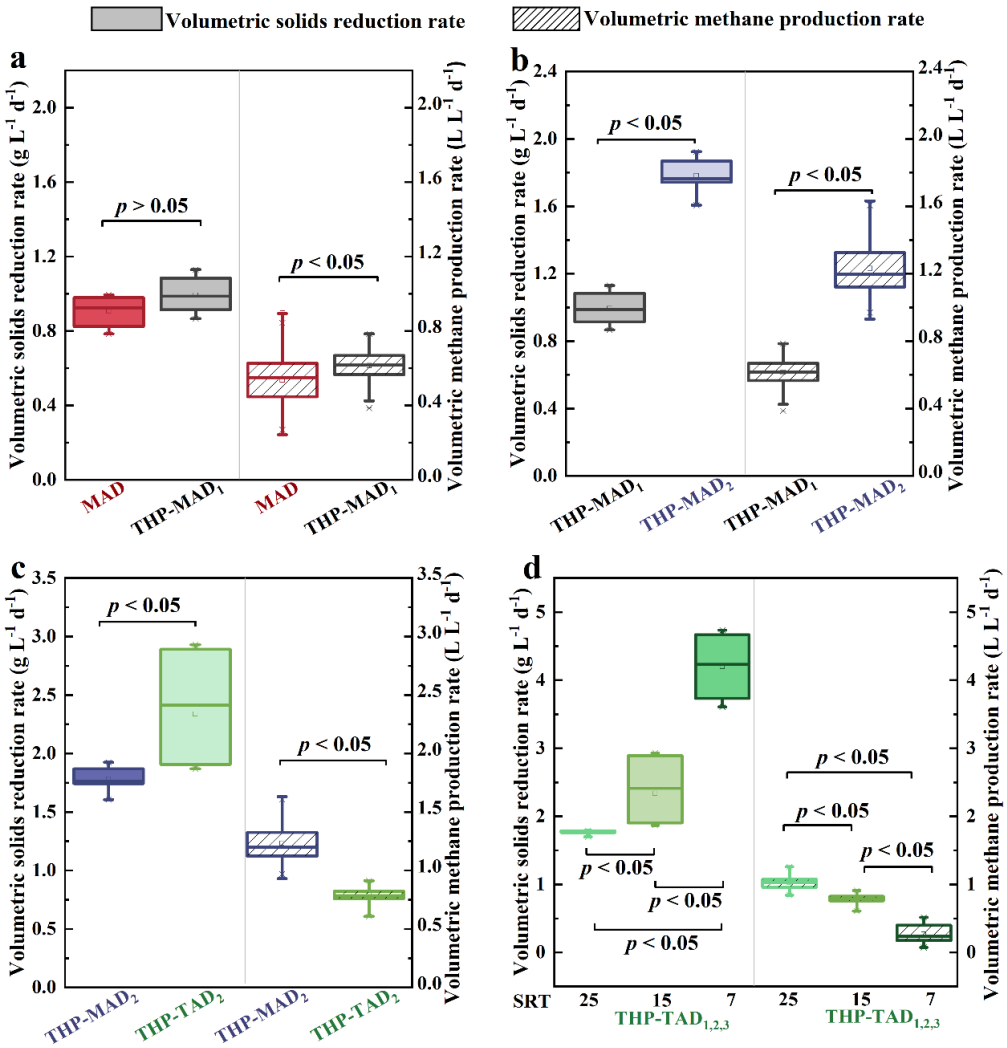

Figure 7.2 Box plots showing the comparative results of volumetric solid reduction rates and volumetric methane production rates of systems under various experimental design in Figure 7.1 c, i.e., a. MAD vs. THP-MAD_1; b. THP-MAD_1 vs. THP-MAD_2; c. THP-MAD_2 vs. THP-TAD_2; d. THP-TAD_1 vs. THP-TAD_2 vs. THP-TAD_3. Data under steady states of all systems (Figure 7.3) were used except for THP-TAD_3 which did not have a steady state. The data from THP-TAD_3 were all included

Table 7.2 Performance of anaerobic digesters under various scenarios

	MAD	**THP-MAD$_1$**	**THP-MAD$_2$**	**THP-TAD$_1$**	**THP-TAD$_2$**	**THP-TAD$_3$**
SRT (days)	15	15	15	25	15	7
Feedstock TS (%)	4.0 ± 0.1	4.0 ± 0.1	8.0 ± 0.1	8.0 ± 0.1	8.0 ± 0.1	8.0 ± 0.1
Feedstock VS (%)	85.0 ± 0.2	85.0 ± 0.2	85.0 ± 0.2	85.0 ± 0.2	85.0 ± 0.2	85.0 ± 0.2
Volumetric solids reduction rate (g L^{-1} d^{-1})	0.91 ± 0.09	0.99 ± 0.10	1.78 ± 0.12	1.76 ± 0.04	2.34 ± 0.46	4.20 ± 0.55
Volumetric methane production rate (L L^{-1} d^{-1})	0.54 ± 0.13	0.61 ± 0.08	1.23 ± 0.15	1.03 ± 0.10	0.80 ± 0.07	0.28 ± 0.12
VSR (%)	46.8 ± 3.7	50.7 ± 4.2	44.1 ± 2.3	63.4 ± 1.1	51.2 ± 7.3	41.0 ± 4.5
VFAs (mg Acetate L^{-1})	1237.5 ± 317.5	1228.1 ± 398.4	3849.6 ± 332.7	4031.5 ± 110.5	5733.6 ± 224.4	7303.9 ± 273.9
Alkalinity (mg $CaCO_3$ L^{-1})	4183.2 ± 329.4	4319.1 ± 427.4	6212.3 ± 549.1	6287.2 ± 499.3	5048.8 ± 818.8	4188.7 ± 781.6
VFA-to-Alkalinity ratio	0.25 ± 0.02	0.24 ± 0.02	0.62 ± 0.04	0.80 ± 0.16	0.96 ± 0.09	2.20 ± 0.34
pH	7.16 ± 0.08	7.16 ± 0.06	7.33 ± 0.07	7.75 ± 0.07	7.66 ± 0.06	6.88 ± 0.25
CH_4 content in biogas (%)	60.8 ± 1.4	60.1 ± 1.6	57.7 ± 0.50	57.7 ± 0.3	63.3 ± 0.2	20.2 ± 0.1
TAN (mg L^{-1})	698 ± 3	1380 ± 42	1538 ± 3	1960 ± 10	1750 ± 10	1570 ± 10
FAN (mg L^{-1})	11.0 ± 0.1	26.8 ± 0.8	35.1 ± 0.1	349.4 ± 2.2	276.9 ± 1.9	155.4 ± 1.5

Noted: Data under steady state from all systems (Figure 7.3) were used except for THP-TAD$_3$. The data from THP-TAD$_3$ were all included.

Table 7.3 Comparison of THP-TAD performance between previous and this study

Reactor configuration	SRT (Days)	THP (°C)	OLR (kg VS $m^{-3} \cdot d^{-1}$)	TS feed (%)	TSR (%)	VSR (%)	Volumetric methane production rate (L L^{-1} d^{-1})	References
Batch	32	134	ND	4.4	ND	ND	0.03	Climent, *et al.*
Batch	ND	90	ND	8.0	ND	ND	0.13	Yao, *et al.*
Continuous	10	70	ND	5.4	31.2	36.6	0.61	Ferrer, *et al.*
Continuous	15	160	3.50	5.7	54.7	60.4	0.95	Han, *et al.*
Continuous	15	134	1.00	2.1	ND	46.0	0.22	Gianico, *et al.*
Continuous	15	165-170	3.35	8.3	ND	ND	0.74	Chen, *et al.*
Continuous	25	165-170	1.88	6.8	ND	ND	0.66	Chen, *et al.*
Semi-continuous	25	170	2.61	8.0	55	62.0	1.03	This study
Semi-continuous	15	170	4.34	8.0	48	53.0	0.80	This study

ND - not determined.

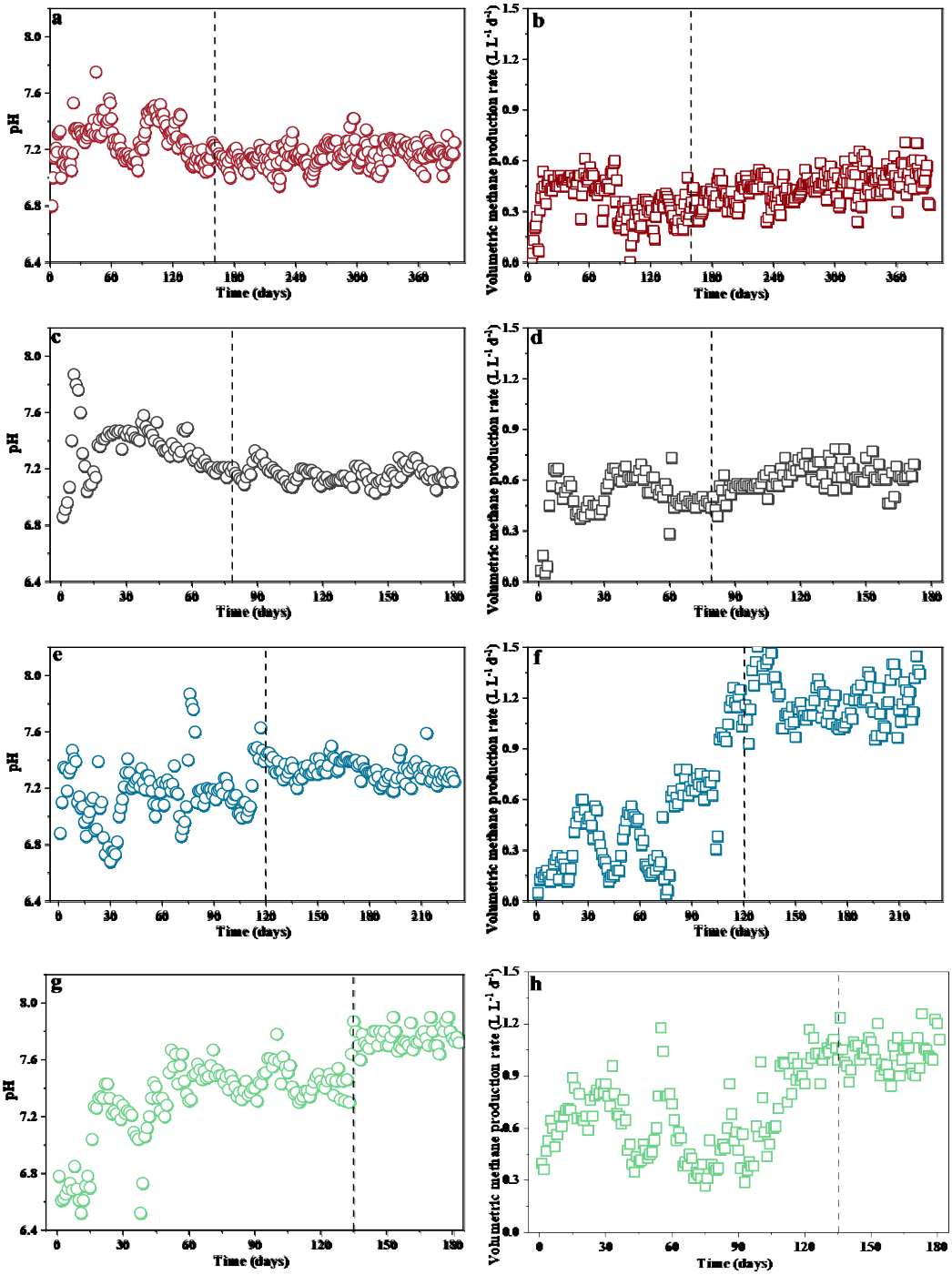

Figure 7.3 Profiles of pH and volumetric methane production rates for systems under various experimental design described in Figure 7.1, i.e., (a, b) MAD; (c, d) THP-MAD$_1$; (e, f) THP-MAD$_2$; (g, h) THP-TAD$_1$; (i, j) THP-TAD$_2$; and (k, l) THP-TAD$_3$. Date after dash lines represent data under steady states as determined from T-Tests.

7.6 Discussion

Judging from the horizontal comparison in Table 7.2 and Figure 7.2, the best setup for achieving maximum VSR, namely 63%, is THP-TAD_1 operated at an SRT of 25 days, which is expected in that all three factors, i.e., the high temperatures of both AD and THP and the longest SRT, e.g., 25 days, have collectively contributed to the solid hydrolysis in this one combination. Meanwhile, the volumetric solids reduction rate of this setup was also comparable to that achieved in the THP-MAD_2 operated at an SRT of 15 days, which is the most common setup used across the world (Labatut and Pronto, 2018). The 16.3% lower volumetric methane production rate has to do with the 10 times FAN accumulation as a result of the 55 °C used as well as the greatest VSR and pH values measured in the THP-TAD_1. This is because FAN with a concentration greater than 297 mg L^{-1} has been shown inhibitory to methanogenesis (Capson-Tojo et al., 2020; Rajagopal et al., 2013). As mentioned above, FAN is an end product of AD that cannot be reduced by AD itself unless a separate TAN removal process is incorporated. Besides, FAN level is actually very sensitive to the AD temperature used. According to the ideal equilibrium equation (Emerson et al., 1975), an increase of AD temperature from 35 °C to 55 °C will increase the FAN level for 3 times even when the pH and TAN remain at the same level of 7 and 1000 mg L^{-1}, respectively. With this FAN inhibition in mind, it is not difficult to understand the impeded methanogenesis rate and in turn the elevated VFA accumulation (Figure 7.2 d and Table 7.2) in face of the accelerated hydrolysis rates brought by THP and TAD. As a consequence, both the VFA concentration and the VFA-to-Alkalinity ratio became higher in all THP-TAD than those in THP-MAD as a result of the methanogenesis inhibition (Table 7.2), causing a feedback inhibition loop between FAN and VFAs as described by (Capson-Tojo et al., 2020). Given the exceptionally higher VSR and VFA production obtained in THP-TAD over THP-MAD, the THP-TAD setup might be more conducive to the applications that emphasize more on the solid removal or VFA recovery than on the methane production because the high temperatures of THP and TAD have improved the hydrolysis so well that the methanogenesis can no longer keep up with anymore.

According to the U.S. Environmental Protection Agency (USEPA) reports, out of the 1484 municipal wastewater treatment facilities that digest sludge to produce biogas in the U.S., only less than 10% of those plants commercially utilize biogas, leaving the rest just flaring the biogas into the atmosphere or merely combust biogas in boilers (Naik-Dhungel, 2010). Meanwhile, VFAs is an important carbon substrate to assist mainstream enhanced biological phosphorus removal (EBPR) and biological nutrient

removal (BNR) (Atasoy et al., 2018; Luo et al., 2019). Technically, VFAs accumulated in TAD effluent can be recovered and utilized through filtrate recirculation (Yesil et al., 2021). Many studies have shown that better EBPR performance was obtained using VFAs derived from the fermenter than dosing equivalent amounts of synthetic acetic acid (Atasoy et al., 2018; Luo et al., 2019). Meanwhile, 31.5% more solids can be further reduced in unit reactor volume on a daily basis when using the configuration of THP-TAD at SRT of 15 days (THP-TAD_2) than THP-MAD_2 at the same SRT (Table 7.2). However, the seven times higher FAN measured in this configuration (THP-TAD_2) accounted for a 53.8% less volumetric methane production rate than that of the THP-MAD at SRT of 15 days (Table 7.2). This FAN inhibitory problem might be addressable with the application of in-situ ammonia recovery techniques under development. Example technologies include in-situ ammonia stripping using either biogas (Bi et al., 2020; Walker et al., 2011) or nitrogen (Yao et al., 2017) as stripping gas without pH or temperature modification. Palakodeti et al. (2021) and Zhang et al. (2020b) have also reported that adding biochar into continuous or semi-continuous digesters can not only alleviate FAN inhibition but also increase digestate properties as a fertilizer. Shi et al. (2019) even demonstrated that submerging a hydrophobic gas-permeable expanded polytetrafluoroethylene (ePTFE) membrane tube into the AD reactor and recirculating an adsorption solution of sulfuric acid through the membrane tube can effectively achieve in-situ and real-time ammonia recovery from ongoing AD systems. It is anticipated that the rate-limiting step of the municipal sludge anaerobic digestion can be further alleviated in the future with the application of similar in-situ ammonia removal technologies.

7.7 Conclusions

The following concluding remarks can be drawn from this study:

1) All THP-TAD investigated in this study can offer equal or faster volumetric solids reduction rates than all the THP-MAD do.
2) FAN inhibition appears to be an ultimate limiting factor constraining the volumetric methane production rate in THP-TAD.
3) THP-MAD_2 operated at an SRT of 15 days with 8% TS influent sludge offered the greatest volumetric methane production rate.

4) THP-TAD_1 operated at an SRT of 25 days offered the greatest VSR at a volumetric methane production rate similar to that achieved in THP-MAD_2 and thus should be considered for full-scale application.
5) In-situ ammonia removal technique should be developed to further unblock the rate-limiting step of THP-TAD_1.

7.8 References

APHA (2012) Standard methods for the examination of water and wastewater, 22nd Edition, American Public Health Association, Washington DC.

Appels, L., Baeyens, J., Degrève, J. and Dewil, R. 2008. Principles and potential of the anaerobic digestion of waste-activated sludge. Progress in energy and combustion science 34(6), 755-781.

Atasoy, M., Owusu-Agyeman, I., Plaza, E. and Cetecioglu, Z. 2018. Bio-based volatile fatty acid production and recovery from waste streams: current status and future challenges. Bioresource technology 268, 773-786.

Batstone, D.J., Keller, J., Angelidaki, I., Kalyuzhnyi, S., Pavlostathis, S., Rozzi, A., Sanders, W., Siegrist, H. and Vavilin, V. 2002. The IWA anaerobic digestion model no 1 (ADM1). Water Science and technology 45(10), 65-73.

Bi, S., Qiao, W., Xiong, L., Mahdy, A., Wandera, S.M., Yin, D. and Dong, R. 2020. Improved high solid anaerobic digestion of chicken manure by moderate in situ ammonia stripping and its relation to metabolic pathway. Renewable Energy 146, 2380-2389.

Capson-Tojo, G., Moscoviz, R., Astals, S., Robles, Á. and Steyer, J.-P. 2020. Unraveling the literature chaos around free ammonia inhibition in anaerobic digestion. Renewable and Sustainable Energy Reviews 117, 109487.

Chen, Z., Li, W., Qin, W., Sun, C., Wang, J. and Wen, X. 2020. Long-term performance and microbial community characteristics of pilot-scale anaerobic reactors for thermal hydrolyzed sludge digestion under mesophilic and thermophilic conditions. Science of The Total Environment 720, 137566.

Climent, M., Ferrer, I., del Mar Baeza, M., Artola, A., Vázquez, F. and Font, X. 2007. Effects of thermal and mechanical pretreatments of secondary sludge on biogas production under thermophilic conditions. Chemical Engineering Journal 133(1-3), 335-342.

Di Capua, F., Spasiano, D., Giordano, A., Adani, F., Fratino, U., Pirozzi, F. and Esposito, G. 2020. High-solid anaerobic digestion of sewage sludge: challenges and opportunities. Applied Energy 278, 115608.

Emerson, K., Russo, R.C., Lund, R.E. and Thurston, R.V. 1975. Aqueous ammonia equilibrium calculations: effect of pH and temperature. Journal of the Fisheries Board of Canada 32(12), 2379-2383.

Ferrer, I., Serrano, E., Ponsa, S., Vazquez, F. and Font, X. 2009. Enhancement of thermophilic anaerobic sludge digestion by 70 C pre-treatment: energy considerations. Journal of Residuals Science and Technology 6(1), 11-18.

Ge, H., Jensen, P.D. and Batstone, D.J. 2011. Relative kinetics of anaerobic digestion under thermophilic and mesophilic conditions. Water Science and Technology 64(4), 848-853.

Gianico, A., Braguglia, C., Cesarini, R. and Mininni, G. 2013. Reduced temperature hydrolysis at 134 C before thermophilic anaerobic digestion of waste activated sludge at increasing organic load. Bioresource technology 143, 96-103.

Han, D., Lee, C.-Y., Chang, S.W. and Kim, D.-J. 2017. Enhanced methane production and wastewater sludge stabilization of a continuous full scale thermal pretreatment and thermophilic anaerobic digestion. Bioresource technology 245, 1162-1167.

Holm-Nielsen, J.B., Al Seadi, T. and Oleskowicz-Popiel, P. 2009. The future of anaerobic digestion and biogas utilization. Bioresource technology 100(22), 5478-5484.

Jain, S., Jain, S., Wolf, I.T., Lee, J. and Tong, Y.W. 2015. A comprehensive review on operating parameters and different pretreatment methodologies for anaerobic digestion of municipal solid waste. Renewable and Sustainable Energy Reviews 52, 142-154.

Labatut, R.A. and Pronto, J.L. (2018) Sustainable food waste-to-energy systems, pp. 47-67, Elsevier.

Liu, W., Yang, H., Ye, J., Luo, J., Li, Y.-Y. and Liu, J. 2020. Short-chain fatty acids recovery from sewage sludge via acidogenic fermentation as a carbon source for denitrification: A review. Bioresource technology 311, 123446.

Lossie, U. and Pütz, P. 2008. Targeted control of biogas plants with the help of FOS/TAC. Practice Report Hach-Lange.

Luo, K., Pang, Y., Yang, Q., Wang, D., Li, X., Lei, M. and Huang, Q. 2019. A critical review of volatile fatty acids produced from waste activated sludge: enhanced strategies and its applications. Environmental Science and Pollution Research 26(14), 13984-13998.

Mei, R., Narihiro, T., Nobu, M.K., Kuroda, K. and Liu, W.-T. 2016. Evaluating digestion efficiency in full-scale anaerobic digesters by identifying active microbial populations through the lens of microbial activity. Scientific reports 6(1), 1-10.

Mills, N., Pearce, P., Farrow, J., Thorpe, R. and Kirkby, N. 2014. Environmental & economic life cycle assessment of current & future sewage sludge to energy technologies. Waste management 34(1), 185-195.

Müller, J. 2000. Pretreatment processes for the recycling and reuse of sewage sludge. Water Science and Technology 42(9), 167-174.

Naik-Dhungel, N. 2010. The opportunities for and benefits of combined heat and power at wastewater treatment facilities. Proceedings of the Water Environment Federation 2010(4), 557-566.

Nielsen, S.S. (2010) Food analysis laboratory manual. Nielsen, S.S. (ed), pp. 47-53, Springer US, Boston, MA.

Palakodeti, A., Azman, S., Rossi, B., Dewil, R. and Appels, L. 2021. A critical review of ammonia recovery from anaerobic digestate of organic wastes via stripping. Renewable and Sustainable Energy Reviews 143, 110903.

Pandey, A., Soccol, C.R. and Larroche, C. (2008) Current developments in solid-state fermentation, Springer Science & Business Media.

Pilli, S., Yan, S., Tyagi, R.D. and Surampalli, R.Y. 2015. Thermal pretreatment of sewage sludge to enhance anaerobic digestion: a review. Critical Reviews in Environmental Science and Technology 45(6), 669-702.

Rajagopal, R., Massé, D.I. and Singh, G. 2013. A critical review on inhibition of anaerobic digestion process by excess ammonia. Bioresource technology 143, 632-641.

Shi, X., Zuo, J., Zhang, M., Wang, Y., Yu, H. and Li, B. 2019. Enhanced biogas production and in situ ammonia recovery from food waste using a gas-membrane absorption anaerobic reactor. Bioresource technology 292, 121864.

Walker, M., Iyer, K., Heaven, S. and Banks, C. 2011. Ammonia removal in anaerobic digestion by biogas stripping: an evaluation of process alternatives using a first order rate model based on experimental findings. Chemical Engineering Journal 178, 138-145.

Wang, Z.-W., Ma, J. and Chen, S. 2011. Bipolar effects of settling time on active biomass retention in anaerobic sequencing batch reactors digesting flushed dairy manure. Bioresource technology 102(2), 697-702.

Xu, Y., Gong, H. and Dai, X. 2021. High-solid anaerobic digestion of sewage sludge: achievements and perspectives. Frontiers of Environmental Science & Engineering 15(4), 1-18.

Yao, Y., Huang, Y. and Hong, F. 2016. The influence of sludge concentration on its thermophilic anaerobic digestion performance based on low temperature thermal hydrolysis pretreatment. Procedia Environmental Sciences 31, 144-152.

Yao, Y., Yu, L., Ghogare, R., Dunsmoor, A., Davaritouchaee, M. and Chen, S. 2017. Simultaneous ammonia stripping and anaerobic digestion for efficient thermophilic conversion of dairy manure at high solids concentration. Energy 141, 179-188.

Yesil, H., Calli, B. and Tugtas, A.E. 2021. A hybrid dry-fermentation and membrane contactor system: Enhanced volatile fatty acid (VFA) production and recovery from organic solid wastes. Water Research 192, 116831.

Zhang, D., Santha, H., Pallansch, K., Novak, J.T. and Wang, Z.-W. 2020a. Repurposing pre-pasteurization as an in situ thermal hydrolysis pretreatment process for enhancing anaerobic digestion of municipal sludge: a horizontal comparison between temperature-phased and standalone thermophilic or mesophilic anaerobic digestion. Environmental Science: Water Research & Technology 6(12), 3316-3325.

Zhang, L., Li, F., Kuroki, A., Loh, K.-C., Wang, C.-H., Dai, Y. and Tong, Y.W. 2020b. Methane yield enhancement of mesophilic and thermophilic anaerobic co-digestion of algal biomass and food waste using algal biochar: semi-continuous operation and microbial community analysis. Bioresource technology 302, 122892.

Zhen, G., Lu, X., Kato, H., Zhao, Y. and Li, Y.-Y. 2017. Overview of pretreatment strategies for enhancing sewage sludge disintegration and subsequent anaerobic digestion: Current advances, full-scale application and future perspectives. Renewable and Sustainable Energy Reviews 69, 559-577.